DOT HS-801 440

EHICLE-IN-USE LIMIT PEFORMANCE ND TIRE FACTORS. RE IN USE. PPENDIX A,B,C

Contract No. DOT-HS-031-3-693
March 1975
Final Report

PREPARED FOR:

U.S. DEPARTMENT OF TRANSPORTATION

NATIONAL HIGHWAY TRAFFIC SAFETY ADMINISTRATION

WASHINGTON, D.C. 20590

TECHNICAL REPORT STANDARD TITLE PAGE

1. Report No.	2. Government Accession No.	3. Recipient's Catalog No.
DOT-HS - 801-440	31973	

4. Title and Subtitle	5. Report Date
Vehicle-In-Use Limit Performance and Tire Factors The Tire in Use	MARCH 1975 6. Performing Organization Code
7. Author(s)	**8. Performing Organization Report No.**
James E. Bernard, Paul S. Fancher, Rajiv Gupta Howard Moncarz, Leonard Segel	UM-HSRI-PF-75-1-2
9. Performing Organization Name and Address	**10. Work Unit No.**
Highway Safety Research Institute The University of Michigan Huron Parkway & Baxter Road Ann Arbor, Michigan 48105	**11. Contract or Grant No.** DOT-HS-031-3-693
12. Sponsoring Agency Name and Address	**13. Type of Report and Period Covered**
National Highway Traffic Safety Administration U.S. Department of Transportation Washington, D.C. 20590	Appendix A, B, C 6/73 - 2/75 **14. Sponsoring Agency Code**

15. Supplementary Notes

16. Abstract The influence of tire-in-use factors (inflation pressure, replacement mixes, and wear) on the steering and braking response of automobiles is examined through analysis, simulation, laboratory and over-the-road tire testing, and vehicle testing. Results for a 1971 Mustang and a 1973 Buick station wagon illustrate the influence of tire-in-use factors on (a) the open-loop braking and/or turning performance in drastic maneuvers on wet and dry surfaces, and (b) the understeer/oversteer factor for maneuvers involving lateral accelerations below 0.3 g.

This investigation shows that differences in tire mechanical properties between the front and rear wheels (as caused by tire-in-use factors) can cause significant and potentially dangerous changes in limit response and from the stability and control characteristics intended by the vehicle manufacturer. The report recommends that (1) inspection limits for inflation pressure be within ±1 psi of the manufacturer's recommended level, (2) minimum tread-groove depth exceed 2/32", and (3) further research be conducted to develop a cost-effective means for indicating the lateral force characteristics of a tire.

17. Key Words Tire shear force, vehicle mechanics, tire wear, tire inflation pressure, replacement tire mixes, emergency maneuvers, linear analysis of directional response, vehicle simulation.

18. Distribution Statement
Document is available to the public through the National Technical Information Service, Springfield, Virginia 22151

19. Security Classif. (of this report)	20. Security Classif. (of this page)	21. No. of Pages	22. Price
Unclassified	Unclassified	259	

Form DOT F 1700.7 (8-69)

TABLE OF CONTENTS

APPENDIX A

LITERATURE SURVEY

Howard Moncarz

A1. INTRODUCTION

The purpose of this literature survey is to gather, organize, and summarize information relative to the influence of tire-in-use factors on vehicle performance. The tire-in-use factors considered in this survey are: (1) the performance characteristics of different replacement tires, (2) tread wear (both uniform and shoulder wear), (3) inflation pressure, (4) vertical loading, (5) tire temperature, and (6) vehicle speed. Additionally, the interaction between circumferential and lateral force, as well as the effect of wet surfaces on tire performance characteristics, are considered.

A search was undertaken to find those papers that present experimental results and conclusions concerning: (1) the effect of tire-in-use factors on the mechanical properties of pneumatic tires, (2) the effect of tire-in-use factors on vehicle dynamics, and (3) the generation of accelerated wear to simulate actual tire wear. The search was also extended to those papers presenting theories on tire mechanics considered relevant to the project.

The manner in which people actually use and maintain their tires serves as a good introduction to the study of tire-in-use factors. Harvey and Brenner [54]* did such a study relying on two surveys—one aimed at obtaining data of the condition of tires from an unbiased sample of passenger car tires in normal use and the second one aimed at obtaining similar data for passenger car tires used mainly in long distance traveling. The tire-in-use factors they examined were tread depth and wear pattern, wheel loading, inflation pressure, tire mix (in regard to using tires of different inflation pressures and/or tread wear), and the effects of temperature. Additionally, they correlated these tire-in-use factors and traffic accidents based on previously published accident data. Highlights quoted from the report are:

---

*Numbers in brackets designate references in the Annotated Bibliography at end of text.

"--A greater percentage of severely worn tires were found on vehicles in accidents than in the general tire population.

--Vehicles in accidents have a larger number of severely worn tires on their rear axles than on the front suggesting that it is safer to have newer or less worn tires on the rear axle.

--There is a considerable body of evidence indicating that the risk of tire disablement and of loss of vehicle control rises sharply for tires having less than about 2/32-inch of tread depth remaining.

--Air towers at service stations are generally not accurate. A motorist relying on a tower gage will have only about a 20 percent change of getting within ± 1 psi of the inflation pressure he wants. A single point calibration of the tower gage could decrease the error substantially.

--More than one out of four cars has at least one seriously underinflated tire (4 psi or more below the recommended normal inflation pressure for the vehicle).

--About 2 percent of cars are overloaded by 10 percent or more; about 6 percent are overloaded to some extent. Most overloading occurs on station wagons and light trucks, and on passenger cars during vacation trips.

--On the average most cars are loaded to about 80 percent of their allowable load (at the existing equivalent cold tire inflation pressure)."

A2. REPLACEMENT TIRES

There are numerous design variables that go into the making of a tire, and each one can have an effect on the performance characteristics of the tire [115]. The tire carcass is made of a woven fabric of cords, set at a specified angle to the plane of the tire. The cords may be made from a number of materials. Additionally, rigid breakers, or belts, are attached on a layer of cords and these belts have been made from a variety of materials as well. There are several different types of rubber compounds that are used on the same tire—one type for the tread, another for the sidewalls, a third for the inner lining, etc. Each rubber compound is made from a variety of substances in different ratios to each other to give it the desired properties the designer intends. And of course, tread designs are numerous.

With all these design variables there are still others which are important in the actual manufacture of the tire. The same materials put together in different sequences, or treated for different time spans, heated to different temperatures, etc., can produce quite different tires.

A2.1 MANUFACTURER

Because of the complexity of a tire, no two tire manufacturers can be said to make any tire in exactly the same way. Thus, in a technical sense it is inappropriate to study the performance differences of the same type of tires made by different manufacturers, because, in fact, the tires are not the same.

However, in the marketplace, the consumer has only limited information concerning the design variables of a tire, including the size, the aspect ratio, the general construction, the tread pattern. These variables (with price, of course) will determine which tires a consumer will buy as replacement tires. Thus it

is reasonable (in a practical sense) to study manufacturers as a tire-in-use factor, keeping the design variables just mentioned fixed. It should be noted that production by a single manufacturer of several batches of a specified tire may still result in tires being made having significantly different performance characteristics among them. This is due to variables encountered in the actual manufacture of the tire. These variables could vary from day to day, from plant to plant, or possibly even in the same batch of tires manufactured at the same place at the same time.

Several investigators have dealt with manufacturer as a variable in determining performance characteristics of tires. They have not made specific conclusions, except to say that there exist substantial differences in performance characteristics between tires of the same size and construction type but different manufacturers [32, 66, 95, 114].

A2.2 DESIGN VARIABLES

A literature survey by Schuring, et al. [112], investigated the influence of (1) tire construction type, (2) tread geometry, (3) tread compound, (4) road wheel dimensions, (5) tire aspect ratio, and (6) cord material of OE tires on vehicle performance. A general discussion is provided that indicates the state of the art in each of these six categories, following which is a brief summary of each of the 82 articles deemed pertinent to the survey. This survey serves as an important source of information concerning replacement tires, since it has dealt with six of the important tire design variables that have an important effect on vehicle performance.

A3. GENERATION OF TREAD WEAR

Tread wear can substantially change the mechanical characteristics of a tire, and hence is an important tire-in-use factor. To study tread wear, means must be used to generate tread wear at an accelerated time scale, but in a manner in which the processed tires will have the same performance characteristics as tires with tread wear obtained by normal driving. Thus it is necessary to designate and understand the mechanisms by which a tire wears naturally.

As early as 1943 Moyer [90] published a comprehensive report discussing the numerous factors affecting tread wear. He found the factors "to affect tread wear are, in the approximate order of their importance: (1) car speed; (2) brake application and car acceleration; (3) type and condition of road surface; (4) tire inflation pressures and wheel loads; (5) mechanical condition of car and alignment and balance of wheels; (6) air temperature and tire temperature; (7) wheel position and attention given to tire rotation; (8) tire mileage; (9) highway curves and grades; (10) design of cars; (11) type, grade, and age of rubber; and (12) drivers' practices." More recently Brenner and Kondo [12] discussed the factors affecting tread wear relevant to developing a test for rating tread wear. They concluded that the course on which tires are to be rated should include several different pavements and a variety of maneuvers of unequal severity to have general usefulness. This was corroborated by Snyder [118] who found that large differences in the rate of tread wear are obtained in different locales across the U.S., based on a statistical study of tread wear of contemporary belted tires.

Several papers have dealt with the generation of accelerated tread wear. Using a two-wheeled trailer designed by Schallamach [51], Southern [119] described a method for obtaining accelerated tread wear and the corresponding measurement for

the rate of tread wear. McIntosh [82] described a method to duplicate road testing of tires on a laboratory tread wear tester.

Bergman and Crum [9] developed a theory based on experiment to explain the generation of tread wear. Their theory is expressed by the following points:

(1) Grip is defined as an intimate instantaneously stationary contact between tire tread rubber and road asperities, during which contact no relative motion between the tire and the road takes place. Therefore, grip expresses a static condition.

(2) "Grip is the key factor in the first phase of tire-road interaction. The grip enables the tire to transmit or generate shear forces (cornering, braking, or driving)."

(3) There are two types of grip:

   (a) Deformation grip is due to road asperities which act like the teeth in gears and produce localized pressures between the road and tire.

   (b) Adhesion grip is due to molecular forces. Hence the tire and road must be in close proximity. Adhesion grip occurs where localized pressure is high. Therefore, it only exists at certain points throughout the contact patch.

(4) Grip between the tire and road is primarily affected by road surface, and to a much lesser extent, the tire surface.

(5) Less than 0.1 mm of the surface of tread affects grip.

(6) Tire-road friction is defined as a resistance to relative motion between the tire tread rubber and the road surface. Friction prevails during the second phase of the tire-road interaction, when the elements disengage themselves from a grip and slide back toward their initial position with respect to the wheel rim.

(7) The length of travel of tread rubber during the sliding phase of the contact patch and the friction drag force are the two main factors determining tread wear on a given road surface under given operating conditions.

Based on experiment, they observed the following:

(1) Cornering produces uneven wear which starts from the corners of individual tread ribs. Stiffness of the tread ribs increase with wear. Therefore uneven wear decreases with accumulated wear. (S. Tsuchiya, et al., [128] also found that tread rubber stiffness increases with wear.)

(2) Increased inflation pressure decreases tire contact patch area.

(3) Tread wears more in cornering than in braking or traction. This is due to a lower cornering stiffness compared to braking or driving stiffness. Also, in cornering, wear increases at a greater than constant rate with increasing lateral force. In braking or traction, wear increases linearly with those respective forces.

This last point was corroborated by Veith [131] who found that cornering force is a much more important factor in tire wear than longitudinal force. Using an instrumented test trailer [130], he found that wear rate varies with cornering force

raised to an exponent between 2 and 4, depending on the pavement texture, tire temperature, and tread composition (in the tire cornering force range of 0-500 lb.).

Additionally, he discussed test severity and concluded that severity must be broken up into three components:

(1) Tire cornering force level (the most important factor)

(2) Pavement texture

(3) Tire surface temperature

These effects are not simply additive. The predominant wear mechanism varies depending on the conditions (particularly pavement texture), and completely different results are found depending on the mechanism of wear actually occurring. In making note of this point, good correlation of experimental data with the theory developed was obtained.

Other conclusions reached by Veith were:

(1) With current tread compounds, the wear rate increases about 2 percent per degree centigrade.

(2) Radial tires are superior to bias tires in wear, due primarily to the belt which stabilizes the tread elements.

(3) Pavement microtexture is a major factor determining wear rate. The pavement macrotexture has only a slight effect on wear rate.

(4) The wear rate decreases on wet roads for two reasons:

    (a) The tire surface temperature decreases.

    (b) The friction between tire and road decreases.

One final point concerning tread wear noted by Lippman and Oblizajek [79] is that the front tires of a car wear more severely at the tread edges than at the center, whereas the rear tires tend to wear more uniformly. (Presumably, this assumes equal inflation pressures in front and rear tires.)

A4. INFLUENCE OF TREAD WEAR ON TIRE CHARACTERISTICS

A4.1 UNIFORM WEAR

An OE tire shows traction performance characteristics quite different than what they are after the tire has been run sufficiently to be "worn in." OE tires were tested at Karlsruhe University on an internal drum tire testing machine. The cornering force and aligning torque rose from their initial values as running time increased. These values finally leveled off as the tires became "worn in."

Once the tires are "worn in," further wear, as well as the type of wear, has a very important influence on the performance characteristics of a tire. In general, for uniform tread wear, traction increases as tread depth decreases on dry surfaces and decreases with decreasing tread depth on wet surfaces [25, 31, 36, 43, 53, 56, 66, 69, 102, 128].* It should be noted, however, that in a study by Fancher, et al., on tire traction fields using wet surfaces, it was found that in a few cases, fully worn radial tires as well as fully worn belted-bias tires exceeded the traction performance of half-worn radials and half-worn belted-bias tires, respectively [31].

Finally, Leland [74] found that the friction level of a tire on wet roads deteriorates gradually with tread wear until the tread is 80% worn, after which point the friction level deteriorates rapidly. Further, based on a tire's footprint, a tire may be considered completely bald insofar as its friction capability is concerned when its tread is 95% worn, due to the load on the tire bearing down on it [74].

---

*See Lippman and Oblizajek [79] and Tsuchiya, et al. [128], in annotated bibliography for more detailed analysis of the effect of tread wear on the performance characteristics of a tire.

A4.2 SHOULDER WEAR

In several studies it was found that tread shoulder wear can have a significant effect on the performance characteristics of a tire. Rasmussen and Cortese [102] found that tires with their treads shaved on a tire-truing machine produced greater lateral forces and aligning torques on dry surfaces when the shoulders were rounded. Recent experiments at HSRI reported by Segel [114] show that a tire displays a "remarkable sensitivity" of dry traction to tread shoulder wear. Tires with belted-bias construction were particularly sensitive.

A5. INFLATION PRESSURE

Varying the inflation pressure of a tire changes its performance characteristics. A number of studies have shown that lateral stiffness and force levels increase with increasing inflation pressure (for a particular load and slip angle) until a maximum is reached, after which point the stiffness and force level decreases [33, 36, 37, 61, 63, 95, 96]. Also, aligning torque levels and aligning torque stiffness decrease with increasing inflation pressure [37, 61, 95, 96]. However, on dry to slightly damp surfaces, the above effects are reduced, particularly with regard to braking coefficients and longitudinal forces which show little if any sensitivity to inflation pressure on such surfaces [63, 123].

Nordeen and Cortese [95] determined that camber thrust also increased with increasing inflation pressure. Additionally, they found that the sensitivity of cornering stiffness and camber stiffness to changing inflation pressure varies considerably with different tires of the same size. Peterson and Rasmussen [99] found that the sensitivity of traction characteristics of radial tires to changing inflation pressure is smaller than the sensitivity of bias tires.

Finally, Nordeen and Cortese [96] noted that changing the inflation pressure of tires affects the response time of a vehicle to force inputs through the tires—causing a quicker response time with higher inflation pressure.

A6. LOAD

There is a consensus in the literature that the following results generally hold true for the effects of load on the performance characteristics of tires:

(1) The peak lateral force that can be obtained increases with load to a maximum value and then decreases with a further increase in load [31, 37, 61].

(2) The peak longitudinal force shows the same behavior as the peak lateral force [31].

(3) Cornering stiffness also increases with load to a maximum, and then decreases gradually at higher loads [31, 37].

(4) Aligning torque increases with load [61], and additionally, tends toward zero as the load tends toward zero [95].

There were several papers that presented equations of lateral forces and moments as functions of wheel loading and other quantities [94, 111]. Schallamach [111] presented the development of a method to transform theoretical side force versus slip angle curves at different loads to one master curve. He found good agreement with experimental data. An attempt to do the same with aligning torque did not meet with good agreement based on experimental data. He believed the reason for this discrepancy was that his theory underestimates the length of the pneumatic trail at small slip angle.

A7. SPEED

The performance characteristics of tires are more speed-dependent on wet roads than they are on dry roads. In fact, some investigators have concluded that speed is the most important factor in determining the wet weather tractive ability of a tire [23, 63]. (However, this is not conclusive. Dijks [24] found that road surface parameters are more important in influencing the tractive performance of a tire on a wet surface.)

In 1939, however, Ball [15] found that speed has very little effect on the lateral force of a tire under practically all conditions. However, in more recent times investigators have found that speed does have an effect on the lateral force developed by a tire. In fact, the lateral force decreases as speed increases. This effect is particularly significant on wet roads [16, 38].

Krempl [69] found that speed has a greater influence on maximum longitudinal force than on maximum lateral force. Several investigators have studied the effects of speed on longitudinal force.

(1) Using a towed trailer, Harned, et al. [53] found that the locked-wheel brake force coefficient of a tire on dry asphalt decreased with speed in the speed range 5-20 mph, but in the range 20-60 mph, the locked-wheel brake force coefficient increased with increasing speed.

(2) Using a mobile tire tester on wet roads, Holmes, et al. [56] found that increasing the speed lowered the brake force versus longitudinal slip curve. Further, the locked-wheel brake force dropped more so than the peak brake force for an increase in speed. Finally, they found that the brake force developed from smooth tires was very speed sensitive on smooth textured surfaces.

A8. INTERACTION OF LONGITUDINAL AND LATERAL FORCES

The longitudinal and lateral forces developed by a tire are not independent of each other. Mounting tires on a test fixture attached to a truck, Byrdsong [16] found that a tire develops considerable side force up to the maximum wheel braking force. Past this point, the side force decreases rapidly to zero when the tire is in full skid. Gengenbach and Weber, using an internal drum tire test rig at the University of Karlsruhe, found that the side force of a tire increased with increased braking force and decreased with increased driving force at low to moderate force levels. (This was corroborated by Sakai [109].) Gengenbach and Weber [43] also found that aligning torques decreased more sharply with braking forces than with driving forces. Krempl [69] found that the static friction force, braking force, and side force are usually of different magnitudes. The envelope of the shear forces transmitted is a circle only for special cases. In fact, deviations from the static friction circle may be as high as 20%.

Holmes and Stone did a rather complete study of the interaction of longitudinal and lateral forces of tires on wet surfaces [56]. They did a series of tests to study the effect of pure braking (with no slip angle) and then pure cornering (with no longitudinal slip). They then investigated interaction effects. The results they found were:

(1) The curves of side force versus slip angle had smaller initial slopes when a brake force was applied. Also, the peak side force obtainable was reduced and it occurred at higher slip angles than for the free-rolling case.

(2) The curves of brake force versus brake slip had smaller initial slopes in the presence of a side force. The peak brake force obtainable was smaller and shifted to higher values

of longitudinal slip. However, the drop-off of brake force near lockup still occurred.

(3) The friction circle concept did not agree with the experimental data.

(4) The plot of resultant shear force versus resultant slip showed a shape very similar to those of brake force versus longitudinal slip and cornering force versus slip angle, where

$$S = 100\sqrt{\sin^2\alpha + Q^2\cos^2\alpha/10^4}$$

S = resultant slip in percent
α = slip angle
Q = % brake slip

In 1970, Fancher, et al. [29] studied tire characteristics using the HSRI Mobile Tire Tester. This allowed on-the-road measurements of tire shear forces under combined slip and slip angle operation at highway speeds. They corroborated other experimentors by showing that as slip angle increases, the peak of the longitudinal force versus longitudinal slip curve occurs at higher values of longitudinal slip. At high slip angles the peak longitudinal force is obtained at lockup. Also, lateral force may be greatly reduced by increasing longitudinal slip. An additional result they found was that in lockup the direction of wheel slide is not necessarily in the direction to oppose the shear forces, indicating that the tire-road friction coefficient should be treated as two constants—one for the longitudinal direction and one for the lateral direction.

Because of the importance of side slip and longitudinal slip on a tire's shear forces, several mathematical models have been developed which take explicit account of the influence of both these slips on the traction forces produced.

Bergman [8] developed a mathematical model for a tire in which the tire was modeled as a series of three interacting springs spaced about the tire's circumference. Using this model, he discussed the effect of load on lateral force and showed how the theory could be applied to predict the effect of traction on cornering force. He found that calculated values of lateral tire force during power application correlated very well with experimental data.

Tielking and Mital [127] compared five tire models which simulated tire traction forces and moments due to both lateral and longitudinal slip. A summary of each of these models (with references in brackets) is quoted from the report:

MODEL	RESUME
HSRI-NBS-I [27]	Elastic tread blocks on rigid wheel, uniform contact pressure, uniform deformation in sliding region, tire-road friction decreasing linearly with slip speed. Aligning moment not simulated.
HSRI-NBS-II [31]	Elastic tread blocks on foundation allowed to translate uniformly, finite transition between adhesion and fully developed sliding, uniform contact pressure, distinction between static and dynamic friction which decreases linearly with slip speed.
Goodyear [81]	Elastic tread blocks on rigid wheel, parabolic or experimentally determined contact pressure, deformation in sliding region decreases with shear force, constant friction. Deformation discontinuity avoided by assuming sliding shear force to act in same direction as shear force in the adhesion region.
Sakai [109]	Elastic tread blocks on flexible elastically-supported beam carcass (subsequently reduced to rigid beam with uniform translation) with an artificial mechanism connecting longitudinal stiffness with lateral stiffness (but not vice-versa), parabolic contact pressure, distinction between static and sliding friction which is considered to be orthotropic. Prescribed stress in sliding region produces a displacement discontinuity for unequal longitudinal and lateral traction stiffnesses. Traction forces and moment computed by

MODEL	RESUME
	integrating across a stress discontinuity which is more severe for bias tires than for radial tires.
HSRI-NBS-III [127]	Parabolic contact pressure, otherwise identical to HSRI-NBS-II model.

A9. WET ROAD SURFACES

A large number of studies have been done to examine the tractive qualities of tires on wet roads. It is interesting to note that the friction coefficient of a tire drops significantly from a dry to just damp road (as might occur from a light rain) [3, 75, 76, 123]. As the water level is increased further the friction coefficient continues to decrease, until the water depth reaches about 3 to 4 mm, after which the friction coefficient decreases only slightly as the tire hydroplanes [24, 123].

Road surface parameters have an important influence on the wet tractive ability of tires. A road with an open (rough) macrotexture will allow drainage of water under the tire and will yield larger friction coefficients than would a surface with a fine macrotexture, regardless of the microtexture [3].

The most important tire variable in wet traction at high speeds and shallow water is the tread pattern. Its effect is greatest on surfaces with poor drainage [3, 87]. The tread compound can also be important, and in fact, when taking into account all conditions of road surface, speed, water depth, etc., tread compound should be given equal importance to tread pattern [3].

There are certain distinct differences between the tractive properties of a tire on a wet or dry surface. The traction coefficients, in addition to being much smaller on wet surfaces than dry, are also much more speed sensitive on wet surfaces, while showing only a slight speed sensitivity on dry surfaces [16, 36]. Further, the ratio of the peak braking coefficient of a tire to its slide coefficient is much greater on wet than dry surfaces [36].

Using a statistical approach to study the factors important in wet traction allows for a study of interaction effects among

parameters. This approach was used by Dijks [24]. Previously, all parameters except one were held fixed. It was found that the factors influencing wet skid resistance in order of their significance are (1) road surface parameters, (2) speed of travel, (3) tread depth, and (4) tire parameters. Further, all two-factor interactions with road surface were important. Three-factor interactions had only minor effects.

A10. ANNOTATED BIBLIOGRAPHY

The following section contains an annotated bibliography. Those papers of most significance to the literature survey are described in detail. Others are only listed. The papers annotated in the literature survey done by Schuring [112] are included, since these papers include information concerning replacement tires.

1. Alexander, K. R., "Bias Angle Versus Radial Ply Versus Bias Belted Tires - Materials and Construction Comparisons." SAE Paper 680386, May, 1968, 5 pp.

2. Allbert, B.J., "Tires and Hydroplaning." SAE Paper 680140, January 1968, 11 pp.

3. Allbert, B.J. and Walker, J.C., "Tyre to Wet Road Friction at High Speeds." Institution of Mech. Engineers, Proceedings, Vol. 180, Part 2A, No. 4, 1965-1966, pp. 105-121.

The level of friction obtainable between a tire and a wet road is related primarily to the ability of the tire to remove a water film from the contact area. It was assumed that the contact patch was divided into three zones:

(1) Unbroken water film (at front of contact patch)

(2) Partial breakdown of film

(3) "Dry" area.

An experimental investigation was conducted employing both road and indoor rig techniques to study limiting tire cornering and braking properties on wet roads under a wide range of operating conditions. It was found that the size of the dry contact area at the rear of the contact patch is the most significant factor in determining the friction force available. A speed increase reduces this area. Tread pattern, tread material, and road surface also have a considerable influence on the size of this area.

Tread pattern and tread material were investigated. Conclusions reached concerning the effect of these on the wet tractive properties of a tire are quoted:

"Tread pattern

(1) Tyre performance at high speeds is dominated by the characteristics of the tread pattern.

(2) Smooth tyres give poor performance at all but the very slowest speeds and offer negligible braking coefficients at speeds over 50-60 mile/h.

(3) Tread patterns, even those of the simplest type, give considerable improvements compared with the smooth tyre at all speeds.

(4) The reduction of recorded peak braking force coefficients caused by increasing the speed is least with the modern pattern having large numbers of narrow cuts or slots in its tread surface.

Tread Material

(1) Variations of the tread material have small influences upon the slope of the braking force/speed relationship.

(2) For the patterned tyres, the effect of improving the tread material is to give a straightforward increase in the braking force coefficient. This increase is roughly independent of speed.

(3) Tread material changes have a negligible effect upon the performance of the smooth tyre at the highest speeds."

4. Anon., "A Review of Current Constructions, Developments, Performance." Automobile Engineers, Vol. 49, No. 8, July, 1969, pp. 274-288.

5. Anon., Oil-Extended Natural Rubber in Winter Tyre Treads. Natural Rubber Prod. Res. Assoc., Inc., England, Report No. TB-15/68, 1968, 22 p.

6. Bandel, P., Cederi, F., Chiesa, A., and Mazza, C., "The Tyre is a Link between the Vehicle and the Road." J. Mech. E., Auto. Div., Conference on Drive-Line Eng., Paper 40, 1970.

7. Beauregard, C. and McNall, R.G., "Tire Cornering/Traction Test Methods." SAE Paper 730147, Jan. 8-12, 1973.

A "tire cornering/traction trailer" was designed to measure the traction and steering performance of passenger car tires. Sample test data of lateral and longitudinal friction characteristics of tires as affected by tire construction, inflation pressure, camber angle, normal load, road surface, and speed are included.

8. Bergman, W., "Theoretical Prediction of the Effect of Traction on Cornering Force." SAE Paper 186A, 1960.

A model was developed for the pneumatic tire in which the tire was considered to be composed of circumferential spring elements—each element being a three-dimensional spring. The concept of "interaction effect" was developed to explain the effect of traction on cornering force. In the model developed, this effect was included by assuming a change in spring constant of one elemental spring when one or both of the other two springs in the element were deflected. A change in inflation pressure was treated as a change in the spring constants. A load increase causes an increase in tire contact patch and was treated as an increase in the coefficient of friction.

9. Bergman, W. and Crum, W.B., "New Concepts of Tire Wear Measurement and Analysis." SAE Paper 730615, May 1973.

An analysis is presented of tire tread wear utilizing new experimental and analytical techniques. The following points were made:

(1) Grip is defined as an intimate instantaneously stationary contact between tire tread rubber and road asperities, during which contact no relative motion between the tire and the road takes place. Therefore grip expresses a static condition.

(2) "Grip is the key factor in the first phase of tire-road interaction. The grip enables the tire to transmit or generate shear forces (cornering, braking, or driving)."

(3) There are two types of grip:

(a) Deformation grip is due to road asperities which act like the teeth in gears and produce localized pressures between the road and tire.

(b) Adhesion grip is due to molecular forces. Hence, the tire and road must be in close proximity. Adhesion grip occurs where localized pressure is high. Therefore, it only exists at certain points throughout the contact patch.

(4) Tire-road friction is defined as a resistance to relative motion between the tire tread rubber and the road surface. Friction prevails during the second phase of the tire-road interaction, when the elements disengage themselves from a grip and slide back toward their initial position with respect to the wheel rim.

(5) It was proposed that road texture be classified in a quantitative manner:

(a) Microtexture—road texture of asperities between 0.1 and 0.4 mm in diameter.

(b) Macrotexture—road texture with asperity sizes larger than 0.4 mm.

(c) Smooth surface—surface texture with asperity sizes less than 0.1 mm.

(6) Grip between the tire and road is primarily affected by road surface, and to a much lesser extent, the tire surface.

(7) Less than 0.1 mm of the surface of tread affects grip.

(8) The length of travel of tread rubber during the sliding phase of the contact patch and the friction drag force are the two main factors determining tread wear on a given road surface under given operating conditions.

(9) Tread wears more in cornering than in braking or traction. This is due to a lower cornering stiffness compared to braking or driving stiffness. Also, in cornering, wear increases at a greater than constant rate with increasing lateral force. In braking or traction, wear increases linearly with those respective forces.

(10) Cornering produces uneven wear which starts from the corners of individual tread ribs. Stiffness of the tread ribs increase with wear. Therefore, uneven wear decreases with accumulated wear.

(11) Increased inflation pressure decreases tire contact patch area.

10. Bidwell, J.B., "Car-Tire Relationships," General Motors Publication GMR-502, presented at Akron Rubber Group Winter Meeting, Nov. 1965, 17 pp.

Tire properties which affect vehicle ride motions and directional control were discussed, and a comparison was made between radial and bias ply tires in relation to these properties. It was concluded that the vehicle must be designed to utilize the characteristics of the specific tires which are to be used in order to get maximum performance. Radial and bias ply tires were found to be non-interchangeable on the same vehicle without causing variations in vehicle performance characteristics.

11. Bogan, R.F. and Dobie, W.J., "Performance Comparison - 2-Ply Versus 4-Ply Passenger Car Tires." SAE Paper 660378, pp. 557-562.

12. Brenner, F.C. and Kondo, A., "Elements in the Road Evaluation of Tire Wear." Tire and Science Technology, TSTCA, Vol. 1, No. 1, Feb. 1973.

The procedural steps to be followed to achieve tread wear evaluation are described. Results of such experiments are discussed and recommendations are made on the course over which the tires should be run.

13. Briggs, G.J., Hutchison, E.J., and Klingender, R.C., "Factors Affecting Skid Resistance of Polybutadiene." Rubber World, Vol. 150, No. 6, Sept. 1964, pp. 41-53.

14. Buddenhagen, F.E., "Design and Construction Considerations of Radial Passenger Car Tires." SAE Paper 670470, May 1967, 5 pp.

15. Bull, A.W., "Tire Behavior in Steering." SAE Journal (Transactions), Vol. 34, 1939, pp. 344-350.

Experiments were done on a tire testing drum machine to study the effects of surface wetness, tire brand, tire size, wheel loading, inflation pressure, and tractive force on the cornering force and aligning torque of a tire.

16. Byrdsong, T.A., Investigation of the Effect of Wheel Braking on Side-Force Capability of a Pneumatic Tire. NASA TN D-4602, 1968.

"An experimental investigation was made to determine the effect of wheel braking on the side-force capability of a pneumatic tire. Data were obtained from tests of a smooth-tread pneumatic tire with an inflation pressure of 30 pounds per square inch at ground speeds of 10, 20, and 30 miles per hour at wheel yaw angles of 4° and 8° on both wet and dry paved surfaces.....The wheel and tire were mounted on a test fixture and attached to a 2 1/2 ton truck. The test fixture was located forward of and in line with the right front wheel of the truck."

Results:

(1) The side force developed was less on wet roads than on dry roads. The effect became significant as speed increased. At 30 mph there was a 50% reduction.

(2) Considerable side force was developed during wheel braking up to the maximum wheel braking force. Past this point, the side force decreased rapidly to zero at full skid.

17. Carr, G.W. and Holt, A.J., "A Comparison of the Rolling Resistance of Radial and Cross-Ply Tyres." MIRA Bulletin No. 5, Sept./Oct. 1970, pp. 4-7.

18. Chiesa, A., Gough, V.E., Jones, F.B., and Udall, W.S., "Take the Bias Out of Tires?" SAE Journal, May 1965, pp. 32-39.

19. Cox, J.H., "The Fleeting Tire Footprint." SAE Paper 970 D, Detroit, Jan. 1965.

20. Curtiss, W.W., "Low Power Loss Tires." SAE Paper 690108, Jan. 1969, 14 pp.

21. Curtiss, W.W., "Principles of Tire Design." Tire Science and Technology, TSTCA, Vol. 1, No. 1, Feb. 1973, pp. 77-98.

22. Davisson, J.A., "Design and Application of Commercial Type Tires." SAE Paper SP-344, Jan. 1969, 39 pp.

23. DeVinney, W.E., "Factors Affecting Tire Traction." SAE Paper 670461, May 1967, 8 pp.

Conclusions reached are:

(1) Speed is the most significant factor affecting wet traction.

(2) Different tread compounds may show opposite relative ranking under different conditions insofar as traction is concerned.

(3) Studded tires improve traction significantly on ice.

(4) As ice warms, traction decreases drastically because of the slippery water layer between the ice and the tire.

(5) Temperature has an effect on dry traction also—particularly above about 85°F. As temperature increases, traction decreases.

24. Dijks, I.A., "A Multifactor Examination of Wet Skid Resistance of Car Tires." SAE Paper 741106, 1974.

A statistical study of the factors important to the traction of tires on wet surfaces was conducted. This study examined the interaction among the factors in affecting traction instead of holding all but one factor constant. Traction was rated by three coefficients: peak brake force, locked wheel brake force, and maximum side force—all normalized by the loading.

The test matrix was composed of the following:

(1) 6 road surfaces

(2) 4 types of tires—all radial in construction. Two were steel belted and the other two were textile belted.

(3) 3 speeds—50, 75, and 100 km/hr

(4) 2 tread depths—new and 1 mm.

It was found that the factors affecting wet traction in order of their significance are road surface parameters, speed of travel, tread depth, and tire parameters. Additionally, it was found that all two-factor interactions with road surface were important. Three-factor interactions had only minor effects.

25. Dijks, A., "Tests to Determine the Minimum Permissible Tread-Depth for Passenger-Car Tyres." Automobiltechnische Zeitschrift (ATZ) (In German), Vol. 75, No. 1, Jan. 1973, pp. 1-6.

"Experiments were conducted on three different types of standard radial tyres and one type of cross-ply tyre to determine the effect of tread depth on tyre adhesion to wet road-surfaces....Results showed that, for all tyres tested, the coefficient of adhesion on wet roads fell with decreasing tread depth, and that the extent of the reduction in tyre/road adhesion was heavily dependent upon road surface, vehicle speed, and tyre construction."

26. Dijks, A., "Wet Skid Resistance of Car and Truck Tires." Tire Science and Technology, TSTCA, Vol. 2, No. 2, May 1974, pp. 102-116.

27. Dugoff, H., Fancher, P.S., and Segel, L., "An Analysis of Tire Traction Properties and Their Influence on Vehicle Dynamic Performance." 1970 International Automobile Safety Conference Compendium, New York, 1970, pp. 341-366.

A mathematical model was developed for the vehicle dynamics of an automobile. The vehicle was represented as an eight-degrees-of-freedom system—longitudinal and lateral translation and yaw rotation of the vehicle considered as a rigid body, angular rotation for each wheel mass, and steer angular displacement. Main emphasis was placed on the tire mechanics, and the mathematical model was built around this part of the simulation. Elsewhere in the model, large simplifications were made, so the simulations would not exceed computer capacity. The major simplification was that roll and pitch were omitted and their effects included indirectly using a quasi-static approach.

Explicit account was taken of the influence of both side and longitudinal tire slip on the traction forces produced at the tire-road interface. This was done so that limit maneuvers could be simulated. In the past, some form of "friction circle"

concept was used in such treatments, and hence did not take explicit account of the longitudinal tire slip. This was a serious flaw, since experiments have shown that longitudinal slip is important in the development of traction forces.

In the model presented here, the traction mechanics include:

(1) Shear force components as functions of a friction coefficient which varies with sliding speed.

(2) Various parameters describing the relevant mechanical properties of the tire.

(3) Variables describing the tire contact patch kinematics.

28. Elliott, D.R., Klamp, W.K., and Kraemer, W.E., "Passenger Tire Power Consumption." SAE Paper 710575, June 1971, 14 pp.

29. Fancher, P.S., Jr., Dugoff, H., Ludema, K.C., and Segel, L., Experimental Studies of Tire Shear Force Mechanics—A Summary Report. Highway Safety Research Institute, The Univ. of Michigan, Ann Arbor, July 30, 1970, 16 pp.

30. Fancher, P.S., Jr. and Segel, L., "Tire Traction Assessed by Shear Force and Vehicle Performance." Tire Science and Technology, TSTCA, Vol. 1, No. 4, Nov. 1973, pp. 363-381.

31. Fancher, P.S., Segel, L., MacAdam, C.C., and Pacjka, H.B., Tire-Traction Grading Procedures as Derived from the Maneuvering Characteristics of a Tire-Vehicle System. Vols. 1 & 2, Highway Safety Research Institute, Report No. HSRI-71-129, June 13, 1972.

Ten tire configurations were studied using the HSRI Mobile Tire Tester. The tire configurations consisted of three carcass constructions, each one having three levels of tread wear, plus an SAE-type reference tire. Carpet plots were generated for

(a) Longitudinal force vs. longitudinal slip, and vertical load.

(b) Lateral force vs. lateral slip and vertical load.

Three surfaces were used:

(a) wet concrete
(b) wet asphalt
(c) wet jennite

Additionally, the complete traction field of a radial tire consisting of lateral and longitudinal force measurements at three speeds, three loads, seven slip angles, with longitudinal slip varied from 0 (free rolling) to 1 (locked) was recorded in order to develop detailed mathematical representation of tire shear force characteristics.

Results

(1) Radial tires produced larger shear forces than belted-bias tires, and belted-bias tires produced larger shear forces than standard unbelted bias tires.

(2) In some cases, fully-worn radials and fully-worn belted-bias tires exceeded the performance of half-worn radials and half-worn belted-bias tires, respectively.

(3) Values for longitudinal friction coefficient were found to be much higher than the values for lateral friction coefficient.

(4) Friction coefficients varied with speed and load on wet surfaces.

(5) It was found that the peak lateral tire shear force correlated well with the limit velocity in a J-turn maneuver.

32. Formgren, C. and Nordström, O., Side Force Characteristics of Passenger Car Tyres. Difference Between Tyres of Same Type and Manufacture, and Difference Between Tyres of Various Manufacture." The National Swedish Road and Traffic Research Institute, Report No. 8, 1972.

The side force characteristics and peak and locked-wheel brake force coefficients for a number of production snow tires and standard tread tires of radial ply, bias ply, and bias-belted construction were investigated. A flat bed machine was used to obtain cornering stiffness and camber stiffness of the tires. A towed trailer was used to obtain the braking coefficients. Force characteristics as affected by the variation in tires of the same manufacturer and size, and the variation on tires of different manufacturer but the same size, tire construction, inflation pressure, and load were examined.

Results:

(1) There were no significant variations in side force characteristics and braking coefficients between tires of the same construction and manufacturer.

(2) There existed substantial differences in tires of different constructions.

(3) There were large variations between tires of the same construction but different manufacturer.

33. Förster, B., Tests to Determine the Adhesive Power of Passenger-Car Tires. NASA Technical Memorandum 1416, Aug. 1956.

Tire forces were determined experimentally using a single-wheel towing axle and varying speed, inflation pressure, load, tread design, tire construction, slip angle, and, simultaneously, longitudinal slip. The tests were conducted on wet, dry, snow-covered, and ice-covered roads.

On dry roads, it was found that the best tire in terms of largest friction coefficient (out of a group of similar tires except for tread wear and pattern) was one with discontinuous narrow transverse grooves and somewhat wider longitudinal grooves.

34. French, T., "Construction and Behavior Characteristics of Tyres." IME Paper, Inst. of Mech. Eng., 1960, 15 pp.

35. Gardner, E.R., "Recent Trends in Tyre Compounding." Institution of Rubber Industry Transactions and Proceedings, Vol. 13, Dec. 1966, pp. 248-260.

36. Gauss, F., "Braking and Guiding Forces Between Tyre and Road." Automobiltechnische Zeitschrift (ATZ) (In German), Vol. 63, No. 2, Feb. 1961.

The effect of variations in operating variables on the peak and locked-wheel brake force and side force coefficients was investigated on both wet and dry surfaces. A towed trailer was used to determine the brake force coefficients, while both road and drum testing were employed to determine the side force coefficients.

Results:

(1) The difference between peak and locked-wheel brake force coefficient was small on dry roads and greater on wet roads. The difference became greater as speed increased.

(2) On a dry road, as tread depth decreased, locked-wheel brake force coefficient increased. The variation with speed was small.

(3) On a wet road, as tread depth decreased, locked-wheel brake force coefficient decreased. Tire pressure had little effect within the range of normal loads and tire pressures.

(4) Side force coefficient decreased as tire load increased, as inflation pressure decreased, and as speed increased. The decrease with speed was more rapid on wet than on dry roads.

(5) The difference in side force coefficients on wet and dry roads was small at slip angles up to 5°.

37. Gauss, F. and Wolff, H., "On the Lateral Guiding Force of Passenger Car Tires." Deutsche Kraftfahrtforschung und Strassenverkehrstechnik, (D.K.S.), No. 133, 1959.

Tires of different sizes were tested on a wet and dry drum to determine the effect of slip angle, camber angle, normal load, inflation pressure, tread depth, and wheel rim width on lateral force and aligning moment.

38. Gengenbach, W., "Experimental Investigation of Tires on Wet Tracks." Automobiltechnische Zeitschrift (A.T.Z), (In German), Pt. 2, 1968.

The effect of traction and braking forces, speed, slip angle, and water depth on side force and aligning torque was studied.

39. Gengenbach, W., "Experimental Investigation of Tires on Wet Tracks." Automobiltechnische Zeitschrift (A.T.Z), (In German), Pt. 3, 1968.

The effect of inflation pressure, camber angle, speed, water depth, tread pattern, and groove width on wet road braking force coefficient and side force coefficient was studied.

40. Gengenbach, W. and Weber, R., "The Cornering Forces of Vehicle Tires in Winter Conditions." Auto Industrie, Vol. 13, No. 3, Sept. 1968.

"The cornering forces of different tyres were measured on typical winter surfaces, and, for comparison, on dry asphalt." Tires used were cross-ply and radial, with and without studs, and a tire with snow chains. They were mounted on the front axle of the test vehicle. On dry, rough asphalt the studded tire gave the highest adhesion coefficients. The studded tire and the chained tire gave the highest coefficients on the winter surfaces—and the longer the studs, the higher the coefficient. The lowest coefficients were given on the dry surface with the chained tire and on the winter surfaces with the smooth and unstudded tire.

41. Gengenbach, W. and Weber, R., "The Influence of Road Surface, Speed and Tyre-Tread Depth on the Adhesion Under Wet Conditions." Auto. Industrie, Vol. 15, No. 4, Nov. 1970, pp. 69-73. MIRA Translation No. 34171.

42. Gengenbach, W. and Weber, R., "Measurement of Tire Deflection of Bias-Ply and Radial Tires." (In German) Automobiltechnische Zeitschrift (A.T.Z), Vol. 71, No. 6, June 1969, pp. 196-198.

43. Gengenbach, W. and Weber, R., "The Restoring Moment of Motor-Vehicle Tyres Under the Combined Influence of Circumferential and Lateral Forces." Auto. Industrie, Vol. 15, No. 3, Aug. 1970, pp. 85-96. MIRA Translation No. 2071.

The study was conducted using the tire test rig at the Institute for Motor Vehicle Mechanics of the University of Karlsruhe. Many graphs were generated of tire forces as a function of circumferential force for varying side slip angles to show the effect of wheel loading, tread depth, and inflation pressure on tire characteristics for cross-ply and radial-ply tires.

The results were:

(1) Side force increased with increasing braking force and decreased with increasing driving force at low to moderate force levels.

(2) The greatest aligning torques were reached at side slip angles between 2° and 5°.

(3) Aligning torques for bald tires were over 1 1/2 times as large as those for tires with 90% tread.

(4) Tread effects were less significant for cross-ply tires than for radial-ply tires.

(5) Aligning torques increased significantly as wheel loading was increased.

(6) Aligning torques decreased more sharply with braking forces than with driving forces.

(7) Aligning torques increased with decreasing inflation pressure.

44. Giles, C.G. and Sabey, B.E., "Rubber Hysteresis and Skidding Resistance." Engineering, Vol. 186, December 1958, pp. 840-842.

45. Goudie, J. J., Jr., "Performance Requirements for Passenger Car Tires." SAE Paper 660375, June 1966, 3 pp.

46. Gough, V.E., "Practical Tire Research." SAE Transactions, Vol. 64, 1956.

The paper discussed:

(1) The distribution of side force in the contact patch.

(2) Wear patterns and their meanings.

(3) Tire characteristic curves (Gough diagrams) and their application.

47. Gough, V.E. and Allbert, B.J., "Tyres and the Design of Vehicles and Road for Safety." Vehicle and Road Design for Safety, The Inst. of Mechanical Engineers, Paper 8, July 1968, 10 pp.

48. Gough, V.E. and French, T., "Tyres and Skidding from a European Viewpoint." Proceedings, 1st International Skid Prevention Conf., Virginia Council Highway Invest. and Research, Charlottesville, Aug. 1959, pp. 189-209.

49. Gough, V.E., Jones, F.B., and Udall, W.S., "Radial Ply, Rigid Breaker Tires." SAE Paper 990A, Jan. 1965, pp. 1-12.

50. Grosch, K.A. and Maycock, G., "Influence of Test Conditions on Wet Skid Resistance of Tire Tread Compounds." Rubber Chemistry and Technology, Vol. 41, 1968, pp. 477-494.

51. Grosch, K.A. and Schallamach, A., Wear, Vol. 4, 1961, p. 356.

52. Hales, F.D. and Berter, N.F., The Effect of Roll Stiffness and Tyre Type on Vehicle Steady-State Response. The Motor Industry Research Assoc., Report No. 1968/1, Nov. 1967.

53. Harned, J.L., Johnston, L.E., and Scharpf, G., "Measurement of Tire Brake Force Characteristics as Related to Wheel Slip (Anti-Lock) Control System Design." SAE Paper 690214, 1969.

Characteristic μ-slip curves* were determined for a variety of tire-road pairings to aid in the design of anti-lock braking systems. Ten types of automobile tires including snow tires, studded snow tires, and highway tires of radial ply, bias ply, and bias-belted construction were tested by the transient μ-slip method. In this method, "the instantaneous tire brake force, vertical load, wheel speed, and vehicle speed are recorded during the transient wheel slip change period and the μ-slip curve is then reconstructed from these recorded data." A towed trailer was used at a number of speeds between 5 and 60 mph on a large number of wet and dry surfaces, including gravel and ice.

The results were:

(1) From 5 to 20 mph the locked-wheel brake force coefficient on dry asphalt decreased and from 20 to 60 mph it increased.

---

*μ = brake friction coefficient.

(2) Peak brake force coefficients on gravel occurred with locked wheel.

(3) Brake force coefficients decreased as water depth increased. The differences became more significant at higher speeds.

(4) On wet roads higher locked-wheel brake force coefficients occurred with studded snow tires than with unstudded snow tires. This result was believed to have occurred because the studs gouged the road surface. Highway tires had the lowest coefficient of braking friction on wet roads at 40 and 60 mph.

(5) Decreased tread depth on wet roads decreased braking friction coefficients.

54. Harvey, J.L. and Brenner, F.C., Tire Use Survey, the Physical Condition, Use, and Performance of Passenger Car Tires in the United States of America. NBS Technical Note 528, issued May 1970.

The way in which people maintain and use their tires was determined based on two surveys—one aimed at obtaining data for an unbiased sample of passenger car tires in normal use and the second aimed at data for passenger car tires used mainly in long distance traveling. Further, the correlation between various tire-in-use factors and traffic accidents was determined based on previously published accident data.

55. Holmes, K.E., Braking Force/Braking Slip: Measurements Over a Range of Conditions between 0 and 100 Percent Slip. Road Research Laboratory Report LR 292, 1970, 31 pp.

An experimental investigation was conducted to determine the braking force coefficient as a function of slip for various tires on a number of wet road surfaces. Variables investigated included tread pattern, tread material, road surface texture, speed, and tire construction.

56. Holmes, K.E. and Stone R.D., "Tyre Forces as Functions of Cornering and Braking Slip on Wet Road Surfaces." Published in HS-011 272, Handling of Vehicles under Emergency Conditions, 1969, pp. 35-55.

The study was conducted to experimentally investigate:

(1) the brake force vs. slip relationship,

(2) the cornering force and aligning torque vs. slip angle relationship, and

(3) the resultant shear force vs. resultant slip relationship for combined cornering and braking forces

as affected by road surface, tire construction, tread, speed, and rubber resilience.

The Road Research Laboratory mobile tire tester was used. Load, cornering force, braking force, and aligning torque were measured with strain gages. Magnetic pulse generators measured brake slip. Five road surfaces ranging from polished to rough in texture were used. The water depth was varied between .5 and .75 mm.

The conclusions reached were:

(1) Pure braking

(a) In general, increased speed lowered the brake force vs. slip curve; the locked-wheel brake force dropped further than the peak brake force with increasing speed.

(b) The brake force was speed sensitive on smooth textured surfaces and using smooth tires. Surface microtexture appeared to be more important than macrotexture.

(c) Treaded tires gave higher friction at high speed than smooth tires.

(d) Low rubber resilience improved traction under all conditions, but did not affect the shape of the force-slip curve.

(e) Radial tires gave slightly higher peak force values than bias ply tires.

(2) Pure cornering

(a) Cornering forces showed qualitatively similar variations with surface, speed, tread pattern, rubber resilience, and construction as did brake force.

(3) Aligning torque in pure cornering

(a) Aligning torque became zero when cornering force reached its peak value.

(4) Combined braking and cornering

(a) The presence of a brake force did not affect the initial slope of the side force-slip angle relationship, but the peak value was reduced.

(b) Curves of brake force vs. brake slip were reduced in initial slope and peak value when a constant sideslip angle was applied. The peak was shifted to higher slip values, but the drop-off approaching lock-up still appeared.

(c) The friction circle concept did not agree with the experimental data.

(d) The plot of resultant shear force vs. resultant slip showed a shape very similar to those of brake force vs. brake slip and cornering force vs. slip angle.

$$S = 100 \sqrt{\sin^2\alpha + Q^2 \cos^2\alpha / 10^4}$$

S = resultant slip in percent

α = slip angle

Q = % brake slip

(e) Regression analysis showed that tread rubber resilience had a significant effect on all road surfaces.

57. Horne and Leland, Influence of Tire Tread Pattern and Runway Surface Condition on Braking Friction and Rolling Resistance of a Modern Aircraft Tire. NASA TN D-1376, Sept. 1962.

58. Hutchinson, J.F., "Development of the Low Profile Passenger Tire." SAE Paper 983C, Jan. 1965, 4 pp.

59. Hutchinson, J.F. and Becker, H.D., "Determination of Passenger Tire Performance Levels - Traction." SAE Paper 690510, May 1969, 7 pp.

60. Johnson, W.C., "Factors in Tires that Influence Skid Resistance, Part III - The Effect of Carcass Construction, Size, Cord Angle, and Number of Plies." Proceedings from First International Skid Prevention Conf., Part I, Virginia Council of Highway Invest. and Research, Charlottesville, Aug. 1959, pp. 163-166.

61. Joy, T.J.P. and Hartley, D.C., "Tyre Characteristics as Applicable to Vehicle Stability Problems." Proceedings of the Automobile Division, The Inst. of Mech. Engrs., No. 6, 1953-54, pp. 113-122.

The effect of changes in sideslip, tire load, camber angle, rim diameter, speed, inflation pressure, longitudinal force, rim width, section width, and wear on lateral force and aligning torque were examined using a drum type tire tester.

62. Keller, R.C., "Improvement of Tire Traction with Chlorobutyl Rubber." Tire Science and Technology, TSTCA, Vol. 1, No. 2, May 1973, pp. 190-201.

63. Kelley, J.D., Jr., "Factors Affecting Passenger Tire Traction on the Wet Road." SAE Paper 680138, Jan. 1968, 13 pp.

The objectives of this investigation were to determine the effects of tread pattern, tire construction, tread compound, speed, surface friction coefficients, wheel load, ambient temperature, and inflation pressure on braking and cornering forces of tires on wet roads.

Among the conclusions were:

(1) Tread pattern design is the most significant "tire variable" as far as wet weather traction is concerned.

(2) Radial ply tires are not significantly better than bias ply tires for stopping traction but the radial ply construction is better for wet cornering traction.

(3) Speed is the most important single operating factor for wet weather tractive ability.

64. Kern, W.F., "Coefficient of Wet Friction of Tire Treads." Rubber Chemistry and Technology, translated by G. Leuca from Kautschuk und Gummi-Kunststoffe, 19, (2)91, 1966.

65. Klamp, W.K. and Milligan, W.J., "Performance Characteristics - Radial Ply Tires." SAE Paper 670471, May 1965, 12 pp.

66. Koessler, P. and Senger, G., "Comparative Investigations of the Lateral Guiding Characteristics of Passenger Car Tires." Deutsche Kraftfartforsh., No. 172, 1964.

The objectives of this study were to determine the effect of tire size, tire tread design, tread wear, and manufacturer on side force and aligning torque of automobile tires. Testing was done on a flat bed machine.

Results:

(1) There were variations in side force and aligning moment on tires of the same size and manufacturer.

(2) There existed large differences in side force and moments between tires of the same size but different manufacturer.

(3) As tread depth decreased, lateral force at a given slip angle increased and peak lateral force also increased.

(4) As tread width increased, with a given diameter wheel and inflation pressure, lateral force increased.

(5) As inflation pressure increased, lateral force increased and aligning torque decreased.

(6) At low slip angles a snow tire developed less lateral force than a standard tire. At high slip angles the reverse was true.

67. Krebs, H.C., "Cornering Characteristics of Car Tyres." International Colloquium on the Interrelation of Skidding Resistance and Traffic Safety on Wet Roads, Wehner, B. and Schulze, K.H., Wilhelm Ernst & Sohn, Berlin, Chap. 9, pp. 483-499.

68. Krempl, G., "Experimental Contribution to Investigations on Automobile Tires." Ph.D. Dissertation, Technische Hochschule Karlsruhe, Germany, Feb. 1965, Published in Automobiltechnische Zeitschrift (A.T.Z.), Vol. 69, No. 1, Jan. 1967, pp. 1-8 and No. 8, Aug. 1967, pp. 262-268.

69. Krempl, G., "Investigations of Automobile Tires." Automobiltechnische Zeitschrift (ATZ), Vol. 69, No. 1, Jan. 1967 and Vol. 69, No. 8, Aug. 1967.

Using an internal drum tire testing machine at Karlsruhe University, force and moment characteristics of automobile tires were determined (1) as a function of tread wear and (2) under the influence of braking and tractive forces. The following dry traction results were found:

(1) Side force increases with wear. Though not proportional to load, the side force increase is relatively larger for small wheel loads.

(2) Worn tires develop larger longitudinal forces than unworn tires. The same trend is true of side forces, though the magnitudes involved are much less.

(3) The envelope for the side forces and longitudinal forces at the limit of tire-road adhesion is a circle only for special cases. Deviations from the static friction circle were found to be as high as 20%.

(4) Speed has a greater influence on the peak longitudinal force developed than on the peak side force developed.

70. Kullberg, G. and Kihlgren, B., Undersökning av Vinterdäck och Slirskydd ur Friktionssynpunkt (Investigation of Frictional Properties of Winter Tires and Anti-Skid Devices). The National Road Research Institute, Stockholm, Sweden, Report No. 36, 1960.

71. Kummer, H.W., "Lubricated Friction of Rubber Discussion." Rubber Chemistry and Technology, Vol. 41, 1968.

A discussion of the likely friction mechanisms of rubber sliding on lubricated surfaces is presented in this paper. The significant topics are:

(1) The significance of skidding accidents data.

(2) Minimum tire-road friction to prevent skidding during "normal" vehicle maneuvers.

(3) Frictional characteristics of roads at the start of rain.

(4) Adhesion and abrasion.

(5) Merits of portable devices and skid trailers intended for field use.

72. Kummer, H.W. and Meyer, W.E., Tentative Skid-Resistance Requirements for Main Rural Highways. National Cooperative Highway Research Program, Report 37, 1967, 80 pp.

73. Lane, J.H., McCall, C.A., and Gunberg, P.F., "Predicting Tire Tread Performance from Composition I." Rubber Chemistry and Technology, Vol. 43, No. 5, Sept. 1970, pp. 1070-1081.

74. Leland, T.J.W., An Evaluation of Some Unbraked Tire Cornering Force Characteristics. National Aeronautics & Space Admin., Langley Research Center, TND-6964, Nov. 1972, 36 pp.

An experimental investigation was done to determine the effects of pavement surface condition on the cornering forces of a group of tires of different tread designs. Dry, damp, and flooded pavements were used. Both tread pattern and type of surface were found to be significant factors in determining cornering force.

75. Leland, T.J.W. and Taylor, G.R., An Investigation of the Influence of Aircraft Tire-Tread Wear on Wet-Runway Braking. NASA TN D-2770, April 1965.

The effect that tread wear has on braking effectiveness as influenced by the type of wear (uniform or non-uniform), amount of wear, tire groove width, inflation pressure, and speed was examined on wet runways.

76. Leland, T.J.W., Yager, T.J. and Joyner, V. T., Effects of Pavement Texture on Wet Runway Braking Performance. NASA Technical Note D-4323, 1968.

77. Leyden, J.J., "Radial Tire Compounding." Rubber Age, Vol. 104, No. 4, Apr. 1972, pp. 51-53.

78. Lippman, S.A. and Oblizajek, K.L., "The Distribution of Stress Between the Tread and the Road for Freely Rolling Tires." SAE Paper 740072, 1974.

The interfacial stress distributions of tires were measured using specially designed equipment. The distribution of stresses

in the contact patch of a radial ply tire studied was much more uniform across the profile of the tire than for a bias-belted tire studied. In particular, the bias-belted tire had much higher lateral traction at the side edges of the contact patch than the radial ply tire.

79. Lippmann, S.A. and Oblizajek, K.L., "The Influence of Tire Wear on Steering Properties and the Corresponding Stresses at the Tread-Road Interface." SAE Paper 741102, 1974.

Transducers were placed at various positions on a flat bed tire tester to obtain the interfacial stresses at different points in the contact patch of a tire. In this manner, the lateral force and moment distributions could be obtained.

Three types of tires were examined: (1) steel-belted radial tires, (2) glass-belted bias tires, and (3) standard bias tires. The tires were tested at three levels of wear:

(1) Unworn

(2) 1/4 tread worn in the manner as occurs on the front tires of a passenger car

(3) 1/4 tread worn in the manner as occurs on the rear tires of a passenger car.

It should be noted that a front tire wears more severely at the tread edges than at the center. Wear on the rear tires, however, tends to be uniform.

Results

Cornering Stiffness, C_α

(1) The load sensitivity of C_α increases with wear.

(2) Unworn radials have a higher C_α than the other two types of tires. However, if the tires are worn, the bias-belted tire has the highest C_α of the three types.

Aligning Torque Stiffness, AT_α

(1) AT_α increases with wear, but the two types of wear (front or rear) give about the same AT_α.

(2) AT_α is about the same for all three types of tires in the unworn condition. However, with wear, steel-belted radials have the highest AT_α and the standard bias tires have the lowest AT_α.

Stress Distribution

(1) The shear force increases in magnitude through the contact patch and then quickly decreases to zero at its exit.

(2) For the bias and bias-belted tires, the increase in shear force with position in the contact patch was exponential. The increase for the radial tire, however, was linear with position.

(3) The region at the entrance of the contact patch does not contribute to the shear force. This length increases with wear. Additionally, the shape of the shear force distribution changes with wear. The maximum amplitude is higher and the exponent of the increasing shear force is higher. AT_α increases, since the forces are shifted rearward.

(4) For an inflation pressure increase, the entire contact length decreases. The exponent gets smaller and the inactive zone shrinks. The result is an increase in C_α with no change in AT_α.

(5) The fore/aft interfacial stresses are important in determining the aligning torque. The pneumatic trail concept arose assuming that only lateral interfacial stresses contribute to the aligning torque. Hence, in this paper the longitudinal stresses were subtracted from the total stress distribution before computing the pneumatic trail to be consistent with its definition, i.e.,

$$\text{pneumatic trail} = \frac{F_y}{AT} \text{ or } = \frac{C_\alpha}{AT_\alpha} \text{ at small } \alpha.$$

In fact, the longitudinal stresses contribute from 25 to 40% to the aligning torque.

(6) The pneumatic trail is sensitive to the exponent of the lateral stress distribution and to the extent and location of the inactive zone at the entrance of the contact patch. It is not determined by a rearward shift of the contact patch.

80. Litzler, C.A., "Advances in Tire Cord Processes. Pt. 1: Reinforcing Materials." Rubber Age, Vol. 105, No. 2, Nov. 1972, pp. 27-32.

81. Livingston, D.I. and Brown, J.E., "Physics of the Slipping Wheel. II. Slip Under Both Tractive and Lateral Forces." Rubber Chemistry and Technology, Vol. 43, No. 2, 1970, pp. 244-261.

An elementary theory was proposed for the origin of the camber force. Results based on the theory are consistent with experiment for small camber angles.

82. McIntosh, K.W., "Laboratory Tire Treadwear Testing." Tire Science and Technology, TSTCA, Vol. 1, No. 1, Feb. 1973.

83. Marick, L., "Factors in Tires that Influence Skid Resistance, Part II: The Effect of Tread Design." Proceedings, First International Skid Prevention Conference, Part I, Virginia Council of Highway Invest. and Research, Charlottesville, Aug. 1959, pp. 155-162.

84. Masaki, R., Saito, T., Ikeya, C., and Haranda, I., "Cornering Characteristics of Automobile Tires (I)." Jour. of Mech. Laboratory of Japan, Vol. 4, No. 2, 1958.

A mathematical model was developed to determine side force and aligning torque as a function of slip angle for a non-rolling tire.

85. Masaki, R., Saito, I., Ikeya, C., and Haranda, I., "Cornering Characteristics of Automobile Tires (II)." Jour. of Mech. Laboratory of Japan, Vol. 5, No. 2, 1959.

A description of an apparatus developed to observe the transformation of the contact area of the rolling tire was presented, and several of the results obtained were shown.

86. Maycock, G., Experiments on Tyre Tread Patterns. Road Research Laboratory Report LR 122, 1967, 11 pp.

The experimentation was conducted to investigate the influence of certain features of tread pattern design on the skid resistance of tires.

A test vehicle was operated on five surfaces—polished concrete, fine cold asphalt, asphalt with chippings (white), rounded gravel carpet, and asphalt with chippings (black). "Spray bars" were used to wet the road surfaces to the desired water depth. "Measurements were made of peak and locked wheel braking force coefficients, on several wet surfaces at speeds between 20 and 105 mile/hr., using a front wheel braking technique."*

*Quotations are from the report.

"In the first experiment four tyres were used having respectively 5, 7, 9 and 13 straight cut ribs and having the same overall tread area. The results showed that the differences between these tyres were small, except on the most polished surface, where the 5-rib tyre gave a larger decrease of coefficient with increasing speed."

"In the second experiment, the rib width was held constant, and the groove width varied. Initially, six tyres were tested: a 2 1/2" wide smooth tyre, and six ribbed tyres having five 1/2 in. ribs and a range of groove widths. The results showed that no appreciable increase in coefficient was obtained when the groove width exceeded a critical value. The optimum value of groove to rib width ratio for these tyres was 0.4."

87. Maycock, G., "Studies on the Skidding Resistance of Passenger-Car Tyres on Wet Surfaces." Proceedings, Institution of Mechanical Engineers, Vol. 180, No. 4, 1965-1966, pp. 122-157.

88. Meades, J.K., "Braking Force Coefficients Obtained with a Sample of Currently Available Radial Ply and Crossed Ply Car Tyres." Road Research Laboratory, 1967, 17 pp.

89. Meades, J.K., The Effect of Tyre Construction on Braking Force Coefficients. Road Research Laboratory Report No. LR 224, 1969, 14 pp.

Radial ply and bias ply tires with winter tread patterns and siped rib tread patterns were tested on seven wet road surfaces at speeds between 30 mph and 60 mph to determine the effect of tire construction on peak and locked-wheel brake force coefficients. The tires were made with identical tread materials and tread patterns. Testing was done with a front wheel braking car.

Results:

(1) Differences in results produced by type of construction were independent of type of tread (i.e., winter or siped).

(2) Radial ply tires gave higher peak brake force coefficients than bias ply tires on all road surfaces. The differences were independent of speed and were greater on fine textured surfaces than coarse textured surfaces.

(3) Radial ply tires gave higher locked-wheel brake force coefficients than bias ply tires on fine textured surfaces but lower coefficients on coarse textured surfaces. The differences were generally smaller than those observed for peak brake force coefficients.

90. Moyer, R.A., Tire Wear and Tire Failures on Various Road Surfaces. Available from Clearinghouse, Springfield, Virginia 22151, Accession No. PB 191039, June 1943, 44 pp.

91. Neill, A.H., Jr., "Claims that Siping Increases Wet Traction of Tires Not Borne Out by NBS Test." Automotive Engineering, Vol. 79, No. 7, July 1971, pp. 33-35.

92. Neill, A.H., Jr., "Wet Traction of Tractionized Tires." Nat. Bur. Stand., (U.S.), Tech. Note 566, Feb. 1971, 14 pp.

93. Neill, A.H., Jr. and Boyd, P.L., "Research on Wet Tire Traction." Tire Science and Technology, TSTCA, Vol. 1, No. 2, May 1973, pp. 172-189.

94. Nordeen, D.L., "Analysis of Tire Lateral Forces and Interpretation of Experimental Tire Data." SAE Paper 670173, Jan. 9-13, 1967.

This paper described an easy method for computing the steady-state directional control characteristics for a particular tire-vehicle system. A method for characterization of the effect

of slip angle and vertical load on lateral force was developed. Normalized load transfer, load sensitivity, and normalized lateral force were the principle tire characteristics that affected vehicle handling in this model.

95. Nordeen, D.L. and Cortese, A.D., "Force and Moment Characteristics of Rolling Tires." SAE Paper 713A, June 1963, 13 pp.

A flat bed tire testing machine was used to generate tire performance data. The objectives of the testing were to determine the influence of slip angle, camber angle, normal force, and inflation pressure on the steady-state characteristics of the tires and to determine the differences of these characteristics with tires of the same size but different manufacturer.

Results:

(1) Lateral force was a linear function of slip angle only for slip angles less than 2 degrees.

(2) Normal force significantly affected lateral force for slip angles larger than 2 degrees.

(3) As normal force tended towards zero at a constant slip angle, the aligning torque tended towards zero.

(4) Maximum lateral force at a given slip angle was obtained with some braking (about 200 to 300 lb. braking force for slip angle between -4 and -8 degree with normal load of -1000 lb.).

(5) An increase in inflation pressure caused an increase in lateral force and a decrease in aligning torque at a given slip angle.

(6) The sensitivity of tires of different manufacturer to changes in inflation pressure was significant.

96. Nordeen, D.L. and Cortese, A.D., "Small Differences in Tire Properties = Large Differences in Vehicle Handling." SAE Journal 71(7), 1963, pp. 83-90.

Lateral force and aligning torque were determined as functions of camber, loading, tractive force, and inflation pressure. Results include:

(1) An increase in inflation pressure increases lateral force and decreases the aligning torque.

(2) Increasing the pressure in all tires of a car increases the speed of response of the vehicle.

(3) Increasing the inflation pressure in the rear tires contributes to understeer.

(4) Adjusting the inflation pressure in the tires of different cars can cause them to respond similarly to small steering inputs.

97. Nordeen, D.L., Rasmussen, R.E. and Bidwell, J.B., Tire Properties Affecting Vehicle Ride and Handling. General Motors Engineering Staff, Engineering Publication 3759, July 12, 1968.

"This paper discusses many of the tire factors which affect vehicle ride and handling. The significance of certain tire properties to vehicle behavior is described. The paper also discusses other tire properties which influence vehicle dynamic performance, but for which a quantitative relationship between component characteristics and vehicle performance has not been established. The state of the art with respect to the capability and utility of laboratory measurements of the tire properties is indicated."*

*Quotation from the paper.

98. Odgers, B.J., The Performance and Failure of Car Tyres. Melbourne University, Mech. Eng. Dept., June 1966, 50 pp.

99. Peterson, K.G. and Rasmussen, R.E., "Mechanical Properties of Radial Tires." SAE Paper 730500, May 1973, 7 pp.

Conclusions which are generally true of radial tires on typical cars are:

(1) "Properties of radial tires vary over a wide range. Although the cornering coefficient average is higher, there is obviously overlap between the two distributions. Camber properties are most different and very rarely overlap.

(2) Application of radial tires reduces vehicle understeer in the amount of 1.0-3.0 deg/g. Most of this is due to reduced camber stiffness.

(3) The reduction in understeer coupled with higher cornering stiffness causes an increase in steering sensitivity or the amount of lateral acceleration produced by a given level of steering input. The increase is small at low speeds, but may be in the range of 50-100% at expressway speeds.

(4) The reduction in understeer would normally produce longer vehicle response times and increased vehicle sensitivity to wind disturbances. Higher front and rear cornering stiffnesses compensate for this in most cases.

(5) Road feel is generally reduced with radial tires because the front tires operate at lower slip angles for a given maneuver and generate proportionally less aligning torque.

(6) In addition to the above, vehicles equipped with radial tires are generally less sensitive to service factors like load and inflation pressure. Thus, vehicle characteristics are likely to be more constant in customer service, but also more difficult to modify with tire inflation specifications."*

*Quotation from the paper.

100. Phillips, B., "The Static Steady-State and Dynamic Characteristics of Pneumatic Tires." PhD Thesis, Lanchaster Polytechnic, Coventry, April 1973.

101. Rasmussen, R.E. and Cortese, A.D., "Dynamic Spring Rate Performance of Rolling Tires." SAE Paper 680408, May 1968, 7 pp.

102. Rasmussen, R.E. and Cortese, A.D., The Effect of Certain Tire-Road Interface Parameters on Force and Moment Performance. Engineering Staff/General Motors Corp., Report A-2526, July 1969, 24 pp.

This study was undertaken to:

(1) Investigate the effect of different road surfaces on tire characteristics.

(2) Investigate the effect of tread wear and several different tire constructions on tire characteristics.

A flat bed force and moment tire test machine was used. The surfaces studied were: Safety Walk, nylon, teflon, steel, various tungsten carbide grits, grooved aluminum, and wet ice. Carpet plots of many of the results were included.

The results obtained were:

(1) Grooved surfaces increased the lateral and tractive force capabilities of tires.

(2) Studs on snow tires produced a significant increase in lateral tractive force capability.

(3) Studs substantially altered the normal balance of front and rear lateral and tractive force capability when used on only one end of the car.

Wear conditions were produced by shaving new tires on a tire truing machine.

(4) Lateral force and aligning torque increased greatly between new and half-worn conditions (on dry surfaces).

(5) Mixing of worn and new tires on front and rear of the car substantially altered the usual balance of tire properties that affects vehicle handling performance.

Shoulder wear was simulated by shaving tires to a half-worn condition at 6-inch and 8-inch crown radii.

(6) Lateral force and aligning torque increased with shoulder wear.

103. Reinhart, M.A., "Factors in Tires that Influence Skid Resistance, Part IV: The Effect of Tread Components," Proceedings, First International Skid Prevention Conf., Part I, Virginia Council of Highway Invest. and Research, Charlottesville, Aug. 1959, pp. 167-171.

104. Rice, R.S., Jr. and Milliken, W.F., Jr., "The Effects of Loadings and Tire Characteristics on the Steering Behavior of an Automobile." First International Conference on Vehicle Mechanics, 1968.

The steady-state steering behavior of the test vehicle was varied by changing certain characteristics of the vehicle related to tires and loading. Variations in tire pressure (absolute and front-to-rear differential), tire design (radial, bias ply, and snow tires), vehicle loading (up to 1000 lbs.), and distribution of load as they affected vehicle handling were studied at speeds up to 50 mph. Extreme combinations of variables produced configurations ranging from oversteer with a critical speed of less than 50 mph to understeer with a characteristic speed of about 35 mph.

It was concluded that consistency of steering behavior can be drastically degraded by unfavorable loading and tire combinations.

105. Robson, J.J., "High-Speed Cornering Forces." SAE Trans., Vol. 64, 1956.

This paper described an experiment in which a standard chassis was mounted on a 10-foot test wheel to study traction of tires at speeds up to 100 mph.

106. Sabey, B.E., Williams, T., and Lupton, G.N., "Factors Affecting Friction of Tires on Wet Roads." SAE Paper 700376, 1970.

The object of this investigation was to put into perspective the roles of "drainage" and "energy loss" properties of tires in providing good traction on wet roads. Experiments were conducted to determine locked wheel force coefficient and spin-down speed on a variety of surfaces, at different water depths. The effect of changes in tread pattern, tread material, and inflation pressure were examined.

107. Saito, T. and Ikeya, C., "Cornering Characteristics of Automobile Tires (III)." Journal of Mech. Laboratory of Japan, Vol. 7, No. 1, 1961.

The effects of speed, tire temperature, load, inflation pressure, and tire tread design on the cornering force and aligning torque of tires are examined using a steel drum tire tester. A mathematical model yielding side force and aligning torque is refined from previous work as the result of the experimentation done.

108. Saito, T. and Ikeya, C., "Cornering Characteristics of Automobile Tires (IV)." Journal of Mech. Laboratory of Japan, Vol. 7, No. 1, 1961.

This paper is a continuation of the work from the preceding paper. The effect of inflation pressure, load, speed, and road texture on the cornering characteristics of two different size tires on a wet surface is examined.

109. Sakai, H., "Theoretical Study of the Effect of Tractive and Braking Forces on Cornering Characteristics of Tires." Paper No. 4 of Safety Research Tour in the U.S.A. from the Viewpoint of Vehicle Dynamics (Vehicle Handling, Automobile Aerodynamics and Tire Mechanics), 1969.

110. Schallamach, A., "The Load Dependence of Side Force and Self-Aligning Torque of Pneumatic Tires." Rubber Chemistry and Technology, 43(2), 1970.

A method is developed to transform theoretical side force versus slip curves at different loads to a single master curve normalized by load.

111. Schallamach, A., "Skid Resistance and Directional Control." (Chap. 6), Mechanics of Pneumatic Tires, S. K. Clark, Ed., National Bureau of Standards Monograph 122, 1971, pp. 501-544.

112. Schuring, D., "Literature Survey and Annotated Bibliography." The Influence of Tire Properties on Passenger Vehicle Handling, Vol. III, DOT-HS-053-3-7272, Final Report, 1974, Appendix A.

113. Schuring, D., Notes on the Influence of Road Wheel Dimensions on Tire Performance. Internal Document of TIRF Center, Calspan Corp., May 1974.

114. Segel, L., "Tire Traction on Dry, Uncontaminated Surfaces." The Physics of Tire Traction—Theory and Experiment, Edited by Hays and Browne, Plennum Press, New York-London, 1974.

A summary of the theory of tire mechanics as it is understood today was presented, and some of the latest results on tire properties found at HSRI were shown.

$$\begin{bmatrix} F_x \\ F_y \\ F_z \\ M_x \\ M_y \\ M_z \end{bmatrix} = f(R_\ell, \gamma, \frac{1}{\rho}, S_x, S_y, u)$$

where

R_ℓ is the rolling radius of the tire

γ is the inclination of the tire center plane with respect to the vertical z-axis

$\frac{1}{\rho}$ is the curvature of the tire path

S_x is the tire's longitudinal slip

S_y is the tire's side slip

u is the tire's longitudinal speed.

This equation constitutes a complete definition of the tire traction field. These characteristics are determined by the mechanical properties of the tire carcass and by the frictional coupling developed at the tire-road interface.

Simplifications of this equation are shown and qualitative explanations are given to explain tire traction performance.

Some of the recent results found at HSRI are:

(1) A tire shows a lateral force dependency on slip angle different than its longitudinal force dependency on slip for a particular surface. This asymmetric behavior in the shear forces generated by a tire varies in magnitude depending on the surface on which the tire is tested.

(2) The influence of tire design variables on longitudinal shear force performance is more significant on asphalt than on concrete. Substantial testing with specially constructed tires is needed to further the understanding of how design variables influence dry traction behavior.

(3) A recent experiment shows a "remarkable sensitivity" of dry traction to tread shoulder wear. Also, tires with belted-bias construction are particularly sensitive to tread shoulder wear.

115. Setright, L.J.K., Automobile Tires. Published by Chapman and Hall, London, 1972.

116. Sinnamon, J.F., Literature Survey of Tire-Road Experiments. Highway Safety Research Inst., Report No. UM-HSRI-PF-74-5, Feb. 1974.

This survey was conducted to report on published experimental work representing the state of the art of the testing of automobile and aircraft tires and the results obtained. Thirty-eight references are cited and annotated. Several sections from the summary, appearing at the beginning of the survey and based on the literature examined, are quoted below:

TIRE CONSTRUCTION. When compared to a bias ply tire of the same size, rubber compound, and tread pattern, the radial ply tire gives somewhat higher values of peak braking force coefficient, but no difference in locked wheel coefficient (the differences are small). However, compared to a typical production bias ply tire, much larger differences are observed because radial construction allows greater freedom in tread pattern design and tread rubber compounding.

Radial ply tires have higher cornering stiffness than do bias ply tires.

TIRE LOAD AND INFLATION PRESSURE. An increase in load usually causes a decrease in both braking and cornering traction on both wet and dry surfaces.

An increase in inflation pressure causes a decrease in dry friction and a decrease in wet braking friction at speeds below the hydroplaning speed. But in deep water at high speeds,

traction is improved when inflation pressure is increased because the hydroplaning speed is raised.

With respect to tire-road friction, changes in load and inflation pressure in the range that can be used in automobile tires have a relatively small effect, but these variables are very important for aircraft tires which may be operated over a greater range of loads and inflation pressures.

An increase of inflation pressure causes an increase in cornering stiffness.

WATER DEPTH AND TIRE SPEED. Even a very small amount of water, enough to make the surface "just damp," can cause a large decrease in friction coefficient, especially on surfaces having a polished microtexture.

An increase in water depth causes a decrease of wet friction. The effect is greatest at high speed on smooth surfaces. Most of the decrease occurs in the first 3-4 mm of water depth. At greater depths, for most tires, the tread grooves become flooded and no further effect of increasing depth is seen.

In deep water (more than 3-4 mm), tread pattern and surface texture have a large effect only at speeds below the hydroplaning speed; but in shallow water tread pattern and surface texture continue to have an effect at higher speeds.

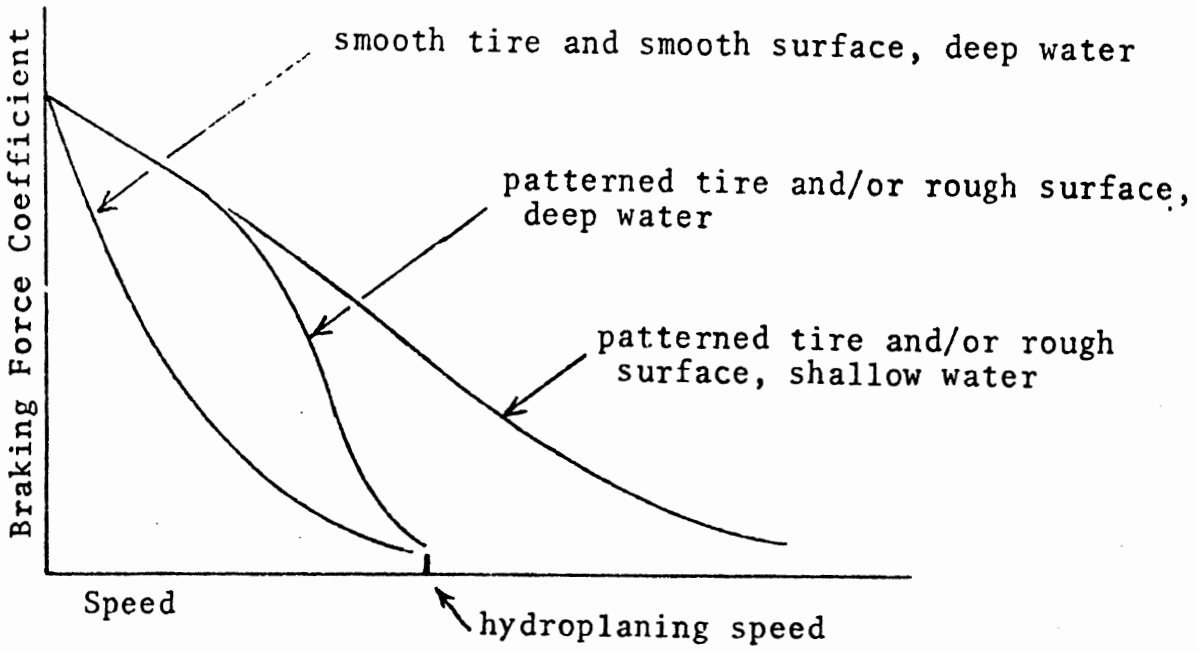

COMBINED BRAKING AND CORNERING. In pure braking, a curve of braking force coefficient versus wheel slip shows a rapid initial rise to a peak between 7% and 25% slip, followed by a gradual decrease as wheel slip increases toward lockup.

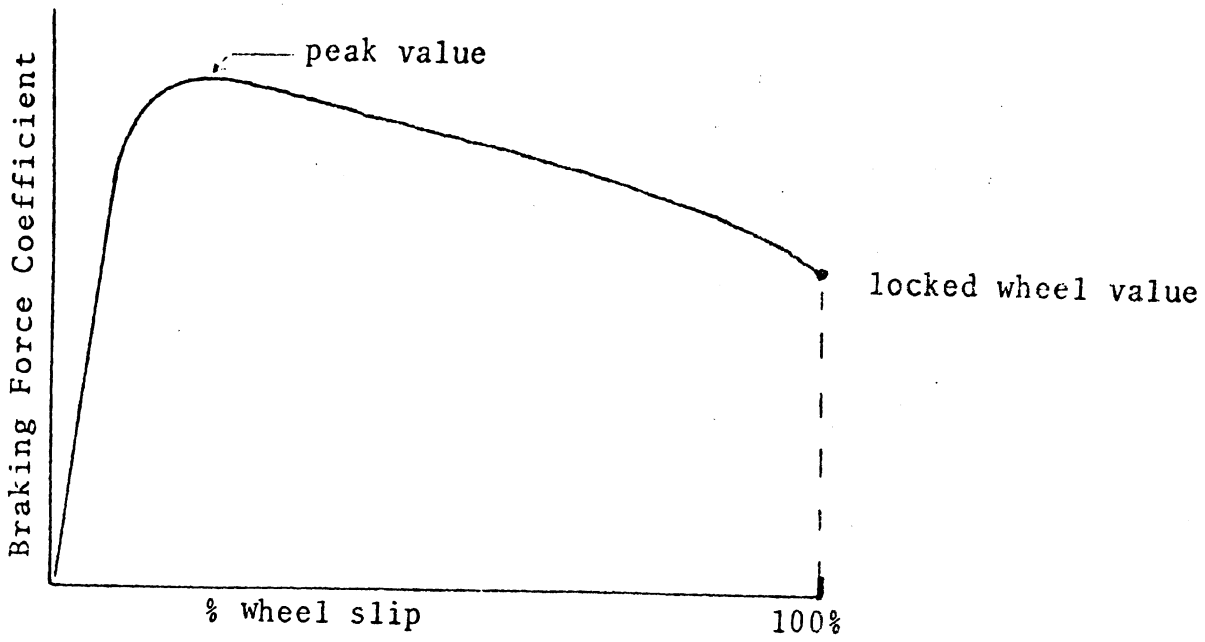

The effect of a slip angle upon the BFC versus wheel slip curve is to decrease the initial slope, shift the peak to a higher value of slip, and to decrease the maximum available braking force. At large slip angles, maximum braking force is obtained at lockup. Also cornering force obtained at a given slip angle is reduced when a braking force is applied.

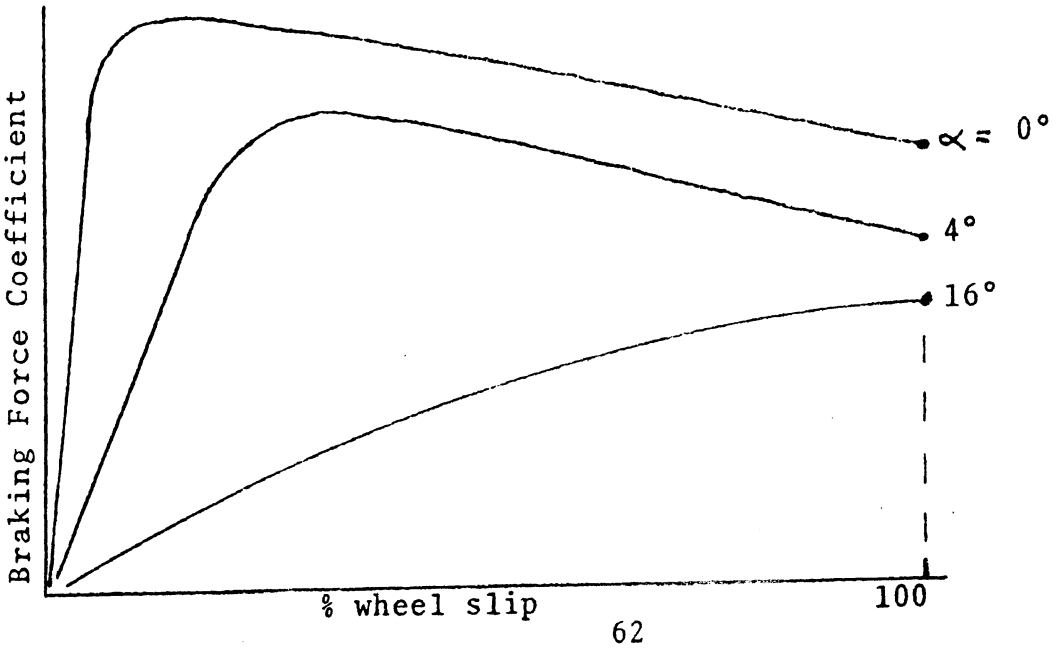

Considerable progress has been made in the field of tire traction research which has led to significant improvements in tire and road performance. However, it is still not possible to predict the traction performance of a tire-road system based on the many tire and surface variables. Indeed, there is, as yet, no agreement as to how to quantify many of these variables in a meaningful way. It is clear that there is a great deal of definitive work yet to be done in this field.

117. Smithson, F.D. and Herzegh, F.H., "Investigation of Tire-Road Traction Properties." SAE Paper 710091, Jan. 1971, 16 pp.

118. Snyder, R.H., "Environmental Effects on Tire Treadwear." Tire Science and Technology, TSTCA, Vol. 1, No. 2, May 1973.

Statistical studies were conducted on the tire treadwear of contemporary belted tires on a nationwide basis. One result found was that the treadwear behavior of a tire varies greatly in different geographical regions.

119. Southern, E., "Rapid Tire Wear Measurements Using Two-Wheeled Trailer." Tire Science and Technology, Vol. 1, No. 1, Feb. 1973.

A method has been developed using a two-wheeled trailer previously designed by Schallamach [53] to obtain accelerated wear data on tires.

120. Southern, E. and Walter, R.W., "The Performance of Natural and Synthetic Radial-Ply Winter Tyres on Ice and Hard Packed Snow." I.R.I.J., Vol. 6, No. 6, Dec. 1972, pp. 249-252.

121. Spelman, R.H., Tarpinian, H.D., Johnson, D.E., and Campbell, K.L., "SAE Study - Wet Pavement Braking Traction." SAE Paper 700462, May 1970, 26 pp.

122. Staughton, G.C., The Effect of Tread Pattern Depth on Skidding Resistance. Road Research Laboratory Report LR 323, 1970, 9 pp.

123. Staughton, G.C. and Williams, T., Tyre Performance in Wet Surface Conditions. Road Research Laboratory Report LR 355, 1970, 89 pp.

This report gave the results of an investigation of the tire-road adhesion of a single wheel towed through various depths of water. The effects of water depth, road surface texture, speed, inflation pressure, and tread pattern on locked-wheel brake force coefficient and hydroplaning speed were discussed.

124. Taft, P.H., "New Trends in Tires." Published in Interagency Motor Equipment Advisory Committees Management Conference Minutes, 1969, pp. 12-17.

125. Thieme, van Eldik, H.C.A. and Pacejka, H.B., "The Tire as a Vehicle Component." (Chap. 7), Mechanics of Pneumatic Tires, S.K. Clark, Ed., National Bureau of Standards Monograph 122, Nov. 1971, pp. 545-839.

126. Tielking, J.T., Construction and Profile Study, Part I: Tire Traction Data Measured by the HSRI Mobile Tire Tester. Highway Safety Research Institute, March 1973, 186 pp.

127. Tielking, J.T. and Mital, N.K., A Comparative Evaluation of Five Tire Traction Models. Interim Document 6, Highway Safety Research Inst. Project 329180, Jan. 1974.

128. Tsuchiya, S., Watanabe, T., and Matsuoka, Y., "The Effects of Tire Wear on Vehicle Behavior." SAE Paper 741100, 1974.

The tires to be studied were driven on a winding course to generate different levels of wear, after which the cornering force of the tires as a function of slip angle and load were determined. The tires used for the experiment were bias-belted and radial in construction.

The results found were:

(1) Cornering force increases with wear.

(2) Aligning torque increases with wear in the small slip angle region, but it decreases with wear in the region of large slip angles.

(3) The cornering stiffness, C_α, increases at small loads with wear.

(4) The pneumatic trail increases with wear in the region of small slip angles, but it decreases with wear at large slip angles.

A tire model was developed to calculate the cornering characteristics of a tire in different states of wear to agree with the experimental data. The tire is modeled as a stretched beam on an elastic foundation:

$$EI \frac{d^4y}{dx^4} - K \frac{EI}{AG} \frac{d^2y}{dx^2} + Ky = q(x) - \frac{EI}{AG} \frac{d^2q(x)}{dx^2} \qquad (1)$$

where

$y = y_b + y_s$

y_b is the lateral deflection of the beam with bending moment only

y_s is the lateral deflection of the beam with shear force only

EI is the bending stiffness and

AG is the shear stiffness.

Introducing the tire parameters

$$a = \left(\frac{K}{2AG}\right)^{1/2} \quad , \quad b = \left(\frac{K}{4EI}\right)^{1/4}$$

the solution to Equation (1) is

$$y = e^{-ux}[C_1 \cos(vx) + C_2 \sin(vx)]$$

where

$$u = \sqrt{2}\, b \cos\left[\frac{1}{2} \cos^{-1}\left(\frac{a^2}{2b^2}\right)\right]$$

and

$$v = \sqrt{2}\, b \sin\left[\frac{1}{2}\cos^{-1}\left(\frac{a^2}{2b^2}\right)\right]$$

a, b, K, and C_o (the tread rubber stiffness) are shown to have different values depending on the construction of the tire. a, b, and K is found to vary negligibly with increasing wear, though C_o increases with wear.

Using an iterative procedure to determine the shear force distribution, the cornering force and aligning torque are then determined by integrating the shear force distribution.

The theory developed shows good correlation with the data obtained in determining the cornering characteristics of a tire with the progress of wear.

Conclusions

Concerning cornering characteristics of tires:

(1) For bias-belted tires, the bending stiffness can be considered infinite, and the cornering characteristics depend only on shear stiffness.

(2) For radial tires both bending stiffness and shear stiffness must be taken into account.

(3) Tread rubber stiffness increases with wear.

129. Umland, C.W., Bannister, E., and Tomlinson, C.B., "The Skid Resistant Properties of Butyl Tyres." Instn. Mech. Engrs., Symposium on Control of Vehicles, 1963, pp. 91-97.

130. Veith, A.G., "Accelerated Tire Wear Under Controlled Conditions - Part I: Description of the Test System." Rubber Chem. Tech., Vol. 46, No. 4, Sept. 1973, pp. 801-820.

131. Veith, A.G., "Accelerated Tire Wear Under Controlled Conditions - Part II: Some Factors that Influence Tire Wear." Rubber Chem. Tech., Vol. 46, No. 4, Sept. 1973, pp. 821-842.

This paper discusses the results obtained using the instrumented trailer test system described in the author's preceding paper [130].

Three primary factors causing tire wear are:

(1) Tire force level (the most important factor).

(2) Pavement texture

(3) Tire surface temperature.

The concept of test severity was discussed, and it was concluded that severity must be broken up into the three components listed above. The effects are not simply additive. The predominant wear mechanism varies depending on the conditions (particularly pavement texture), and completely different results are found with different mechanisms. In making note of this point, good correlation of experimental data with the theory developed was obtained.

Other conclusions are:

(1) Cornering force is a much more important factor in tire wear than longitudinal force.

(2) Wear rate varies with cornering force raised to an exponent between 2 and 4 depending on the pavement texture, tire temperature, and tread composition (in the tire force range of 0-500 lb.).

(3) With current tread compounds, the wear rate increases about 2% per degree centigrade.

(4) Radial tires are superior to bias tires in wear—due mainly to the belt, which stabilizes the tread elements.

(5) Pavement microtexture has a significant effect on wear whereas pavement macrotexture has only a slight effect.

(6) Water on a tire lowers the tire's surface temperature and reduces the tire-road friction—both contributing to reduced wear.

132. Veith, A.G., Cooperative Correlation Program: University of Michigan HSRI Mobile Tire Tester vs. B.F. Goodrich Cornering Trailer. Company Document, B.F. Goodrich Company, Aug. 15, 1972.

133. Veith, A.G., "Measurement of Wet Cornering Traction of Tires." Rubber Chemistry & Tech., Vol. 44, No. 4, 1971.

A cornering test trailer was used to measure the cornering traction of tires in free-rolling in the 30-60 mph speed range.

The cornering force of tires at various slip angles was found at different speeds while the test trailer was traveling at a constant velocity. The test surface contained a specified water depth. Cornering coefficients (μ_c) were calculated where:

$$\mu_c = \frac{F_c}{L}$$

F_c = cornering force

L = static tire load

The results were:

(1) Tread rubber composition showed a wide range of performance ratings at low speeds (30-35 mph) and a narrower range at high speeds (55-60 mph). On the contrary, the opposite effect was exhibited for tread pattern showing a narrow range of performance ratings at low speeds and a higher range at high speeds.

(2) For any given rubber, high-speed traction improved with increasing rubber hardness.

(3) Tread rubbers ranked in order of high to low traction characteristics were: styrene-butadiene rubber, Butyl rubber, natural rubber, and polybutadiene rubber.

(4) Lack of microtexture in roads produced low friction coefficients.

(5) At low speeds, boundary layer lubrication predominated on all but the smoothest surfaces. At high speeds both thick and thin film elastohydrodynamic lubrication predominated. This mode yields minimum friction coefficients smaller than the mode of touching boundary layers of two surfaces or the pure hydrodynamic mode (thick film).

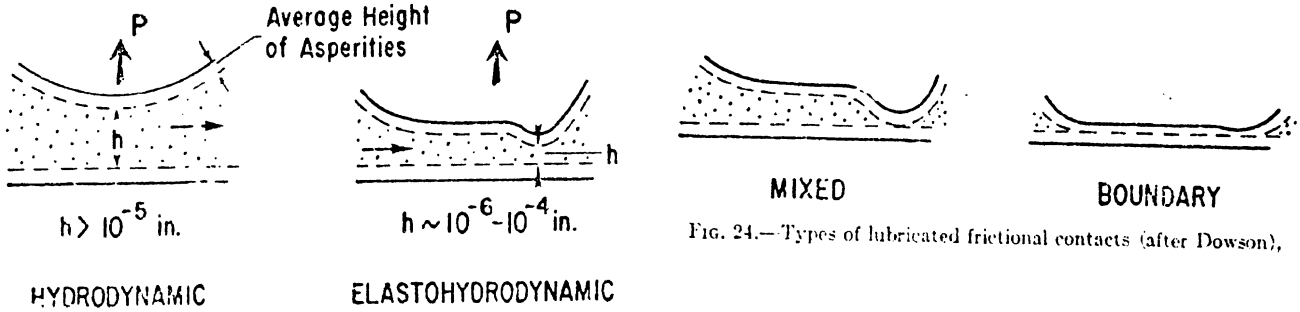

FIG. 24.—Types of lubricated frictional contacts (after Dowson).

(6) It was "postulated that the fraction of contact area of a cornering tire that is in the elastohydrodynamic mode of lubrication is a linear function of speed. This accounts for the good linearity of the plots of traction as a function of speed."

(7) Statistically designed test programs were advocated for wet traction testing due to difficulty in measuring a constant water depth and also to enable the investigator to "uncover the strong interaction between tire and test variables that underline all wet traction testing."

134. Wild, R.E., Wet Traction Test Program. Final Report, Highway Safety Res. Inst., Univ. of Michigan, Ann Arbor, Report No. HSRI-PF-73-3, Aug. 1973.

In the study conducted "86 tires (2 each of 43 different types representing 90% of the OE population) were measured for longitudinal and lateral traction capability on 3 different, wetted surfaces." For each tire the longitudinal and lateral traction coefficients (both peak and locked-wheel values) were found.

The tests were conducted at the Texas Transportation Institute with the HSRI Mobile Tire Tester. Three surfaces were used: (1) Portland cement concrete; (2) jennite flush seal; and (3) a crushed gravel hot mix.

The results found were:

(1) The "skid number" proved to be a poor measure for characterizing a tire-pavement combination.

(2) Lateral and longitudinal traction showed independent natures.

(3) One trend, though inconclusive, was improvement of traction with increasing diameter tires.

(4) Second inconclusive trend showed traction improvement with increasing vertical wheel loading.

(5) "Traction uniformity on concrete between identical tires was found to be excellent, while the traction differences on concrete between tires of the same size but of different manufacture were found to be statistically significant."

(6) Studs produced slightly lower peak traction coefficients but did not affect the locked-wheel longitudinal traction coefficient.

(7) No one type of tire construction stands out as producing traction levels consistently above or below the overall OE means.

135. Wilson, M.A., "Tire Progress - Past, Present, and Future." SAE Paper 721A, Aug. 1963, 7 pp.

136. Wolff, H., "Investigations on the Guiding Forces of Rubber Tyres." Automobiltechnische Zeitschrift (A.T.Z.) (In German), Vol. 58, No. 1, Jan. 1956.

137. Zeranski, P., "Factors Affecting Force Transmission at the Pneumatic Tyre." K.F.T. (In German), No. 3, March 1973, pp. 78-81.

138. Zoeppritz, H.P., "Requirements and Performance of Automobile Tires." Automobiltechnische Zeitschrift (A.T.Z) (In German), Vol. 66, No. 9, Sept. 1964, pp. 250-256.

APPENDIX B

TIRE-VEHICLE SYSTEM SIMULATION MODEL

J.E. Bernard
R. Gupta
P.S. Fancher

ACKNOWLEDGEMENT

The programming of the simulation was ably handled by Tae Moon Kim. The graphics package, which was used herein and in the Technical Report, was produced by Paul Messink. Dave Starr was very helpful in the derivation of the tire model.

B1. INTRODUCTION

The problems of vehicle handling appeared in the literature as long ago as 1937, when the pioneering analysis of Olley [1]* was published. Subsequent investigators developed linearized equations whose solution would yield the trajectory of a vehicle subject to time-varying steering or braking. More recently, efforts have been made to analyze various nonlinear aspects of the vehicle system, including, most notably, nonlinear tire properties.

Since the equations of vehicle motion can become quite difficult to handle in the general case, it is not surprising that simulation has been a tool frequently used by vehicle dynamicists. Perhaps the best-known early computer simulation was developed in 1961 by Ellis [2], who developed a three-degrees-of-freedom analog-computer model for studying the lateral motion of an articulated vehicle. Since that time, the advent of more and more sophisticated computing equipment has led to the possibility of simulations of increasing complexity. Presently, many research facilities make use of highly nonlinear passenger-car simulations with at least fourteen degrees of freedom, including six degrees of freedom for the vehicle body (the so-called sprung mass), a vertical or "wheel hop" degree of freedom for each wheel (or unsprung mass), and a spin degree of freedom for each wheel.

The present program also falls into this pattern, i.e., there are the usual fourteen degrees of freedom, plus some quasi-static steering system variables. The distinguishing features which have justified this effort are to be found in the tire model, the input/output (I/O) formating, and in the uniquely economical run costs. This document addresses the mundane details as well as the unique features of the simulation.

---

*Numbers in brackets indicate references.

In Section 2, a discussion of the axis systems used in the simulation is presented. This explanation includes consideration of Euler angles and the appropriate transformation equations. Section 2 also includes a presentation of the equations of motion of the sprung mass. The calculation of the forces and moments to be used in these equations is left to the following section.

In Section 3, the relationships defining important kinematic variables related to tires, such as longitudinal slip and sideslip angle, are given, along with a brief discussion of some time-saving numerical methods of solution for the wheel spin equations. Next, the formulations for the rear suspension, the front suspension, and the steering system are presented, with a detailed discussion of the optional levels of sophistication of the mathematical models. Some comments are given on the trade-offs between the added range of validity of the more detailed options versus the added burden of the increased I/O.

In Section 4, a semi-empirical tire model designed for the simulation of limit maneuvers is presented. While much of the analysis is based on the findings of previous efforts to come to grips with the mechanics of the tire-road interface, two new features have been added. First, the user may set the pressure distribution at the tire-road interface, allowing a realistic representation of both radial- and bias-ply tires in the mid range of slip angle. Secondly, certain tire properties, heretofore assumed constant in semi-empirical models, have been made a function of sideslip angle to permit the user to match the calculated tire traction field more closely to measured data than has been possible previously. Examples are given of "fitting" a few measured data points to arrive at parameters suitable for the calculation of the entire traction field.

In Section 5, a table of guidelines for the use of the simulation are presented. The various potential levels of complexity of the program are used in example runs in support of this table. Flow charts for each of the subroutines discussed throughout this document are presented in Section 6.

B2. AXIS SYSTEMS AND KINEMATICS

B2.1 INTRODUCTION

The vehicle to be simulated by the digital computer program has sixteen degrees of freedom, with calculations taking place in three coordinate systems. In this section, an overview of the mathematical formulation is presented, including some kinematic details necessary for the explanation of the various mathematical models. The coordinate systems and some explanation of the methods of computation of sprung mass and unsprung mass motion are given, but the details of the various suspension and steer models are left to Section B3.

B2.2 THE AXIS SYSTEMS

The large number of translational and rotational degrees of freedom required to represent a vehicle in motion precludes the use of only one coordinate system. In fact, the equations of motion may be most easily written if several systems are used. The purpose of this section is to identify the (1) orientation and purpose of the various axis systems, and (2) to identify the transformation variables used to relate the unit vectors in the various systems. The sets of axes to be described are the inertial axes, the body axes, and the unsprung mass axes.

B2.2.1 SYSTEM I. - THE INERTIAL AXES. Since Newton's laws are valid only for accelerations measured from an inertial reference, it is necessary to have one set of fixed axes. This set of axes, which shall be termed the [XN, YN, ZN] system, has its origin at the sprung mass center of the vehicle at time zero. The vehicle will always be assumed to start with the following orientation:

XN is out the front of the vehicle,
YN is out the right door,
ZN is vertically downward, normal to the plane of the road.

The set of unit vectors in the XN, YN, and ZN directions are defined as $\hat{x}n$, $\hat{y}n$, and $\hat{z}n$, respectively. The [XN, YN, ZN] system is, of course, fixed, and therefore the time derivatives of the unit vectors, $\hat{x}n$, $\hat{y}n$, and $\hat{z}n$, are identically zero. It should be noted that there is no requirement that $\hat{z}n$ be vertical (i.e., in the direction of gravitational forces). It will be shown in a subsequent section that non-vertical $\hat{z}n$ may be chosen to simulate an inclined roadway.

B2.2.2 SYSTEM II. - THE BODY AXES. To facilitate the calculation of the location and velocity of points on the sprung mass, it is convenient to use a system of so-called body axes. This set of axes, which shall be termed the [XB, YB, ZB] system, is coincident with [XN, YN, ZN] at time zero, but remains fixed in the sprung mass. The transformation from this set of axes to the inertial set may be defined as

$$[\hat{x}n\ \hat{y}n\ \hat{z}n] = [\hat{x}b\ \hat{y}b\ \hat{z}b](a_{ij}) \qquad \text{(B2.1a)}$$

$$[\hat{x}b\ \hat{y}b\ \hat{z}b] = [\hat{x}n\ \hat{y}n\ \hat{z}n](a_{ji}) \qquad \text{(B2.1b)}$$

where the a_{ij} are functions of the roll angle, ϕ, the pitch angle, θ, and the yaw angle, ψ. These so-called Euler angles and the transformation equation (B2.1) are considered in detail later in this section.

B2.2.3 SYSTEM III. - THE UNSPRUNG MASS AXES. To facilitate the calculation of shear forces at the tire-road interface, it is convenient to define one more set of axes. This set of axes, which shall be termed the [X1, Y1, Z1] system,

has its origin at the road level on a line in the $\hat{z}n$ direction through the sprung mass center. It is required that

$$\hat{z}1 \equiv \hat{z}n \tag{B2.2}$$

Since $\hat{z}1$ is normal to the road, $\hat{x}1$ and $\hat{y}1$ are in the plane of the road, and the origin of [X1, Y1, Z1] must translate with the component of the sprung mass center velocity which is in the road plane.

This set of axes is constrained to yaw with the vehicle sprung mass. The transformation from this set of axes to the inertial set is

$$[\hat{x}1, \hat{y}1, \hat{z}1] = [\hat{x}n, \hat{y}n, \hat{z}n] \begin{pmatrix} \cos\psi & -\sin\psi & 0 \\ \sin\psi & \cos\psi & 0 \\ 0 & 0 & 1 \end{pmatrix} \tag{B2.3a}$$

where ψ is the yaw angle. In addition, it may be shown that

$$[\hat{x}n, \hat{y}n, \hat{z}n] = [\hat{x}1, \hat{y}1, \hat{z}1] \begin{pmatrix} \cos\psi & \sin\psi & 0 \\ -\sin\psi & \cos\psi & 0 \\ 0 & 0 & 1 \end{pmatrix} \tag{B2.3b}$$

The transformation between the unsprung mass axes and the body axes may be written

$$[\hat{x}1, \hat{y}1, \hat{z}1] = [\hat{x}b, \hat{y}b, \hat{z}b](b_{ij}) \tag{B2.4a}$$

$$[\hat{x}b, \hat{y}b, \hat{z}b] = [\hat{x}1, \hat{y}1, \hat{z}1](b_{ji}) \tag{B2.4b}$$

where

$$b_{ij} = a_{ij}\Big|_{\psi=0} \tag{B2.4c}$$

A schematic diagram of the sprung mass in an arbitrary orientation is shown in Figure B2-1.

B2.3 THE KINEMATICS OF THE SPRUNG MASS

This section will be concerned both with definitions of variables and with certain algebraic manipulations chosen to lay the groundwork for the equations of motion. The velocity of the sprung mass center can be written as

$$\bar{V} = u\,\hat{x}b + v\,\hat{y}b + w\,\hat{z}b \qquad \text{(B2.5a)}$$

where u is called the longitudinal velocity, v the lateral velocity, and w the vertical velocity of the sprung mass center. Use of Equation (B2.1) in Equation (B2.5a) allows the velocity to be expressed with respect to the inertial system, viz:

$$\bar{V} = (\text{XNDOT})\hat{x}n + (\text{YNDOT})\hat{y}n + (\text{ZNDOT})\hat{z}n \qquad \text{(B2.5b)}$$

The components of $\bar{V}$ given in Equation (B2.5b) can be integrated to obtain the inertial coordinate positions XN, YN, and ZN of the sprung mass center.

It becomes necessary to compute the position of other points on the sprung mass to find the suspension forces. This computation may be facilitated by considering a point p on the vehicle sprung mass. Assume a vector $\bar{\rho}$ from the mass center to the point p where

$$\bar{\rho} = \text{XS}\,\hat{x}b + \text{YS}\,\hat{y}b + \text{ZS}\,\hat{z}b \qquad \text{(B2.6a)}$$

In terms of inertial unit vectors, $\bar{\rho}$ may be written

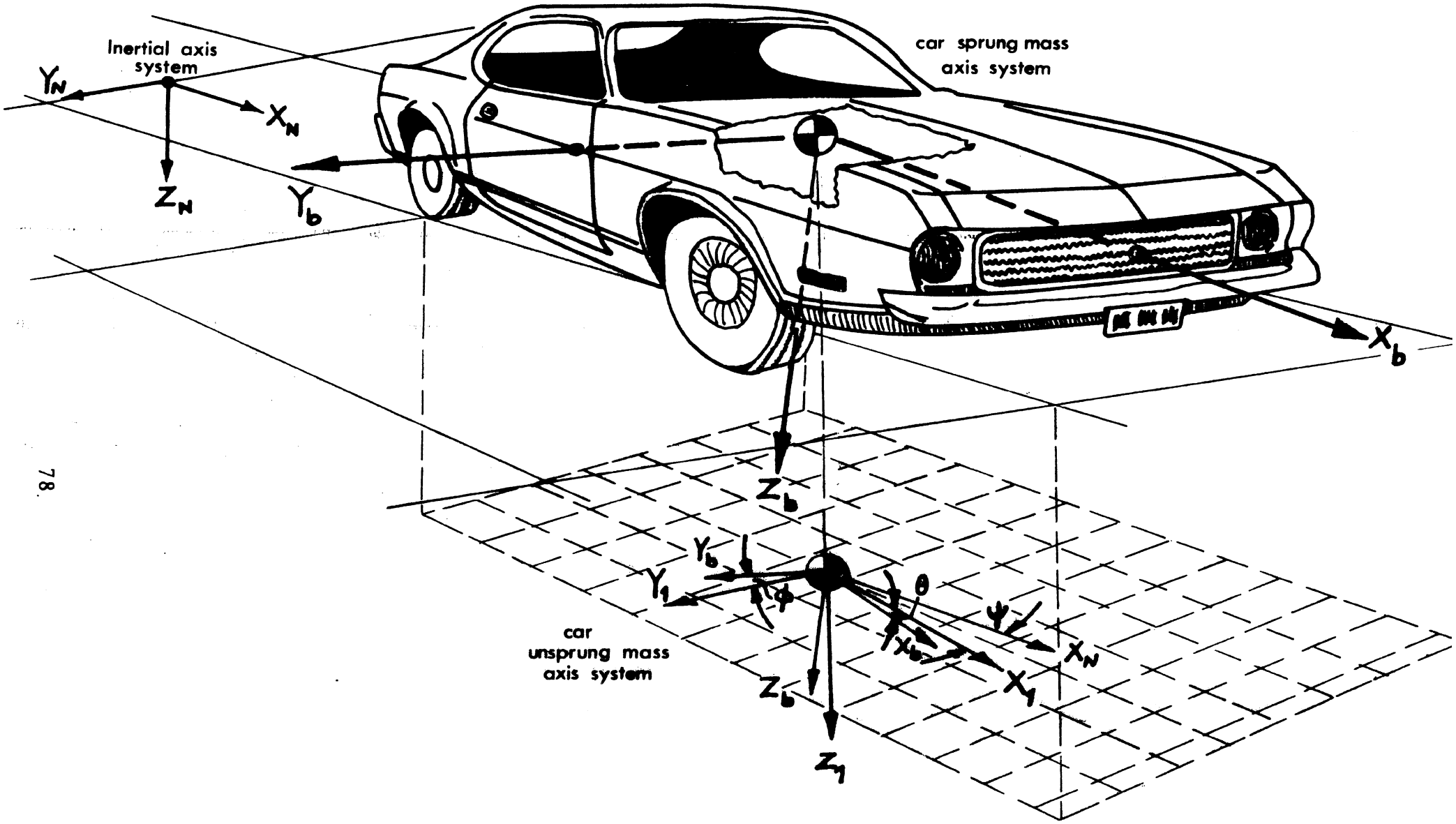

Figure B2-1. Car simulation axis system.

$$\bar{\rho} = (XS\ a_{11} + YS\ a_{21} + ZS\ a_{31})\hat{x}n + (XS\ a_{12} + YS\ a_{22} + ZS\ a_{32})\hat{y}n + (XS\ a_{13} + YS\ a_{23} + ZS\ a_{33})\hat{z}n \quad \text{(B2.6b)}$$

The distance of any sprung mass point below static equilibrium position of the sprung mass center is

$$h = ZN + (\bar{\rho} \cdot \hat{z}n) \quad \text{(B2.7)}$$

Equation (B2.7) will be used in the suspension model.

It is also necessary to calculate the velocity of the arbitrary sprung mass point. Since the vector to the point p from the origin of [XN, YN, ZN] is

$$\bar{P} = XN\ \hat{x}n + YN\ \hat{y}n + ZN\ \hat{z}n + \bar{\rho}\ , \quad \text{(B2.8)}$$

the velocity is

$$\dot{\bar{P}} = (XNDOT)\hat{x}n + (YNDOT)\hat{y}n + (ZNDOT)\hat{z}n + \bar{\omega} \times \bar{\rho} \quad \text{(B2.9)}$$

where the [XB, YB, ZB] system rotates with angular velocity, $\bar{\omega}$. Equation (B2.9) may be written

$$\dot{\bar{P}} = u\ \hat{x}b + v\ \hat{y}b + w\ \hat{z}b + \bar{\omega} \times \bar{\rho} \quad \text{(B2.10)}$$

where u, v, and w are the components of the velocity of the sprung mass center along the directions of the body axes. The angular rotation vector, $\bar{\omega}$, may be defined as

$$\bar{\omega} = p\hat{x}b + q\hat{y}b + r\hat{z}b \quad \text{(B2.11)}$$

where p, q, and r are the rotation rates in roll, pitch, and yaw, respectively. Using $\bar{\rho}$ from Equation (B2.6a), we have

$$\bar{\omega} \times \bar{\rho} = (qZS - rYS)\hat{x}b + (rXS - pZS)\hat{y}b + (pYS - qXS)\hat{z}b \tag{B2.12}$$

Thus, in body axis notation, the velocity of the sprung mass point is

$$\dot{\bar{P}} = (u + qZS - rYS)\hat{x}b + (v + rXS - pZS)\hat{y}b + (w + pYS - qXS)\hat{z}b \tag{B2.13}$$

which may be rewritten

$$\dot{\bar{P}} = (uu)\hat{x}b + (vv)\hat{y}b + (ww)\hat{z}b \tag{B2.14}$$

Using Equation (B2.1), the right-hand side of Equation (B2.14) may be expressed in terms of fixed vectors.

$$\dot{\bar{P}} = (uu\ a_{11} + vv\ a_{21} + ww\ a_{31})\hat{x}n + (uu\ a_{12} + vv\ a_{22} + ww\ a_{32})\hat{y}n + (uu\ a_{13} + vv\ a_{23} + ww\ a_{33})\hat{z}n \tag{B2.15}$$

(The $\hat{z}n$ component of the right-hand side of Equation (B2.15) will be useful in the calculation of the suspension velocity.)

At this stage, it is appropriate to define the acceleration of the sprung mass center. Differentiation of the sprung mass velocity vector given in Equation (B2.5a) leads to

$$\dot{\bar{V}} = \dot{u}\hat{x}_b + \dot{v}\hat{y}_b + \dot{w}\hat{z}_b + \bar{\omega} \times (u\hat{x}_b + v\hat{y}_b + w\hat{z}_b) \qquad \text{(B2.16)}$$

which after carrying out the cross product produces the following result:

$$\dot{\bar{V}} = (\dot{u} + qw - rv)\hat{x}_b + (\dot{v} - pw + ru)\hat{y}_b + (\dot{w} + pv - qu)\hat{z}_b \qquad \text{(B2.17)}$$

Application of Newton's law yields

$$M\dot{\bar{V}} = \bar{F} \qquad \text{(B2.18)}$$

where M is the sprung mass and $\bar{F}$ is the total force applied to the sprung mass. It is convenient to set the scalar components of Equation (B2.17) equal to the appropriate components of the external forces on the sprung mass in order to find $\dot{u}$, $\dot{v}$, and $\dot{w}$. (The velocity components, u, v, and w, are found by integrating $\dot{u}$, $\dot{v}$, and $\dot{w}$, respectively.)

Next, consider the rate of change of angular momentum of the sprung mass about the sprung mass center. This may be written

$$\begin{aligned}\dot{\bar{H}} = {} & \{I_{xx}\dot{p} + qr(I_{zz} - I_{yy}) - I_{xz}(\dot{r} + pq)\}\hat{x}_b \\ & + \{I_{yy}\dot{q} - pr(I_{xx} - I_{zz}) - I_{xz}(r^2 - p^2)\}\hat{y}_b \\ & + \{I_{zz}\dot{r} + pq(I_{yy} - I_{xx}) + I_{xz}(qr - p)\}\hat{z}_b\end{aligned} \qquad \text{(B2.19)}$$

where

I_{xx} is the roll moment of inertia

I_{yy} is the pitch moment of inertia

I_{zz} is the yaw moment of inertia

$I_{xz} = \int xz \, dm$

Lateral symmetry has been assumed (i.e., I_{xy} and I_{yz} are assumed to be zero).

The rate of change of angular momentum, $\dot{\bar{H}}$, is used in the equation

$$\bar{T} = \dot{\bar{H}} \qquad \text{(B2.20)}$$

where $\bar{T}$ is the total moment applied to the sprung mass. The scalar components of Equation (B2.19) are set equal to the appropriate applied moments in order to find $\dot{p}$, $\dot{q}$, and $\dot{r}$. (The angular velocity components, p, q, and r, are found by integrating $\dot{p}$, $\dot{q}$, and $\dot{r}$, respectively.)

These equations of the sprung mass, in scalar form, permit us to:

(1) Integrate the accelerations to obtain the angular and translational velocity components of the sprung mass.

(2) Perform the appropriate transformations to allow integration of the angular and translational velocity to find the angular and translational position of the sprung mass.

To evaluate the forces and moments appearing in Equations (B2.18) and (B2.20), it is required that the location and velocity of the axles be known. This topic is considered below. The mechanics of the forces themselves is discussed in Section B3.

B2.4 KINEMATICS OF THE UNSPRUNG MASSES

In order to compute the reactions at the tire-road interface and the suspension forces, the locations and velocities of the axles relative to the sprung mass must be determined.

Consider an arbitrary point, p', in the unsprung mass system. Assume a vector, $\bar{\rho}$, from the origin of the unsprung mass system to the point p' where

$$\overline{\rho} = (XU)\hat{x}1 + (YU)\hat{y}1 + (ZU)\hat{z}1 \qquad \text{(B2.21)}$$

For all points on the unsprung mass, XU and YU are assumed fixed; ZU, however, is variable. A vector from the origin of the inertial system to p' may be written

$$\overline{PP} = \overline{R} + h\hat{z}1 + \overline{\rho} \qquad \text{(B2.22)}$$

where h is the perpendicular distance from the sprung mass center to the road and $\overline{R}$ is a vector from the origin of the inertial system to the sprung mass center. Thus, the velocity of the point p' (with respect to the inertial reference) is

$$\overline{PP} = \overline{V} + \dot{h}\hat{z}1 + \left.\frac{d\overline{\rho}}{dt}\right|_{[X1\ Y1\ Z1]} + (\dot{\psi}\hat{z}1) \times (\overline{\rho}) \qquad \text{(B2.23)}$$

where

$\overline{V}$ is defined in Equation (B2.5)

$\dot{h}$ is the negative of the $\hat{z}1$ component of $\overline{V}$
(Note: $\hat{z}1 \equiv \hat{z}n$)

$\dot{\psi}$ is the rate of rotation of the unsprung mass axis system [X1, Y1, Z1].

Equation (B2.23) may be expanded into a more useful form. First, the sprung mass velocity, $\overline{V}$, may be written in terms of the unit vectors, $\hat{x}1$, $\hat{y}1$, and $\hat{z}1$.

$$\overline{V} = U1\hat{x}1 + V1\hat{y}1 + W1\hat{z}1 \qquad \text{(B2.24)}$$

Expansion of the cross product in Equation (B2.23) yields

$$\dot{\psi}\hat{z}1 \times \overline{\rho} = \dot{\psi}(-YU\hat{x}1 + XU\hat{y}1) \qquad \text{(B2.25)}$$

Substitution of Equations (B2.24) and (B2.25) into (B2.23) leads to the following result:

$$\dot{\overline{PP}} = (U1 - \dot{\psi}YU)\hat{X}1 + (V1 + \dot{\psi}XU)\hat{Y}1 + \left.\frac{d\overline{\rho}}{dt}\right|_{[X1,\ Y1,\ Z1]} \tag{B2.26}$$

Since XU and YU have been assumed to be constant, $\left.\frac{d\overline{\rho}}{dt}\right|_{[X1,\ Y1,\ Z1]}$ may only be in the $\hat{Z}1$ direction.

$$\left.\frac{d\overline{\rho}}{dt}\right|_{[X1,\ Y1,\ Z1]} = Z\dot{U}\ \hat{Z}1 \tag{B2.27}$$

The above assumption may be restated in the following way: The track and wheelbase, when viewed from the $\hat{Z}1$ direction, remain constant. This may be expected to be very accurate in the presence of the magnitude roll and pitch angles encountered in even very severe maneuvers.

In order to compute the forces of constraint between the unsprung masses and the sprung mass, it is necessary to express the acceleration of the unsprung mass point. Differentiation of Equation (B2.23) leads to

$$\ddot{\overline{PP}} = \dot{\overline{V}} + (\ddot{h} + \dot{Z}\dot{U})\hat{Z}1 + \ddot{\psi}\hat{Z}1 \times \overline{\rho} + \dot{\psi}\hat{Z}1 \times \frac{d\overline{\rho}}{dt} \tag{B2.28}$$

Noting that

$$\frac{d\overline{\rho}}{dt} = Z\dot{U}\hat{Z}1 + \dot{\psi}\hat{Z}1 \times \overline{\rho} \tag{B2.29}$$

and that $\dot{\overline{V}}$, which was given in Equation (B2.17), may be rewritten

$$\dot{\bar{V}} = UD1\ \hat{x}1 + VD1\ \hat{y}1 + WD1\ \hat{z}1 \qquad (B2.30)$$

where

$$WD1 = -\ddot{h}\ , \qquad (B2.31)$$

a more useful form of Equation (B2.28) is obtained, viz.,

$$\ddot{\overline{PP}} = [UD1 - (XU)\dot{\psi}^2 + (XU)\ddot{\psi}]\hat{x}1 + [VD1 - (YU)\dot{\psi}^2 + (XU)\ddot{\psi}]\hat{y}1 + \dot{Z}\dot{U}\hat{z}1 \qquad (B2.32)$$

Equation (B2.32) is used in calculating the forces of constraint between the sprung and unsprung masses.

B2.5 AXIS SUMMARY

Since it is quite tedious just to keep track of the various reference systems, all of the reference systems are listed in Table B2.1.

Table B2.1

Reference Systems

Name	Notation	Rotation Vector	Use
Inertial	XN, YN, ZN	0	Location of the vehicl Observation point for accelerations and velocities.
Body	XB, YB, ZB	$p\hat{x}b + q\hat{y}b + r\hat{z}b$	Convenient for calculation of rotational equations of sprung mass.
Unsprung Mass	X1, Y1, Z1	$\dot{\psi}\hat{z}1$	Convenient for calculation of shear forces at the tire-road interface.

The transformation equations, which are given briefly in Equation (B2.1), are used in the representation of the forces, moments, and velocities in the various coordinate systems. The equations of motion yielding the components of the translational acceleration and the components of the rate of change of angular momentum are derived from Equations (B2.18) and (B2.20), respectively. Equation (B2.30) is used to compute the translational acceleration of the unsprung masses; these accelerations are used to calculate the constraint forces between the sprung and unsprung masses. It is assumed that the unsprung masses must yaw with the sprung mass, but they can roll as determined by the forces and moments applied to them. This topic is discussed in some detail in Section B3. At this point it is appropriate to discuss transformation equations (B2.1) in detail.

B2.6 THE TRANSFORMATION EQUATIONS

Euler angles are used to specify the orientation of the body axes of the vehicle with respect to a fixed set of axes (inertial axes).

The angles of interest are:

(1) ψ, a yaw angle measured in a plane perpendicular to the inertial system vertical unit vector, $\hat{z}n$,

(2) θ, a pitch angle measured in a plane perpendicular to the unsprung mass lateral unit vector, $\hat{y}1$,

and

(3) ϕ, a roll angle measured in a plane perpendicular to the sprung mass forward unit vector, $\hat{x}b$.

The angles ψ, θ, and ϕ are shown in Figure B2-2. In this discussion four sets of axis systems are used. These axis systems are specified by the following sets of unit vectors:

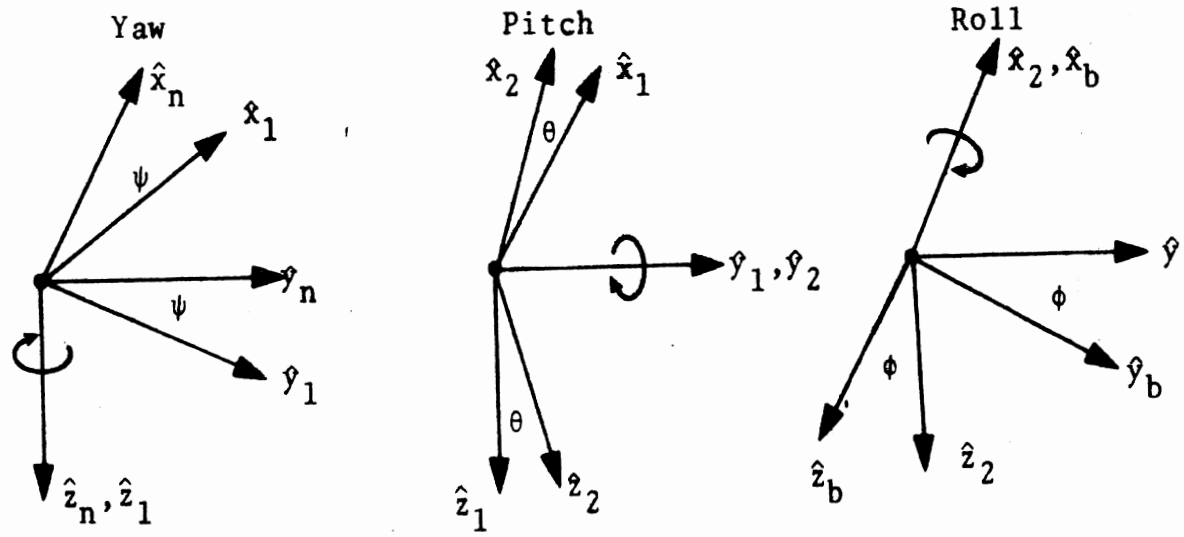

1. ψ about $\hat{z}_n$ (yaw) 2. θ about $\hat{y}_1$ (pitch) 3. ϕ about x_b (rol

Figure B2-2. Euler angles.

(1) $[\hat{x}n, \hat{y}n, \hat{z}n]$ the inertial set of unit vectors

(2) $[\hat{x}1, \hat{y}1, \hat{z}1]$ the unsprung mass set of unit vectors

(3) $[\hat{x}2, \hat{y}2, \hat{z}2]$ an auxiliary set of unit vectors

(4) [xb, yb, zb] the sprung mass set of unit vectors

The $[\hat{x}b, \hat{y}b, \hat{z}b]$ unit vectors can be expressed in terms of the $[\hat{x}n, \hat{y}n, \hat{z}n]$ unit vectors by three rotations through the angles ψ, θ, and ϕ consecutively. Consider these rotations one at a time. For ψ, a rotation about the $\hat{z}n$ unit vector, as shown in Figure B2-2

$$\begin{aligned} \hat{x}1 &= \cos\psi\,\hat{x}n + \sin\psi\,\hat{y}n \\ \hat{y}1 &= -\sin\psi\,\hat{x}n + \cos\psi\,\hat{y}n \\ \hat{z}1 &= \hat{z}n \end{aligned} \qquad \text{(B2.33)}$$

(Note that $[\hat{x}1, \hat{y}1, \hat{z}1]$ are the unit vectors used in deriving the unsprung mass equations of motion.) For θ, a rotation about the $\hat{y}1$ axis:

$$\begin{aligned} \hat{x}2 &= \hat{x}1\cos\theta - \hat{z}1\sin\theta \\ \hat{y}2 &= \hat{y}1 \\ \hat{z}2 &= \hat{x}1\sin\theta + \hat{z}1\cos\theta \end{aligned} \qquad \text{(B2.34)}$$

and for ϕ, a rotation about the $\hat{x}2$ axis:

$$\begin{aligned} \hat{x}b &= \hat{x}2 \\ \hat{y}b &= \hat{y}2\cos\phi + \hat{z}2\sin\phi \\ \hat{z}b &= -\hat{y}2\sin\phi + \hat{z}2\cos\phi \end{aligned} \qquad \text{(B2.35)}$$

(Note that $\hat{x}2 = \hat{x}b$ where $\hat{x}b$ is the forward body axis of the sprung mass.)

At this point it is convenient to express Equations (B2.33), (B2.34), and (B2.35) in matrix notation. For example, Equation (B2.33) can be written as:

$$[\hat{x}1,\ \hat{y}1,\ \hat{z}1] = [\hat{x}n,\ \hat{y}n,\ \hat{z}n] \begin{bmatrix} \cos\psi & -\sin\psi & 0 \\ \sin\psi & \cos\psi & 0 \\ 0 & 0 & 1 \end{bmatrix}$$

$$= [\hat{x}n,\ \hat{y}n,\ \hat{z}n] \quad (C^{n1}) \qquad \text{(B2.36)}$$

where (C^{n1}) is equal to the matrix used to express the $[\hat{x}1,\ \hat{y}1,\ \hat{z}1]$ unit vectors in terms of the $[\hat{x}n,\ \hat{y}n,\ \hat{z}n]$ unit vectors. Similarly, Equations (B2.34) and (B2.35) may be expressed as:

$$[\hat{x}2,\ \hat{y}2,\ \hat{z}2] = [\hat{x}1,\ \hat{y}1,\ \hat{z}1] \quad (C^{12}) \qquad \text{(B2.37)}$$

where

$$(C^{12}) = \begin{bmatrix} \cos\theta & 0 & \sin\theta \\ 0 & 1 & 0 \\ -\sin\theta & 0 & \cos\theta \end{bmatrix}$$

and

$$[\hat{x}b,\ \hat{y}b,\ \hat{z}b] = [\hat{x}2,\ \hat{y}2,\ \hat{z}2] \quad (C^{2b}) \qquad \text{(B2.38)}$$

where

$$(C^{2b}) = \begin{bmatrix} 1 & 0 & 0 \\ 0 & \cos\phi & -\sin\phi \\ 0 & \sin\phi & \cos\phi \end{bmatrix}$$

Using (B2.37) to substitute for $[\hat{x}2,\ \hat{y}2,\ \hat{z}2]$ in (B2.38),

$$[\hat{x}b,\ \hat{y}b,\ \hat{z}b] = [\hat{x}1,\ \hat{y}1,\ \hat{z}1] \quad (C^{12})(C^{2b}) \qquad \text{(B2.39)}$$

where $(C^{12})(C^{2b})$ can be evaluated by matrix multiplication, that is,

$$(C^{12})(C^{2b}) = \begin{bmatrix} \cos\theta & \sin\theta\sin\phi & \sin\theta\cos\phi \\ 0 & \cos\phi & -\sin\phi \\ -\sin\theta & \cos\theta\sin\phi & \cos\theta\cos\phi \end{bmatrix} = (b_{ji}) \qquad \text{(B2.40)}$$

(Note that $(C^{12})(C^{2b}) = (b_{ji})$ where (b_{ji}) is used in Equation (B2.4b) of the text. Also note that (b_{ij}) is the matrix obtained by transposing the horizontal rows of (B2.40) with the vertical columns of (B2.40).)

Now proceeding to substitute for $[\hat{x}1,\ \hat{y}1,\ \hat{z}1]$ using Equation (B2.36), the following expression is obtained:

$$[\hat{x}b,\ \hat{y}b,\ \hat{z}b] = [\hat{x}n,\ \hat{y}n,\ \hat{z}n] \quad (C^{n1})(C^{12})(C^{2b})$$

The matrix product, $(C^{n1})(C^{12})(C^{2b})$, is equal to the matrix for the transformation (a_{ji}) which is used in Equation (B2.1b) of the text. Thus,

$$[\hat{x}b,\ \hat{y}b,\ \hat{z}b] = [\hat{x}n,\ \hat{y}n,\ \hat{z}n]\ (a_{ji}) \qquad \text{(B2.41)}$$

Carrying out the indicated multiplication (i.e., using Equations (B2.36) and (B2.40)),

$$(a_{ij}) = \begin{bmatrix} \cos\psi\cos\theta & \cos\psi\sin\theta\sin\phi-\sin\psi\cos\phi & \cos\psi\sin\theta\cos\phi+\sin\psi\sin\phi \\ \sin\psi\cos\theta & \sin\psi\sin\theta\sin\phi+\cos\psi\cos\phi & \sin\psi\sin\theta\cos\phi-\cos\psi\sin\phi \\ -\sin\theta & \cos\theta\sin\phi & \cos\theta\cos\phi \end{bmatrix}$$

(B2.42)

and transposing (a_{ji}) one obtains

$$(a_{ij}) = \begin{bmatrix} \cos\psi\cos\theta & \sin\psi\cos\theta & -\sin\theta \\ \cos\psi\sin\theta\sin\phi-\sin\psi\cos\phi & \sin\psi\sin\theta\sin\phi+\cos\psi\cos\phi & \cos\theta\sin\phi \\ \cos\psi\sin\theta\cos\phi+\sin\psi\sin\phi & \sin\psi\sin\theta\cos\phi-\cos\psi\sin\phi & \cos\theta\cos\phi \end{bmatrix}$$

(B2.43)

In summary, if the Euler angles are known, the matrix (a_{ji}) can be used to obtain the inertial axis components of a vector whose body axis components are given. To illustrate the statement above, consider the sprung mass velocity vector which is expressed, in body axis coordinates, as

$$\bar{V} = [\hat{x}b, \hat{y}b, \hat{z}b] \begin{bmatrix} u \\ v \\ w \end{bmatrix} \qquad \text{(B2.44)}$$

and, in inertial coordinates, as

$$\bar{V} = [\hat{x}n, \hat{y}n, \hat{z}n] \begin{bmatrix} XNDOT \\ YNDOT \\ ZNDOT \end{bmatrix} \qquad \text{(B2.45)}$$

Using Equation (B2.41) in (B2.44), one obtains

$$\bar{V} = [xn, yn, zn] (a_{ji}) \begin{bmatrix} u \\ v \\ w \end{bmatrix} \qquad \text{(B2.46)}$$

Equating the components of $\bar{V}$ in Equations (B2.45) and (B2.46), one obtains

$$\begin{bmatrix} XNDOT \\ YNDOT \\ ZNDOT \end{bmatrix} = (a_{ji}) \begin{bmatrix} u \\ v \\ w \end{bmatrix} \qquad \text{(B2.47)}$$

Thus the inertial components of the velocity vector, $\bar{V}$, can be calculated from the body axis components of $\bar{V}$ and the matrix, (a_{ji}), which is a function of ψ, θ and ϕ.

Since the body axes of the sprung mass are rotating with the sprung mass, the Euler angles are changing with time during a vehicle maneuver. In the following discussion the differential equations for the time rates of change of the Euler angles are derived. In the computer simulation the Euler angles are found by integrating these equations.

The time rates of change of the Euler angles are $\dot{\psi}$, $\dot{\theta}$, and $\dot{\phi}$. These angular rates can be represented by the vectors $\dot{\psi}\hat{z}n$, $\dot{\theta}\hat{y}1$, and $\dot{\phi}\hat{x}b$ (see Reference 3 for an explanation of treating angular rates as vectors.) The angular rotation vector of the sprung mass, $\bar{\omega}$, is the sum of these rates, that is,

$$\bar{\omega} = \dot{\psi}\hat{z}n + \dot{\theta}\hat{y}1 + \dot{\phi}\hat{x}b \qquad \text{(B2.48)}$$

In Equation (B2.11) $\bar{\omega}$ was defined by:

$$\bar{\omega} = p\,\hat{x}b + q\,\hat{y}b + r\,\hat{z}b \qquad \text{(B2.49)}$$

Thus, since (B2.48) and (B2.49) are two expressions for the same vector,

$$p\,\hat{x}b + q\,\hat{y}b + r\,\hat{z}b = \dot{\psi}\hat{z}n + \dot{\theta}\hat{y}1 + \dot{\phi}\hat{x}b \qquad \text{(B2.50)}$$

Now consider expressing $\hat{z}n$ and $\hat{y}1$ in the body axis system. From Figure B2-2 it can be seen that

$$\hat{y}1 = \hat{y}2 = \hat{y}b\cos\phi - \hat{z}b\sin\phi \qquad \text{(B2.51)}$$

(This result could also be derived from the matrix (b_{ij}).) It is not easy to visualize $\hat{z}n$ and thus $\hat{z}n$ is more readily obtained from the expression $[\hat{x}n, \hat{y}n, \hat{z}n] = [\hat{x}b, \hat{y}b, \hat{z}b](a_{ij})$. The answer is

$$\hat{z}n = -\sin\theta\ \hat{x}b + \cos\theta\sin\phi\ \hat{y}b + \cos\theta\cos\phi\ \hat{z}b \qquad \text{(B2.52)}$$

Using (B2.51) and (B2.52) in (B2.50) and equating the $\hat{x}b$, $\hat{y}b$, $\hat{z}b$ components, the following set of equations are obtained:

$$\left.\begin{aligned} p &= \dot{\phi} - \sin\theta\ \dot{\psi} \\ q &= \dot{\psi}\cos\theta\sin\phi + \dot{\theta}\cos\phi \\ r &= -\dot{\theta}\sin\phi + \dot{\psi}\cos\theta\cos\phi \end{aligned}\right\} \qquad \text{(B2.53)}$$

Solving (B2.53) for $\dot{\psi}$, $\dot{\theta}$ and $\dot{\phi}$, yields

$$\left.\begin{aligned} \dot{\psi} &= \frac{(q\sin\phi + r\cos\phi)}{\cos\theta} \\ \dot{\theta} &= q\cos\phi - r\sin\phi \\ \dot{\phi} &= p + \dot{\psi}\sin\theta \end{aligned}\right\} \qquad \text{(B2.54)}$$

Equations (B2.54) are integrated in the simulation to find ψ, θ, and ϕ which are used throughout the computer program to convert vector components from one axis system to another.

B3. THE MATHEMATICAL MODELS

B3.1 INTRODUCTION

The simulation consists of a large number of interconnected algorithms, each one made up of equations derived to model some aspect of the motion of the vehicle. The purpose of this section is to list the pertinent assumptions and demonstrate the analytical basis for these models.

Certain kinematic aspects of the tire model are discussed first, since the forces at the tire-road interface are a necessary part of the explanations of the other models. This discussion is divided into sections dealing respectively with the forces generated at the tire-road interface, complications arising in the wheel rotational equations and difficulties in simulating low vehicle speeds. The details of the assumed relationship between kinematics and the shear forces at the tire-road interface are left to Section B4.

Next, the equations of motion of a solid axle rear suspension are considered in depth, followed by a less detailed explanation on the independent front suspension. These analyses are followed by an explanation of the steering system. The last two parts of this section concern the equations of motion of the vehicle on an inclined roadway, and an explanation of the use of the program to simulate wind loading.

B3.2 THE TIRE MODEL

B3.2.1 NORMAL FORCES AT THE TIRE-ROAD INTERFACE. The normal force at the tire-road interface is assumed to be the sum of the static normal load on the tire plus (1) the product of the change in distance between the wheel center and the road and the tire spring rate, KT, and (2) the product of the vertical velocity of the wheel center and the tire dissipation constant, CT. In all cases, the normal force is in the $\hat{2}1$ direction, i.e., perpendicular to the road. As was pointed out in Section B2, the $\hat{2}1$ direction need not be aligned with the direction of

the gravitational force. The unit vector is, however, a constant.

It should be noted that it is not assumed that the road surface is smooth. A road profile description, in functional or coordinate form, may be introduced into the programs. However, the direction of the normal force at the tire-road interface is assumed to be constant, thus the fore-aft or lateral forces that might be expected due only to the particular shape of road undulations will not be predicted by this model.

B3.2.2 SHEAR FORCES AT THE TIRE-ROAD INTERFACE. The velocity of any wheel center (see Equation (B2.26)), is repeated here for convenience.

$$\dot{\overline{PP}} = (U1 - \dot{\psi}YU)\hat{x}1 + (V1 + \dot{\psi}XU)\hat{y}1 + \dot{Z}U\hat{z}1 \qquad (B3.1)$$

where U1, V1, and $\dot{Z}U$ indicate the velocity of the sprung mass center in the $\hat{x}1$, $\hat{y}1$, and $\hat{z}1$ direction, respectively

$\dot{\psi}$ is the rate of change of vehicle yaw angle

YU is the half track

XU is the distance in the $\hat{x}1$ direction from the sprung mass center to the wheel center.

The velocity of the wheel center in the plane of the road is precisely the first two terms of Equation (B3.1). Thus, the velocity components ui and vi of the wheel center in the $\hat{x}1$ and $\hat{y}1$ directions, respectively, are:

$$ui = U1 - \dot{\psi}YU \qquad (B3.2a)$$

$$vi = V1 + \dot{\psi}XU \qquad (B3.2b)$$

It is also necessary to determine uw, the longitudinal velocity component in the wheel plane:

$$uw = ui \cdot \cos\delta + vi \cdot \sin\delta \qquad \text{(B3.3)}$$

where δ is the steer angle. Finally, the tire sideslip angle, α, is given by (see Figure B3-1)

$$\alpha = \tan^{-1}\frac{vi}{ui} - \delta \qquad \text{(B3.4)}$$

and the longitudinal slip ratio, S, is defined as

$$S = 1 - \frac{RR \cdot \Omega}{u_w} \qquad \text{(B3.5)}$$

where Ω is the wheel spin velocity and RR is the effective rolling radius. The orientation of the tire is shown schematically in Figure B3-2.

B3.2.3 WHEEL SPIN DYNAMICS. As was pointed out in [4], there is sufficient reason to include the wheel rotational degree of freedom in a straight-line braking simulation; namely, the control devices presently used in anti-skid devices require explicit or implicit information about the rotation of the wheels. Furthermore, in developing a simulation of braking and handling maneuvers, one finds that wheel rotation rate must be calculated if the interaction between longitudinal slip and sideslip is to be taken with account.

Figure B3-3 is a free-body diagram of a rotating wheel. The equation of rotational motion is

$$JS(\dot{\Omega}) = -TT - FXW \cdot RR \qquad \text{(B3.6)}$$

where

FXW is the longitudinal force at the tire-road interface

JS is the polar moment of inertia

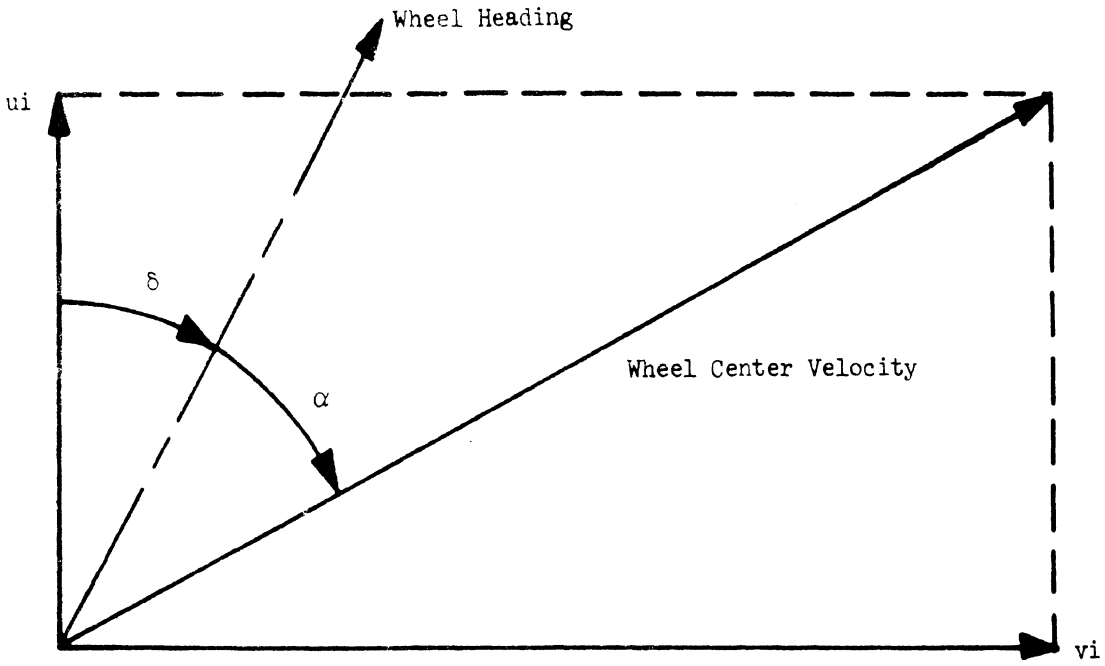

Figure 3-1. Tire-road interface kinematics

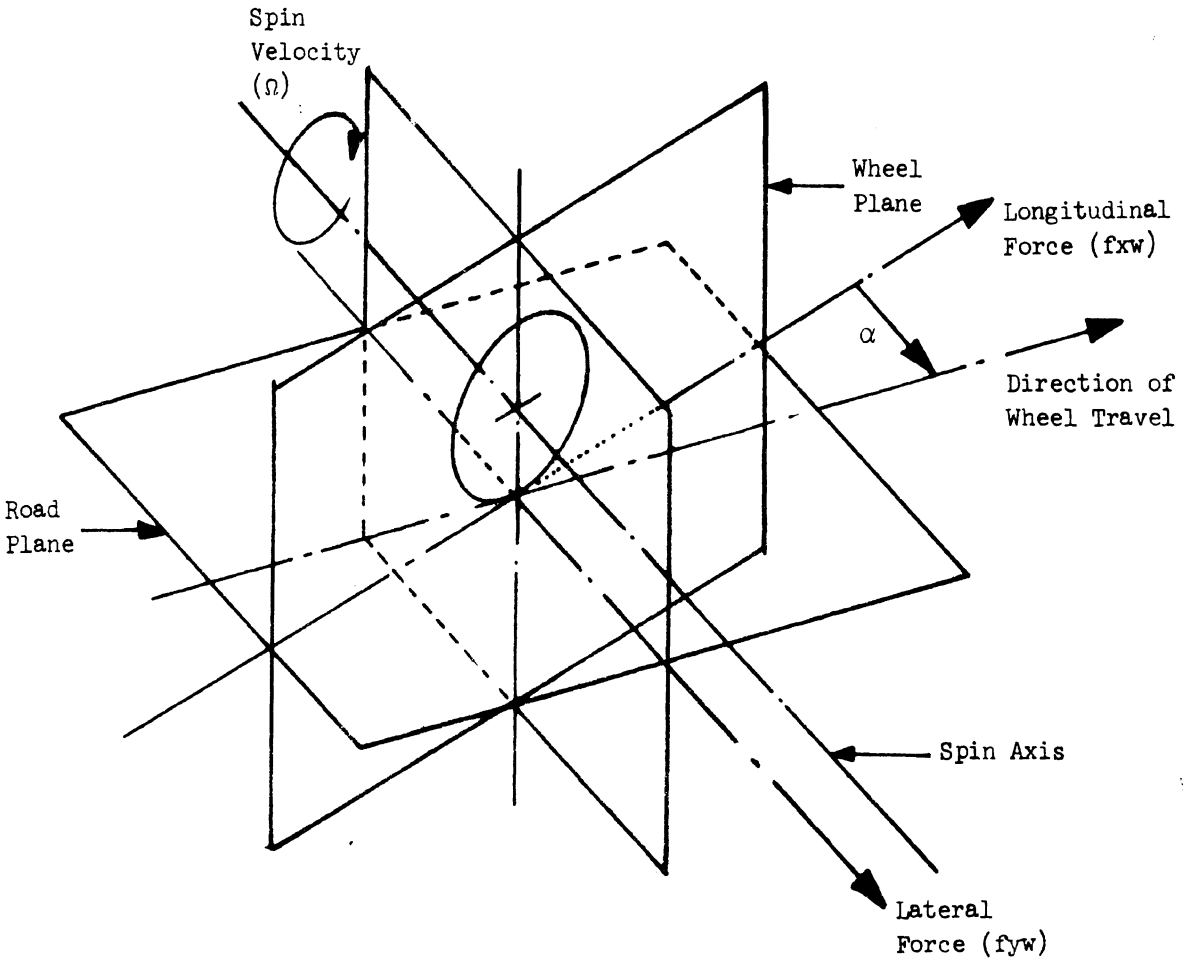

Figure 3-2. Longitudinal and lateral force components in tne tire axis system

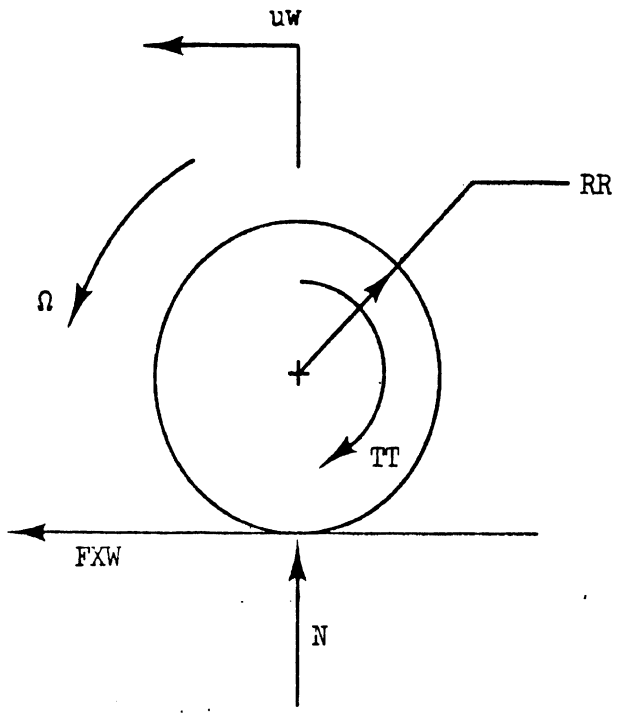

Figure B3-3. Free-body diagram: wheel with braking

The assumption may be made that, for a short time lapse, Δt (in this case, the integration time step of .005 sec), all variables with the exception of FXW on the right side of Equation (B3.7) may be approximated by a constant value. Furthermore, it may be assumed that during the time interval, Δt, FXW is a linear function of S only. The other variables affecting FXW, such as load, velocity, and slip angle, are held constant during Δt. This leads to a particularly convenient and economical formulation which allows calculation of S rather than integration of Equation (B3.6). Details may be found in [5].

B3.2.4 THE LOW SPEED APPROXIMATIONS. The calculation of the tire sideslip angle, α, given in Equation (B3.4), depends on the ratio $\frac{vi}{ui}$. For small ui, small errors in ui produce large errors in sideslip angle, resulting in inaccurate calculations of lateral force. Rather than shorten the integration time step, Δt, to preserve necessary accuracy in ui, the shear forces at the tire-road interface are assumed to remain constant when ui becomes small. Since any ui cannot be greatly different

from the longitudinal speed of the sprung mass center, U1, the following procedure is used. (See Equation (B3.2a). Note $|\dot{\psi}|$ may be expected to be significantly less than 1, |YU| is normally about 3 feet.) If U1 falls below 5 ft/sec, all the FXW and FYW values will be assumed to remain "frozen" to the value calculated at the last time when U1 was greater than 5 ft/sec. Normally this phenomenon will only be seen in a maneuver in which the vehicle is braked to a stop, or in a violent spin.

3.3 THE SUSPENSION MODELS

B3.3.1 THE SOLID REAR AXLE. A sketch of the rear axle is given in Figure B3-4. The forces at the tire-road interface and the forces between the sprung and unsprung mass must be calculated at the beginning of each new integration time step, these forces being used to calculate the accelerations of the sprung mass. The forces at the tire-road interface and the suspension forces, SF (the number 1 denotes the left side and 2 denotes the right side), are functions only of the positions and velocities of the sprung and unsprung masses, and may therefore be calculated in a straightforward manner. However, the longitudinal and lateral constraint forces between the sprung mass and the unsprung masses also depend on the acceleration of the unsprung masses, and thus computational complications arise.

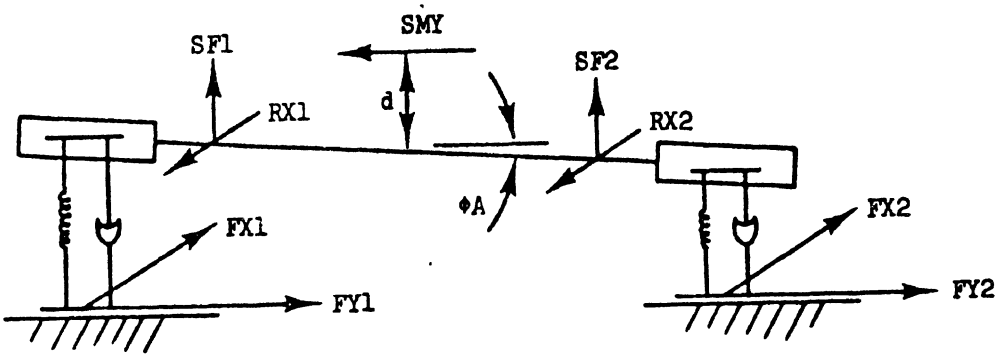

Figure B3-4. Schematic diagram: single axle model.

B3.3.1.1 The Vertical Force Calculations. The suspension force, SF, is assumed to be the sum of the force in the spring, the shock absorber, and Coulomb friction. Each of these will be considered in some detail in this section.

First consider the spring force. This must be expected to be a nonlinear function of the relative displacement between the axle center (at the spring) and the sprung mass. Thus, table lookup points of force versus deflection are input data, with the input deflection value set to zero at the rebound stop. Force values are then entered* as increasingly positive numbers corresponding to the various displacement positions.

Prior to any integrations, the static load on the suspension is calculated based on the magnitude and orientation of the sprung mass. From this load, the static position, Z1, of the suspension may easily be found as shown in Figure B3-5. The dynamic spring force may now be computed as a function of displacement from the static equilibrium condition.

It should be noted that this table may be left out by proper use of keys in the input data, as explained in Section 6, and a linear spring rate, in pounds per inch, entered in its place.

*A typical experimental setup would be to put the vehicle up on the rack and allow the rear axle to hang on the rebound stops. As the axle is picked up from below, the relative motion between the axle and the frame is measured along with the corresponding force levels. Note that this leads to a tensile load (negative) of one-half the unsprung weight at zero displacement.

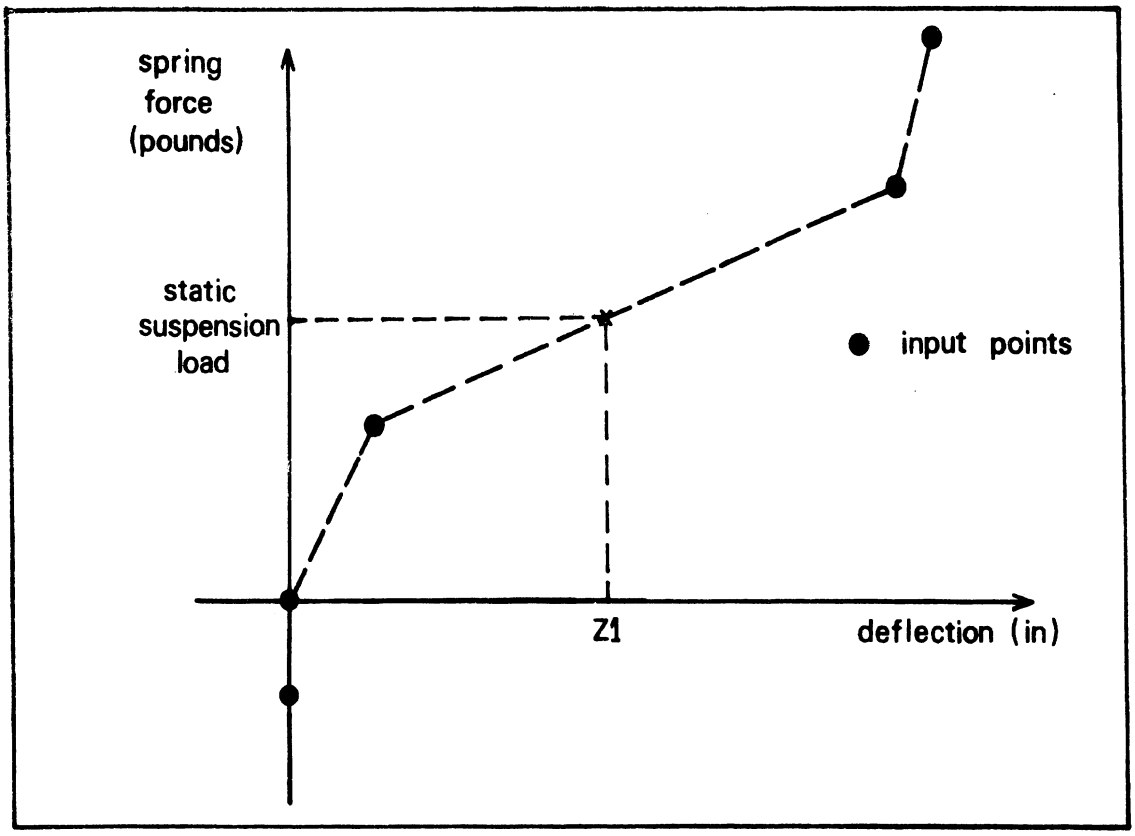

Figure B3-5. Nonlinear spring force vs. deflection.

The shock absorber force is assumed to be a bilinear* function of the suspension velocity as shown in Figure B3-6. The input paramters are the absolute values C1 and C2 of the compression and rebound slopes, respectively. It should be noted that the appropriate C1 and C2 values may be much lower than test machine data would indicate since the shock absorber may be mounted at an angle. Further, note that a linear force-velocity relationship may be attained by setting C1 = C2.

*For rough road maneuvers, a more detailed shock absorber model is in order to take blowoff into account. While such an option is not available in the present simulation, it could easily be added.

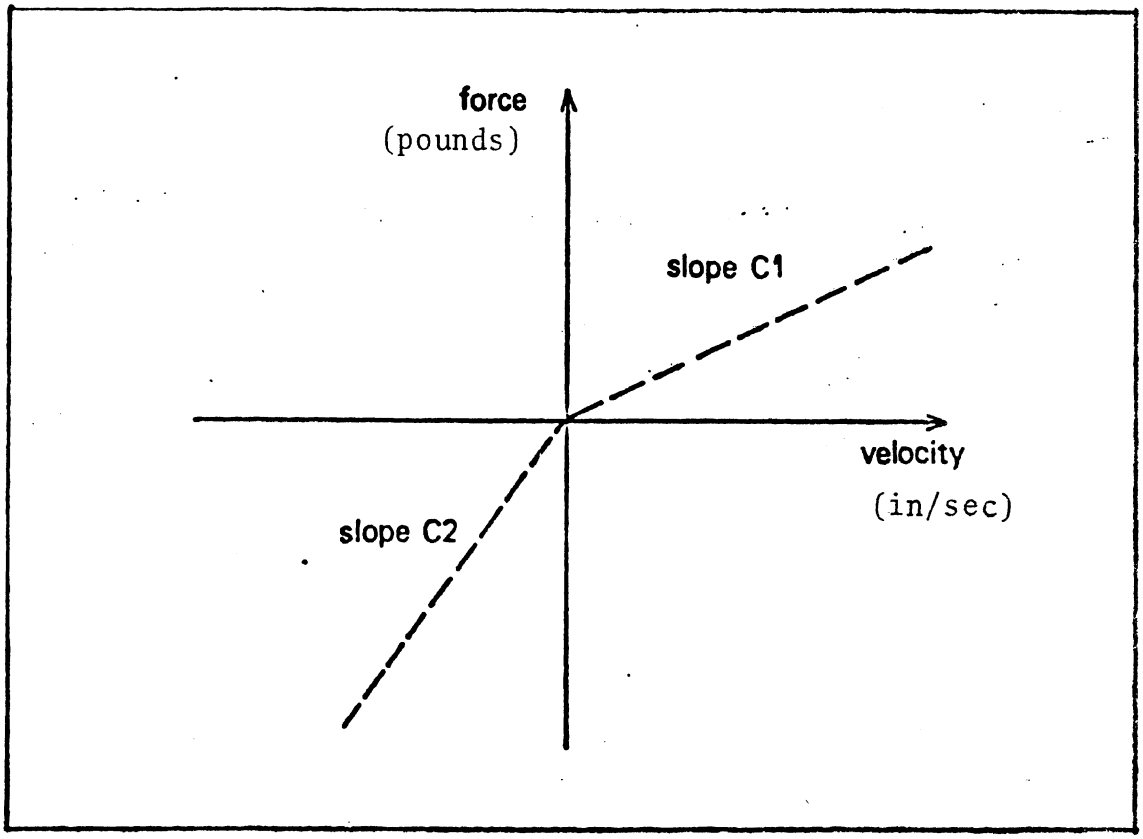

Figure B3-6. Shock absorber force vs. velocity.

The Coulomb friction force, which has maximum value, CF, is also a nonlinear function of velocity as is shown in Figure B3-7. The break points, $\delta(I)$, are calculated based on the sprung and unsprung mass inertial properties and the integration time step to assure that the suspension will not "chatter" at static equilibrium. These calculations, which are discussed in detail in Reference [6], usually lead to $\delta(I)$ substantially less than one inch per second.

B3.3.1.2 The Horizontal Force Calculations. Consideration of a free-body diagram of a wheel and of the axle will be of assistance in the analysis of this system. Consider the wheel diagrammed in Figure B3-8, in which xw, yw, and zw axles are fixed with the origin at the axle center. At the instant of interest, $\hat{2}w$ is in the $\hat{2}1$ direction, and $\hat{X}w$ is in the plane of the wheel. The axis system rotates at angular velocity, $\overline{\omega 1}$, where

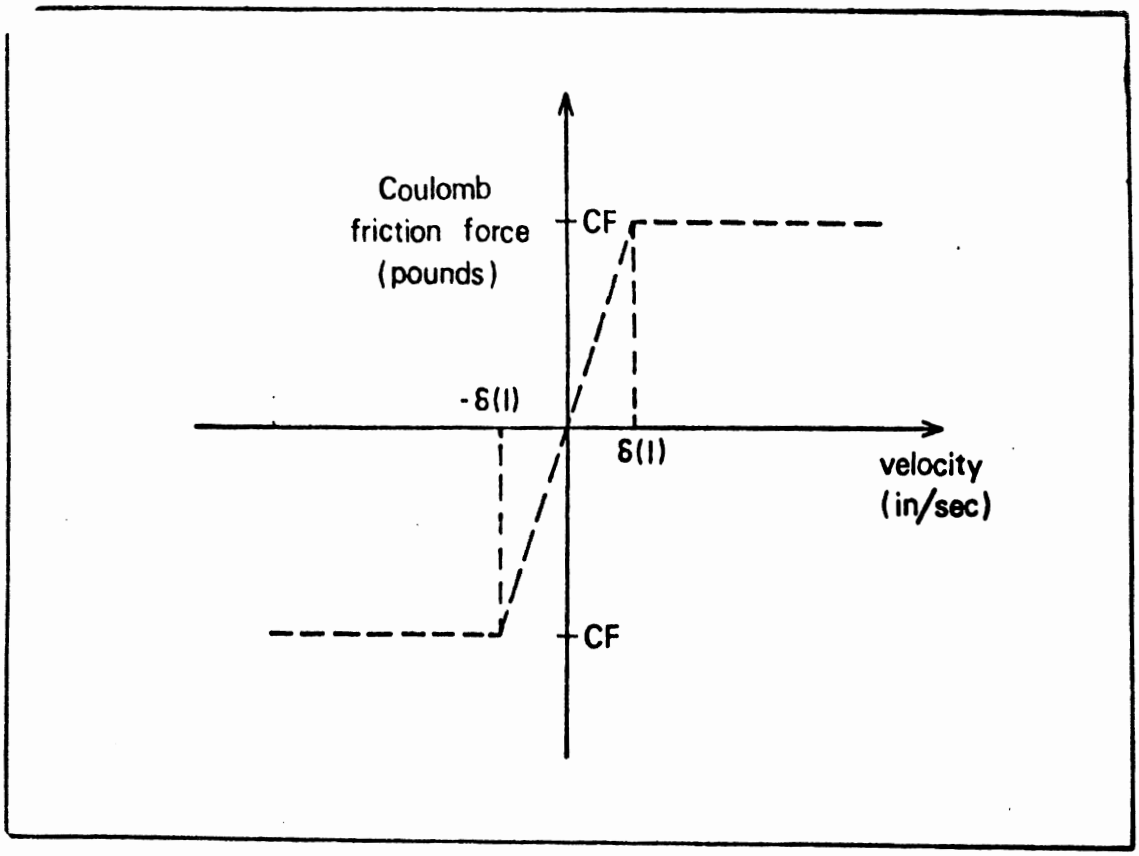

Figure B3-7. Coulomb friction force vs. velocity.

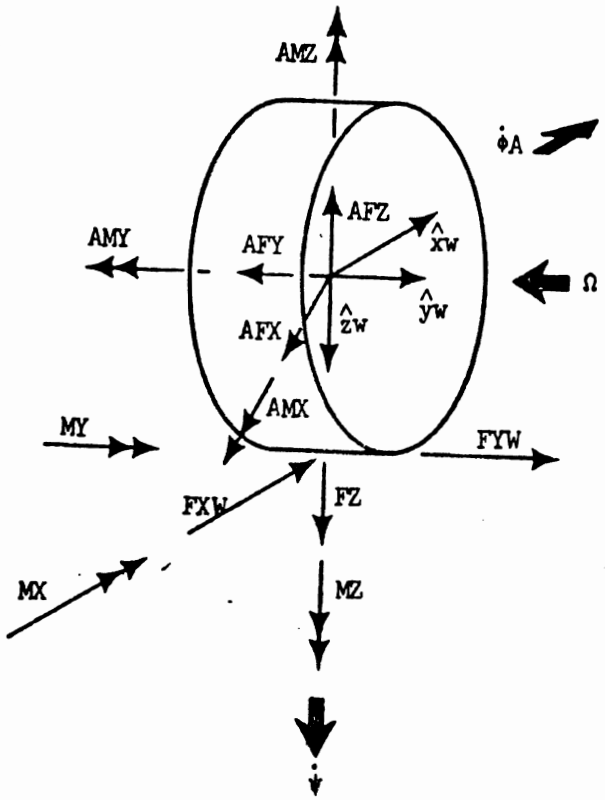

Figure B3-8. Free-body diagram: rolling wheel.

$$\overline{\omega 1} = \dot{\phi}A\ \hat{x}w - \Omega\ \hat{y}w + \dot{\psi}\ \hat{z}w \qquad (B3.7)$$

where

$\dot{\phi}A$ is the roll rate of the axle

$\dot{\psi}$ is the rotation rate of $\hat{x}1$, $\hat{y}1$, $\hat{z}1$; the yaw rate of the unsprung mass system.

Since the solid axle may reasonably be assumed to deviate only slightly from the $\hat{y}1$ direction,* it will be assumed in the following analysis that

$$\hat{y}w = \hat{y}1 \qquad (B3.8)$$

The reaction forces and moments from the axle on the wheel are AFX, AFY, AFZ, and AMX, AMY, and AMZ, respectively. The forces at the tire-road interface are FXW, FYW, and FZW; MX, MY, and MZ are the moments. Application of Newton's laws leads to (see Equation B2.32)):

$$\begin{aligned}&(FX-AFX)\hat{x}1 + (FY-AFY)\hat{y}1 + (FZ-AFZ)\hat{z}1\\ &= M_w([UD1 - \dot{\psi}^2(XU) - \ddot{\psi}(YU)]\hat{x}1\\ &+ [VD1 - \dot{\psi}^2(YU) + \ddot{\psi}(XU)]\hat{y}1 + \dot{Z}\dot{U}_w\hat{z}1)\end{aligned} \qquad (B3.9)$$

where

XU is the half track

YU is the distance in the $\hat{x}1$ direction from the sprung mass center to the mass center of the wheel

*The possible deviations are those due to roll steer and to roll angle ϕA of the axle assembly.

UD1 is the acceleration of the sprung mass center in the $\hat{x}1$ direction

VD1 is the acceleration of the sprung mass center in the $\hat{y}1$ direction

$\ddot{ZU}$ is the vertical acceleration of the wheel mass center

M_W is the mass of the wheel.

Now using the same free-body diagram, we can write the equations of rotational motion. Assuming that the polar moments of inertia of the tire about the xw, yw, zw axes are principal moments (i.e., wheel imbalance is neglected), the rotational equations for the wheel become

$$MX\text{-}AMX = JT \cdot \ddot{\phi}A + JS \cdot \dot{\psi} \cdot \Omega \qquad \text{(B3.10a)}$$

$$FX(RR) + MY\text{-}AMY = JS\ \dot{\Omega} \qquad \text{(B3.10b)}$$

$$MZ\text{-}AMZ = JT \cdot \ddot{\psi} - JS \cdot \Omega \cdot \dot{\phi}A \qquad \text{(B3.10c)}$$

where JT, JS, JT are the polar moments of the wheel about xw, yw, zw, respectively.

Now consider the free-body diagram of the axle in Figure B3-9. (The number 1 in a force or couple indicates the left-hand side, the number 2, the right). The reaction forces from the sprung mass on the axle are RX1 and RX2, SMY, and SF1 and SF2. The moment applied from the frame to the axle is assumed to be only the brake torque TT1 and TT2. The force summation in the $\hat{x}1$ direction leads to

$$RX1 + RX2 = AFX1 + AFX2 - MAX[UD1 - \dot{\psi}^2 \cdot XU] \qquad \text{(B3.11)}$$

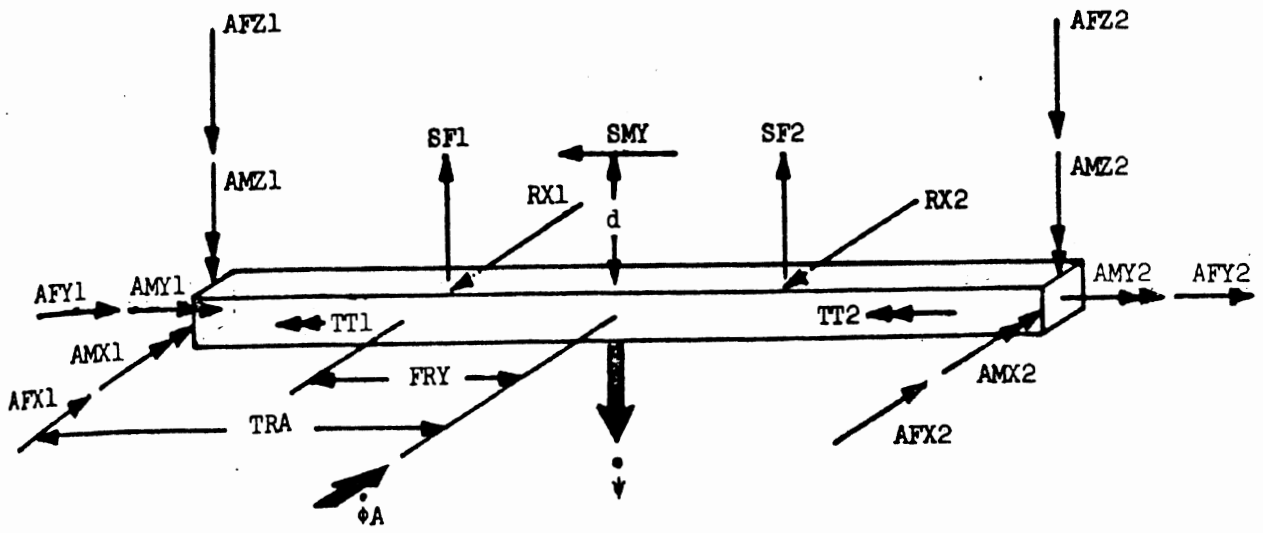

Figure B3-9. Free-body diagram: single axle

where MAX is the mass of the axle, and the axle mass center is assumed to be located such that

$$YU = 0 \tag{B3.12}$$

From Equation (B3.9) we have

$$AFX1 + AFX2 = FX1 + FX2 - 2M_w[UD1 - \dot{\psi}^2 \cdot XU] \tag{B3.13}$$

But the unsprung mass is defined as the mass of the axle plus the mass of the wheel, i.e.,

$$MS = MAX + 2M_w \tag{B3.14}$$

Thus, Equation (B3.11) may be written

$$RX1 + RX2 = FX1 + FX2 - MS[UD1 - \dot{\psi}^2 XU] \tag{B3.15a}$$

In the same way, it can be shown that

$$SMY = FY1 + FY2 - MS[VD1 + \ddot{\psi}\, XU] \qquad \text{(B3.15b)}$$

$$-SF1 - SF2 + FZ1 + FZ2 = MS \cdot \dot{Z}\dot{A} \qquad \text{(B3.15c)}$$

where ZA is the vertical position of the mid-point of the axle. Now, under the assumption that the principle moments of inertia of the axle are Ja, 0, Ja, about axes in the $\hat{x}1$, $\hat{y}1$, $\hat{z}1$ directions with origin at the axle center (i.e., the dynamics of axle "wrap up" are neglected), the Euler equations may be written for the axle.

$$(SF1-SF2)FRY + (AFZ2-AFZ1)TRA - SMY\ (d) + AMX1 + AMX2 = J_a\dot{\phi}\dot{A} \qquad \text{(B3.16a)}$$

$$AMY1 + AMY2 - TT1 - TT2 = 0 \qquad \text{(B3.16b)}$$

$$AMZ1 + AMZ2 + (AFX1 - AFX2)TRA + (RX2-RX1)FRY = J_a\ddot{\psi} \qquad \text{(B3.16c)}$$

By combination of Equations (B3.16c) and (B3.12c) we can eliminate AMZ1 and AMZ2, yielding

$$MZ1 + MZ2 + (AFX1-AFX2)TRA + (RX2-RX1)FRY$$

$$= 2(JT)\ddot{\psi} + -Js(\phi\dot{A})[\Omega_1 + \Omega_2] + J_a\ddot{\psi} \qquad \text{(B3.17)}$$

But from the $\hat{x}1$ component of Equation (B3.9) we have

$$FX1 - AFX1 = M_w[UD1 - \dot{\psi}^2 XU + \ddot{\psi}(TRA)] \qquad \text{(B3.18a)}$$

$$FX2 - AFX2 = M_w[UD1 - \dot{\psi}^2 XU - \ddot{\psi}(TRA)] \qquad \text{(B3.18b)}$$

Thus,

$$AFX1 - AFX2 = FX1 - FX2 - 2M_w \cdot \ddot{\psi} \cdot TRA \qquad (B3.19)$$

Substitution of Equation (B3.19) in (B3.16) yields

$$MZ1 + MZ2 + (FX1-FX2)TRA - 2M_w\psi(TRA)^2 + (RX2-RX1)FRY$$

$$= 2(JT)\ddot{\psi} - J_s\dot{\phi}A[\Omega_1 + \Omega_2] + J_a\ddot{\psi} \qquad (B3.20)$$

But the polar moment of inertia of the axle wheel assembly may be written as

$$JA = J_a + 2JT + 2M_w(TRA)^2 \qquad (B3.21)$$

Thus,

$$MZ1 + MZ2 + (FX1-FX2)TRA + (RX2-RX1)FRY + (JS)(\dot{\phi}A)[\Omega_1 + \Omega_2] = JA(\ddot{\psi})$$

(B3.22)

Both equations (B3.15a) and (B3.22) contain the unkown constraint forces RX1 and RX2. However, there is a major complication to using these two equations to solve for RX1 and RX2; namely, the sprung mass acceleration, UD1, and the unsprung mass angular acceleration, $\ddot{\psi}$, are unknown at this stage of this development. A rigorous solution would require the added consideration of the sprung mass equations of motion in order to solve the system of equations for the constraint forces and the accelerations.

Since we have not constrained the suspensions to remain perpendicular to the sprung mass, a rigorous approach is tedious and numerically time consuming, requiring a matrix inversion to solve for the accelerations at each time step. We have elected instead to apply an alternate, approximate method. In this method, it is assumed that the unknown accelerations of the

unsprung masses may be successfully estimated based on the assumption that the entire vehicle is moving as a single rigid body in the yaw plane.

The acceleration of the mass center of the entire vehicle is assumed to be

$$\bar{A} = \frac{GVW}{g} \sum_I (FXI\ \hat{x}1 + FYI\ \hat{y}1) \tag{B3.23}$$

where the summation sign indicates a sum over all the tires. The yaw acceleration may be written

$$\ddot{\psi}\hat{z}1 = \frac{1}{IZ} \sum_I \bar{r}_I \times (FXI\ \hat{x}1 + FYI\ \hat{y}1) \tag{B3.24}$$

where IZ is the yaw moment of the entire vehicle (assuming no roll or pitch), the $\bar{r}_I$ are the appropriate moment arms and the sum is again over all of the tires. The yaw plane components of the individual unsprung masses may now be found from Equations (B3.23) and (B3.24).

$$\bar{a}_I = \bar{A} - \dot{\psi}^2\ \bar{r}_I + \ddot{\psi}(\hat{z}1 \times \bar{r}_I) \tag{B3.25}$$

Thus, given the forces at the tire-road interface, the $\bar{a}_I$ may be used in Equations (B3.15a) and (B3.25) to calculate the forces on the sprung mass from the unsprung mass. A schematic diagram of this process is shown in Figure B3-10.

Similar equations will now be derived combining the force equations in the $\hat{z}1$ directions and moments about the $\hat{x}1$ axis.

By combining Equations (B3.16a) and (B3.22a), AMX1 and AMX2 are eliminated, yielding

$$(SF1-SF2)FRY - SMY \cdot d + MX1 + MX2 + (AFZ2-AFZ1)TRA$$

$$= (J_a + 2JT)\dot{\phi}\dot{A} + (JS)\dot{\psi}[\Omega_1 + \Omega_2] \tag{B3.26}$$

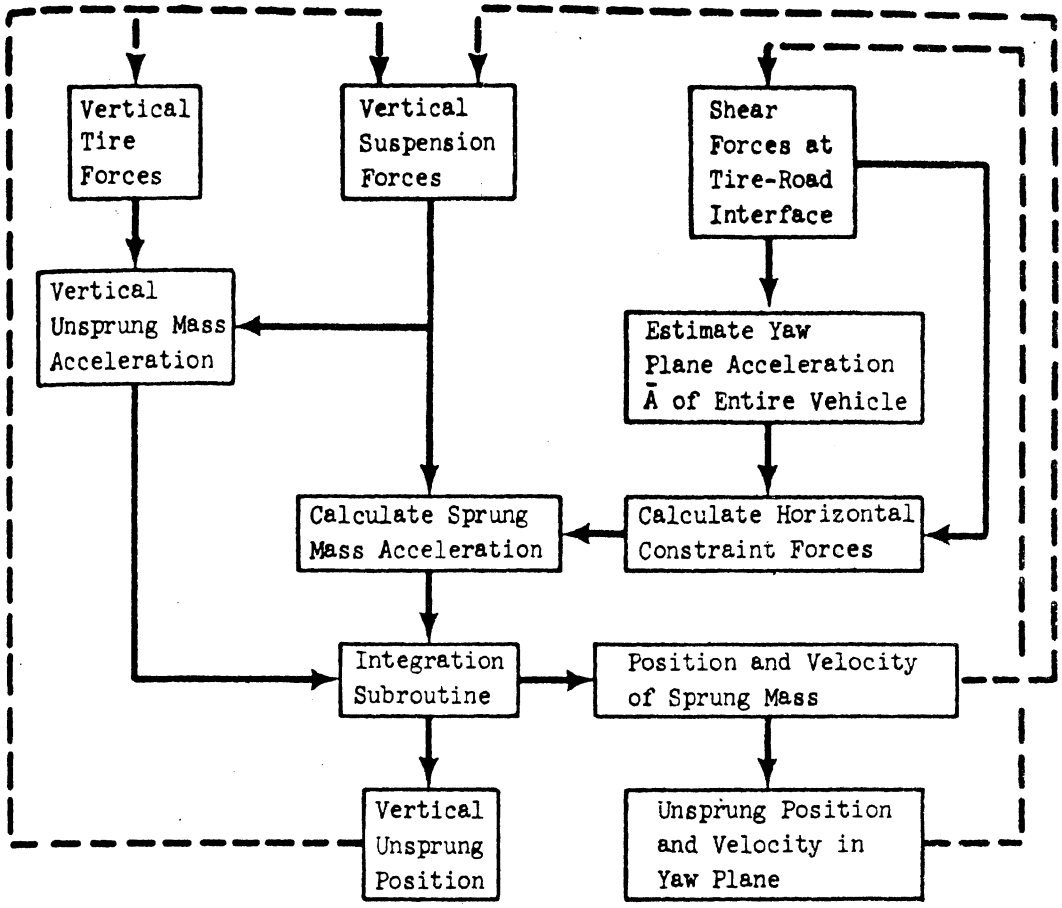

Figure B3-10. Flow diagram: method of computation of the constraint forces.

But from the $\hat{z}1$ component of Equation (B3.9) we have

$$\begin{aligned} FZ1 - AFZ1 &= M_{w1}\dot{\dot{Z}}_{w1} \\ FZ2 - AFZ2 &= M_{w2}\dot{\dot{Z}}_{w2} \end{aligned} \tag{B3.27}$$

Thus,

$$AFZ2-AFZ1 = FZ2-FZ1 + M_{w1}\dot{\dot{Z}}_{w1} - M_{wz}\dot{\dot{Z}}_{wz} \tag{B3.28}$$

The acceleration terms on the right-hand side of Equation (B3.28) may be written as

$$M_{w1}[\dot{Z}\dot{A} - TRA \cdot \dot{\phi}\dot{A}] - M_{w2}[\dot{Z}\dot{A} + TRA \cdot \dot{\phi}\dot{A}] \qquad (B3.29)$$

where ZA is the vertical position of the axle center. The use of Equations (B3.19) and (B3.28) in Equation (B3.26) leads to

$$MX1 + MX2 + (SF1-SF2)FRY - SMY(d) + [FZ2-FZ1-2M_w(TRA)\dot{\phi}\dot{A}]TRA$$

$$= (J_a + 2JT)\dot{\phi}\dot{A} + (JS)\dot{\psi}(\Omega_1 + \Omega_2) \qquad (B3.30)$$

But

$$J_a + 2JT + 2M_w(TRA)^2 = JA \qquad (B3.31)$$

where JA is the total moment of inertia of the axle and wheels around an axis in the $\hat{x}1$ direction through the axle center. Thus,

$$MX1 + MX2 - JS \cdot \dot{\psi} \cdot (\Omega_1 + \Omega_2) + (FZ2-FZ1)TRA$$

$$+ (S1-S2)FRY - SMY(d) = JA(\dot{\phi}\dot{A}) \qquad (B3.32)$$

Equations (B3.15c) and (B3.32) are used to calculate the accelerations of the axle, the former equation yielding the "bounce" acceleration of the axle center, the latter yielding the roll acceleration of the axle. The lateral constraint force, SMY, may be calculated using Equation (B3.15b) and the methods of Figure B3-10.

B3.3.1.3 Roll Steer. When the rear axle is displaced toward or away from the sprung mass while remaining parallel to the ground plane, a side view of the wheel center motion will typically show fore-aft as well as vertical motion. Thus when the sprung mass and the unsprung mass roll relative to each other, the axle must take on a so-called roll steer angle.

This steer angle may be computed in a straightforward manner. Consider the schematic diagram B3-11 in which a rear axle is shown along with a typical plot of fore-aft versus vertical deflection taken from data in which the rear axle was moved toward the sprung mass while remaining parallel to the sprung mass.

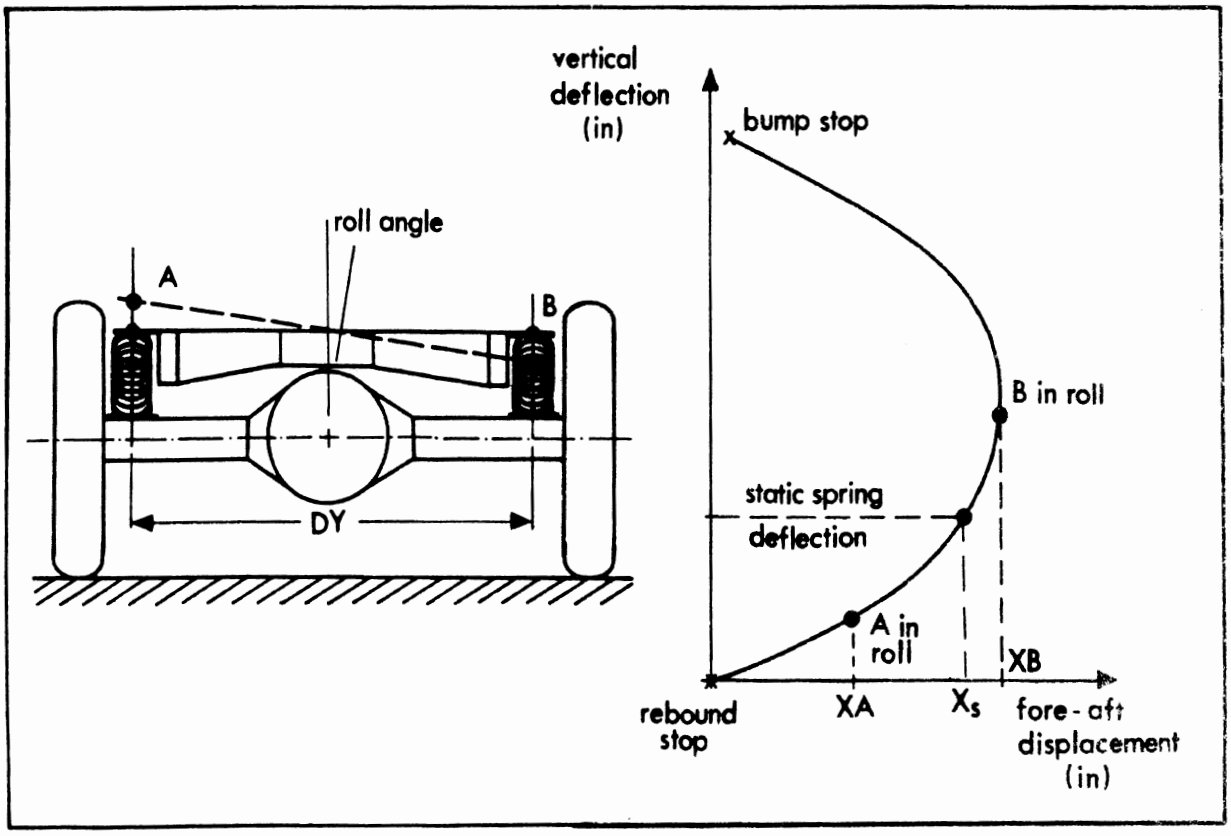

Figure B3-11. Typical plot of fore-aft vs. vertical deflection of the rear axle.

Points A and B are arbitrary points on the axle spaced DY apart, centered about the axle center line. When the sprung mass rolls relative to the axle (as in a left turn), points A and B take on different fore/aft positions as shown in the diagram. The steer angle of the rear axle is thus

$$\delta_R = \frac{XA - XB}{DY} \qquad (B3.33)$$

The input to the simulation is the table of vertical versus horizontal displacement of the axle in inches. (Vertical displacement is zero at the rebound stop, and positive as the axle moves toward the sprung mass.) The values of XA and XB are computed for the wheel centers, and thus DY is the track.

It should be noted that a simplified version of this roll steer algorithm may be called for by proper use of the keys in the input data as shown in Section 6. In this case, a simple roll steer parameter, designating degrees steer (to the right) per degree of relative roll angle between the sprung mass and the axle (i.e., body roll minus axle roll) is used to calculate the roll steer. It can easily be shown that the appropriate input value is the slope of the curve shown in Figure B3-11 at the static equilibrium position of the suspension.*

B3.3.1.4 A Summary of the Assumptions Used in the Rear Axle Model. A number of simplifying assumptions were made in the derivation of the equations of motion of the single axle in the preceding section. These are listed below.

1. Deviations of the axle from the $\hat{y}1$ direction were ignored since axle steer displacements and axle roll angle, ϕA, are expected to be small. (Note, the effects of roll steer and axle roll on tire slip angles are not neglected; rather, the effects of roll steer and axle roll angle on the orientation of the wheel axis system are neglected. Roll steer is computed as a function of the relative roll angles between the sprung mass and the axle.

*Even if the linearization is deemed accurate enough (say roll angles are expected to be small), one particularly nice feature of using a table here is that changes in load on the suspension (as by adding a payload to the vehicle) are automatically accounted for, while the single parameter would require changing with payload.

2. The wheels are balanced. Thus the mass center of the wheel is assumed to be at the axle center, and the polar moments about the xw, yw, zw axes are assumed to be principal moments.

3. Axle rotation about an axis in the $\hat{y}1$ direction (i.e., wrap up) is neglected.

4. Various assumptions have been made concerning the forces between the sprung and unsprung masses.

   a. The reactions in the $\hat{x}1$ direction are applied at the height of the axle center, and the torque about the axle is the brake torque. (Anti-pitch geometry is not considered.)

   b. The constraint in the $\hat{y}1$ direction is assumed to be a point force applied at constant distance d above the axle. (In the simulation, the input variable is the distance of RCH above the ground, i.e., the roll center height.)

   c. The suspension forces, SF, are assumed to act in the $\hat{z}1$ direction.

These assumptions lead to equations which predict the forces on the sprung mass only if the acceleration of the unsprung mass is known. These accelerations are found through an approximate method which assumes motion in the yaw plane. A diagram of the procedure is given in Figure B3-10. Using this procedure, the constraint forces RX and SMY may be computed and then used to find the acceleration of the sprung mass.

In spite of the many assumptions made, the equations given are quite detailed. Since for each added feature of the simulation the user must pay the price in both the tedium of dealing with the added input variables as well as increasing computation costs, it was decided to drop from the equations certain terms which may be considered negligibly small. Among these are

overturning moments at the tire-road interface and the gyroscopic effects caused by the yaw velocity of the axis of tire rotation. Through a straightforward modification of the program, these terms may easily be added by the user should they be considered significant.

B3.3.2 THE INDEPENDENT FRONT SUSPENSION.

B3.3.2.1 The Solution for the Constraint Forces, Vertical Position, and Spin Rate. A schematic rear view of the front suspension is shown in Figure B3-12. Just as was the case for the rear suspension, all "suspension forces," SF, are assumed to be normal to the ground plane. The springs and shocks are assumed to be at the wheel center, thus the spring rate and viscous damping must be measured corresponding to relative motion between the wheel and the sprung mass.

Lateral equilibrium is assured by the imaginary link between the tire-road interface and the front roll center. It should be noted that the link is pinned at the roll center, but fixed at the tire-road interface, thus an overturning moment may be transmitted by the link to the unsprung mass, and the vector sum of Z and Y is not necessarily along the link.

To simplify the following analysis, we will initially (rather than later as in the solid axle equations) make the following bold but nevertheless reasonable assumption:

> The front wheels may be considered to be a point mass for all calculations except the wheel spin equation.

Thus we are dropping all inertial effects due to the interaction of camber, steer and yaw angle changes. We may now write straightforward equations for this simplified system using the free-body diagram given in Figure B3-12. Application of Newton's Laws yields

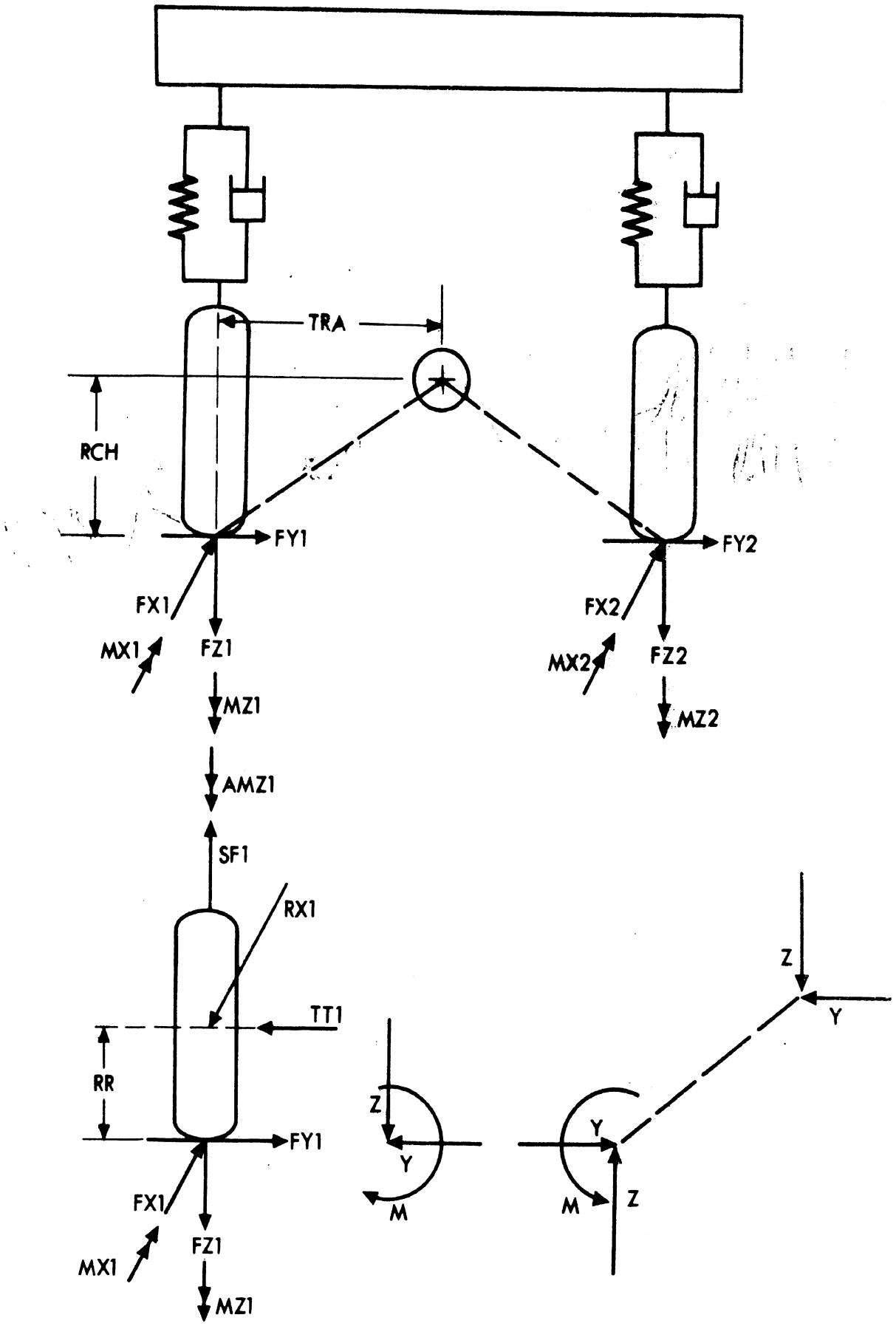

Figure B3-12. Schematic diagram, front suspension.

$$RX1 = FX1 - M_w(UD1 - \dot{\psi}^2 \cdot XU - \ddot{\psi} \cdot YU) \qquad \text{(B3.34a)}$$

$$Y = FY1 - M_w(VD1 - \dot{\psi}^2 \cdot YU + \ddot{\psi} \cdot XU) \qquad \text{(B3.34b)}$$

$$Z - M_w\dot{ZU} = SF1 - FZ1 \qquad \text{(B3.34c)}$$

where the tire-road interface forces, FX, FY, and FZ, are in the $\hat{x}1$, $\hat{y}1$, $\hat{z}1$ systems, i.e., they are not, in general, in the plane of the wheel, which is steered and cambered with respect to the unsprung mass systems.

Note that in this case the constraint forces, RX1 and Y, may be calculated immediately using the methods of Figure B3-10. Equation (B3.34c) contains two unknowns, namely, the constraint force Z and the unknown acceleration $\dot{ZU}$. But setting the moment around the $\hat{x}1$ axis to zero yields

$$M = (FY1 - Y)RR \qquad \text{(B3.35)}$$

and the vertical constraint can be found from the link equilibrium condition, i.e.,:

$$Z \cdot TRA = Y(RCH) + M \qquad \text{(B3.36)}$$

The vertical motion of the wheel may now be defined through equations (B3.36) and (B3.34c). Lastly, the wheel spin equation is elementary, viz:

$$JS\ \dot{\Omega} = - TT1 - FXW \cdot RR \qquad \text{(B3.37)}$$

where in this case shear force FXW is in the plane of the wheel and TT1 is the brake torque.

B3.3.2.2 Camber and Toe. Camber and toe must be expected to be nonlinear functions of the relative displacement between the axle center and the sprung mass. In each case, table lookup points of camber and toe versus suspension deflection are used in lieu of a complicated analytical methodology.

The camber of the left front wheel (rotation about the $\hat{x}1$ axis is considered positive) and toe of the left front wheel (rotation about the $\hat{z}1$ axis is considered positive) versus suspension deflection are input data. Left to right symmetry is assumed. The suspension deflection points should be input to the table in inches, with zero denoting the rebound stop and suspension compression positive.

It should be noted that both these tables may be left out by proper use of the keys in the input data as shown in Section 6. In this case, the camber angle is assumed to be the roll angle, and toe is neglected.

B3.4 THE STEERING SYSTEM

The most complex steering system option will be explained here. Judicious choice of simpler models may be effected by proper usage of keys set in the input data, as explained in Section 6.

First consider the flow diagram given in Figure B3-13. Note that the user must supply a steering wheel angle versus time table of points. The steer data points are each input to a table of left and right wheel angles versus steering wheel angle in the absence of aligning torque. The use of these tables leads to computed tables of desired left and right steer angles, $\overline{\delta L}$ and $\overline{\delta R}$, versus time. Note that all these calculations, which are shown schematically above the dashed line in Figure B3-13, take place as a prelude to the simulation of the vehicle response to the input steering wheel angle. The resultant $\overline{\delta L}$ and $\overline{\delta R}$ include the effects of lash and Ackerman geometry,

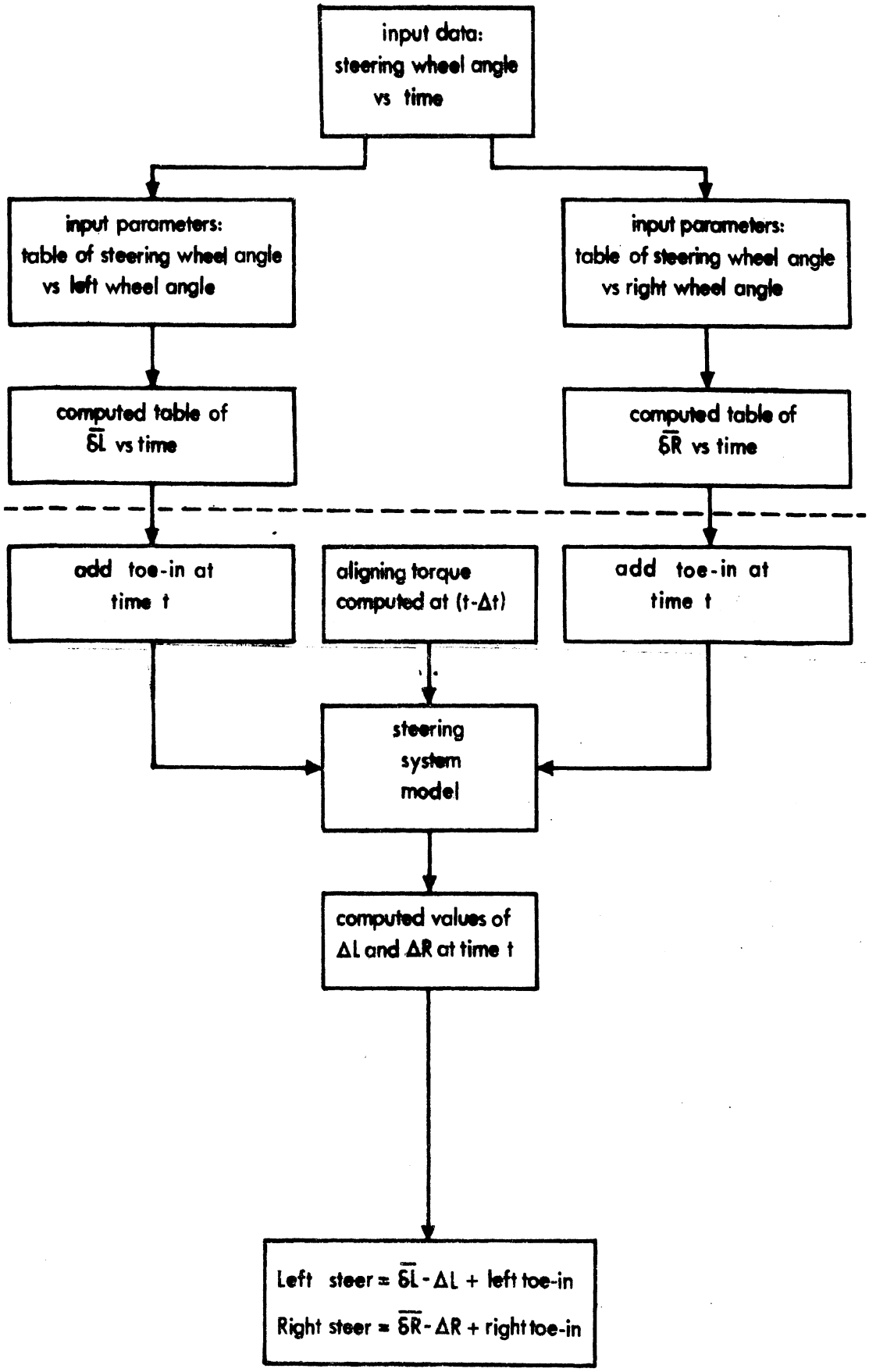

Figure B3-13. Flow diagram, steering system model.

but not the effects of aligning torque and toe-in* which must be computed "on the fly" during the integration procedure.

The variations from the desired steer angles, $\overline{\delta L}$ and $\overline{\delta R}$ to the action of aligning torque on the steering system are computed quasi-statically during the course of the simulation. These computations are shown schematically below the dashed line in Figure B3-13.

Note that since the steer angle depends on the aligning torque and the aligning torque depends on the steer angle (this latter relationship is nonlinear), the solution for α may be a complicated procedure. However, we have chosen to obviate any complications with an "updating" scheme which will be explained below.

The aligning torque acting on the steering system derives from three sources, namely,

1. The moment of the lateral force about the kingpin due to caster. This moment is computed as

$$M1 = -FY \cdot TRAIL \qquad \text{(B3.38)}$$

where TRAIL is the moment arm from the projections of the wheel center to the ground plane forward to the kingpin axis. (The negative sign is used to signify that positive aligning torque, which is in the $\hat{z}1$ direction, results from negative FY.)

2. The moment of the longitudinal force about the kingpin. This moment is computed as

$$\begin{aligned} M2L &= FXL \cdot KPOFF \\ M2R &= -FXR \cdot KPOFF \end{aligned} \qquad \text{(B3.39)}$$

---

* For details of the toe calculation, see Section B3.2.2.

where KPOFF is the kingpin offset. Note the signs change from side to side since the kingpin is always inboard of the longitudinal force.

3. The aligning torque due to the displacement of the shear force application point away from the projection of the wheel center in the ground plane. This value is taken directly from tabular input test data as a table lookup function of normal load and sideslip angle. An explanation of the use of this table lookup is given in Section 6.

It should be noted that the aligning torque derives from a knowledge of the sideslip angle, α, both implicitly in the FX and FY calculations and explicitly in the table lookup. Since the aligning torque has a first-order effect on the value of α, an exact solution for α and aligning torque would be quite tedious. Rather than attempting an analytical solution or applying iteration techniques, we have computed the above three aligning torque components using the shear force values and α value which were valid during the previous digital integration time step as shown in Figure B3-13. While the technique results in a major simplification in the computations, no significant lags are introduced since the digital integration time step is very small (usually .005 sec.).

The quasi-static model for the changes in steer due to compliance may be explained with the aid of Figure B3-14. The springs are, of course, torsional, and the outputs of the model are the changes ΔL and ΔR in left and right steer angle due to the application of aligning torques ATL and ATR. (Positive aligning torque is shown to the right.) The spring rate, KSL, represents the steering linkage, and KSC represents the steering column. The parameter GR represents the steering gear ratio.

The torque applied to the steering column is

$$T = \frac{ATL + ATR}{GR}$$

thus the angular displacement of point A is

$$\delta A = \frac{ATL + ATR}{KSC \cdot GR^2}$$

The change in angular displacement of the left and right wheels from the desired steer angles are therefore

$$\Delta L = \frac{ATL + ATR}{KSC \cdot GR^2} + \frac{ATL}{KSL} \qquad \text{(B3.42a)}$$

$$\Delta R = \frac{ATL + ATR}{KSC \cdot GR^2} + \frac{ATR}{KSL} \qquad \text{(B3.42b)}$$

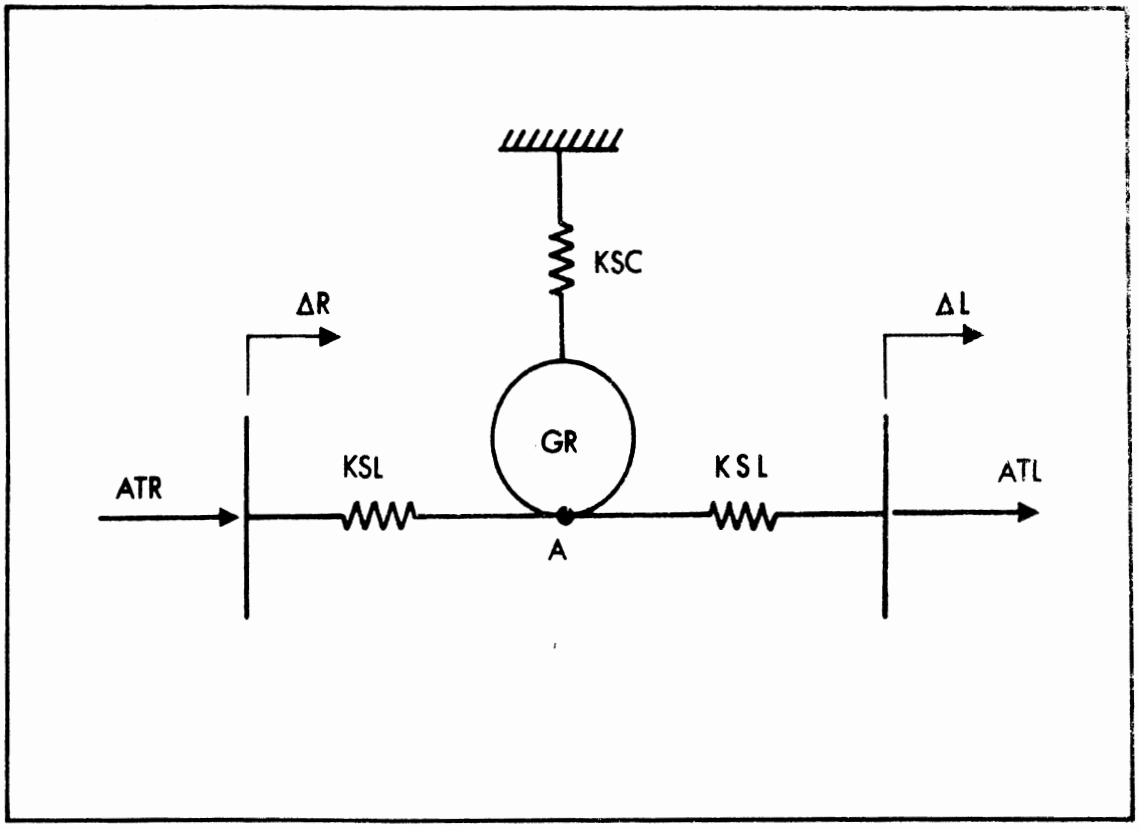

Figure 3-14. Schematic diagram, steering system.

B3.5 THE INCLINED ROADWAY

There is good reason to wish to simulate vehicle performance on real roads. Careful simulation of an actual site could provide insight into the effects of the surface, grade, superelevation and curvature on vehicle performance, and the combinations of vehicle and roadway factors which simulation shows to be causes for loss of control might be compared with the accident data from that site. However, there are serious difficulties to contend with before such a simulation is feasible.

The first, and perhaps most serious, difficulty is the necessity to "close the loop" if a real road is to be simulated, i.e., to calculate the steer angles during the course of the simulation such that the vehicle model will follow the roadway, rather than to give an input set of steer and braking data and calculate the path of the vehicle model. Simple closed loop models have been attempted (for example, [7], [8], [9]). However, it is the belief of the authors of this work that the simulation of an actual driver is a complex task beyond the capabilities of simplified techniques, and that a simple model might, in some cases, hide meaningful results available from open loop simulation. The user may, however, elect to "close the loop" himself, since a driver model such as those given in [8] and [9] may be easily added to the present simulation.*

In lieu of a driver model, one might wish to specify a realistic terrain and try to gain insight through the analysis of open loop vehicle simulation on such a terrain. This work has been accomplished successfully by McHenry and Deleys for an automobile [10]. The equations of the terrain, however, are much more complicated than those presented herein, and it was felt

*The steer model given in [8] is different conceptually from those considered here. The front wheel steer and the braking are degrees of freedom in this model, and the desired trajectory is the input function of time.

that such additional complications would not be in the overall user interest in the case of the present model.

In view of these considerations, it was decided to use a roadway model in which the normal forces at the tire-road interface are assumed to have only a $\hat{z}_n$ component. Thus the model may be thought of as a planar surface, possibly inclined, extending as far as is necessary in the XN and YN directions. It is not, however, assumed that this road surface is smooth. Road profile data in functional or coordinate form may be introduced. But since the normal forces at the tire-road interface do not vary in direction, the fore-aft or lateral forces that might be expected due to surface undulations will not be predicted by the model.

B3.5.1 THE EQUATIONS OF THE INCLINED ROADWAY. The initial speed in the longitudinal direction is a user input variable; all other initial conditions are set to zero. Thus, initially, on a level surface the suspension forces add up to the weight of the sprung mass and the moment of the suspension forces about any point is identically zero. The normal forces at the tire-road interface add up to the gross vehicle weight.

This choice of initial conditions, together with the assumption that the vertical suspension forces do not change direction as a function of the orientation of the sprung mass, allow an important simplification of the equations of motion if the roadway is not inclined. In the summation of forces on the sprung mass, only the change in load in the suspensions need be considered, since the static loads will always be equal and opposite the weight of the sprung mass. Thus this choice of coordinates allows consideration of the sprung and unsprung mass equations of motion without any consideration of the force of the weight of the sprung and unsprung masses.

The problem becomes slightly more complicated if the roadway is inclined, since the suspension forces and normal forces

remain normal to the road rather than opposite in direction to the gravitational forces. The following is the procedure for adjusting the equations of motion to accommodate an inclined roadway:

1. The [X1, Y1, Z1] and [XN, YN, ZN] systems (the unsprung mass system and the inertial system, respectively) are again taken to be colinear initially. The direction of $\hat{x}1$ and $\hat{y}1$ will, of course, change in time with the vehicle yaw angle. Note that $\hat{x}n$ and $\hat{y}n$ are in the road plane and $\hat{z}n$ is perpendicular to the road.

2. The gravity force field, whose direction will be defined by the unit vector $\hat{g}$, may be at an angle with $\hat{z}n$. The user input variables are g1 and g2 where

$$\hat{g} = g1\ \hat{x}n + g2\ \hat{y}n + g3\ \hat{z}n \qquad \text{(B3.43)}$$

and

$$g3 = \sqrt{1 - g1^2 - g2^2} \qquad \text{(B3.44)}$$

Thus the components of the vector $\hat{g}$ define the direction of gravitational forces, or, from a different point of view, the orientation of the "road." A few examples may be helpful.

$$\text{(a)} \qquad g1 = g2 = 0 \qquad \text{(B3.45)}$$

The gravitational field vector $\hat{g}$ has no component in the $\hat{x}1$ or $\hat{y}1$ directions. Therefore, this surface has no inclination angle.

$$\text{(b)} \qquad g1 = .05 \qquad g2 = 0 \qquad \text{(B3.46)}$$

The cosine of the angle between $\hat{g}$ and $\hat{x}n$ is 0.05. Thus the XN axis inclines downward. The included angle β may be found to be

$$\beta = 90° - \cos^{-1}(.05) \cong 3° \qquad \text{(B3.47)}$$

This corresponds to an initial orientation of the vehicle as facing directly downhill on a 5% grade.

(c) g1 = 0, g2 = .05 (B3.48)

The cosine of the angle between $\hat{g}$ and $\hat{y}n$ is 0.05. Thus the YN axis inclines downward as shown in Figure 3-15. The angle labeled β is again about 3°.

The choice of non-zero g1 or g2 or both implies that the gravitational forces applied to the sprung and unsprung masses are not opposite in direction to the suspension forces and the normal forces at the tire-road interface. The appropriate adjustments, however, may be made in a straightforward manner. The initial position of the vehicle will be chosen to be the trim position of the vehicle whether or not the vehicle is on a flat surface. Thus, just as in the case of the flat surface, all initial conditions except the initial speed are zero. As a result, the sprung and unsprung masses cannot be in equilibrium initially unless g1 and g2 are zero.

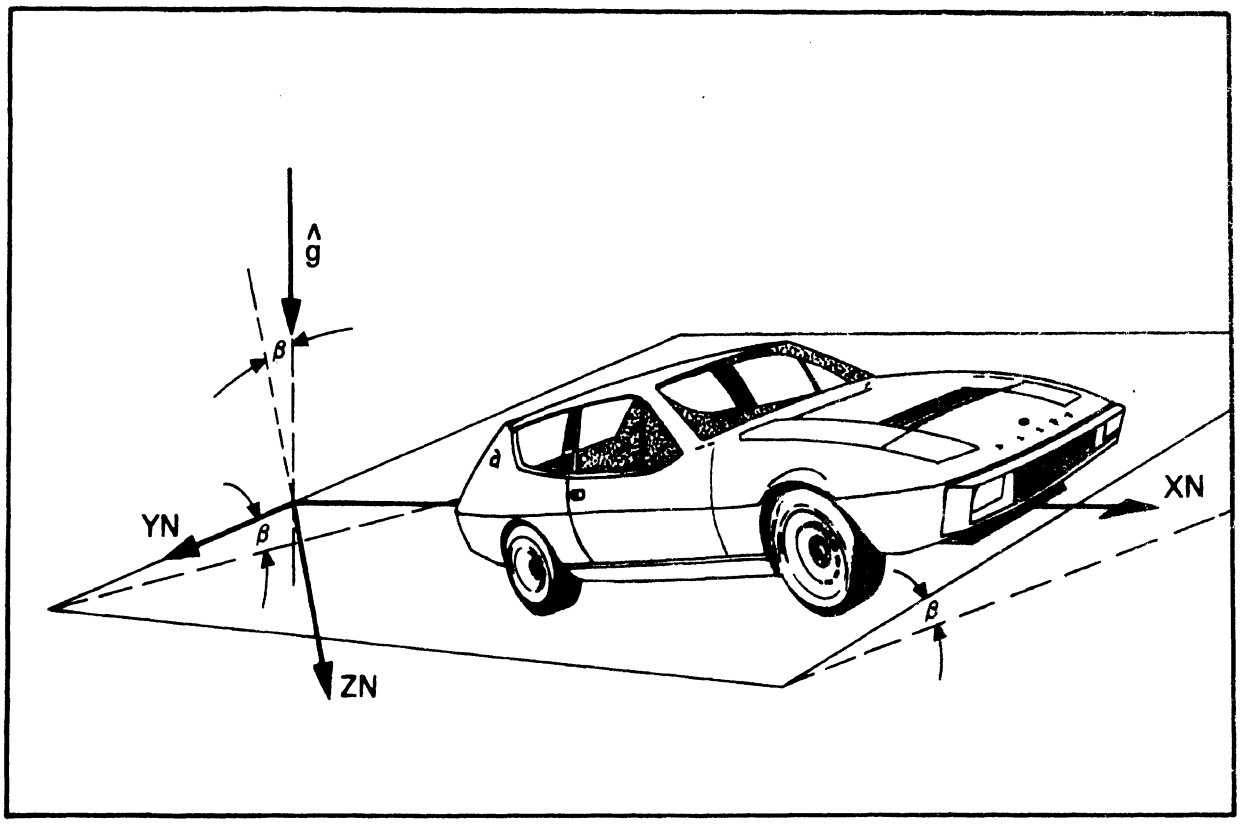

Figure 3-15. The inclined roadway: g1 = 0.0, g2 = 0.05.

In the case of non-zero g1 and g2, initially there must be a force imbalance on both the sprung and unsprung masses. On the sprung mass the combination of the suspension forces and the weight may be written

$$\Sigma\bar{F} = (\Sigma SF)\hat{z}n + W[g1\ \hat{x}n + g2\ \hat{y}n + g3\ \hat{z}n] \qquad (B3.49)$$

where the first term on the right side is the total suspension force and the second is the sprung weight. Note that, since initially the SF have no net moment about the sprung mass center, there is no moment imbalance.

Equation (B3-49) may be rewritten

$$\Sigma\bar{F} = (\Sigma SF + W)\hat{z}n + W[g1\ \hat{x}n + g2\ \hat{y}n + (g3-1)\hat{z}n] \qquad (B3.50)$$

The first term in Equation (B3.50) is calculated by the algorithm used for a level surface and the second, which is constant, is an additional force applied at the sprung mass center.

The same analysis may be done in the case of the unsprung masses. At each unsprung mass center the force

$$\bar{F} = MS \cdot g[g1\ \hat{x}n + g2\ \hat{y}n + (g3-1)\hat{z}n] \qquad (B3.51)$$

where MS is the appropriate mass, and g is the gravitation constant, may be applied, with the calculation of normal forces and slip angles taking place in the usual way.

B3.6 AERODYNAMIC DRAG

The possible modes of application of wind drag are many and varied. While analytical work has been done and has offered insight into the problem, a purely theoretical base on which one might draw in order to write equations suitable for use in vehicle simulation is by no means complete. Nevertheless,

aerodynamic drag may be an important factor in the calculation of the speed of the vehicle as, for example, during the coast-down period before initiation of a trapezoidal steer maneuver. To facilitate the simulation of an approximate drag force without undue user effort, we have in this case chosen a very simple approach. The total drag force has been assumed to apply in the $-\hat{x}1$ direction at the vehicle mass center. The magnitude of this force $|F|$ is

$$|F| = \text{WIND} \cdot u^2 \qquad \text{(B3.52)}$$

where WIND is a user input constant and u is the longitudinal speed of the vehicle in feet/sec.

B4. A TIRE MODEL FOR USE IN THE SIMULATION OF LIMIT MANEUVERS

B4.1 INTRODUCTION

The most important and most difficult single aspect of the simulation of the braking and directional response of vehicles is the formulation of the analytical representation to yield the shear forces at the tire-road interface. These representations are invariably "semi-empirical," i.e., tire models which combine certain known and/or hypothetical characteristics of the physics of the tire-road interface with measured test data.

Many semi-empirical models have been presented in the literature (see, for example, [11, 12, 13]). These models have been used, with varying success, to explain the shear-force generation process at the tire-road interface, and, in some cases, to compute these forces for purposes of vehicle simulation. None of these models, however, is ideally suited for simulating limit maneuvers. Accordingly, an improved tire model has been produced for use in the present program.

Our goals for this model are listed below:

1. The model should adequately predict (a) the lateral forces generated by a steered tire, (b) the longitudinal forces generated by a straight-running tire under the influence of braking, and (c) combinations of the two. By "adequately", we mean that we expect computed data to be within 5% or less of measured data under all conditions.

2. The model should be economical to use from the point of view of (a) the expense involved in the empirical generation of tire data suitable for the derivation of parameters for use in the computations, (b) the user time required to feed these parameters into the computer, and (c) the expense involved in the computations.

3. The model should be based, as much as possible, upon the physics perceived at the tire-road interface.

The last of these goals tends to conflict to a certain extent with the others, particularly with respect to the stipulations on expense. However, it will be shown below that a reasonable trade-off has been conceived such that, while the newly developed algorithm requires only routinely measured data as input and lends itself to quite economical computations, the connection to the physics of the tire-road is sufficient to allow the user to "estimate" a reasonable tire traction field based on sparse data. (This practice is not, however, recommended, and has not been necessary in the present program in which sufficient tire data has been generated.)

It is important to note that no attempt has been made here to model the generation of moments at the tire-road interface. It was felt that accurate and economical computations of aligning moment are not feasible at this time, thus, provision has been made to directly load tabular data points of measured aligning moment versus slip angle and load for use in straightforward interpolation. (Data supporting this position have been presented in Reference 14.) In this same spirit, overturning moments have been neglected as a small effect, and rolling resistance has been assumed to be equal to 2% of the normal load on the tire.

In Section B4.2, the kinematic considerations will be presented, and the basic constitutive relations governing the adhesion or sliding of tire elements relative to the road. In B4.3, the equations for the shear forces are derived, and in B4.4 a detailed discussion of each of the various parameters of the model is presented. Finally, in Section B4.5, comparisons are given between computed and measured tire traction fields.

B4.2 KINEMATICS

This derivation is based on an idealization of the tire-road contact region geometry as shown in Figure B4-1. The tire is considered to have zero inclination angle with the effects of inclination on the forces produced accounted for in an approximate manner through the introduction of an "equivalent slip angle", which is a function of the inclination angle and the tire's camber stiffness. This approximation is discussed in detail in Reference [11].

Line 0-1-2 (in Figure B4-1) is the longitudinal centerline of the tire-road contact patch. The ξ-η ground plane coordinate system has its origin at point 0, the tread touchdown point, with the ξ axis passing through point 2, the tread liftoff point. Line 3-4 is the longitudinal centerline of the tire carcass. Each point on the carcass centerline is assumed to be elastically connected to the tread (line 0-1-2) through orthogonal "springs" producing independent forces in the ξ and η directions. Thus a point on the tread follows the path of the carcass so long as no shear force acts on it.

In the analysis performed by Fiala [12], the configuration of the carcass centerline, line 3-4, is derived by assuming it to behave as an elastically-supported beam subjected to a point (lateral) load at its center. The resulting infinite series is approximated by a parabola. In the present analysis, we make the more arbitrary assumption that the carcass centerline deformation may be approximated by a contant; thus line 3-4 lies in the vertical plane passing through the ξ axis. The validity of this rather bold but often used assumption (see [13]) can only be assessed from a practical standpoint on the basis of comparisons between calculated and measured results.

Point 1 of the tire tread centerline represents the "sliding boundary"; points on the tread forward of point 1 (line segment 0-1) adhere to the ground surface without sliding.

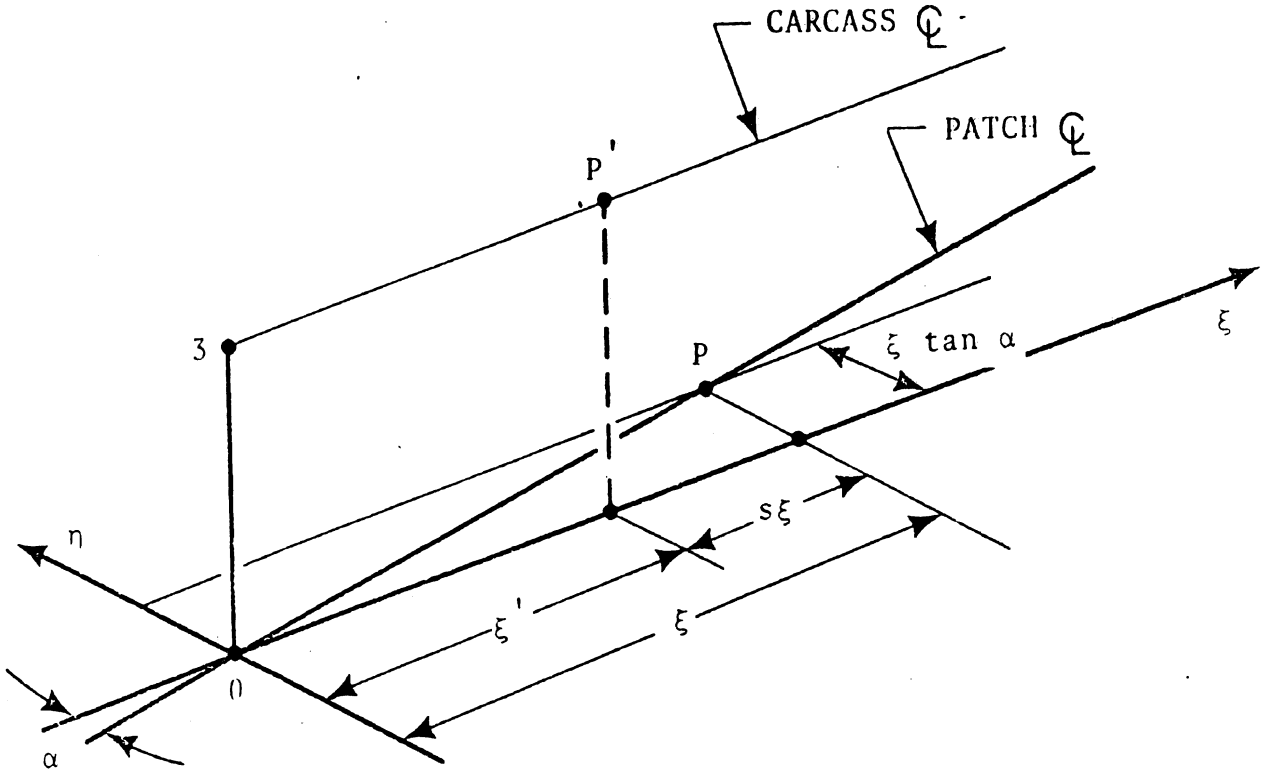

Figure B4-2. Strain condition in non-sliding portion of contact patch.

At point 1, the elastic stresses due to tread deformation reach a value corresponding to the tire-road shear stress limit and the rubber begins to slide relative to the ground. Accordingly, the shear deformation along line segment 1-2 is a function of the local sliding friction potential.

Figure B4-2 is a sketch depicting the hypothesized deformation condition prevailing at a typical point $P(\xi,\eta)$ on the non-sliding segment (0-1) of the patch centerline. The longitudinal coordinate of point P is equal to the product of the tire's longitudinal velocity (u_w) and the time interval, Δt, from the instant when P entered the patch at 0 to the instant pictured, i.e.,

$$\xi = u_w \Delta t \tag{B4.1}$$

During the same interval Δt, point P' on the carcass centerline (which coincided with point 3 at the start of the interval) has moved a distance ξ' given by

$$\xi' = \Omega R_e \Delta t \tag{B4.2}$$

where R_e is the rolling radius of the tire and Ω is the wheel spin velocity. Thus the longitudinal deformation of point P relative to point P' is given by

$$\begin{aligned} \xi - \xi' &= u_w \Delta t - \Omega R_e \Delta t \\ &= \left(1 - \frac{\Omega R_e}{u_w}\right) u_w \Delta t \\ &= s\xi \end{aligned} \tag{B4.3}$$

and the longitudinal component of stress at point P is equal to

$$\sigma_\xi = K_x s \xi \tag{B4.4}$$

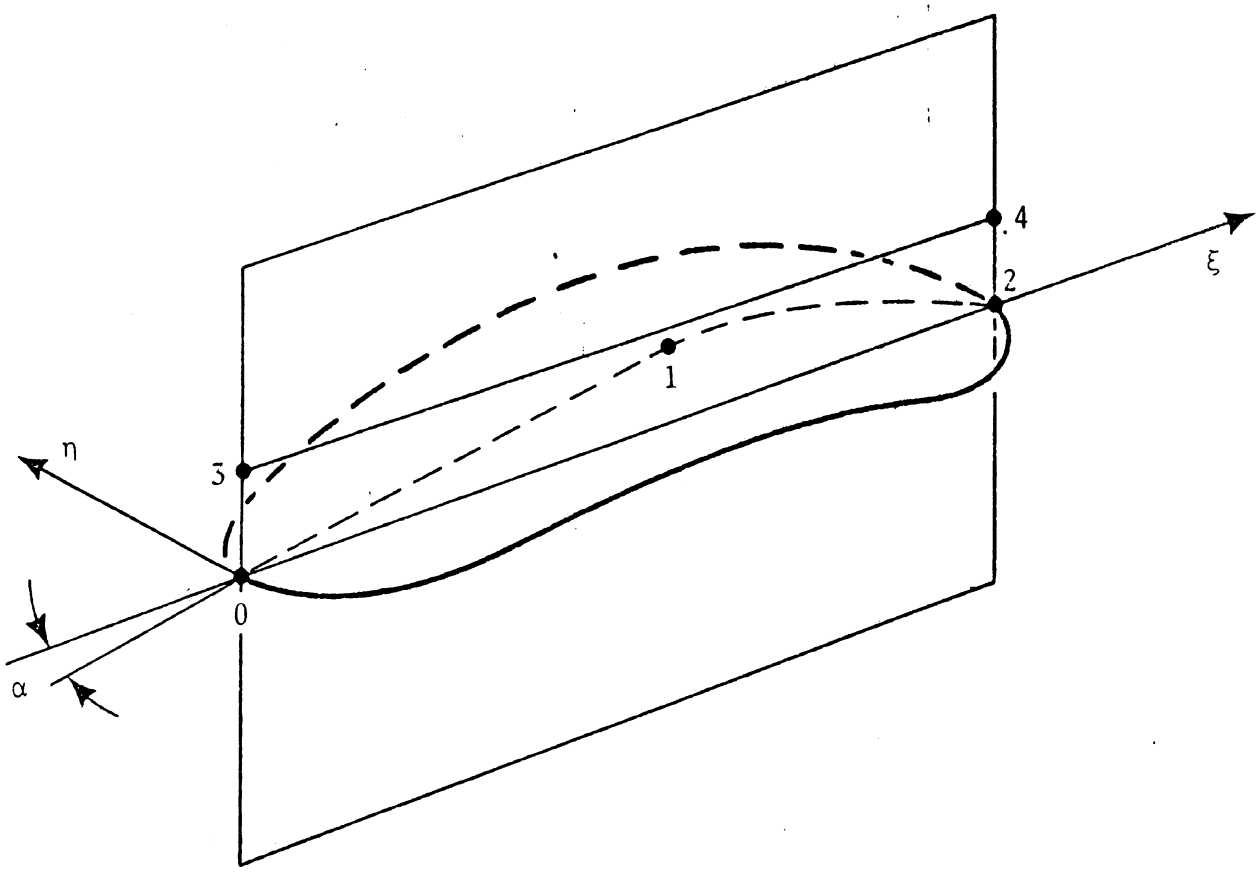

Figure B4-1. Tire-road contact region geometry.

where K_x is the "longitudinal tire stiffness," in pounds per unit length, per unit width, per unit longitudinal deflection.

The lateral deformation of point P is given by* (see Figure B4-2):

$$\eta = -\xi \tan \alpha \tag{B4.5}$$

Thus the lateral stress component at P is equal to

$$\sigma_\eta = -K_y(\tan \alpha)\xi \tag{B4.6}$$

where K_y is the "lateral tire stiffness," in pounds per unit length, per unit width, per unit lateral deflection.

The maximum allowable total shear stress at any point in the contact patch, σ_{max}, is assumed to vary with ξ'. One of the main factors determining σ_{max} is the distribution of the normal pressure, p, over the contact patch. It will be assumed that the pressure distribution over the contact patch area will be trapezoidal** in form in the longitudinal direction and uniform in the lateral direction as illustrated in Figure B4-3.

The summation of forces in the vertical direction yields a simple expression for the maximum pressure in terms of the total normal load, F_z, the length of the contact patch, 2ℓ, the width of the contact patch, w, and the length of the increasing and decreasing pressure zones, a.

$$P_{max} = \frac{|F_z|}{(2\ell - a)w} \tag{B4.7a}$$

---

*Note that the sideslip angle, α, shown in Figure B4-2 is a negative angle.

**This assumption allows the use of a uniform pressure distribution, as in Reference [11], by setting a = 0. It has been shown (see Reference [14]),however, that a uniform pressure distribution is not reasonable in many cases, thus the variable slope at the extremes of the contact patch.

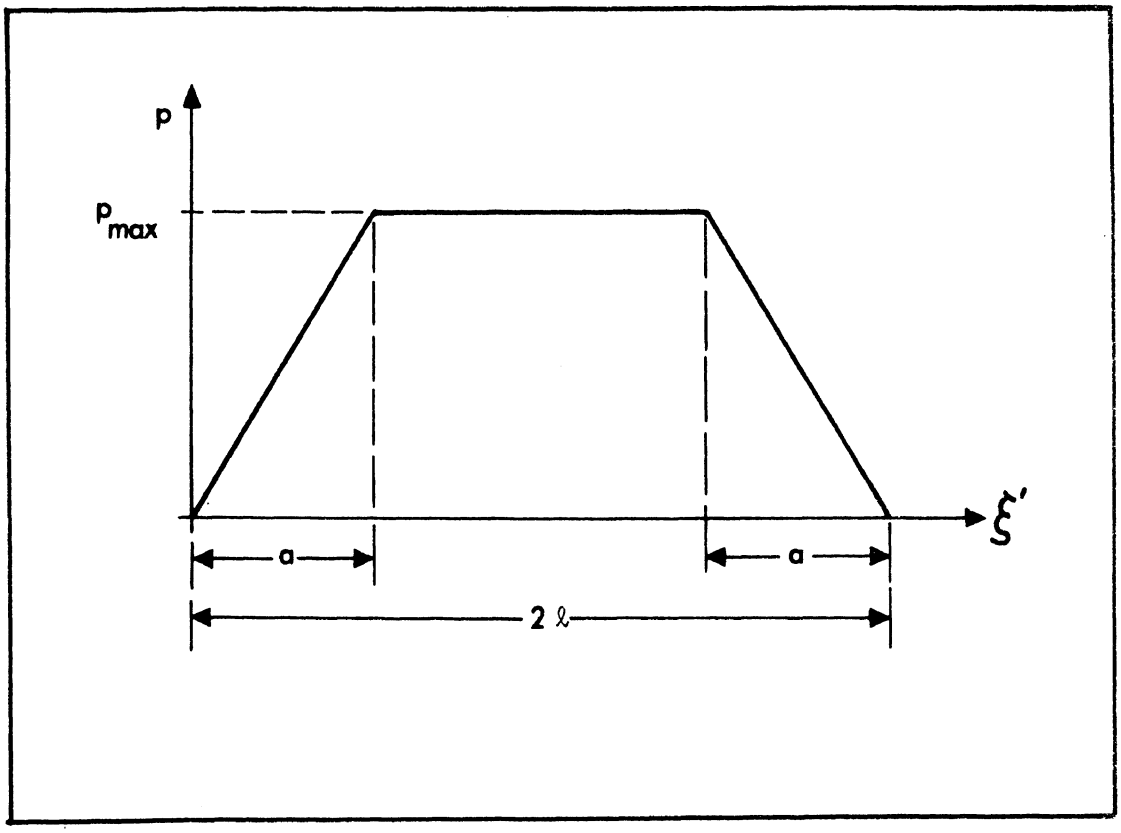

Figure B4-3. Pressure distribution in the contact patch.

The pressure in each of the three regions of the contact patch may therefore be written

$$P = \begin{cases} \dfrac{P_{max}\xi'}{a} & 0 \leq \xi' \leq a \\ P_{max} & a < \xi' < 2\ell - a \\ \dfrac{P_{max}}{2\ell - a}(2\ell - \xi') & 2\ell - a \leq \xi' \leq 2\ell \end{cases} \qquad \text{(B4.7b)}$$

The tire-road shear stress limit, σ_{max}, is assumed to derive from a finite frictional coupling such that

$$\sigma_{max} = \mu p \qquad \text{(B4.8)}$$

where μ is the coefficient of friction at the interface. The quantity μ will be discussed below. It should, however, be noted here that μ may be assumed to be a function of the direction of the shear stresses with no loss in generality in the following discussion.

Using Equation (B4.8), we can determine the position of the sliding boundary point (point 1 in Figure B4-1) where the resultant elastic deformation stress just equals the tire-road shear stress limit, i.e., where

$$(\sigma_\xi^2 + \sigma_\eta^2)^{1/2} = \sigma_{max} = \mu p \tag{B4.9}$$

Let ξ_s denote the longitudinal coordinate of the sliding boundary point. On substituting into Equation (B4.9) from Equations (B4.4) and (B4.6), we obtain

$$\xi_s = \sigma_{max}[(K_x s)^2 + (K_y \tan \alpha)^2]^{-1/2} \tag{B4.10}$$

Let ξ'_s denote the longitudinal coordinate of the point on the tire carcass associated with point ξ_s, as per Figure B4-2. Then, from Equation (B4.3), we have that

$$\begin{aligned} \xi'_s &= (1-s)\xi_s \\ &= \mu p(1-s)\,[(K_x s)^2 + (K_y \tan \alpha)^2]^{-1/2} \end{aligned} \tag{B4.11}$$

The resultant of the shear stresses in the adhesion region may now be computed in a straightforward fashion. This exercise has two parts, namely, (1) the location of the sliding boundary, ξ'_s, and (2) the integration of the shear stresses over the area from $\xi' = 0$ to $\xi' = \xi'_s$.

It has been assumed that the shear stress in the sliding region is equal to μp and is oriented to oppose sliding velocity. Thus a second integration, in this case over the area from ξ'_s to 2L, will yield the shear force in the sliding region.

Due to the assumed trapezoidal form of pressure distribution, there are three separate regions in which ξ'_s may be located:

(1) A point in the decreasing pressure zone.

(2) A point in the central region of the pressure distribution.

(3) A point in the increasing pressure zone.

Case (1): $$2\ell - a \leq \xi'_s \tag{B4.12}$$

From Equations (B4.11) and (B4.7), we have

$$2\ell - a < \frac{\mu p_{max}(2\ell - \xi')(1-s)}{a[(K_x s)^2 + (K_y \tan \alpha)^2]^{1/2}} \tag{B4.13}$$

Inserting the limit ξ' value in Equation (B4.13), namely

$$\xi' = 2\ell - a \tag{B4.14}$$

and the p_{max} value as defined in Equation (B4.7), and re-arranging terms yields the criterion for the initiation of sliding in this region.

$$\frac{s}{1-s} \leq \frac{\mu |F_z| s}{2(1-\frac{a}{2\ell})^2 C_s \lambda} \tag{B4.15}$$

where

$$C_s = -2\ell^2 w K_x \tag{B4.16a}$$

$$C_\alpha = -2\ell^2 w K_y \tag{B4.16b}$$

$$\lambda = [s^2 + (\frac{C_\alpha}{C_s} \tan \alpha)^2]^{1/2} \tag{B4.16c}$$

The parameters C_s and C_α are normally referred to as the longitudinal stiffness and the cornering stiffness of the tire.

Case (2): $$a < \xi'_s < 2\ell - a \tag{B4.17}$$

From Equations (B4.11) and (B4.7), we have

$$a < \frac{\mu |F_z| p_{max} (2\ell - \xi'_s)(1-s)}{a(2\ell-a)w [(K_x \cdot s)^2 + (K_y \tan \alpha)^2]^{1/2}} < 2\ell - a \tag{B4.18}$$

Using the lower limit value, namely,

$$\xi'_s = a \tag{B4.19}$$

and rearranging terms yields one of the criteria for the initiation of sliding in the center region.

$$\frac{s}{1-s} < \frac{\mu |F_z| s}{2 \frac{a}{2\ell} (1 - \frac{a}{2\ell}) C_s \lambda)} \tag{B4.20}$$

Taking note of Equation (B4.15), we may now stipulate that initiation of sliding will take place in the center region if

$$\frac{\mu |F_z| s}{2(1-\frac{a}{2\ell})^2 C_s \lambda} < \frac{s}{s-1} < \frac{\mu F_z s}{2 \frac{a}{2\ell} (1-\frac{a}{2\ell}) C_s \lambda} \tag{B4.21}$$

Case (3): $$\xi'_s < a \tag{B4.22}$$

If the first of inequalities (B4.20) is violated, sliding must occur in the leading shoulder region. This condition may be written

$$\frac{s}{1-s} > \frac{\mu|F_z|s}{2\frac{a}{2\ell}\left(1-\frac{a}{2\ell}\right)C_s} \tag{B4.23}$$

Note that since both the pressure and the stress are linear functions of ξ'_s in this case, aliding will occur at all points $0 < \xi_s < a$, i.e.,

$$\xi'_s = 0 \tag{B4.24}$$

Two important assumptions are made with regard to the forces in the sliding region, namely (1) the resulting force opposes the direction of relative motion between the tire and the road surface, and (2) the velocity of deformation of the sliding region relative to the undeformed tire centerline is neglected.* The average longitudinal component of sliding velocity, therefore, is (see Figure B4-2)

$$V_x = (V\cos\alpha - \Omega R_e) \tag{B4.25}$$

and the average lateral component is

$$V_y = V\sin\alpha \tag{B4.26}$$

Thus, the angle, θ, between the sliding direction and the undeformed centerline may be written

*These assumptions are necessary to keep the numerical work down to a reasonable level. Fortunately, reasonable calculations seem to result. A more detailed discussion of options available for the sliding region is given in Reference [13].

$$\tan \theta = \frac{V \sin \alpha}{V \cos \alpha - \Omega R_e} \tag{B4.27}$$

But

$$s = \frac{V \cos \alpha - \Omega R_e}{V \cos \alpha} \tag{B4.28}$$

Thus

$$\tan \theta = \frac{\tan \alpha}{s} \tag{B4.29}$$

B4.3 THE COMPUTATION OF THE SHEAR FORCES

The shear force produced at the tire-road interface may now be calculated using the following procedure:

1) Inequalities (B4.15), (B4.21), and (B4.23) yield the sliding region

2) Equation (B4.11) will yield ξ'_s

3) The total longitudinal force, F_ξ, and lateral force, F_η, may be computed through an integration of the shear stress over the contact patch, viz:

$$F_\xi = w\left(\int_o^{\xi'_s} \sigma_\xi(\xi')d\xi' + \cos\theta \int_{\xi'_s}^{2\ell} \sigma_{max}(\xi')d\xi'\right) \tag{B4.30}$$

and

$$F_\eta = w\left(\int_o^{\xi_s} \sigma_\eta(\xi')d\xi' + \sin\theta \int_{\xi'_s}^{2\ell} \sigma_{max}(\xi')d\xi'\right) \tag{B4.31}$$

where the first terms on the right-hand side of Equations (B4.30) and (B4.31) indicate the force contribution from the adhesion region, and the second terms indicate the force from the sliding region.

The magnitude of the shear stresses σ_ξ and σ_η may be computed from Equations (B4.3), (B4.4), and (B4.6), viz.:

$$\sigma_\xi = \frac{K_x \, s \, \xi'}{1-s} \tag{B4.32}$$

and

$$\sigma_\eta = \frac{-K_y \tan \alpha \, \xi'}{1-s} \tag{B4.33}$$

and from Equation (B4.7b)

$$\sigma_{max} = \mu p \tag{B4.34}$$

The results of the integrations (B4.30) and (B4.31) are summarized below for Cases 1 through 3:

Case (1): $2\ell - a < \xi'_s$

Repeating Equation (B4.11), we note that

$$\xi'_s = \frac{\mu \, p \, (1-s)}{\sqrt{(K_x s)^2 + (K_y \tan \alpha)^2}}$$

where from Equation (B4.7b) we have

$$p = \frac{p_{max}}{a} \, (2\ell - \xi'_s)$$

The combination of Equations (B4.11) and (B4.7b) leads to

$$\xi'_s = \frac{\mu \frac{p_{max}}{a} \, (2\ell - \xi'_s)(1-s)}{\sqrt{(s \, K_x)^2 + (K_y \tan \alpha)^2}} \tag{B4.35}$$

Equation (B4.35) may be rewritten as

$$\frac{\xi'_s}{2\ell} = \frac{\mu F_z(1-s)}{(1-s)\mu F_z + (2\ell-a)aW K_x \sqrt{s^2 + \left(\frac{K_y}{K_x} \tan \alpha\right)^2}} \qquad \text{(B4.36)}$$

The above result simplifies to

$$\frac{\xi'_s}{2\ell} \qquad \frac{1}{1 + \frac{2(a/2\ell)(1 - a/2\ell)C_s\lambda}{\mu F_z(1-s)}} \qquad \text{(B4.37)}$$

Equation (B4.36) yields the limits of integration for use in Equations (B4.29) and (B4.30). Carrying out these integrations, we obtain the following expressions:

$$F_\xi = \frac{C_s s}{1-s}\left(\frac{\xi'_s}{2\ell}\right)^2 + \frac{\mu|F_z|\cos\theta}{2\left(\frac{a}{2\ell}\right)\left(1-\frac{a}{2\ell}\right)}\left[1 - \frac{\xi'_s}{\ell} + \left(\frac{\xi'_s}{2\ell}\right)\right] \qquad \text{(B4.38a)}$$

$$F_\eta = \frac{C_\alpha \tan\alpha}{1-s}\left(\frac{\xi_s}{2\ell}\right)^2 + \frac{\mu|F_z|\sin\theta}{2\left(\frac{a}{2\ell}\right)\left(1-\frac{a}{2\ell}\right)}\left[1 - \frac{\xi'_s}{\ell} + \left(\frac{\xi'_s}{2\ell}\right)^2\right] \qquad \text{(B4.38b)}$$

Case 2: $\quad a < \xi'_s < 2\ell - a$

In this case, the combination of Equations (B4.11) and (B4.7b) leads to

$$\frac{\xi'_s}{2\ell} = \frac{\mu F_z (1-s)}{2C_s\lambda(1 - a/2\ell)} \qquad \text{(B4.39)}$$

Equation (B4.39) yields the limits of integration for use in Equations (B4.30) and (B4.31). Carrying out these integrations, we obtain the following expressions:

$$F_\xi = \frac{C_s s}{1-s}\left(\frac{\xi'_s}{2\ell}\right)^2 + \frac{\mu|F_z|\cos\theta}{1-\frac{a}{2\ell}}\left(1 - \frac{1}{2}\left(\frac{a}{2\ell}\right) - \frac{\xi'_s}{2\ell}\right) \quad \text{(B4.40a)}$$

$$F_\eta = \frac{C_\alpha \tan\alpha}{1-s}\left(\frac{\xi_s}{2\ell}\right)^2 + \frac{\mu|F_z|\sin\theta}{1-\frac{a}{2\ell}}\left(1 - \frac{1}{2}\left(\frac{a}{2\ell}\right) - \frac{\xi'_s}{2\ell}\right) \quad \text{(B4.40b)}$$

Case 3: $\xi'_s < a$

It has been noted above that the point $\xi'_s = a$ results in a sliding boundary which includes all points $0 < \xi'_s < a$. Thus, Equations (B4.31) and (B4.32) reduce to the following expressions:

$$F_\xi = \cos\theta \int_0^{2L} \sigma_{max}(\xi')d\xi' \quad \text{(B4.41a)}$$

$$F_\eta = \sin\theta \int_0^{2L} \sigma_{max}(\xi')d\xi' \quad \text{(B4.41b)}$$

Carrying out these integrations, we obtain the following expressions:

$$F_\xi = \mu|F_z|\cos\theta \quad \text{(B4.42a)}$$

$$F_\eta = \mu|F_z|\sin\theta \quad \text{(B4.42b)}$$

B4.4 THE TIRE PARAMETERS

In previous sections of this appendix an algorithm has been presented for the simulation of the shear forces at the tire-road interface. It is required that certain physical variables, such as the normal load, F_z, and the longitudinal and lateral slip, s and α, be calculated elsewhere in the

computer program. In addition, values of μ, $a/2\ell$, C_s, and C_α must be supplied. These latter four variables are discussed below.

B4.4.1 THE SATURATION FRICTION LEVEL, μ. The coefficient of tire-road friction is assumed to be given by the following equation:

$$\mu = \mu_o(1 - FA \cdot V_s) \tag{B4.43}$$

where V_s, the sliding velocity, is given by

$$V_s = uw\ (s^2 + \tan^2\alpha)^{1/2} \tag{B4.44}$$

This formulation, first suggested in Reference 11, indicates that at any given s and α the shear forces at the tire-road interface are assumed to fall off with the product of sliding velocity at the interface and the "friction reduction parameter" FA. In fact, the most important effect of the $FA \cdot V_s$ product is that so-called "μ-slip" curves (straight running $|F_x/F_z|$ plotted against longitudinal slip) will reach a peak at some small slip value and decline until the lock point at s = 1 is reached.

The friction levels have been assumed to be anisotropic by setting

$$\mu_o = \mu_x + \frac{2}{\pi}(\mu_y - \mu_x)|\theta| \tag{B4.45}$$

where θ indicates the sliding direction.

Thus at low speeds (i.e., neglecting the effects of sliding speed on the saturation friction levels), the maximum free-rolling lateral force is

$$|F_y| = \mu_y F_z \qquad \text{(B4.46a)}$$

and the maximum straight-running longitudinal force is

$$|F_x| = \mu_x F_z \qquad \text{(B4.46b)}$$

For combined braking and turning, the maximum forces are limited by an intermediate friction value as defined in Equations (B4.44), and the force in the sliding region opposes the sliding direction.

The parameters, μ_x, μ_y, and FA can easily be derived from measured data—the μ_x and FA values may be derived from the peak and locked-wheel force levels of longitudinal force versus longitudinal slip data, and μ_y may be derived from the saturation levels of side force versus sideslip angle data. (Note the effects of the friction reduction parameter are small here since the product FA · tan α remains small even for quite large α.)

B4.4.2 THE PRESSURE DISTRIBUTION PARAMETER, $a/2\ell$. The assumed distribution of the contact pressure has a first-order effect on the lateral and longitudinal forces which will be predicted by any semi-empirical model. In previous research, the pressure distribution has been assumed to be uniform [11], parabolic [12], and elliptical [15]. Other investigators have made an effort to solve for the appropriate distribution to cause measured data to be predicted by their model [16]. In the present analysis, we have assumed the pressure distribution to be trapezoidal, with the width of

the rising and falling area, $a/2\ell$, to be set by the user. Thus a uniform distribution may be obtained by setting $a/2\ell$ equal to zero, and increasingly nonuniform distribution may be obtained by setting $a/2\ell$ to values between zero and .5.

In practice, we have found that the uniform distribution leads to an excellent fit to free-rolling lateral force data for radial tires. Further, the choice of

$$\frac{a}{2\ell} = .25$$

has been found to lead to an excellent fit to the free-rolling lateral force data for many bias and bias-belted tires.* It should be noted that these latter results also agree very well with lateral force data computed using a parabolic pressure distribution, verifying that the pressure distribution resulting from $a/2\ell = .25$ is similar to a parabola.

B4.4.3 THE LONGITUDINAL STIFFNESS, C_s. The name "longitudinal stiffness" derives from the fact that C_s is the derivative of F_ξ with respect to s evaluated at $\alpha = s = 0$. (This may be verified by differentiation of F_ξ as given in Equation (B4.37a), with ξ'_s from Equation (B4.36).) The value of C_s has a first-order effect on the slip value at which peak longitudinal force occurs, with increasing C_s resulting in the occurrence of the peak F_ξ at lower slip values. Since the value of s at peak F_ξ is quite important in some applications (e.g., antiskid brake simulations), and since the physics of wheel spin dictate that, for very small slip, the value of F_ξ will rapidly tend toward the value of

*The thrust of this finding is in agreement with the commonly accepted premise that radial tires have a more uniform pressure distribution than bias or bias-belted tires.

the brake torque divided by the rolling radius, independent of C_s, we tend to choose C_s to locate the peak of the μ-slip curves appropriately rather than to try to exactly match the slope indicated by the empirical data near s = 0. (It should also be noted that this slope is difficult to measure accurately since relatively large forces are generated at very small values of s.)

B4.4.4 THE CORNERING STIFFNESS, C_α. The name "cornering stiffness" derives from the fact that C_α is the derivative of F_η with respect to α at α = s = 0. (This may be verified by differentiation of Equation (B4.37b), with ξ'_s from Equation (B4.36).) The value of C_α is chosen to exactly match the appropriate lateral force versus α data at the lowest measured slip angle. Usually the angle is 1°. Thus, in the case of a uniform pressure distribution, which can be shown to lead to zero curvature in the F_η, α relationship at α = s = 0, the cornering stiffness, C_α, will be set to the F_η value corresponding to α = 1°. For nonuniform pressure distributions, it can be shown that the F_η, α relationship has curvature at α = 0; thus, the C_α value will be set slightly higher than the force measured at α = 1°.

The appropriate choice of the above discussed parameters, namely, μ_x, μ_y, $a/2\ell$, C_s, and C_α will, in our experience, lead to a good match between measured data and prediction. The accuracy should be expected to be excellent for low α and s and for high α or high s. In the intermediate range of α, however, this formulation may be subject to errors as high as 15%. This is not surprising as the assumptions that the pressure distribution, and the cornering stiffness and the longitudinal stiffness* are themselves independent of the shear stresses at the tire-road interface have limited validity.

---

*These are, it should be recalled, dependent on the length and width of the contact patch, and the lateral and longitudinal "spring rates." See Equation (B4.16).

It should be noted here that a 15% error in the force values at intermediate α and s values does not indicate that the net result will be 15% errors in the prediction of the force levels at the tire-road interface. If, for example, the predictions were 15% high for a given α (the predictions do tend to be high), one would expect lower α values to be predicted by the simulation, and thus force (and acceleration) values more in accord with measured results.

However, there are clearly cases in which these errors, whatever their effect, are intolerable. We have found it convenient to introduce two additional parameters, CA1 and CA2, which may be used to ensure that the lateral force data is in very close accord with the measured data points. In particular, we have assumed

$$C_\alpha = C_{\alpha 0}(1 - CA1 \cdot \bar{\alpha}) \qquad \text{(B4.47a)}$$

where

$$\bar{\alpha} = |\alpha| \quad , \quad |\alpha| < CA2 \qquad \text{(B4.47b)}$$

$$\bar{\alpha} = CA2 \qquad |\alpha| > CA2 \qquad \text{(B4.47c)}$$

where $C_{\alpha 0}$ is the slope of the F_η versus α curve at $\alpha = 0$.

The dependence of C_α on α is shown in Figure B4-4.

The parameters C_α, CA1 and CA2 may now be thought of as tire "properties." The effect of increasing CA1 values is to provide more curvature in the $\alpha < CA2$ region of F_η versus α curves. With these added parameters, we have found that our predicted lateral force versus sideslip angle curves match within 5% or less of measured data.

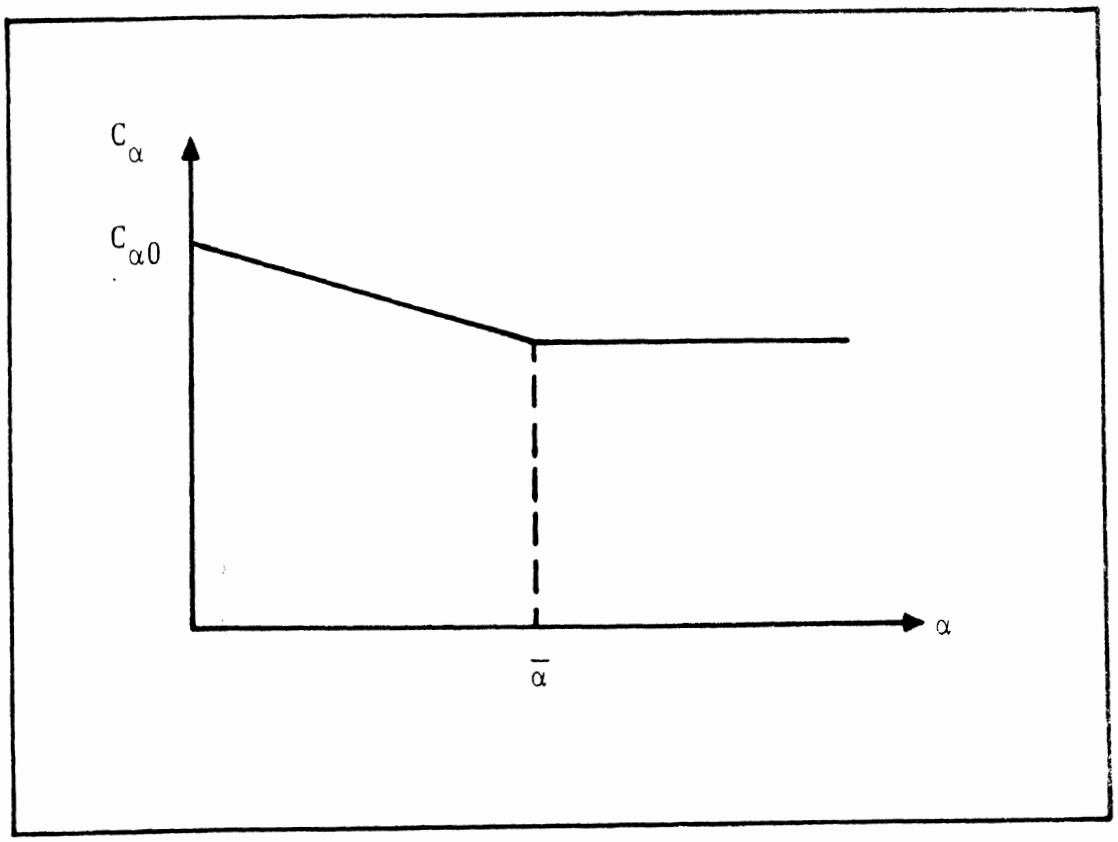

Figure B4-4.

It is appropriate at this point to present some sample results obtained with the model.

B4.5 SOME SAMPLE CALCULATIONS

It is our purpose here to give examples of the procedures used to determine tire parameters for insertion into the simulation. In these examples, extensive use will be made of an interactive stand-alone algorithm which has been written to compute the shear forces FX and FY as a function of α and s based on user input tire parameters. The algorithm is listed with a sample run at the end of this section.

The Firestone Deluxe Champion Sup-R-Belt H78-14 and the Bridgestone 225R-14 will be the subject tires for our examples. The tire traction fields for each of these tires, which have been measured using the mobile tire tester on the asphalt skid pad at TTI, are presented in Appendix D.

Consider the Deluxe Champion. Initially, we restrict our attention to the straight-line braking data. During a trial and error use of the interactive program, the values presented in Table B4-1 were chosen.

Table B4-1. Straight-Line Braking Parameters for the Deluxe Champion, 28 psi

Load	μ_x	C_s (lbs/slip)	FA (sec/ft)
800 lbs.	.96	7000	.002
1100 lbs.	.93	10000	.002

Note that our primary consideration has been to match the peak and slide data, and to make the peak FX values occur at the appropriate longitudinal slip values. This is a straightforward task and quite reasonable agreement was produced, as is shown in Figure B4-5.

The rest of the parameters may be derived from the free-rolling data. Since this is a bias-belted tire, $a/2\ell = .25$ is selected. Then, at each load, C_α is chosen to match the low slip angle data, μ_y is chosen to match the sixteen degree data, and CA1 and CA2 are used as necessary to fine tune the intermediate points. The values of μ_y, $C_{\alpha 0}$, CA1 and CA2 are presented in Table B4-2.

Table B4-2. Free-Rolling Parameters for the Deluxe Champion, 28 psi

Load	μ_y	$C_{\alpha 0}$ (lbs/deg)	CA1	CA2
800	1.0	195.	1.5	10
1100	.95	220.	2.5	6
1700	.9	210.	.5	8

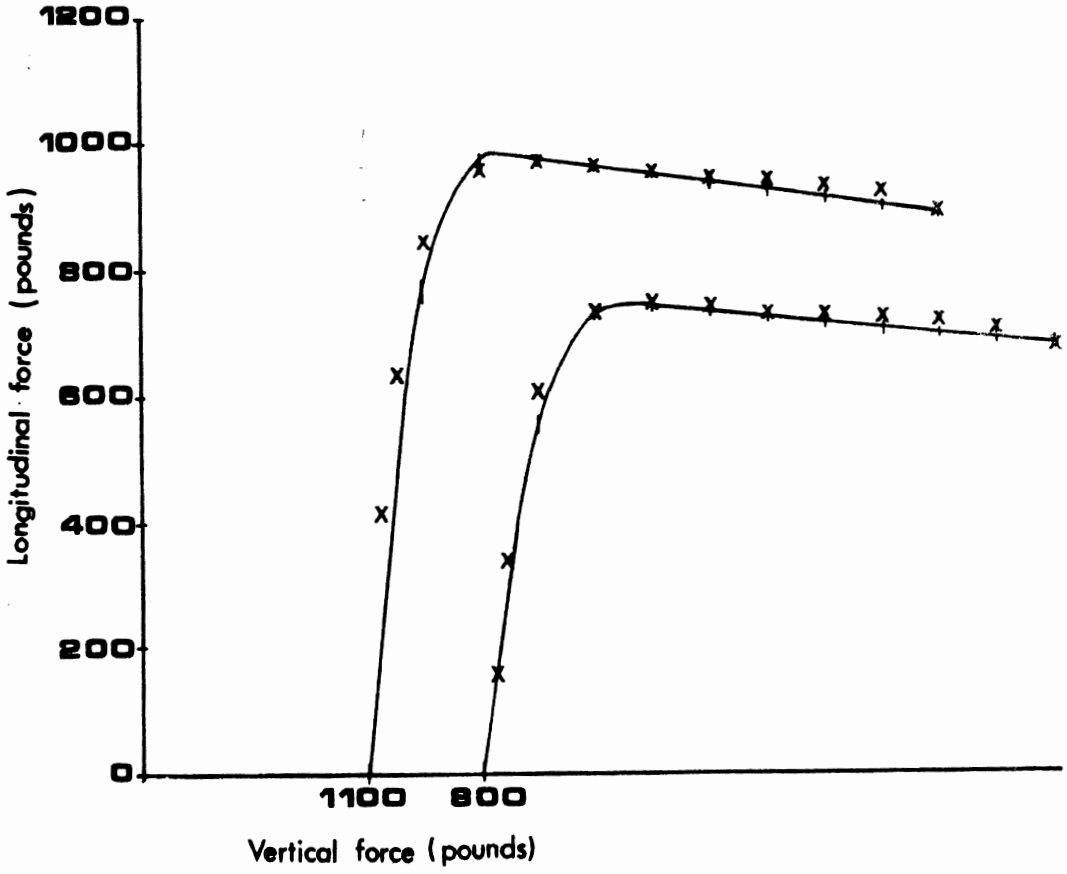

Figure B4-5. Longitudinal force vs. slip for the Firestone Deluxe Champion H78-14, 28 psi.

Use of these values in the model lead to computed results in close agreement with the measured data, as shown in Figure B4-6.

As a check on the fidelity of the model, it is useful to compare measured and predicted braking and turning data. Note that these measured data were procured from tests independent of the tests leading to the parameters used in the model. This comparison, which is presented in Figure B4-7, leads to a good measure of confidence in the model.

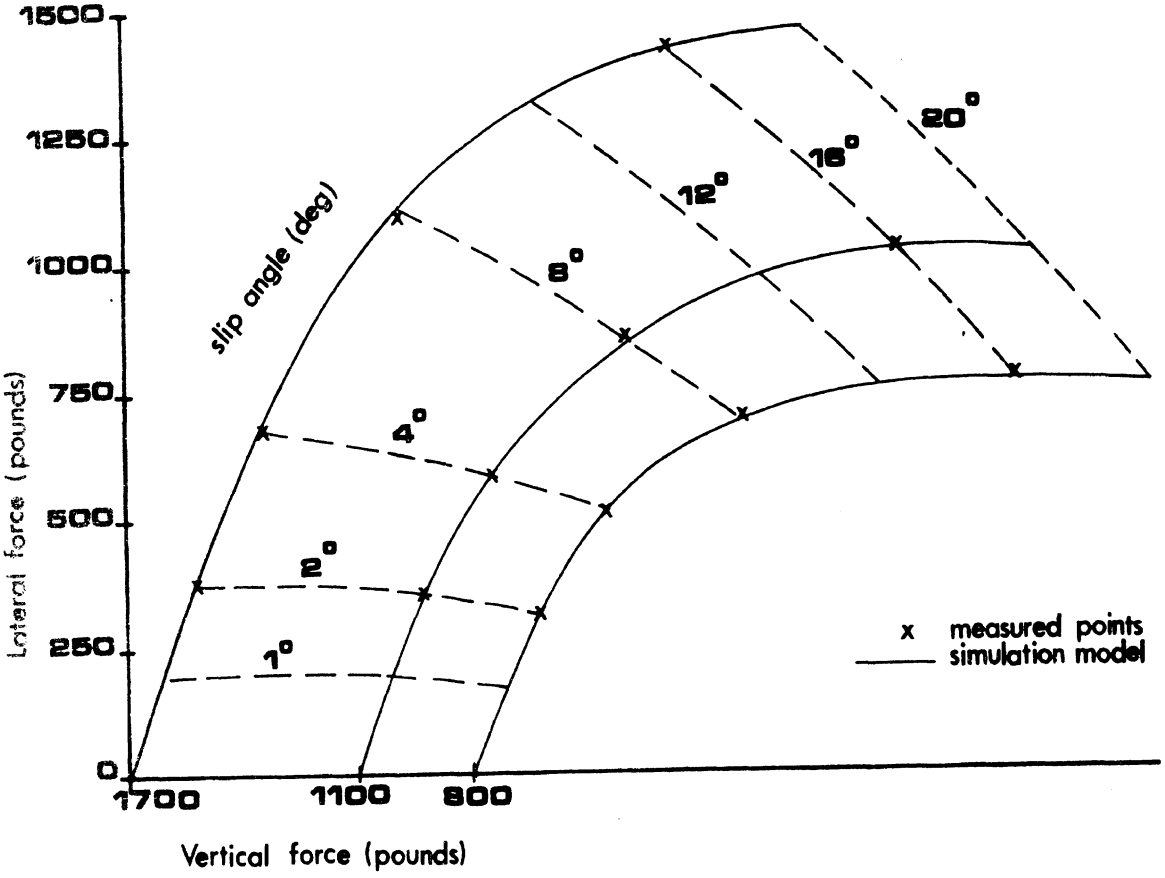

Figure B4-6. Lateral force vs. slip angle for the Firestone Deluxe Champion H78-14, 28 psi.

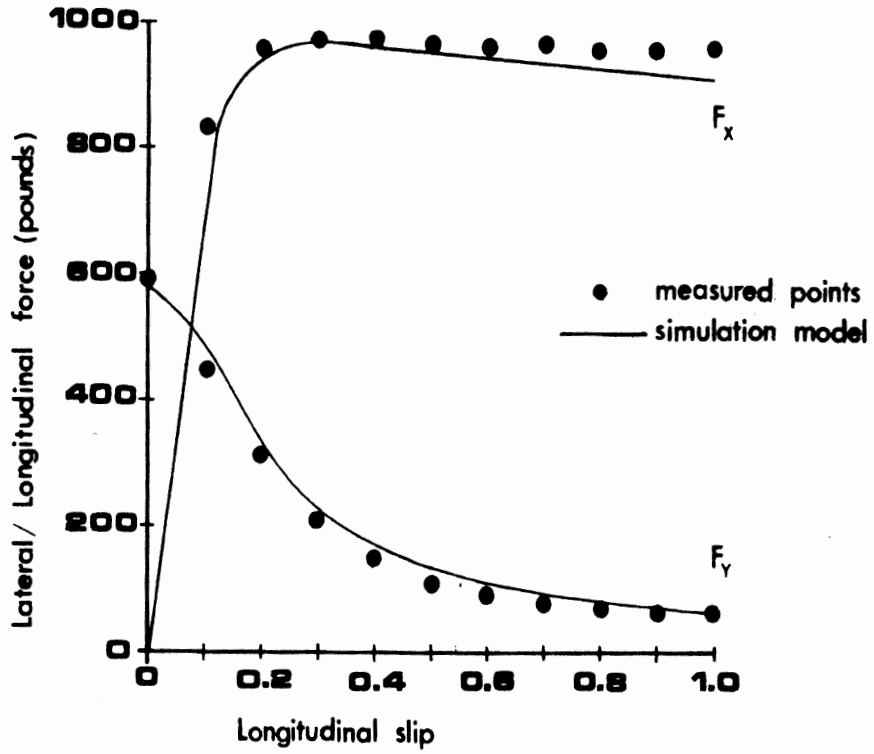

Figure B4-7. Lateral force and longitudinal force vs. slip at $\alpha = 4°$, Firestone Deluxe Champion H78-14, 28 psi.

Consider now the Bridgestone 225R-14. The tire parameters are found using the same procedure as for the above example. In this case, however, we choose $a/2\ell = 0$ for the radial tire. A list of the parameters selected is given in Table B4-3, and a plot of the simulated lateral force versus sideslip angle and the measured data is shown in Figure B4-8.

Table B4-3. Free-Rolling Parameters for the Bridgestone 225R-14, 28 psi.

Load	μ_y	$C_{\alpha 0}$ (lbs/deg)	CA1	CA2
800	.95	240	0.0	0.0
1100	.93	270	1.5	2.0
1700	1.02	290	0.0	0.0

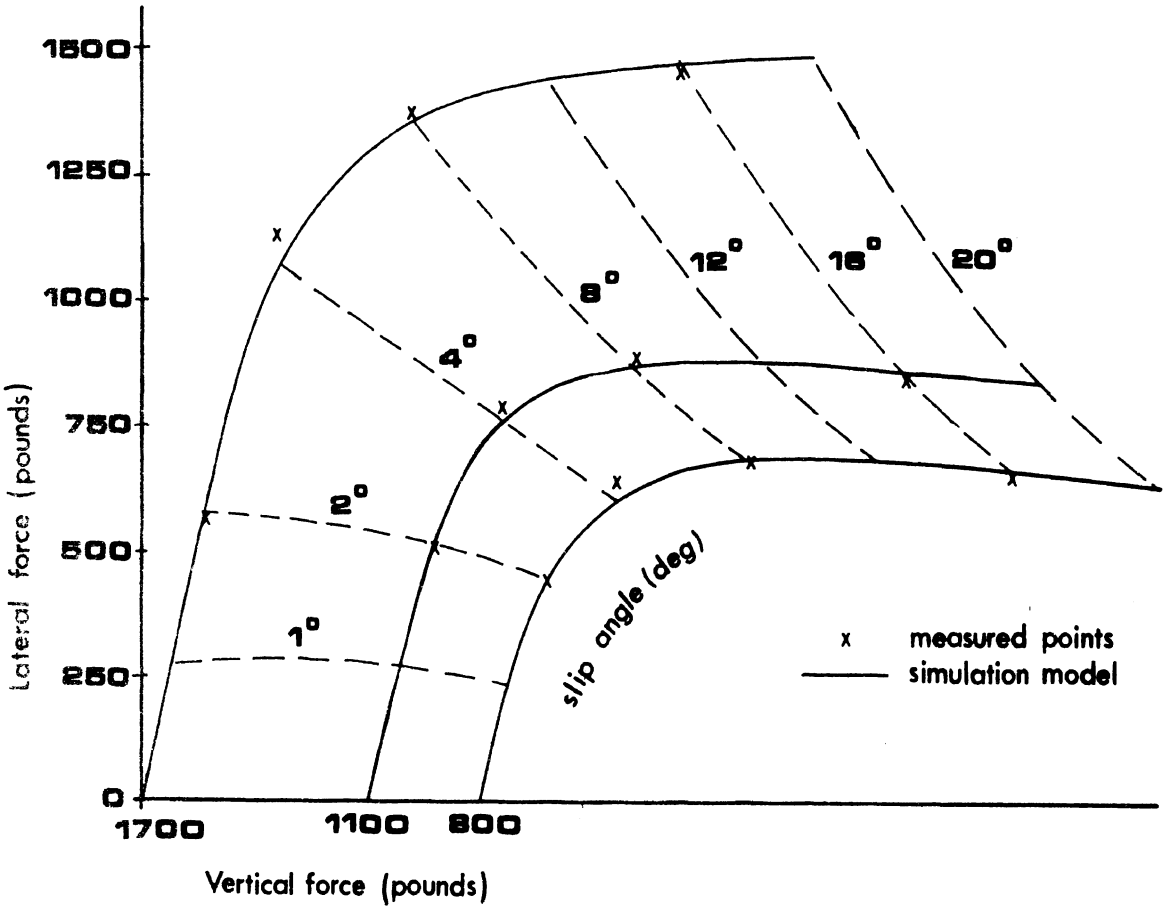

Figure B4-8. Lateral force vs. slip angle for the Bridgestone 225R-14, 28 psi.

While it is not obvious from the above tables and figures, the change to $a/2\ell = 0$ is an important one. To illustrate this point, we have computed the traction field of the Bridgestone tire using $a/2\ell = .25$ and the other parameters tabulated in Table B4-3. In Figure B4-9, these results are compared to the values corresponding to $a/2\ell = 0$, i.e., the simulated data from Figure B4-8. Clearly, the assumed pressure distribution influences the curvature predicted near $\alpha = 0$. Since radial tires tend to exhibit a linear relationship of force versus sideslip angle up to fairly high force levels, the accuracy of the simulation is improved by using $a/2\ell = 0$.

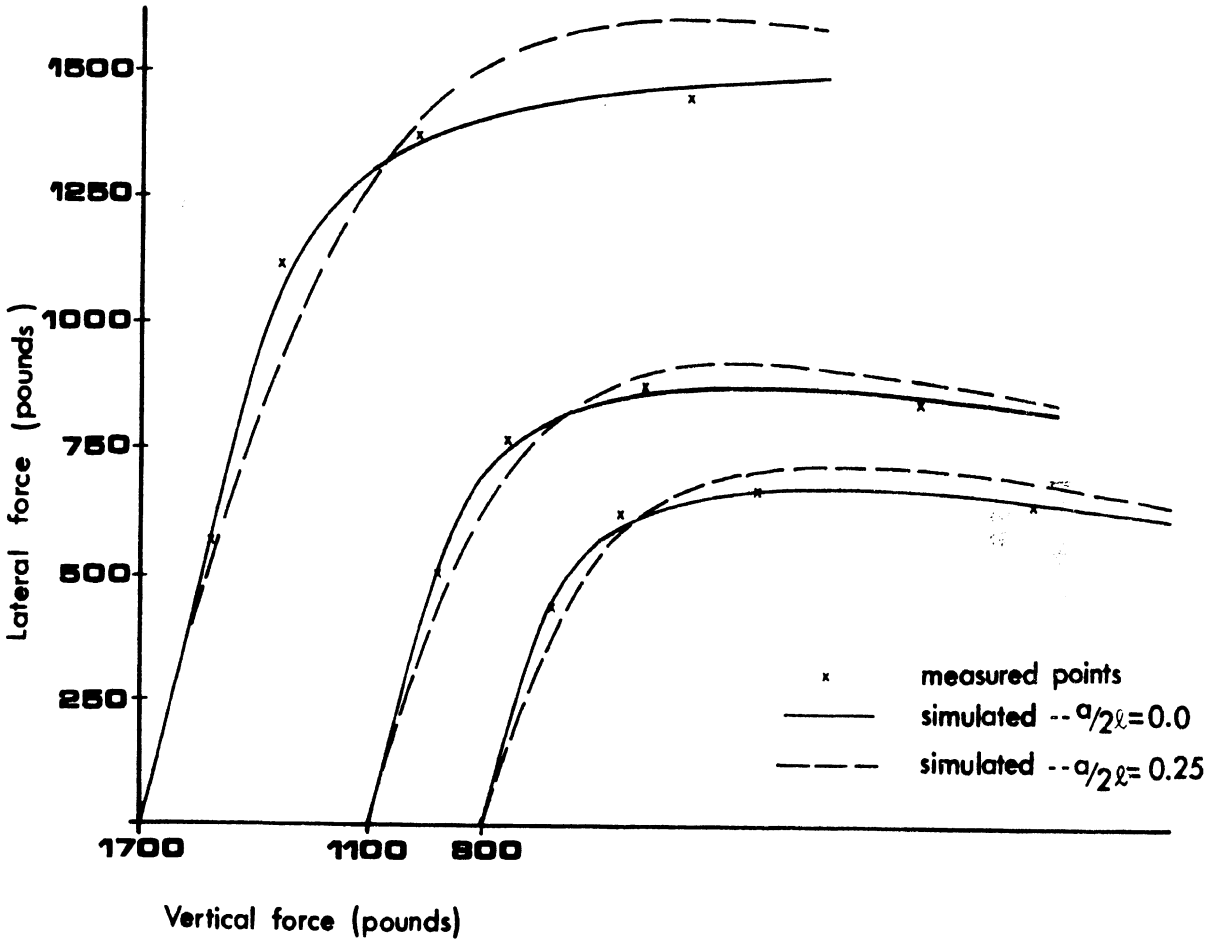

Figure B4-9. Lateral force vs. sideslip angle for the Bridgestone 225R-14, 28 psi.

B4.6 AN INTERACTIVE ALGORITHM FOR THE CALCULATION OF THE SHEAR FORCES

The curve fitting procedure described in the previous section requires the use of a short stand-alone algorithm by which lateral and longitudinal forces may be calculated. The source listing for this algorithm and two sample runs are presented in this section. Note that the input parameters for the sample runs are taken from Tables B4-1 and B4-2. The output variable designated as EPS indicates the $\xi'_s/2\ell$ value for each condition.

```
      C TIRE MODEL
    C ******************************************************************
    C
    C READING IN PARAMETERS
    C
          REAL K,MU,MUFY,KY,MUSL,MUSLFZ,MUFZ
          DATA YES/'Y'/
          KCOR=0
          ICHAN=0
          IR=5
          IW=6
          PI=3.141592653
          PI2=PI/2.
      100 FORMAT(2F14.3)
       30 FORMAT(A1)
       31 FORMAT(I2)
        1 WRITE(IW,101)
      101 FORMAT( '& 1 COEFFICIENTS (X AND Y) OF FRICTION(STATIC
          READ(IR,100) XMUX,XMUY
          IF(KCOR.NE.0) GO TO 13
        2 WRITE(IW,102)
      102 FORMAT('& 2 NORMAL LOAD ON TIRES(LBS.)=
          READ(IR,100) FZ
          IF(KCOR.NE.0) GO TO 13
        8 WRITE(IW,110)
      110 FORMAT('& 8 DO YOU WANT MU-SLIP DATA(Y OR N)?
          READ(IR,30) SL
          IF(SL.NE.YES) GO TO 112
      221 WRITE(IW,219)
      219 FORMAT('&   ENTER RANGE LOWER LIMIT,UPPER LIMIT, AND I
          READ(IR,220) RLL,RUL,XINC
      220 FORMAT(3F6.3)
          IF (RLL.GE.RUL.OR.XINC.LE.0.0) GO TO 221
        3 WRITE(IW,103)
      103 FORMAT('& 3 TIRE SIDE SLIP ANGLE(DEGREES)=
          READ(IR,100) ALPH
          ALPHA=ALPH*PI/180.
          IF(KCOR.NE.0) GO TO 13
          GO TO 5
      112 WRITE(IW,113)
          RLL=0.0
          RUL=1.0
          XINC=0.05
      113 FORMAT('  FY-ALPHA DATA ')
          ALPH=0.
        4 WRITE(IW,104)
      104 FORMAT('& 4 LONGITUDINAL TIRE SLIP=
```

```
      READ(IR,100) S
      IF(KCOR.NE.0) GO TO 13
    5 WRITE(IW,105)
  105 FORMAT('& 5 CORNERING STIFFNESS(LBS/DEG.)=
      READ(IR,100) CALPH
      IF(KCOR.NE.0) GO TO 13
    6 WRITE(IW,106)
  106 FORMAT('& 6 LONGITUDINAL STIFFNESS(LBS./UNIT SLIP)=
      READ(IR,100) CS
      IF(KCOR.NE.0) GO TO 13
    7 WRITE(IW,107)
  107 FORMAT('& 7 PRESSURE DISTRIBUTION FUNCTION=
      READ(IR,100) AN
      IF(AN.EQ.0.) AN=.001
      IF(KCOR.NE.0) GO TO 13
    9 WRITE(Iw,119)
  119 FORMAT('& 9 VEHICLE SPEED(FEET/SEC.)=
      READ(IR,100) VS
      IF(KCOR.NE.0) GO TO 13
   10 WRITE(IW,120)
  120 FORMAT('&10 FRICTION REDUCTION PARAMETER=
      READ(IR,100) FA
      IF(KCOR.NE.0) GO TO 13
 1100 WRITE(IW,1101)
 1101 FORMAT('&11 CA1=
      READ(IR,100) CA1
      IF(KCOR.NE.0) GO TO 13
 1200 WRITE(Iw,1201)
 1201 FORMAT('&12 CA2=
      READ(IR,100) CA2
      CA2=CA2*PI/180.
      IF(KCOR.NE.0) GO TO 13
  111 WRITE(IW,11)
   11 FORMAT('&DO YOU WISH TO CHANGE ANY PARAMETERS(Y OR N)?
      READ(IR,30) CHAN
      IF(CHAN.NE.YES) GO TO 20
  121 WRITE(IW,12)
   12 FORMAT('&HOW MANY PARAMETERS DO YOU WISH TO CHANGE(I2
      READ(IR,31) ICHAN
   13 IF(ICHAN.EQ.0) GO TO 111
      KCOR=1
      ICHAN=ICHAN-1
  114 WRITE(Iw,14)
   14 FORMAT('&ENTER PARAMETER NUMBER TO BE CHANGED IN I2 FO
      READ(IR,31) IGO
      GO TO(1,2,3,4,5,6,7,8,9,10,1100,1200),IGO
   20 WRITE(IW,201)
  201 FORMAT('/'10X,'EPS',9X,'ALPHA',12X,'S',11X,'FX',13X,'FY
```

```
      WRITE(IW,203)
  203 FORMAT(10X,'---',9X,'-----',12X,'-',11X,'--',13X,'--')
C
C CALCULATION OF CONSTANTS
C
      CALPHB=CALPH*180./PI
      NN=IFIX((RUL-RLL)/XINC+.999)+1
      N=NN
      IF(SL.NE.YES) N=8
      IF(SL.EQ.YES) S=RLL
      DO 40 I=1,N
      IF(N.EQ.NN) GO TO 51
      J=I
      IF(I.GT.3) GO TO 52
      ALPH=(FLOAT(J)-1.)
      GO TO 53
   52 ALPH=((FLOAT(J)-4.)*4.+4.)
   53 ALPHA=ALPH*PI/180.
   51 XXX=ALPHA
      IF(ALPHA.GT.CA2) XXX=CA2
      CALPHA=CALPHB*(1.-CA1*XXX)
      RS=CALPHA/CS
      SR=1./RS
      IF(S.GE.RUL) GO TO 22
      K=S/(1.-S)
      GO TO 24
   22 K=10000.
   24 IF(S.NE.RLL) GO TO 23
      IF(ALPHA.EQ.0.) GO TO 25
      THETA=PI2
      TA=TAN(ALPHA)
      GO TO 26
   25 FX=0.
      FY=0.
      EPS=1.
      GO TO 200
   23 TA=TAN(ALPHA)
      A=TA/S
      THETA=ATAN(A)
   26 X=S/(SQRT(S**2+(RS*TA)**2))
      ANGX=COS(THETA)
      ANGY=SIN(THETA)
      MU=XMUY+(XMUX-XMUY)*(1.-ABS(THETA/PI2))
      SQSTA=SQRT(S**2+TA**2)
      MUSL=MU*(1.-FA*VS*SQSTA)
      MUFZ=MUSL*FZ/(1.-AN)
      IF(S.NE.RLL) GO TO 29
      KY=TA/(1.-S)
      Y=TA/(SQRT((SR*S)**2+TA**2))
```

```
145            SLIX=MUFZ*Y/(AN*2.*CALPHA)
146            SLIZ=MUFZ*Y/((1.-AN)*2.*CALPHA)
147            IF(KY.GE.SLIX) GO TO 1000
148            IF(KY.GT.SLIZ) GO TO 2000
149            GO TO 3000
150         29 SLIX=MUFZ*X/(AN*2.*CS)
151            SLIZ=MUFZ*X/((1.-AN)*2.*CS)
152      C
153      C DETERMINATION OF POSITION IN PATCH WHERE SLIDING BEGINS
154      C
155            IF(K.GE.SLIX) GO TO 1000
156            IF(K.GT.SLIZ) GO TO 2000
157      C
158      C SLIDING STARTS IN REAR PART OF PATCH
159      C
160       3000 EPS=MUSL*FZ*(1.-S)/(AN*2.*CS*SQRT(S**2+(RS*TA)**2)*(1.
161           1  MUSL*FZ*(1.-S))
162            FX=CS*S*EPS**2/(1.-S)+MUFZ*ANGX*(.5-EPS+(EPS**2/2.))/A
163            FY=CALPHA*EPS**2*TA/(1.-S)+MUFZ*ANGY*(.5-EPS+(EPS**2/2
164            GO TO 200
165      C
166      C SLIDING STARTS IN CENTRAL PART OF PATCH
167      C
168       3000 EPS=MUFZ*(1.-S)/(2.*CS*SQRT(S**2+(RS*TA)**2))
169            FX=CS*S*EPS**2/(1.-S)+MUFZ*ANGX*(1.-(.5*AN)-EPS)
170            FY=CALPHA*TA*(EPS**2)/(1.-S)+MUFZ*ANGY*(1.-EPS-(.5*AN)
171            GO TO 200
172      C
173      C SLIDING IN TOTAL OF CONTACT PATCH
174      C
175       1000 EPS=0.
176            FX=MUSL*FZ*ANGX
177            FY=MUSL*FZ*ANGY
178        200 WRITE(IW,204) EPS,ALPH,S,FX,FY
179        204 FORMAT(5F14.3)
180            IF(N.EQ.NN) S=S+XINC
181         40 CONTINUE
182            WRITE(IW,301)
183        301 FORMAT('& CHANGES(Y OR N)?')
184            READ(IR,30) ALTER
185            IF(ALTER.EQ.YES) GO TO 121
186            END
 OF FILE
```

B5. THE MECHANICS OF THE USE OF THE SIMULATION

In Table B5-1 a set of guidelines is provided to aid the user in his consideration of the various levels of complexity to be employed in the computations. It should be emphasized that this table is concerned with the prediction of vehicle response on a dry surface in the absence of drive torque or braking. If significant longitudinal forces during a steering maneuver are to be simulated, the predictive task becomes much more difficult, requiring a very careful analysis of the combined longitudinal and lateral forces at the tire-road interface, carefully chosen brake dynamometer data and/or a detailed analysis of the engine-transmission-differential system. Prediction of vehicle performance on a wet surface remains a speculative undertaking because of the variability of the shear forces at the tire-road interface with small changes in water depth.

The simulation utilized in this study has been designed to handle all the nonlinear calculations listed in Table B5-1. For example, consider the simulated and measured performance of a 1971 Dodge Coronet in a drastic steer and brake maneuver, presented in Figure B5-1. The data was measured in an earlier NHTSA-sponsored program [17], and this computer run was performed in the process of tire model refinement which took place during the present investigation.

Predictions of performance were also made for a 1971 Mustang and a 1973 Buick station wagon. These computations were used both to aid in the set-up of the vehicle test program (see Section 3.2.2 of the Technical Report), and to elucidate vehicle test results (see Sections 3.2.2 and 3.2.3 of the Technical Report). To explain the mechanics of the usage of the program, we will consider below the input data in some detail and present some sample runs.

Table B5-1. Guidelines for the Simulation of Handling Response

Objective	Tool	Remarks
Understeer/ oversteer factor, response time	Linear analysis	This matter is discussed in detail in the Technical Report.
Trends in performance in the nonlinear range (over .3g on dry surface)	Nonlinear simulation. Neglect nonlinearities in the suspensions, steering lash, Ackerman effects and steering compliance, and load sensitive tire properties.	As the simulated maneuvers become more severe, the trends become questionable.
Accurate predictions from .3g to .5g	Requires accurate steering wheel-road wheel relationship, load sensitive lateral forces and aligning moments, roll steer, camber	Careful tire modeling accurate to ten degrees slip angle and at least 1.5 times the static load may be necessary.
Accurate predictions over .5g	Add bump stops, accurate tire data to extreme loads and angles.	Static distance to bump stops is important to ensure realistic fore-aft lateral load transfer distribution.

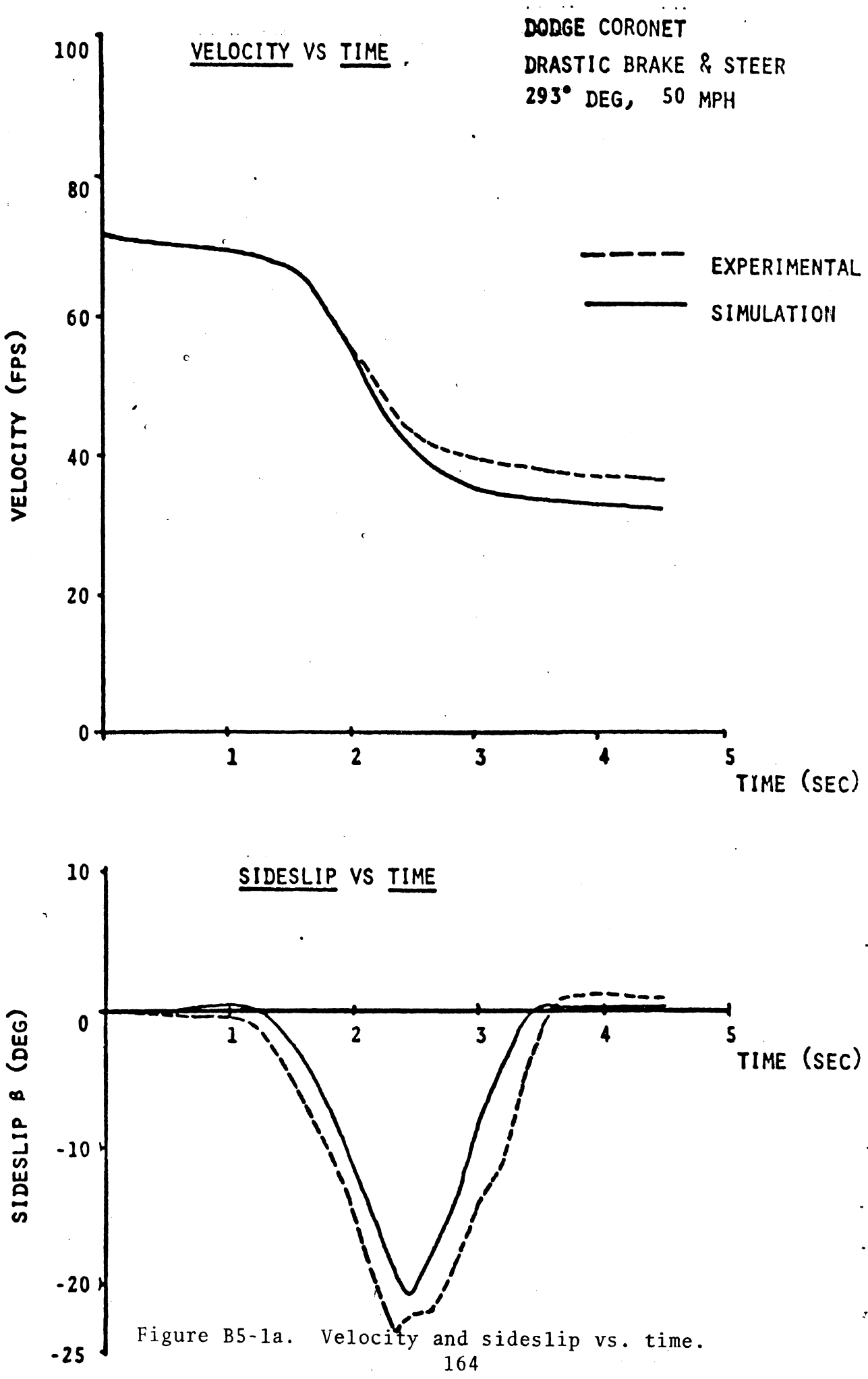

Figure B5-1a. Velocity and sideslip vs. time.

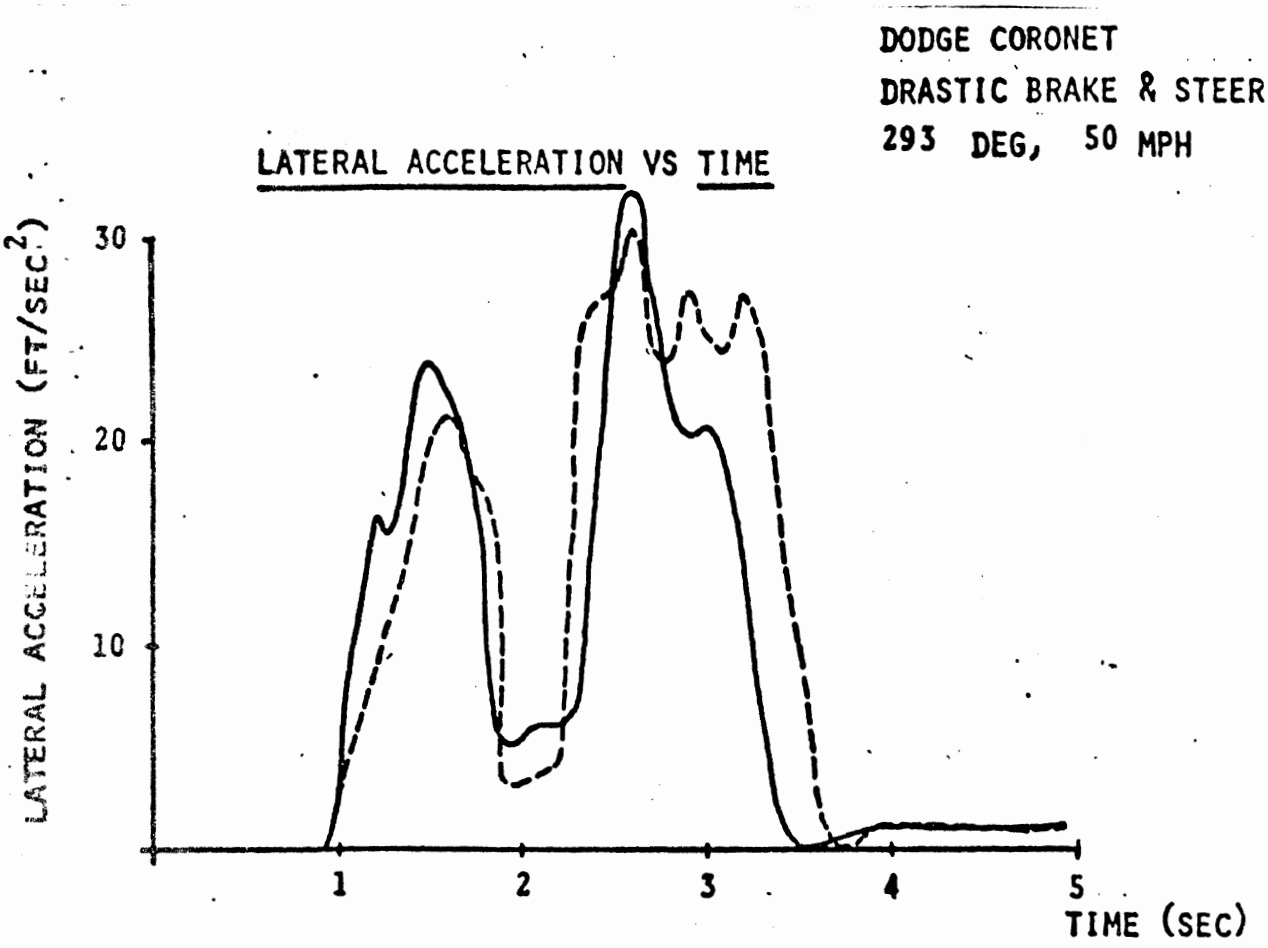

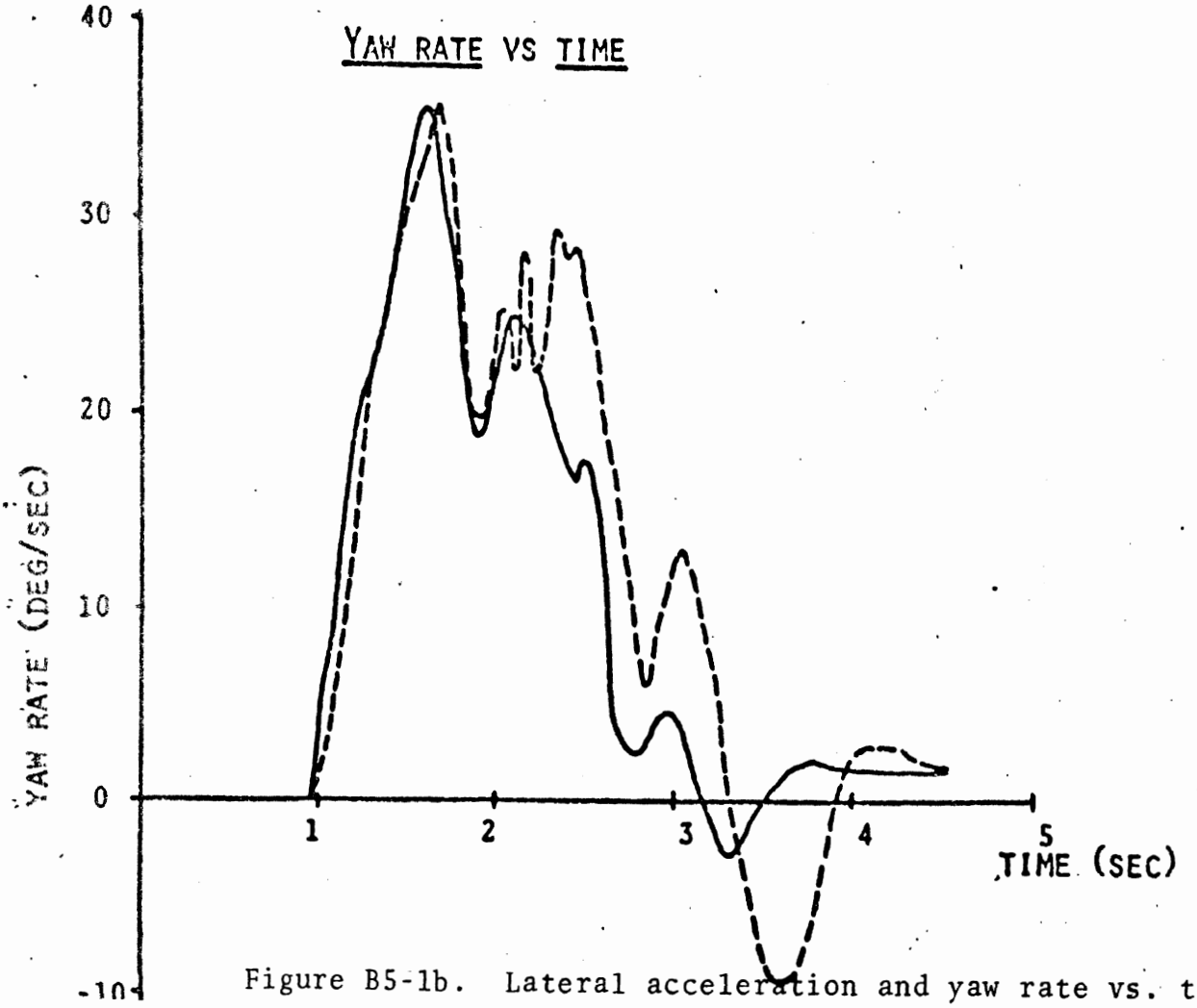

Figure B5-1b. Lateral acceleration and yaw rate vs. time.

Table B5-2 presents all the possible input options with an explanation of each entry added in the right-hand column. Table B5-3 is a list of the data records used for a Buick run. Table B5-4 contains the echo of the data, copied from the computer output. Note all the appropriate parameters and some explanatory remarks are shown on the echo.

In Figures B5-2 through B5-4 simulated results are compared with measured results for the Buick in low-level, middle-range, and high-level trapezoidal steer maneuvers. In this case, as in the majority of the calculations throughout the present research program, good agreement was obtained between simulated and measured responses.

Tables B5-5 and B5-6 contain the input data and the echo for a simplified Buick model using linear springs, a simplified steering system, and neglecting load sensitivities of the tires. While the simplified data list is obviously much more convenient than the previous set, there are potential disparities between the results of the simple and complex formulation which will be discussed briefly here.

For low level runs, simplified data is likely to lead to higher predicted lateral accelerations since aligning torque is neglected. Further deviations may occur due to the simplified roll steer and camber representations. In the present case, the simplified data leads to about 15% higher predicted lateral accelerations than the more complex set for the Buick in a low-level trapezoidal steer maneuver as is shown in Figure B5-5. For mid-range and limit simulations, the aligning torque, roll steer, and camber effects are relatively less important. However, for many tires, it may be crucial to adequately model load transfer sensitivity by use of the extended tables of tire input data. Correct bump stop locations may also be necessary to apportion the lateral load transfer between front and rear tires, and to limit the relative

sprung and unsprung mass roll excursions to realistic values. In the present case, the input data describing the forces generated by the Buick tires are relatively insensitive to load, thus, nearly identical lateral accelerations are predicted in high level trapezoidal steer maneuvers. The simplified data does, however, predict significantly higher roll angles. This is illustrated in Figure 5-5c in which the response of the Buick to a 375° trapezoidal steer input computed using both the simple and the complex data sets are presented.

Note that the transition from a simple to a complex vehicle representation has been human engineered so that the user may shift from one model to the other with minimum inconvenience. It is hoped that this set-up will enhance the utility of the program for users across the entire spectrum of nonlinear calculations listed in Table B5-1.

TABLE B5-2

DATA DOCUMENTATION
HSRI CAR SIMULATION PROGRAM

***** INPUT PARAMETERS *****

SYMBOL	DESCRIPTION	VALUE FOR BUICK WAGON	COMMENT
HEAD	BUICK WAGON:DATA DOCUMENTATION ETC.,.....		(20A4) FORMAT
A1	HORIZONTAL DISTANCE FROM CG TO MIDPOINT OF FRONT SUSPENSION (IN)	51.60	
A2	HORIZONTAL DISTANCE FROM CG TO MIDPOINT OF REAR SUSPENSION (IN)	64.40	
ALPHA1	STATIC DISTANCE, FRONT AXLE TO GROUND (IN)	13.00	
ALPHA2	STATIC DISTANCE, REAR AXLE TO GROUND (IN)	13.00	
AN1	TIRE PRESSURE DISTRIBUTION FUNCTION (FRONT)	0.25	
AN2	TIRE PRESSURE DISTRIBUTION FUNCTION (REAR)	0.25	
C1	VISCOUS DAMPING: JOUNCE ON FRONT AXLE (LB-SEC/IN)	1.90	
C2	VISCOUS DAMPING: REBOUND ON FRONT AXLE (LB-SEC/IN)	5.60	
C3	VISCOUS DAMPING: JOUNCE ON REAR AXLE (LB-SEC/IN)	5.00	
C4	VISCOUS DAMPING: REBOUND ON REAR AXLE (LB-SEC/IN)	15.00	
CALF1	LATERAL STIFFNESS, FRONT TIRE, ONE SIDE (LBS/DEG)	-1.00	IF .LT. ZERO, TABLE LOOK-UP
CALF2	LATERAL STIFFNESS, REAR TIRE, ONE SIDE (LBS/DEG)		OMIT IF CALF1 IS .LT. ZERO
CF1	MAXIMUM COULOMB FRICTION, FRONT SUSPENSION (LB)	40.00	
CF2	MAXIMUM COULOMB FRICTION, REAR SUSPENSION (LB)	60.00	
CGAMMA	CAMBER STIFFNESS, ONE SIDE (LBS/DEG)	15.00	
CS1	FRONT TIRE LONGITUDINAL STIFFNESS (LBS/UNIT SLIP)		OMIT IF CALF1 IS .LT. ZERO
CS2	REAR TIRE LONGITUDINAL STIFFNESS (LBS/UNIT SLIP)		OMIT IF CALF1 IS .LT. ZERO
DELTA1	STATIC VERTICAL DISTANCE, FRONT AXLE TO SPRUNG MASS CG (IN)	15.50	
FA1	FRICTION REDUCTION PARAMETER, FRONT TIRES	0.002	
FA2	FRICTION REDUCTION PARAMETER, REAR TIRES	0.002	
G1	GRAVITY X COMPONENT	0.00	
G2	GRAVITY Y COMPONENT	0.00	
GR	STEERING GEAR RATIO	22.50	
J1	SPRUNG MASS ROLL MOMENT OF INERTIA (IN-LB-SEC**2)	5312.00	
J2	SPRUNG MASS PITCH MOMENT OF INERTIA (IN-LB-SEC**2)	31781.00	
J3	SPRUNG MASS YAW MOMENT OF INERTIA (IN-LB-SEC**2)	39000.00	
JXZ	SPRUNG MASS PITCH PLANE CROSS MOMENT (IN-LB-SEC**2)	0.00	
JA2	ROLL MOMENT OF REAR AXLE (IN-LB-SEC**2)	600.00	
JS1	POLAR MOMENT OF FRONT WHEEL, ONE SIDE (IN-LB-SEC**2)	8.00	
JS2	POLAR MOMENT OF REAR WHEEL, ONE SIDE (IN-LB-SEC**2)	8.00	
K1	SPRING RATE, FRONT SUSPENSION, ONE SIDE (LB/IN)	-1.00	IF .LT. ZERO, TABLE LOOK-UP
K2	SPRING RATE, REAR SUSPENSION, ONE SIDE (LB/IN)	-1.00	IF .LT. ZERO, TABLE LOOK-UP
KPOFF	KINGPIN OFFSET (IN)	3.44	
KSC	STEERING COLUMN SPRING RATE (IN-LB/RAD)	300.00	
KSL	STEERING LINKAGE SPRING RATE, ONE SIDE (IN-LB/RAD)	150000.00	
KSY	STEERING TABLE KEY	3	(I2) FORMAT
KT1	SPRING RATE, FRONT TIRE, ONE SIDE (LB/IN)	1420.00	
KT2	SPRING RATE, REAR TIRE, ONE SIDE (LB/IN)	1420.00	
MUZERO1	FRICTION COEFFICIENT FOR FRONT TIRE		OMIT IF CALF1 IS .LT. ZERO
MUZERO2	FRICTION COEFFICIENT FOR REAR TIRE		OMIT IF CALF1 IS .LT. ZERO
PW	WEIGHT OF PAYLOAD (LBS)	397.00	
PJ1	ROLL MOMENT OF INERTIA OF PAYLOAD (IN-LB-SEC**2)	0.00	OMIT IF PW IS ZERO
PJ2	PITCH MOMENT OF INERTIA OF PAYLOAD (IN-LB-SEC**2)	0.00	OMIT IF PW IS ZERO
PJ3	YAW MOMENT OF INERTIA OF PAYLOAD (IN-LB-SEC**2)	0.00	OMIT IF PW IS ZERO
PX	HORIZONTAL DISTANCE FROM MIDPOINT OF REAR SUSPENSION TO PAYLOAD MASS CENTER (IN)	20.07	OMIT IF PW IS ZERO

TABLE B5-2 (Cont.)

SYMBOL	DESCRIPTION	VALUE FOR BUICK WAGON	COMMENT
PZ	VERTICAL DISTANCE FROM GROUND TO PAYLOAD MASS CENTER (IN)	20.00	OMIT IF PW IS ZERO
RCH1	ROLL CENTER HEIGHT, FRONT SUSPENSION (IN)	3.50	
RCH2	ROLL CENTER HEIGHT, REAR SUSPENSION (IN)	13.00	
ROLLF	FRONT AUXILIARY ROLL STIFFNESS (IN-LB/DEG)	5779.50	
ROLLR	REAR AUXILIARY ROLL STIFFNESS (IN-LB/DEG)	0.00	
RSC	ROLL STEER TABLE KEY	-2.00	IF .LE. -1.0, TABLE LOOK-UP
SY1	HORIZONTAL DISTANCE FROM BODY X-AXIS TO FRONT SUSPENSION (IN)	30.05	
SY2	HORIZONTAL DISTANCE FROM BODY X-AXIS TO REAR SUSPENSION (IN)	20.50	
TIME	MAXIMUM REAL TIME FOR SIMULATION (SEC)	4.40	
TRA1	FRONT HALF TRACK (IN)	30.50	
TRA2	REAR HALF TRACK (IN)	30.50	
TRAIL	MECHANICAL TRAIL (IN)	0.59	
VEL	INITIAL VELOCITY (FPS)	57.50	
WIND	TOTAL DRAG COEFFICIENT (LBS/(FT/SEC)**2)	0.02	
W	SPRUNG WEIGHT OF CAR (LBS)	3770.00	
WS1	WEIGHT OF FRONT SUSPENSION (LBS)	247.40	
WS2	WEIGHT OF REAR SUSPENSION (LBS)	405.30	
ZBAR			OMIT IF K2 IS .LT. ZERO OR RSC IS .GT. -1.0
KEYTQ	BRAKE PARAMETER KEY (EITHER 1 OR 0)	0	(I2) FORMAT
TQ(1,1,1) TQ(1,1,2)	BRAKE PARAMETERS		(2F10.4) FORMAT
TQ(1,2,1) TQ(1,2,2)	TQ(AXLE,SIDE,TYPE)		IF KEYTQ .EQ. ZERO, THEN
TQ(2,1,1) TQ(2,1,2)	SEE FOOT NOTES.		OMIT ALL THE TQ'S(TQ'S ARE
TQ(2,2,1) TQ(2,2,2)			AUTOMATICALLY SET TO ZERO).

***** INPUT TABLES *****

DESCRIPTION		VALUE FOR BUICK WAGON		COMMENT
***** TIME VS. BREAK LINE PRESSURE TABLE *****				
NO. OF PAIRS IN THE TABLE			1	
TIME(SEC)	PRESSURE(PSI)	0.00	0.00	UP TO 25 PAIRS (2F10.2)
.	.			
.	.			
.	.			
TIME	PRESSURE			
***** BRAKE PRESSURE VS. TORQUE TABLE (FRONT,LEFT) *****				
NO. OF PAIRS IN THE TABLE			23	
PRESSURE(PSI)	TORQUE(IN-LBS)	0.00	0.00	UP TO 25 PAIRS (2F10.2)
.	.	50.00	0.00	
.	.	100.00	540.00	
.	.	150.00	1620.00	
.	.	200.00	2700.00	
.	.	250.00	3780.00	
.	.	300.00	4860.00	
.	.	350.00	5940.00	
.	.	400.00	7020.00	
.	.	450.00	8100.00	
.	.	500.00	9180.00	
.	.	550.00	10260.00	
.	.	600.00	11340.00	
.	.	650.00	12420.00	
.	.	700.00	13500.00	
.	.	750.00	14580.00	
.	.	800.00	15660.00	
.	.	850.00	16740.00	
.	.	900.00	17820.00	
.	.	950.00	18900.00	
.	.	1000.00	19980.00	
.	.	1050.00	21060.00	
PRESSURE	TORQUE	1100.00	22140.00	
***** BRAKE PRESSURE VS. TORQUE TABLE (FRONT,RIGHT) *****				
NO. OF PAIRS IN THE TABLE			23	
PRESSURE(PSI)	TORQUE(IN-LBS)	0.00	0.00	UP TO 25 PAIRS (2F10.2)
.	.	50.00	0.00	
.	.	100.00	540.00	
.	.	150.00	1620.00	
.	.	200.00	2700.00	
.	.	250.00	3780.00	

TABLE B5-2 (Cont.)

DESCRIPTION		VALUE FOR BUICK WAGON		COMMENT
.	.	300.00	4860.00	
.	.	350.00	5940.00	
.	.	400.00	7020.00	
.	.	450.00	8100.00	
.	.	500.00	9180.00	
.	.	550.00	10260.00	
.	.	600.00	11340.00	
.	.	650.00	12420.00	
.	.	700.00	13500.00	
.	.	750.00	14580.00	
.	.	800.00	15660.00	
.	.	850.00	16740.00	
.	.	900.00	17820.00	
.	.	950.00	18900.00	
.	.	1000.00	19980.00	
.	.	1050.00	21060.00	
PRESSURE	TORQUE	1100.00	22140.00	
***** BRAKE PRESSURE VS. TORQUE TABLE (REAR,LEFT) *****				
NO. OF PAIRS IN THE TABLE			23	
PRESSURE(PSI)	TORQUE(IN-LBS)	0.00	0.00	UP TO 25 PAIRS (2F10.2)
.	.	50.00	0.00	
.	.	100.00	0.00	
.	.	150.00	900.00	
.	.	200.00	1800.00	
.	.	250.00	2700.00	
.	.	300.00	3600.00	
.	.	350.00	4500.00	
.	.	400.00	5400.00	
.	.	450.00	6300.00	
.	.	500.00	7200.00	
.	.	550.00	8100.00	
.	.	600.00	9000.00	
.	.	650.00	9900.00	
.	.	700.00	10800.00	
.	.	750.00	11700.00	
.	.	800.00	12600.00	
.	.	850.00	13500.00	
.	.	900.00	14400.00	
.	.	950.00	15300.00	
.	.	1000.00	16200.00	
.	.	1050.00	17100.00	
PRESSURE	TORQUE	1100.00	18000.00	
***** BRAKE PRESSURE VS. TORQUE TABLE (REAR,RIGHT) *****				
NO. OF PAIRS IN THE TABLE			23	
PRESSURE(PSI)	TORQUE(IN-LBS)	0.00	0.00	UP TO 25 PAIRS (2F10.2)
.	.	50.00	0.00	
.	.	100.00	0.00	
.	.	150.00	900.00	
.	.	200.00	1800.00	
.	.	250.00	2700.00	
.	.	300.00	3600.00	
.	.	350.00	4500.00	
.	.	400.00	5400.00	
.	.	450.00	6300.00	
.	.	500.00	7200.00	
.	.	550.00	8100.00	
.	.	600.00	9000.00	
.	.	650.00	9900.00	
.	.	700.00	10800.00	
.	.	750.00	11700.00	
.	.	800.00	12600.00	
.	.	850.00	13500.00	
.	.	900.00	14400.00	
.	.	950.00	15300.00	
.	.	1000.00	16200.00	
.	.	1050.00	17100.00	
PRESSURE	TORQUE	1100.00	18000.00	
***** SPRING COMPRESSION VS. FORCE TABLE (FRONT,ONE SIDE) *****				
***** THIS TABLE IS OMITTED IF K1 IS .GE. ZERO *****				
NO. OF PAIRS IN THE TABLE			7	
COMPRESSION(IN)	FORCE(LBS)	-2.00	-2100.00	UP TO 25 PAIRS (2F10.2)
.	.	0.00	-125.00	
.	.	1.00	825.00	
.	.	1.50	915.00	

TABLE B5-2 (Cont.)

DESCRIPTION			VALUE FOR BUICK WAGON			COMMENT
.	.		6.00	1425.00		
.	.		6.50	1495.00		
COMPRESSION	FORCE		7.50	2700.00		
***** SPRING COMPRESSION VS FORCE TABLE (REAR,ONE SIDE) *****						
***** THIS TABLE IS OMITTED IF K2 IS .GE. ZERO *****						
NO. OF PAIRS IN THE TABLE				7		
COMPRESSION(IN)	FORCE(LBS)		-2.00	-2000.00		UP TO 25 PAIRS (2F10.2)
.	.		0.00	-205.00		
.	.		1.00	665.00		
.	.		2.00	825.00		
.	.		6.50	1475.00		
.	.		7.00	1575.00		
COMPRESSION	FORCE		9.00	3570.00		
***** STEERING TABLES *****						
***** ONLY ONE OF THE FOLLOWING THREE OPTIONS MAY BE USED *****						
*** OPTION 1 (KSW=1) : TIME VS. ROAD WHEEL ANGLE ***						
NO. OF PAIRS IN THE TABLE						
TIME(SEC)	ROAD WHEEL ANGLE(DEG)					UP TO 50 PAIRS (2F15.5)
.	.					
.	.					LEFT WHEEL ANGLE IS EQUAL
.	.					TO RIGHT WHEEL ANGLE
TIME	ROAD WHEEL ANGLE					
*** OPTION 2 (KSW=2) : TIME VS. STEERING WHEEL ANGLE ***						
NO. OF PAIRS IN THE TABLE						
PLAY(DEG)						(F15.5) FORMAT
TIME(SEC)	STEERING WHEEL ANGLE(DEG)					UP TO 50 PAIRS (2F15.5)
.	.					
.	.					LEFT WHEEL ANGLE IS EQUAL
.	.					TO RIGHT WHEEL ANGLE
TIME	STEERING WHEEL ANGLE					
*** OPTION 3 (KSW=3) : TIME VS. STEERING WHEEL ANGLE ***						
*** AND STEERING WHEEL ANGLE VS. ROAD WHEEL ANGLE (LEFT,RIGHT) ***						
NO. OF PAIRS IN THE TIME VS. STEERING WHEEL ANGLE TABLE				08		
PLAY(DEG)				10.00		(F15.5) FORMAT
TIME(SEC)	STEERING WHEEL ANGLE(DEG)		0.0000	0.00		UP TO 50 PAIRS (2F15.5)
.	.		0.1000	0.00		
.	.		0.5000	175.00		
.	.		3.6000	175.00		
.	.		4.0000	0.00		
TIME	STEERING WHEEL ANGLE(DEG)		5.0000	0.00		
NO. OF PAIRS IN THE STEERING VS. ROAD WHEEL ANGLE TABLE					15	
STEERING(DEG)	LEFT ROAD(DEG)	RIGHT ROAD(DEG)	-585.00	-34.00	-32.00	UP TO 50
.	.	.	-540.00	-31.00	-29.80	TRIPLES IN
.	.	.	-450.00	-25.00	-24.00	(3F15.5)
.	.	.	-360.00	-19.50	-18.00	FORMAT
.	.	.	-270.00	-14.00	-12.50	
.	.	.	-180.00	-9.00	-7.80	
.	.	.	-90.00	-4.00	-3.00	
.	.	.	0.00	0.00	0.00	
.	.	.	90.00	4.00	5.00	
.	.	.	180.00	8.40	9.60	
.	.	.	270.00	13.00	15.00	
.	.	.	360.00	18.40	20.00	
.	.	.	450.00	23.80	26.00	
.	.	.	540.00	29.40	31.20	
STEERING	LEFT ROAD	RIGHT ROAD	630.00	35.00	37.00	
***** SUSPENSION COMPRESSION VS. CAMBER TABLE *****						
NO. OF PAIRS IN THE TABLE				10		
COMPRESSION(IN)	CAMBER(DEG)		-10.00	0.333		UP TO 25 PAIRS (2F10.2)
.	.		0.00	0.333		
.	.		1.00	0.333		
.	.		2.00	0.333		
.	.		3.00	1.032		
.	.		4.00	0.733		
.	.		5.00	0.331		
.	.		6.00	-0.331		
.	.		6.50	-0.857		
COMPRESSION	CAMBER		10.00	-0.857		
***** VERTICAL LOAD VS. LATERAL STIFFNESS, CA1, CA2 TABLE (FRONT, ONE SIDE) *****						
***** THIS TABLE IS OMITTED IF CALF1 IS .GE. ZERO *****						
NO. OF QUADRUPLETS IN THE TABLE						4
LOAD(LBS)	STIFFNESS(LBS/DEG)	CA1 CA2	0.00	215.00	2.30	6.00
.	.	. .	800.00	215.00	2.30	6.00
.	.	. .	1100.00	195.00	0.50	8.00
LOAD	STIFFNESS	CA1 CA2	1700.00	185.00	0.25	18.00

TABLE B5-2 (Cont.)

DESCRIPTION				VALUE FOR BUICK WAGON			COMMENT
***** VERTICAL LOAD VS. LATERAL STIFFNESS, CA1, CA2 TABLE (REAR, ONE SIDE) *****							
***** THIS TABLE IS OMITTED IF CALF1 IS .GE. ZERO *****							
NO. OF QUADRUPLETS IN THE TABLE							4
LOAD(LBS)	STIFFNESS(LBS/DEG)	CA1	CA2	0.00	195.00	1.50	10.00
.	.	.	.	800.00	195.00	1.50	10.00
.	.	.	.	1100.00	220.00	2.50	6.00
LOAD	STIFFNESS	CA1	CA2	1700.00	210.00	0.50	8.00
***** VERTICAL LOAD VS. LONGITUDINAL STIFFNESS (FRONT, ONE SIDE) *****							
NO. OF PAIRS IN THE TABLE					4		
LOAD(LBS)	STIFFNESS(LBS/DEG)			0.00	7000.00		UP TO 25 PAIRS (2F10.2)
.	.			800.00	7000.00		
.	.			1100.00	10000.00		
LOAD	STIFFNESS			1700.00	15000.00		
***** VERTICAL LOAD VS. LONGITUDINAL STIFFNESS (REAR, ONE SIDE) *****							
NO. OF PAIRS IN THE TABLE					4		
LOAD(LBS)	STIFFNESS(LBS/DEG)			0.00	7000.00		UP TO 25 PAIRS (2F10.2)
.	.			800.00	7000.00		
.	.			1100.00	10000.00		
LOAD	STIFFNESS			1700.00	15000.00		
***** VERTICAL LOAD VS. MUZERO (FRONT) *****							
NO. OF PAIRS IN THE TABLE					4		
LOAD(LBS)	MUZERO			1.00	0.92		UP TO 25 PAIRS (2F10.2)
.	.			800.00	0.92		
.	.			1100.00	0.90		
LOAD	MUZERO			1700.00	0.90		
***** VERTICAL LOAD VS. MUZERO (REAR) *****							
NO. OF PAIRS IN THE TABLE					4		
LOAD(LBS)	MUZERO			1.00	1.00		UP TO 25 PAIRS (2F10.2)
.	.			800.00	1.00		
.	.			1100.00	0.95		
LOAD	MUZERO			1700.00	0.90		
***** ALIGNING TORQUE TABLE (FRONT, ONE SIDE) *****							
NO. OF LOADS IN THE TABLE					5		UP TO 5 LOADS PER TABLE
LOAD	NO. OF PAIRS IN THE SET			0.00	1		(F15.5,I2)FORMAT
SIDE SLIP ANGLE	ALIGNING TORQUE			0.00	0.00		UP TO 5 PAIRS PER SET
LOAD	NO. OF PAIRS IN THE SET			800.00	5		IN (2F10.2) FORMAT
SIDE SLIP ANGLE	ALIGNING TORQUE			0.00	0.00		
.	.			1.00	19.50		
.	.			2.00	26.00		
.	.			4.00	25.00		
SIDE SLIP ANGLE	ALIGNING TORQUE			12.00	2.00		
LOAD	NO. OF PAIRS IN THE SET			1100.00	5		
SIDE SLIP ANGLE	ALIGNING TORQUE			0.00	0.00		
.	.			1.00	32.00		
.	.			2.00	50.00		
.	.			4.00	54.00		
SIDE SLIP ANGLE	ALIGNING TORQUE			15.00	2.50		
LOAD	NO. OF PAIRS IN THE SET			1400.00	5		
SIDE SLIP ANGLE	ALIGNING TORQUE			0.00	0.00		
.	.			1.00	43.00		
.	.			2.00	72.00		
.	.			4.00	90.00		
SIDE SLIP ANGLE	ALIGNING TORQUE			16.00	11.60		
LOAD	NO. OF PAIRS IN THE SET			1700.00	5		
SIDE SLIP ANGLE	ALIGNING TORQUE			0.00	0.00		
.	.			2.00	93.00		
.	.			4.00	126.00		
.	.			8.00	110.00		
SIDE SLIP ANGLE	ALIGNING TORQUE			18.00	24.00		
***** ALIGNING TORQUE TABLE (REAR, ONE SIDE) *****							
NO. OF LOADS IN THE TABLE					5		UP TO 5 LOADS PER TABLE
LOAD	NO. OF PAIRS IN THE SET			0.00	1		(F15.5,I2) FORMAT
SIDE SLIP ANGLE	ALIGNING TORQUE			0.00	0.00		UP TO 5 PAIRS PER SET
LOAD	NO. OF PAIRS IN THE SET			800.00	5		IN (2F10.2) FORMAT
SIDE SLIP ANGLE	ALIGNING TORQUE			0.00	0.00		
.	.			1.00	16.60		
.	.			2.00	24.10		
.	.			4.00	20.50		
SIDE SLIP ANGLE	ALIGNING TORQUE			12.00	1.40		
LOAD	NO. OF PAIRS IN THE SET			1100.00	5		
SIDE SLIP ANGLE	ALIGNING TORQUE			0.00	0.00		
.	.			1.00	28.50		
.	.			2.00	43.70		
.	.			4.00	45.90		
SIDE SLIP ANGLE	ALIGNING TORQUE			15.00	2.60		

TABLE B5-2 (Cont.)

DESCRIPTION		VALUE FOR BUICK WAGON		COMMENT
LOAD	NO. OF PAIRS IN THE SET	1400.00	5	
SIDE SLIP ANGLE	ALIGNING TORQUE	0.00	0.00	
		1.00	40.00	
		2.00	65.50	
		4.00	76.70	
SIDE SLIP ANGLE	ALIGNING TORQUE	16.00	10.30	
LOAD	NO. OF PAIRS IN THE SET	1700.00	5	
SIDE SLIP ANGLE	ALIGNING TORQUE	0.00	0.00	
		1.00	50.00	
		2.00	87.00	
		4.00	112.00	
SIDE SLIP ANGLE	ALIGNING TORQUE	15.00	21.00	
***** SUSPENSION COMPRESSION VS. TOE TABLE *****				
NO. OF PAIRS IN THE TABLE			10	
COMPRESSION(IN)	TOE(DEG)	-10.00	0.8150	UP TO 25 PAIRS (2F15.5)
		0.00	0.8150	
		1.00	0.5820	
		2.00	0.4150	
		3.00	0.3050	
		4.00	0.3050	
		5.00	0.4480	
		6.00	0.6250	
		6.50	0.6950	
COMPRESSION	TOE	10.00	0.6950	
***** ROLL STEER TABLE *****				
***** THIS TABLE IS OMITTED IF RSC IS .GT. -1.0 *****				
NO. OF PAIRS IN THE TABLE			15	
COMPRESSION(IN)	AXLE DISPLACEMENT(IN)	0.00	0.0000	UP TO 25 PAIRS (2F15.5)
		0.50	-0.1120	
		1.00	-0.2120	
		1.50	-0.2950	
		2.00	-0.3550	
		2.50	-0.3980	
		3.00	-0.4170	
		3.50	-0.4180	
		4.00	-0.4040	
		4.50	-0.3680	
		5.00	-0.3170	
		5.50	-0.2470	
		6.00	-0.1540	
		6.50	-0.0300	
COMPRESSION	AXLE DISPLACEMENT	7.00	0.0700	

***** FINAL PARAMETERS *****

SYMBOL	DESCRIPTION	VALUE FOR BUICK WAGON	COMMENT
TIMO	TIME INCREMENT TO BE PRINTED OUT (SEC)	0.05	(F15.5) FORMAT
NEAR	EXIT KEY, IF =1 :ANOTHER CAR DATA FOLLOWS =0 :CALL EXIT	0	(I2) FORMAT

NOTES:

1. FOR THE INPUT PARAMETERS, (F15.5) FORMAT IS USED UNLESS SPECIFIED.
2. FOR THE BRAKE PARAMETERS, TQ(AXLE,SIDE,TYPE)
   AXLE; FRONT=1 REAR=2
   SIDE; LEFT=1 RIGHT=2
   TYPE; 1=THE TIME DELAY BETWEEN FOOT VALVE AND BRAKE LINE.
   2=THE TIME TO RISE TO 63% STEP INPUT LEVEL.
3. FOR THE INPUT TABLES,
   A). THE NO. OF PAIRS IN THE TABLE IS IN (I2) FORMAT.
   B). THE FORMAT FOR THE CONTENTS OF THE TABLE IS MARKED AS COMMENTS.
   C). FOR THE VERTICAL LOAD VS. LATERAL STIFFNESS TABLE(FRONT,REAR), UP TO 50 QUADRUPLETS IN (4F10.2) FORMAT MAY BE USED.
   D). IN THE LOAD VS. LATERAL STIFFNESS TABLES, "CA1" AND "CA2" ARE CURVE FIT PARAMETERS. DETAILED DESCRIPTION IS GIVEN IN THE APPENDIX B ON THE TIRE MODEL.

TABLE B5-3

INPUT DATA LIST
FOR THE BUICK WAGON (COMPLICATED CASE)

INPUT CARD NO.	COLUMN NO. IN THE CARD 12345678901234567890123456789012345678901234567890...	COMMENTS	
1	BUICK WAGON: COMPLICATED CASE, ETC.,.....	HEAD	(20A4) FORMAT
2	51.60000	A1	(F15.5) FORMAT
3	64.40000	A2	
4	13.00000	ALPHA1	
5	13.00000	ALPHA2	
6	0.25000	AN1	
7	0.25000	AN2	
8	1.90000	C1	
9	5.66000	C2	
10	5.00000	C3	
11	15.00000	C4	
12	-1.00000	CALF1	
13	40.00000	CF1	
14	60.00000	CF2	
15	15.00000	CGAMMA	
16	15.50000	DELTA1	
17	0.00200	FA1	
18	0.00200	FA2	
19	0.00000	G1	
20	0.00000	G2	
21	22.50000	GR	
22	5312.00000	J1	
23	31781.00000	J2	
24	39800.00000	J3	
25	0.00000	JXZ	
26	600.00000	JA2	
27	8.00000	JS1	
28	8.00000	JS2	
29	-1.00000	K1	
30	-1.00000	K2	
31	3.44000	KROFF	
32	300.00000	KSC	
33	150000.00000	KSL	
34	05	KSW	(I2) FORMAT
35	1420.00000	KT1	(F15.5) FORMAT
36	1420.00000	KT2	
37	397.00000	PH	
38	0.00000	PJ1	
39	0.00000	PJ2	
40	0.00000	PJ3	
41	26.07000	PX	
42	20.00000	PZ	
43	3.50000	RCH1	
44	13.00000	RCH2	
45	5779.50000	ROLLF	
46	0.00000	ROLLR	
47	-2.00000	RSCKEY	
48	30.05000	SY1	
49	20.50000	SY2	
50	4.40000	TIRF	
51	30.50000	TRA1	
52	30.50000	TRA2	
53	0.59000	TRAIL	
54	57.50000	VEL	
55	0.02400	WIND	
56	3770.00000	W	
57	247.50000	WS1	
58	495.00000	WS2	
59	00	KEYTQ	(I2) FORMAT
60	01	TIME VS. BRAKE PRESSURE	
61	0.00 0.00	(2F10.2)	
62	23	BRAKE PRESSURE VS. TORQUE	
63	0.00 0.00	(2F10.2) FRONT LEFT	
64	50.00 0.00		
65	100.00 540.00		
66	150.00 1620.00		
67	200.00 2700.00		
68	250.00 3780.00		
69	300.00 4860.00		
70	350.00 5940.00		

TABLE B5-3 (Cont.)

INPUT CARD NO.	COLUMN NO. IN THE CARD 12345678901234567890123456789012345678901234567890123456789012345...	COMMENTS
71	400.00 7020.00	
72	450.00 8100.00	
73	500.00 9100.00	
74	550.00 10260.00	
75	600.00 11340.00	
76	650.00 12420.00	
77	700.00 13500.00	
78	750.00 14580.00	
79	800.00 15660.00	
80	850.00 16470.00	
81	900.00 17820.00	
82	950.00 18900.00	
83	1000.00 19980.00	
84	1050.00 21060.00	
85	1100.00 22140.00	
86	23	BRAKE PRESSURE VS. TORQUE
87	0.00 0.00	(2F10.2) FRONT RIGHT
88	50.00 0.00	
89	100.00 540.00	
90	150.00 1620.00	
91	200.00 2700.00	
92	250.00 3780.00	
93	300.00 4860.00	
94	350.00 5940.00	
95	400.00 7020.00	
96	450.00 8100.00	
97	500.00 9180.00	
98	550.00 10260.00	
99	600.00 11340.00	
100	650.00 12420.00	
101	700.00 13500.00	
102	750.00 14580.00	
103	800.00 15660.00	
104	850.00 16470.00	
105	900.00 17820.00	
106	950.00 18900.00	
107	1000.00 19980.00	
108	1050.00 21060.00	
109	1100.00 22140.00	
110	23	BRAKE PRESSURE VS. TORQUE
111	0.00 0.00	(2F10.2) REAR LEFT
112	50.00 0.00	
113	100.00 0.00	
114	150.00 900.00	
115	200.00 1800.00	
116	250.00 2700.00	
117	300.00 3600.00	
118	350.00 4500.00	
119	400.00 5400.00	
120	450.00 6300.00	
121	500.00 7200.00	
122	550.00 8100.00	
123	600.00 9000.00	
124	650.00 9900.00	
125	700.00 10800.00	
126	750.00 11700.00	
127	800.00 12600.00	
128	850.00 13500.00	
129	900.00 14400.00	
130	950.00 15300.00	
131	1000.00 16200.00	
132	1050.00 17100.00	
133	1100.00 18000.00	
134	23	BRAKE PRESSURE VS. TORQUE
135	0.00 0.00	(2F10.2) REAR RIGHT
136	50.00 0.00	
137	100.00 0.00	
138	150.00 900.00	
139	200.00 1800.00	
140	250.00 2700.00	
141	300.00 3600.00	
142	350.00 4500.00	
143	400.00 5400.00	
144	450.00 6300.00	
145	500.00 7200.00	

TABLE B5-3 (Cont.)

INPUT CARD NO.	12345678901234567890123456789012345678901234567890123456789012345...	COMMENTS
146	550.00 8100.00	
147	600.00 9000.00	
148	650.00 9900.00	
149	700.00 10800.00	
150	750.00 11700.00	
151	800.00 12600.00	
152	850.00 13600.00	
153	900.00 14400.00	
154	950.00 15300.00	
155	1000.00 16200.00	
156	1050.00 17100.00	
157	1100.00 18000.00	
158	07	SPRING COMPRESSION VS. FORCE
159	-2.00 -2100.00	(2F10.2) FRONT ONE SIDE
160	0.00 -125.00	
161	1.00 825.00	
162	1.50 915.00	
163	6.00 1425.00	
164	6.50 1495.00	
165	7.50 2700.00	
166	07	SPRING COMPRESSION VS. FORCE
167	-2.00 -2000.00	(2F10.2) REAR ONE SIDE
168	0.00 -205.00	
169	1.00 665.00	
170	2.00 825.00	
171	6.50 1475.00	
172	7.00 1575.00	
173	9.00 3570.00	
174	06	TIME VS. STEER (OPTION 3)
175	10.00000	PLAY (F15.5)
176	0.00000 0.00000	(2F15.5)
177	0.10000 0.00000	
178	0.50000 175.00000	
179	3.50000 175.00000	
180	4.60000 0.00000	
181	5.00000 0.00000	
182	15	STEERING VS. WHEEL ANGLE
183	-585.00000 -34.00000 -32.00000	(3F15.5)
184	-540.00000 -31.00000 -29.00000	
185	-450.00000 -25.00000 -24.00000	
186	-360.00000 -19.00000 -18.00000	
187	-270.00000 -14.00000 -12.50000	
188	-180.00000 -9.00000 -7.80000	
189	-90.00000 -4.00000 -3.00000	
190	0.00000 0.00000 0.00000	
191	90.00000 4.00000 5.00000	
192	180.00000 8.40000 9.60000	
193	270.00000 13.60000 15.00000	
194	360.00000 18.40000 20.00000	
195	450.00000 23.80000 26.00000	
196	540.00000 29.40000 31.20000	
197	630.00000 35.00000 37.00000	
198	10	SUSP. COMPRESSION VS. CAMBER
199	-10.00 0.333	(2F10.3)
200	0.00 0.333	
201	1.00 0.608	
202	2.00 0.997	
203	3.00 1.032	
204	4.00 0.733	
205	5.00 0.331	
206	5.00 -0.331	
207	6.50 -0.857	
208	10.00 -0.857	
209	04	LOAD VS. LATERAL STIFFNESS
210	0.00 215.00 2.30 6.00	(4F10.2) FRONT ONE SIDE
211	800.00 215.00 2.30 6.00	
212	1100.00 195.00 0.50 8.00	
213	1700.00 185.00 0.25 18.00	
214	04	LOAD VS. LATERAL STIFFNESS
215	0.00 195.00 1.50 10.00	(4F10.2) REAR ONE SIDE
216	800.00 195.00 1.50 10.00	
217	1100.00 220.00 2.50 6.00	
218	1700.00 210.00 0.50 8.00	
219	04	LOAD VS. LONGITUDINAL STIFFNESS
220	0.00 7000.00	(2F10.2) FRONT ONE SIDE

TABLE B5-3 (Cont.)

```
INPUT                    COLUMN NO. IN THE CARD
CARD NO.  12345678901234567890123456789012345678901234567890123456789012345...   COMMENTS

221          800.00    7000.00
222         1100.00   10000.00
223         1700.00   15000.00
224      04                                                    LOAD VS. LONGITUDINAL STIFFNESS
225            0.00    7000.00                                 (2F10.2)  REAR ONE SIDE
226          800.00    7000.00
227         1100.00   10000.00
228         1700.00   15000.00
229      04                                                    LOAD VS. MUZERO, FRONT
230            1.00       0.92                                (2F10.2)
231          800.00       0.92
232         1100.00       0.96
233         1700.00       0.90
234      04                                                    LOAD VS. MUZERO, REAR
235            1.00       1.00                                (2F10.2)
236          800.00       1.00
237         1100.00       0.95
238         1700.00       0.90
239      05                                                    ALIGNING TORQUE, FRONT, ONE SIDE
240              0.00000 1                                     LOAD, NO.  (F15.5,I2)
241            0.00       0.00                                ANGLE, TORQUE  (2F10.2)
242            800.00000 5
243            0.00       0.00
244            1.00      10.50
245            2.00      28.00
246            4.00      25.00
247           12.00       2.00
248           1100.00000 5
249            0.00       0.00
250            1.00      32.00
251            2.00      50.00
252            4.00      54.00
253           15.00       2.50
254           1400.00000 5
255            0.00       0.00
256            1.00      43.00
257            2.00      72.00
258            4.00      90.00
259           16.00      11.00
260           1700.00000 5
261            0.00       0.00
262            2.00      93.00
263            4.00     120.00
264            8.00     110.00
265           18.00      24.00
266      05                                                    ALIGNING TORQUE, REAR, ONE SIDE
267              0.00000 1                                     LOAD, NO.  (F15.5,I2)
268            0.00       0.00                                ANGLE, TORQUE  (2F10.2)
269            800.00000 5
270            0.00       0.00
271            1.00      16.60
272            2.00      24.10
273            4.00      20.50
274           12.00       1.40
275           1100.00000 5
276            0.00       0.00
277            1.00      28.50
278            2.00      43.70
279            4.00      45.90
280           14.50       2.60
281           1400.00000 5
282            0.00       0.00
283            1.00      40.00
284            2.00      65.50
285            4.00      70.70
286           16.00      10.30
287           1700.00000 5
288            0.00       0.00
289            1.00      50.00
290            2.00      87.00
291            4.00     112.90
292           15.00      21.00
293      10                                                    SUSP. COMPRESSION VS. TOE
294         -10.00000          0.81500                        (2F15.5)
295           0.00000          0.81500
```

TABLE B5-3 (Cont.)

INPUT CARD NO.	12345678901234567890123456789012345678901234567890123456789012345...		COMMENTS
296	1.00000	0.58200	
297	2.00000	0.41500	
298	3.00000	0.38500	
299	4.00000	0.38500	
300	5.00000	0.44800	
301	6.00000	0.62500	
302	6.50000	0.69500	
303	10.00000	0.69500	
304	15		ROLL STEER
305	0.00000	0.00000	(2F15.5)
306	0.50000	0.00000	
307	1.00000	-0.11200	
308	1.50000	-0.21200	
309	2.00000	-0.29500	
310	2.50000	-0.35500	
311	3.00000	-0.41700	
312	3.50000	-0.41800	
313	4.00000	-0.40400	
314	4.50000	-0.36800	
315	5.00000	-0.31700	
316	5.50000	-0.24700	
317	6.00000	-0.15400	
318	6.50000	-0.03000	
319	7.00000	0.07000	
320	0.05000		TINC (F15.5)
321	09		NCAR (I2)

Table B5-4. [illegible] SIMULATION
BUICK STATION WAGON: 175 DEG. TRAJ., 40 MPH, 0E, 24F, 28R

INPUT PARAMETER TABLE

SYMBOL	DESCRIPTION	INITIAL VALUE
A1	HORIZONTAL DISTANCE FROM CG TO MIDPOINT OF FRONT SUSPENSION (IN)	51.60
A2	HORIZONTAL DISTANCE FROM CG TO MIDPOINT OF REAR SUSPENSION (IN)	64.40
ALPHA1	STATIC DISTANCE, FRONT AXLE TO GROUND (IN)	13.00
ALPHA2	STATIC DISTANCE, REAR AXLE TO GROUND (IN)	13.00
AN1	TIRE PRESSURE DISTRIBUTION FUNCTION, FRONT	0.25
AN2	TIRE PRESSURE DISTRIBUTION FUNCTION, REAR	0.25
C1	VISCOUS DAMPING: JOUNCE ON FRONT AXLE (LB-SEC/IN)	1.90
C2	VISCOUS DAMPING: REBOUND ON FRONT AXLE (LB-SEC/IN)	5.66
C3	VISCOUS DAMPING: JOUNCE ON REAR AXLE (LB-SEC/IN)	5.00
C4	VISCOUS DAMPING: REBOUND ON REAR AXLE (LB-SEC/IN)	15.00
CALP1	LATERAL STIFFNESS, FRONT TIRE, ONE SIDE (LBS/DEG)	-1.00
CF1	MAXIMUM COULOMB FRICTION, FRONT SUSPENSION (LB)	40.00
CF2	MAXIMUM COULOMB FRICTION, REAR SUSPENSION (LB)	60.00
CGAMMA	CAMBER STIFFNESS, ONE SIDE (LBS/DEG)	15.00
DELTA1	STATIC VERTICAL DISTANCE, FRONT AXLE TO SPRUNG MASS CG (IN)	15.50
FA1	FRICTION REDUCTION PARAMETER, FRONT TIRES	0.002
FA2	FRICTION REDUCTION PARAMETER, REAR TIRES	0.002
G1	GRAVITY X COMPONENT	0.0
G2	GRAVITY Y COMPONENT	0.0
GR	STEERING GEAR RATIO	22.50
IXX	SPRUNG MASS ROLL MOMENT OF INERTIA (IN-LB-SEC**2)	5312.00
IYY	SPRUNG MASS PITCH MOMENT OF INERTIA (IN-LB-SEC**2)	31781.00
IZZ	SPRUNG MASS YAW MOMENT OF INERTIA (IN-LB-SEC**2)	39900.00
IXZ	SPRUNG MASS PITCH PLANE CROSS MOMENT (IN-LB-SEC**2)	0.0
JA2	ROLL MOMENT OF REAR AXLE (IN-LB-SEC**2)	600.00
JS1	POLAR MOMENT OF FRONT WHEEL, ONE SIDE (IN-LB-SEC**2)	8.00
JS2	POLAR MOMENT OF REAR WHEEL, ONE SIDE (IN-LB-SEC**2)	8.00
K1	SPRING RATE, FRONT SUSPENSION (LB/IN)	-1.00
K2	SPRING RATE, REAR SUSPENSION (LB/IN)	-1.00
KPOFF	KINGPIN OFFSET (IN)	3.44

Table B5-4 (cont) HSRI SIMULATION

BUICK STATION WAGON: 175 DEG SWEEP., 40 MPH, OE, 24F, 28R

PAGE 2

KSC	STEERING COLUMN SPRING RATE (IN-LB/RAD.)	300.00
KSL	STEERING LINKAGE SPRING RATE, ONE SIDE (IN-LB/RAD.)	150000.00
KSW	STEERING TABLE KEY	3
KT1	SPRING RATE, FRONT TIRE, ONE SIDE (LB/IN)	1420.00
KT2	SPRING RATE, REAR TIRE, ONE SIDE (LB/IN)	1420.00
PW	WEIGHT OF PAYLOAD (LBS)	397.00
PJ1	ROLL MOMENT OF INERTIA OF PAYLOAD (IN-LB-SEC**2)	0.0
PJ2	PITCH MOMENT OF INERTIA OF PAYLOAD (IN-LB-SEC**2)	0.0
PJ3	YAW MOMENT OF INERTIA OF PAYLOAD (IN-LB-SEC**2)	0.0
PX	HORIZONTAL DISTANCE FROM MIDPOINT OF REAR SUSPENSION TO PAYLOAD MASS CENTER (IN)	26.37
PZ	VERTICAL DISTANCE FROM GROUND TO PAYLOAD MASS CENTER (IN)	23.63
RCH1	ROLL CENTER HEIGHT, FRONT SUSPENSION (IN)	3.50
RCH2	ROLL CENTER HEIGHT, REAR SUSPENSION (IN)	13.00
RCLLF	FRONT AUXILIARY ROLL STIFFNESS (IN-LB/DEG)	5779.50
RCLLR	REAR AUXILIARY ROLL STIFFNESS (IN-LB/DEG)	0.0
RSCKEY	ROLL STEER TABLE KEY	-2.00
SY1	HORIZONTAL DISTANCE FROM BODY X-AXIS TO FRONT SUSPENSION (IN)	30.05
SY2	HORIZONTAL DISTANCE FROM BODY X-AXIS TO REAR SUSPENSION (IN)	28.50
TIMF	MAXIMUM REAL TIME FOR SIMULATION (SEC)	4.40
TRA1	FRONT HALF TRACK (IN)	30.50
TRA2	REAR HALF TRACK (IN)	30.50
TRAIL	MECHANICAL TRAIL (IN)	0.59
VEL	INITIAL VELOCITY (FPS)	57.50
WIND	TOTAL DRAG COEFFICIENT (LBS/(FT/SEC)**2)	0.02
W	SPRUNG WEIGHT OF CAR (LBS)	3770.00
WS1	WEIGHT OF FRONT SUSPENSION (LBS)	247.40
WS2	WEIGHT OF REAR SUSPENSION (LBS)	405.30

BRAKE PARAMETERS: TQ(AXLE,SIDE,TYPE)

TYPE=1 - THE TIME DELAY BETWEEN FOOT VALVE AND BRAKE LINE

TYPE=2 - THE TIME TO RISE TO 63 PERCENT STEP INPUT LEVEL WITH DELAY=0

TQ(1,1,1) = 0.000 TQ(1,1,2) = 0.000

TQ(1,2,1) = 0.000 TQ(1,2,2) = 0.000

TQ(2,1,1) = 0.000 TQ(2,1,2) = 0.000

TQ(2,2,1) = 0.000 TQ(2,2,2) = 0.000

Table B5-4 (cont) HEST SIMULATION
BUICK STATION WAGON: 175 DEG TWAP., 40 MPH, OB, 24F, 28R
PAGE 3

TABLE OF CONTENTS

TABLE #	REMARKS
1	TIME VS STEERING WHEEL ANGLE
2	STEERING WHEEL ANGLE VS WHEEL ANGLE
3	TIME VS ROAD WHEEL ANGLE (LEFT)
4	TIME VS ROAD WHEEL ANGLE (RIGHT)
5	TIME VS BRAKE LINE PRESSURE
6	PRESSURE VS TORQUE (FRONT,LEFT)
7	PRESSURE VS TORQUE (FRONT,RIGHT)
8	PRESSURE VS TORQUE (REAR,LEFT)
9	PRESSURE VS TORQUE (REAR,RIGHT)
10	SPRING COMPRESSION VS FORCE (FRONT)
11	SPRING COMPRESSION VS FORCE (REAR)
12	SUSPENSION COMPRESSION VS TOE
13	SUSPENSION COMPRESSION VS AXLE DISPLACEMENT (ROLL STEER TABLE)
14	SUSPENSION COMPRESSION VS CAMBER
15	VERTICAL LOAD VS LATERAL STIFFNESS (FRONT, ONE SIDE)
16	VERTICAL LOAD VS LATERAL STIFFNESS (REAR, ONE SIDE)
17	VERTICAL LOAD VS LONGITUDINAL STIFFNESS (FRONT, ONE SIDE)
18	VERTICAL LOAD VS LONGITUDINAL STIFFNESS (REAR, ONE SIDE)
19	VERTICAL LOAD VS MUZERO (FRONT)
20	VERTICAL LOAD VS MUZERO (REAR)
21	ALIGNING TORQUE LOOK-UP (FRONT)
22	ALIGNING TORQUE LOOK-UP (REAR)

TABLE 1: TIME VS STEERING WHEEL ANGLE (DEG); INPUT TABLE
TOTAL PLAY AT THE STEERING WHEEL
IS 10.00 DEGREES
NO. OF POINTS: 6

0.0	0.0
0.1000	0.0
0.5000	175.0000
3.6000	175.0000
4.6000	0.0
5.0000	0.0

TABLE 2: STEERING WHEEL ANGLE (DEG) VS MEAN WHEEL ANGLE (DEG); INPUT TABLE
NO. OF POINTS: 15

STEERING WHEEL	LEFT WHEEL	RIGHT WHEEL
-585.0000	-34.0000	-32.0000
-540.0000	-31.0000	-29.8000
-450.0000	-25.0000	-24.0000
-360.0000	-19.0000	-18.0000
-270.0000	-14.0000	-12.5000
-180.0000	-9.0000	-7.8000
-90.0000	-4.0000	-3.0000
0.0	0.0	0.0
90.0000	4.0000	5.0000
180.0000	8.4000	9.6000
270.0000	13.6000	15.0000
360.0000	18.4000	20.0000
450.0000	23.8000	26.0000
540.0000	29.4000	31.2000
630.0000	35.0000	37.0000

TABLE 3: TIME VS ROAD WHEEL ANGLE (DEG); OUTPUT TABLE
LEFT ROAD WHEEL
TOTAL PLAY AT THE ROAD WHEEL
IS 0.44 DEGREES
NO. OF POINTS: 8

0.0	0.0
0.1000	0.0
0.1109	0.0
0.5000	7.9333
3.6000	7.9333
3.6545	7.9333
4.6000	0.2222
5.0000	0.2222

TABLE 4: TIME VS ROAD WHEEL ANGLE (DEG); OUTPUT TABLE
RIGHT ROAD WHEEL
TOTAL PLAY AT THE ROAD WHEEL
IS 0.44 DEGREES
NO. OF POINTS: 8

0.0	0.0
0.1000	0.0
0.1095	0.0
0.5000	9.1222
3.6000	9.1222
3.6476	9.1222
4.6000	0.2222
5.0000	0.2222

TABLE 5: TIME VS PRESSURE AT FOOT VALVE (PSI)
NO. OF POINTS: 1

0.0	0.0

TABLE 6: PRESSURE (PSI) VS TORQUE(IN-LBS)
FRONT BRAKES, LEFT SIDE
NO. OF POINTS: 23

0.0	0.0
50.0000	0.0
100.0000	540.0000
150.0000	1620.0000
200.0000	2700.0000
250.0000	3780.0000
300.0000	4860.0000
350.0000	5940.0000
400.0000	7020.0000
450.0000	8100.0000
500.0000	9180.0000
550.0000	10260.0000
600.0000	11340.0000
650.0000	12420.0000
700.0000	13500.0000
750.0000	14580.0000
800.0000	15660.0000
850.0000	16470.0000
900.0000	17820.0000
950.0000	18900.0000
1000.0000	19980.0000
1050.0000	21060.0000
1100.0000	22140.0000

TABLE 7: PRESSURE (PSI) VS TORQUE (IN-LBS)
FRONT BRAKES,RIGHT SIDE
NO. OF POINTS: 23

0.0	0.0
50.0000	0.0
100.0000	540.0000
150.0000	1620.0000
200.0000	2700.0000
250.0000	3780.0000
300.0000	4860.0000
350.0000	5940.0000
400.0000	7020.0000
450.0000	8100.0000
500.0000	9180.0000
550.0000	10260.0000
600.0000	11340.0000
650.0000	12420.0000
700.0000	13500.0000
750.0000	14580.0000
800.0000	15660.0000
850.0000	16470.0000
900.0000	17820.0000
950.0000	18900.0000
1000.0000	19980.0000
1050.0000	21060.0000
1100.0000	22140.0000

TABLE 8: PRESSURE (PSI) VS TORQUE(IN-LBS)
REAR BRAKE, LEFT SIDE
NO. OF POINTS: 23

0.0	0.0
50.0000	0.0
100.0000	0.0
150.0000	900.0000
200.0000	1800.0000
250.0000	2700.0000
300.0000	3600.0000
350.0000	4500.0000
400.0000	5400.0000
450.0000	6300.0000
500.0000	7200.0000
550.0000	8100.0000
600.0000	9000.0000
650.0000	9900.0000
700.0000	10800.0000
750.0000	11700.0000
800.0000	12600.0000
850.0000	13600.0000
900.0000	14400.0000
950.0000	15300.0000
1000.0000	16200.0000
1050.0000	17100.0000
1100.0000	18000.0000

TABLE 9: PRESSURE (PSI) VS TORQUE (IN-LBS)
REAR BRAKE, RIGHT SIDE
NO. OF POINTS: 23

0.0	0.0
50.0000	0.0
100.0000	0.0
150.0000	900.0000
200.0000	1800.0000
250.0000	2700.0000
300.0000	3600.0000
350.0000	4500.0000
400.0000	5400.0000
450.0000	6300.0000
500.0000	7200.0000
550.0000	8100.0000
600.0000	9000.0000
650.0000	9900.0000
700.0000	10800.0000
750.0000	11700.0000
800.0000	12600.0000
850.0000	13600.0000
900.0000	14400.0000
950.0000	15300.0000
1000.0000	16200.0000
1050.0000	17100.0000
1100.0000	18000.0000

TABLE 10: SPRING COMPRESSION (IN) VS FORCE
FRONT SUSPENSION ...ONE SPRING ONLY
NOTE: BOTH FRONT SPRINGS ARE IDENTICAL
REFERENCE SYSTEM: (0.0, -WS2/2.) AT THE REBOUND STOP,
THEN INCREASINGLY POSITIVE FORCES FOR INCREASING
COMPRESSIVE LOADS IN THE SPRING.
NO. OF POINTS: 7

-2.0000	-2100.0000
0.0	-125.0000
1.0000	825.0000
1.5000	915.0000
6.0000	1425.0000
6.5000	1495.0000
7.5000	2700.0000

TABLE 11: SPRING COMPRESSION (IN) VS FORCE
REAR SUSPENSION ...ONE SPRING ONLY
NOTE: BOTH REAR SPRINGS ARE IDENTICAL
REFERENCE SYSTEM: (0.0, -WS1/2.) AT THE REBOUND STOP,
THEN INCREASINGLY POSITIVE FORCES FOR INCREASING
COMPRESSIVE LOADS IN THE SPRING.
NO. OF POINTS: 7

-2.0000	-2000.0000
0.0	-205.0000
1.0000	665.0000
2.0000	825.0000
6.5000	1475.0000
7.0000	1575.0000
9.0000	3570.0000

TABLE 12: SUSPENSION COMPRESSION (IN) VS TOE
(FOR LEFT FRONT WHEEL, TOE FOLLOWS RIGHT HAND RULE.)
ZERO COMPRESSION AT THE REBOUND STOP
NO. OF POINTS: 10

-10.000	0.815
0.0	0.815
1.000	0.582
2.000	0.415
3.000	0.385
4.000	0.385
5.000	0.448
6.000	0.625
6.500	0.695
10.000	0.695

TABLE 13: ROLL STEER
SUSPENSION COMPRESSION(IN) VS FORE-AFT AXLE DISPLACEMENT(IN)
NO. OF POINTS:15

0.0	0.0
0.500	0.0
1.000	-0.112
1.500	-0.212
2.000	-0.295
2.500	-0.355
3.000	-0.417
3.500	-0.418
4.000	-0.404
4.500	-0.366
5.000	-0.317
5.500	-0.247
6.000	-0.154
6.500	-0.030
7.000	0.070

TABLE 14: SUSPENSION COMPRESSION (IN) VS CAMBER (DEG)
ZERO COMPRESSION AT THE REBOUND STOP
NO. OF POINTS: 10

-10.0000	0.3300
0.0	0.3300
1.0000	0.6000
2.0000	0.9900
3.0000	1.0300
4.0000	0.7300
5.0000	0.3300
6.0000	-0.3300
6.5000	-0.8500
10.0000	-0.8500

TABLE 15: VERTICAL LOAD VS LATERAL STIFFNESS (LBS/DEG)
FRONT TIRE, ONE SIDE
AN1= 0.250
FA1= 0.002
NO. OF POINTS: 4

LOAD	STIFFNESS	CA1	CA2
0.0	215.0000	2.3000	6.0000
800.0000	215.0000	2.3000	6.0000
1100.0000	195.0000	0.5000	8.0000
1700.0000	185.0000	0.2500	18.0000

TABLE 16: VERTICAL LOAD VS LATERAL STIFFNESS (LBS/DEG)
REAR TIRE, ONE SIDE
AN2= 0.250
FA2= 0.002
NO. OF POINTS: 4

LOAD	STIFFNESS	CA1	CA2
0.0	195.0000	1.5000	10.0000
800.0000	195.0000	1.5000	10.0000
1100.0000	220.0000	2.5000	6.0000
1700.0000	210.0000	0.5000	8.0000

TABLE 17: VERTICAL LOAD VS LONGITUDINAL STIFFNESS (LBS)
FRONT TIRE, ONE SIDE
NO. OF POINTS: 4

0.0	7000.0000
800.0000	7000.0000
1100.0000	10000.0000
1700.0000	15000.0000

TABLE 18: VERTICAL LOAD VS LONGITUDINAL STIFFNESS (LBS)
REAR TIRE, ONE SIDE
NO. OF POINTS: 4

0.0	7000.0000
800.0000	7000.0000
1100.0000	10000.0000
1700.0000	15000.0000

TABLE 19: VERTICAL LOAD VS MUZERO
FRONT TIRE, ONE SIDE
NO. OF POINTS: 4

1.0000	0.9200
800.0000	0.9200
1100.0000	0.9600
1700.0000	0.9000

TABLE 20: VERTICAL LOAD VS MUZERO
REAR TIRE, ONE SIDE
NO. OF POINTS: 4

1.0000	1.0000
800.0000	1.0000
1100.0000	0.9500
1700.0000	0.9000

TABLE 21: ALIGNING TORQUE LOCK-UP--FRONT TIRE, ONE SIDE

VERTICAL LOAD: 0.0 LBS.

SIDESLIP ANGLE(DEG)	VS ALIGNING TORQUE(FT-LBS)
0.0	0.0

VERTICAL LOAD: 800.000 LBS.

SIDESLIP ANGLE(DEG)	VS ALIGNING TORQUE(FT-LBS)
0.0	0.0
1.000	19.500
2.000	28.000
4.000	25.000
12.000	2.000

VERTICAL LOAD: 1100.000 LBS.

SIDESLIP ANGLE(DEG)	VS ALIGNING TORQUE(FT-LBS)
0.0	0.0
1.000	32.000
2.000	50.000
4.000	54.000
15.000	2.500

VERTICAL LOAD: 1400.000 LBS.

SIDESLIP ANGLE(DEG)	VS ALIGNING TORQUE(FT-LBS)
0.0	0.0
1.000	43.000
2.000	72.000
4.000	90.000
16.000	11.600

VERTICAL LOAD: 1700.000 LBS.

SIDESLIP ANGLE(DEG)	VS ALIGNING TORQUE(FT-LBS)
0.0	0.0
2.000	93.000
4.000	126.000
8.000	110.000
18.000	24.000

TABLE 22: ALIGNING TORQUE LOCK-UP--REAR TIRE, ONE SIDE

VERTICAL LOAD: 0.0 LBS.

SIDESLIP ANGLE(DEG)	VS ALIGNING TORQUE(FT-LBS)
0.0	0.0

VERTICAL LOAD: 800.000 LBS.

SIDESLIP ANGLE(DEG)	VS ALIGNING TORQUE(FT-LBS)
0.0	0.0
1.000	16.600
2.000	24.100
4.000	20.500
12.000	1.400

Table B5-4 (cont) HSRI SIMULATION
BUICK STATION WAGON: 17° DEG TRAP., 40 MPH, OE, 24F, 28R


```
VERTICAL LOAD:    1100.000 LBS.
    SIDESLIP ANGLE(DEG) VS ALIGNING TORQUE(FT-LBS)
     0.0             0.0
     1.000          28.500
     2.000          43.700
     4.000          45.900
    14.500           2.600
VERTICAL LOAD:    1400.000 LBS.
    SIDESLIP ANGLE(DEG) VS ALIGNING TORQUE(FT-LBS)
     0.0             0.0
     1.000          40.000
     2.000          65.500
     4.000          76.700
    16.000          10.300
VERTICAL LOAD:    1700.000 LBS.
    SIDESLIP ANGLE(DEG) VS ALIGNING TORQUE(FT-LBS)
     0.0             0.0
     1.000          50.000
     2.000          87.000
     4.000         112.900
    15.000          21.000

*** END INPUT ***
```

Table B5-4 (cont)

	EMPTY	LOADED
DISTANCE FROM SPRUNG MASS CENTER TO REAR AXLE CENTERLINE (IN)	64.400	60.748
DISTANCE FROM SPRUNG MASS CENTER TO GROUND (IN)	28.500	27.690
ROLL MOMENT OF SPRUNG MASS (IN-LB-SEC**2)	5311.996	5379.887
PITCH MOMENT OF SPRUNG MASS (IN-LB-SEC**2)	31780.996	33215.059
YAW MOMENT OF SPRUNG MASS (IN-LB-SEC**2)	39900.000	41280.555

YAW MOMENT OF ENTIRE VEHICLE IS 48242.62 IN-LB-SEC**2

THE CG OF THE TOTAL VEHICLE IS 57.52 INCHES BEHIND THE FRONT AXLE, 25.70 INCHES ABOVE THE GROUND.

TABLE LOOKUP FOR ONE FRONT SPRING ...IN THE STATIC CONFIGURATION THE DEFLECTION IS 3.05 INCHES FOR 1090. POUNDS

TABLE LOOKUP FOR ONE REAR SPRING ...IN THE STATIC CONFIGURATION THE DEFLECTION IS 3.16 INCHES FOR 992. POUNDS

THE STATIC LOADS ON THE TIRES ARE

AXLE NUMBER	LOAD
1	2429.621
2	2390.074
TOTAL	4819.695

APPROXIMATE NATURAL FREQUENCIES (HZ):

ROLL	1.50
BOUNCE	1.10
PITCH	1.16

STATIC MARGIN:

TWO DEGREES OF FREEDOM	0.047
THREE DEGREES OF FREEDOM	0.032

TIME INCREMENT TO BE PRINTED OUT IS 0.05

*** BEGIN OUTPUT ***

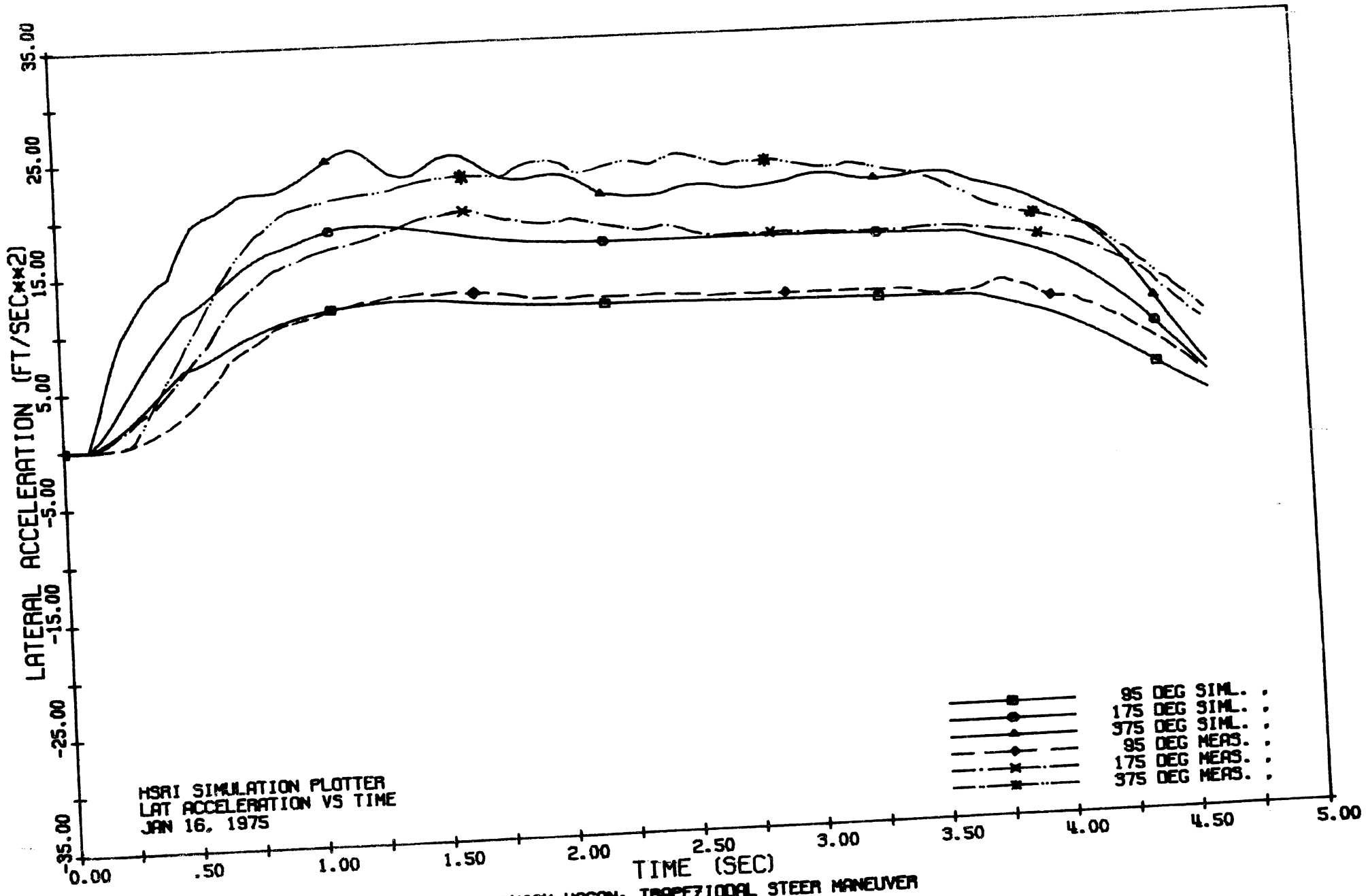
LATERAL ACCELERATION (FT/SEC**2)
35.00
25.00
15.00
5.00
-5.00
-15.00
-25.00
-35.00
0.00
.50
1.00
1.50
2.00
2.50
3.00
3.50
4.00
4.50
5.00
TIME (SEC)
HSRI SIMULATION PLOTTER
LAT ACCELERATION VS TIME
JAN 16, 1975
95 DEG SIML.
175 DEG SIML.
375 DEG SIML.
95 DEG MEAS.
175 DEG MEAS.
375 DEG MEAS.
BUICK WAGON: TRAPEZIODAL STEER MANEUVER

Figure B5-2.

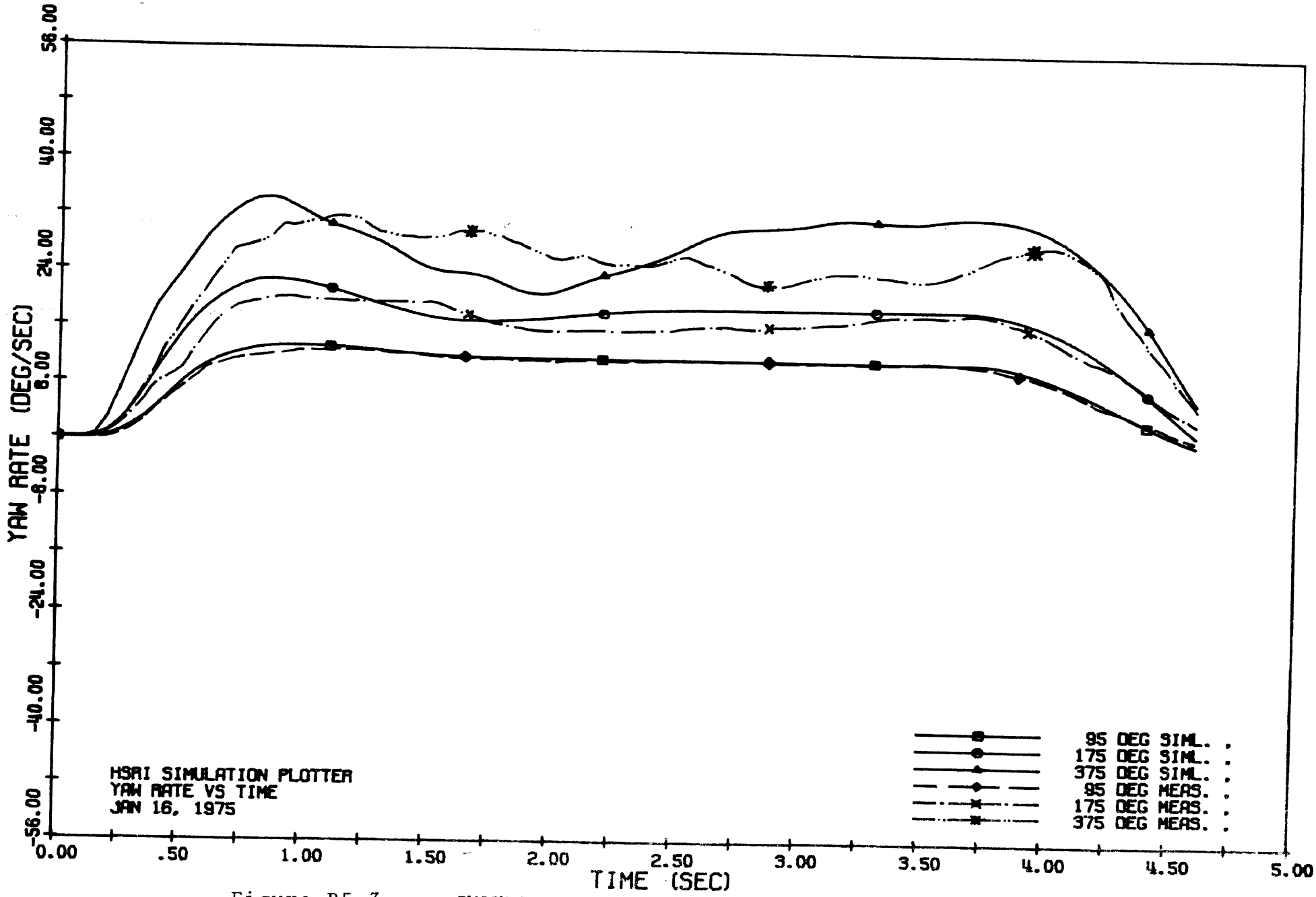
56.00
40.00
24.00
8.00
-8.00
-24.00
-40.00
-56.00
YAW RATE (DEG/SEC)
0.00
.50
1.00
1.50
2.00
2.50
3.00
3.50
4.00
4.50
5.00
TIME (SEC)
HSRI SIMULATION PLOTTER
YAW RATE VS TIME
JAN 16, 1975
95 DEG SIML.
175 DEG SIML.
375 DEG SIML.
95 DEG MEAS.
175 DEG MEAS.
375 DEG MEAS.
BUICK WAGON: TRAPEZIODAL STEER MANEUVER

Figure B5-3.

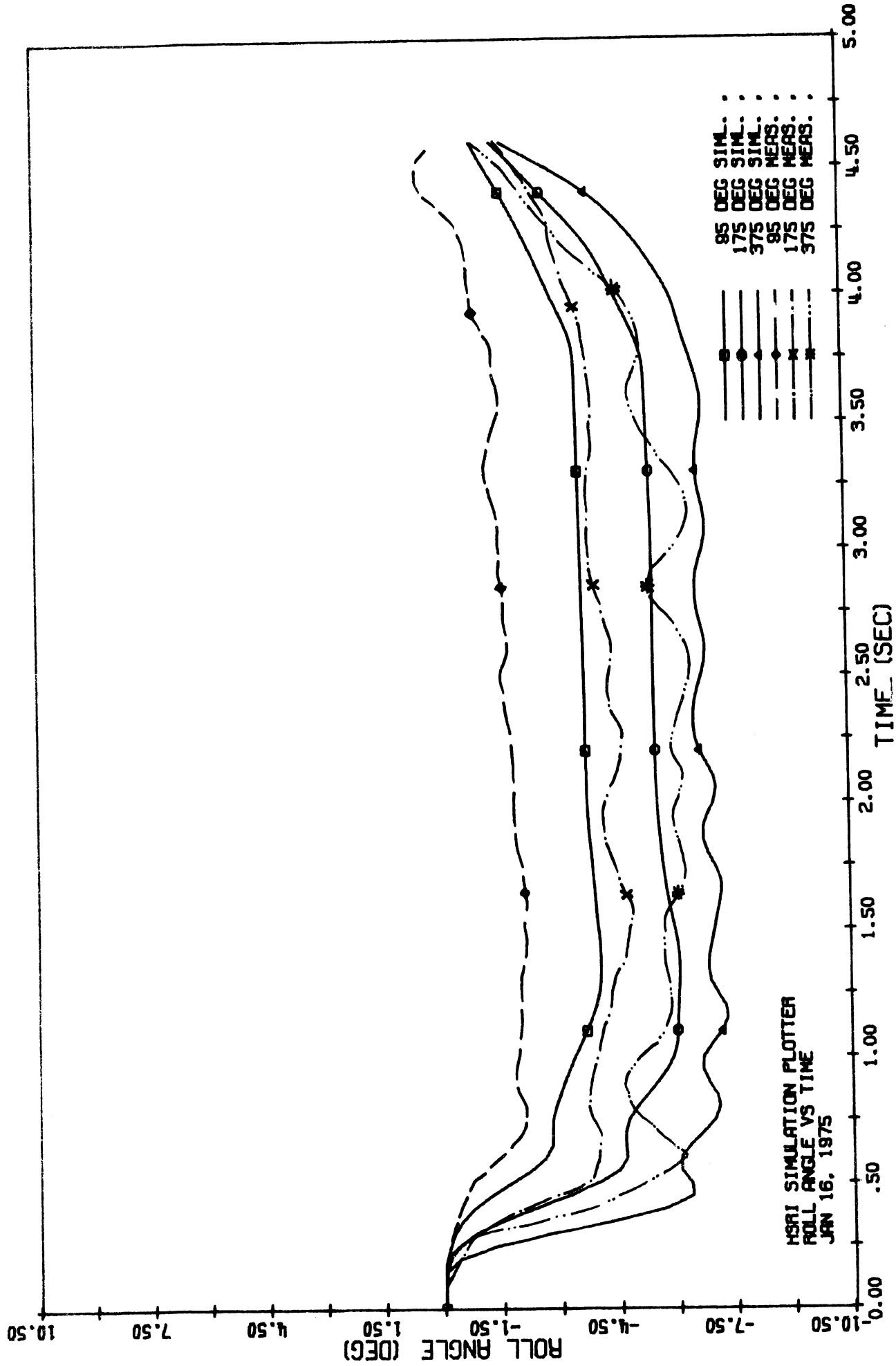
HSRI SIMULATION PLOTTER
ROLL ANGLE VS TIME
JAN 16, 1975
85 DEG SIML.
175 DEG SIML.
375 DEG SIML.
85 DEG MEAS.
175 DEG MEAS.
375 DEG MEAS.
ROLL ANGLE (DEG)
TIME (SEC)
BUICK WAGON: TRAPEZIODAL STEER MANEUVER

Figure B5-4.

TABLE B5-5.

INPUT DATA LIST
FOR THE BUICK WAGON (SIMPLE CASE)

INPUT CARD NO.	COLUMN NO. IN THE CARD 12345678901234567890123456789012345678901234567890123456789012345...	COMMENTS	
1		HEAD	(20A4) FORMAT
2	51.60000	A1	(F15.5) FORMAT
3	64.40000	A2	
4	13.00000	ALPHA1	
5	13.00000	ALPHA2	
6	0.25000	AN1	
7	0.25000	AN2	
8	1.90000	C1	
19	5.66000	C2	
10	5.00000	C3	
11	15.00000	C4	
12	195.00000	CALF1	
13	220.00000	CALF2	
14	40.00000	CF1	
15	60.00000	CF2	
16	15.00000	GGAMMA	
17	10000.00000	GS1	
18	10000.00000	GS2	
19	15.50000	DELTA1	
20	0.00200	FA1	
21	0.00200	FA2	
22	0.00000	G1	
23	0.00000	G2	
24	22.50000	GR	
25	5312.00000	J1	
26	31781.00000	J2	
27	39900.00000	J3	
28	0.00000	IXZ	
29	600.00000	JA2	
30	8.00000	JS1	
31	8.00000	JS2	
32	113.30000	K1	
33	144.40000	K2	
34	3.44000	KPOFF	
35	300.00000	KSC	
36	150000.00000	KSL	
37	01	KSM	(I2) FORMAT
38	1420.00000	KT1	(F15.5) FORMAT
39	1420.00000	KT2	
40	0.92000	MUZERO1	
41	0.05000	MUZERO2	
42	397.00000	PJ	
43	0.00000	PJ1	
44	0.00000	PJ2	
45	0.00000	PJ3	
46	26.07000	PX	
47	20.00000	PZ	
48	3.50000	RCH1	
49	13.00000	RCH2	
50	5779.50000	ROLLF	
51	0.00000	ROLLR	
52	-0.10000	RSC	
53	30.05000	SY1	
54	20.50000	SY2	
55	4.40000	TIMF	
56	30.50000	TRA1	
57	30.50000	TRA2	
58	0.59000	TRAIL	
59	57.50000	VEL	
60	0.02400	WIND	
61	3770.00000	W	
62	247.40000	WS1	
63	405.30000	WS2	
64	3.10000	ZBAR	
65	00	KEYTQ	(I2) FORMAT
66	01	TIME VS. BRAKE PRESSURE	
67	0.00 0.00	(2F10.2)	

TABLE B5-5 (Cont.)

INPUT CARD NO.	12345678901234567890123456789012345678901234567890123456789012345...	COMMENTS
68	02	BRAKE PRESSURE VS. TORQUE
69	0.00 0.00	(2F10.2) FRONT LEFT
70	1100.00 22140.00	
71	02	BRAKE PRESSURE VS. TORQUE
72	0.00 0.00	(2F10.2) FRONT RIGHT
73	1100.00 22140.00	
74	02	BRAKE PRESSURE VS. TORQUE
75	0.00 0.00	(2F10.2) REAR LEFT
76	1100.00 18000.00	
77	02	BRAKE PRESSURE VS. TORQUE
78	0.00 0.00	(2F10.2) REAR RIGHT
79	1100.00 18000.00	
80	05	TIME VS. STEER
81	0.00000 0.00000	(2F15.5)
82	0.10000 0.00000	
83	0.40000 12.20000	
84	3.60000 12.20000	
85	4.60000 0.00000	
86	01	SUSP. COMPRESSION VS. CAMBER
87	0.00 0.00	(2F10.2)
88	0.05000	TIMC (F15.5) ·
89	00	NCAR (I2)

Table B5-6

HSRI SIMULATION:
BUICK WAGON: SIMPLE MODEL , 2400.0 DEG TRAP.,PSI VARIATION RUNS FOR G-E TIRES
PAGE 1

INPUT PARAMETER TABLE

SYMBOL	DESCRIPTION	INITIAL VALUE
A1	HORIZONTAL DISTANCE FROM CG TO MIDPOINT OF FRONT SUSPENSION (IN)	51.60
A2	HORIZONTAL DISTANCE FROM CG TO MIDPOINT OF REAR SUSPENSION (IN)	54.40
ALPHA1	STATIC DISTANCE, FRONT AXLE TO GROUND (IN)	13.00
ALPHA2	STATIC DISTANCE, REAR AXLE TO GROUND (IN)	13.00
AN1	TIRE PRESSURE DISTRIBUTION FUNCTION, FRONT	0.25
AN2	TIRE PRESSURE DISTRIBUTION FUNCTION, REAR	0.25
C1	VISCOUS DAMPING: JOUNCE ON FRONT AXLE (LB-SEC/IN)	1.00
C2	VISCOUS DAMPING: REBOUND ON FRONT AXLE (LB-SEC/IN)	5.00
C3	VISCOUS DAMPING: JOUNCE ON REAR AXLE (LB-SEC/IN)	5.00
C4	VISCOUS DAMPING: REBOUND ON REAR AXLE (LB-SEC/IN)	15.00
CALF1	LATERAL STIFFNESS, FRONT TIRE, ONE SIDE (LBS/DEG)	195.00
CALF2	LATERAL STIFFNESS, REAR TIRE, ONE SIDE (LBS/DEG)	220.00
CF1	MAXIMUM COULOMB FRICTION, FRONT SUSPENSION (LB)	40.00
CF2	MAXIMUM COULOMB FRICTION, REAR SUSPENSION (LB)	80.00
CGAMMA	CAMBER STIFFNESS, ONE SIDE (LBS/DEG)	15.00
CS1	LONGITUDINAL STIFFNESS, FRONT TIRES (LBS)	10000.00
CS2	LONGITUDINAL STIFFNESS, REAR TIRES (LBS)	10000.00
DELTA1	STATIC VERTICAL DISTANCE, FRONT AXLE TO SPRUNG MASS CG (IN)	15.50
FA1	FRICTION REDUCTION PARAMETER, FRONT TIRES	0.002
FA2	FRICTION REDUCTION PARAMETER, REAR TIRES	0.002
G1	GRAVITY X COMPONENT	0.0
G2	GRAVITY Y COMPONENT	0.0
GR	STEERING GEAR RATIO	22.50
IXX	SPRUNG MASS ROLL MOMENT OF INERTIA (IN-LB-SEC**2)	5312.00
IYY	SPRUNG MASS PITCH MOMENT OF INERTIA (IN-LB-SEC**2)	31781.00
IZZ	SPRUNG MASS YAW MOMENT OF INERTIA (IN-LB-SEC**2)	32900.00
IXZ	SPRUNG MASS PITCH PLANE CROSS MOMENT (IN-LB-SEC**2)	0.0
JA2	ROLL MOMENT OF REAR AXLE (IN-LB-SEC**2)	600.00
JS1	POLAR MOMENT OF FRONT WHEEL, ONE SIDE (IN-LB-SEC**2)	8.00
JS2	POLAR MOMENT OF REAR WHEEL, ONE SIDE (IN-LB-SEC**2)	8.00
K1	SPRING RATE, FRONT SUSPENSION (LB/IN)	113.30
K2	SPRING RATE, REAR SUSPENSION (LB/IN)	144.40
KPOFF	KINGPIN OFFSET(IN)	3.44

Table B5-6 (Cont)

HSRI SIMULATION

QUICK MASCHI SIMPLE MODEL , 240.0 DEG F..PSI VARIATION RUNS FOR 0-E ..ES

KSC	STEERING COLUMN SPRING RATE (IN-LB/RAD.)	300.00
KSL	STEERING LINKAGE SPRING RATE, ONE SIDE (IN-LB/RAD.)	150000.00
KSW	STEERING TABLE KEY	1
KT1	SPRING RATE, FRONT TIRE, ONE SIDE (LB/IN)	1420.00
KT2	SPRING RATE, REAR TIRE, ONE SIDE (LB/IN)	1420.00
MUZERO1	COEFFICIENT OF FRICTION, FRONT WHEELS	0.92
MUZERO2	COEFFICIENT OF FRICTION, REAR WHEELS	0.95
PW	WEIGHT OF PAYLOAD (LBS)	307.00
PJ1	ROLL MOMENT OF INERTIA OF PAYLOAD (IN-LB-SEC**2)	0.0
PJ2	PITCH MOMENT OF INERTIA OF PAYLOAD (IN-LB-SEC**2)	0.0
PJ3	YAW MOMENT OF INERTIA OF PAYLOAD (IN-LB-SEC**2)	0.0
PX	HORIZONTAL DISTANCE FROM MIDPOINT OF REAR SUSPENSION TO PAYLOAD MASS CENTER (IN)	26.07
PZ	VERTICAL DISTANCE FROM GROUND TO PAYLOAD MASS CENTER (IN)	20.00
RCH1	ROLL CENTER HEIGHT, FRONT SUSPENSION (IN)	3.50
RCH2	ROLL CENTER HEIGHT, REAR SUSPENSION (IN)	13.00
ROLLF	FRONT AUXILIARY ROLL STIFFNESS (IN-LB/DEG)	5779.50
ROLLR	REAR AUXILIARY ROLL STIFFNESS (IN-LB/DEG)	0.0
RSCS	ROLL STEER COEFFICIENT AT STATIC EQUILIBRIUM (OVERSTEER IS POSITIVE)	-0.10
SY1	HORIZONTAL DISTANCE FROM BODY X-AXIS TO FRONT SUSPENSION (IN)	30.05
SY2	HORIZONTAL DISTANCE FROM BODY X-AXIS TO REAR SUSPENSION (IN)	29.50
TIME	MAXIMUM REAL TIME FOR SIMULATION (SEC)	4.60
TRA1	FRONT HALF TRACK (IN)	30.50
TRA2	REAR HALF TRACK (IN)	30.50
TRAIL	MECHANICAL TRAIL (IN)	0.59
VEL	INITIAL VELOCITY (FPS)	57.50
WIND	TOTAL DRAG COEFFICIENT(LBS/(FT/SEC)**2)	0.02
W	SPRUNG WEIGHT OF CAR (LBS)	3770.00
WS1	WEIGHT OF FRONT SUSPENSION (LBS)	247.40
WS2	WEIGHT OF REAR SUSPENSION (LBS)	405.30
ZBAR	STATIC SUSPENSION DEFLECTION-- REAR SPRINGS	3.100

BRAKE PARAMETERS: TQ(AXLE,SIDE,TYPE)

TYPE=1 - THE TIME DELAY BETWEEN FOOT VALVE AND BRAKE LINE

TYPE=2 - THE TIME TO RISE TO 63 PERCENT STEP INPUT LEVEL WITH DELAY=0

TQ(1,1,1) = 0.000 TQ(1,1,2) = 0.000

TQ(1,2,1) = 0.000 TQ(1,2,2) = 0.000

TQ(2,1,1) = 0.000 TQ(2,1,2) = 0.000

Table B5-6 (Cont) HSRI SIMULATION

BUICK WAGON: SIMPLE MODEL , 240.0 DEG TRAP.,PSI VARIATION RUNS FOR G-E TIRES

TABLE OF CONTENTS

TABLE 1: TIME VS ROAD WHEEL ANGLE (DEG); INPUT TABLE
NO. OF POINTS: 5

0.0	0.0
0.1000	0.0
0.4000	12.2000
3.6000	12.2000
4.6000	0.0

TABLE 2: TIME VS PRESSURE AT FOOT VALVE (PSI)
NO. OF POINTS: 1

0.0	0.0

TABLE 3: PRESSURE (PSI) VS TORQUE(IN-LBS)
FRONT BRAKES, LEFT SIDE
NO. OF POINTS: 2

0.0	0.0
1100.0000	22140.0000

TABLE 4: PRESSURE (PSI) VS TORQUE (IN-LBS)
FRONT BRAKES,RIGHT SIDE
NO. OF POINTS: 2

0.0	0.0
1100.0000	22140.0000

TABLE 5: PRESSURE (PSI) VS TORQUE(IN-LBS)
REAR BRAKE, LEFT SIDE
NO. OF POINTS: 2

0.0	0.0
1100.0000	18000.0000

TABLE 6: PRESSURE (PSI) VS TORQUE (IN-LBS)
REAR BRAKE, RIGHT SIDE
NO. OF POINTS: 2

0.0	0.0
1100.0000	18000.0000

TABLE 7: SUSPENSION COMPRESSION (IN) VS CAMBER (DEG)
ZERO COMPRESSION AT THE REBOUND STOP
NO. OF POINTS: 1

0.0 0.0

*** END INPUT ***

Table B5-6 (Cont.)

HSRI SIMULATION
QUICK WAGON: SIMPLE MODEL , 240.0 DEG TRAP.,PSI VARIATION RUNS FOR O-E TIRES
PAGE 6

	EMPTY	LOADED
DISTANCE FROM SPRUNG MASS CENTER TO REAR AXLE CENTERLINE (IN)	64.490	60.746
DISTANCE FROM SPRUNG MASS CENTER TO GROUND (IN)	28.500	27.690
ROLL MOMENT OF SPRUNG MASS (IN-LB-SEC**2)	5311.996	5379.887
PITCH MOMENT OF SPRUNG MASS (IN-LB-SEC**2)	31780.996	33215.059
YAW MOMENT OF SPRUNG MASS (IN-LB-SEC**2)	39900.000	41280.555

YAW MOMENT OF ENTIRE VEHICLE IS 48242.62 IN-LB-SEC**2

THE CG OF THE TOTAL VEHICLE IS 57.52 INCHES BEHIND THE FRONT AXLE, 25.70 INCHES ABOVE THE GROUND.

THE STATIC LOADS ON THE TIRES ARE

AXLE NUMBER	LOAD
1	2429.421
2	2390.074
TOTAL	4819.495

APPROXIMATE NATURAL FREQUENCIES (HZ):

ROLL	1.50
BOUNCE	1.10
PITCH	1.16

STATIC MARGIN:

TWO DEGREES OF FREEDOM	0.054
THREE DEGREES OF FREEDOM	0.023

TIME INCREMENT TO BE PRINTED OUT IS 0.05

*** BEGIN OUTPUT ***

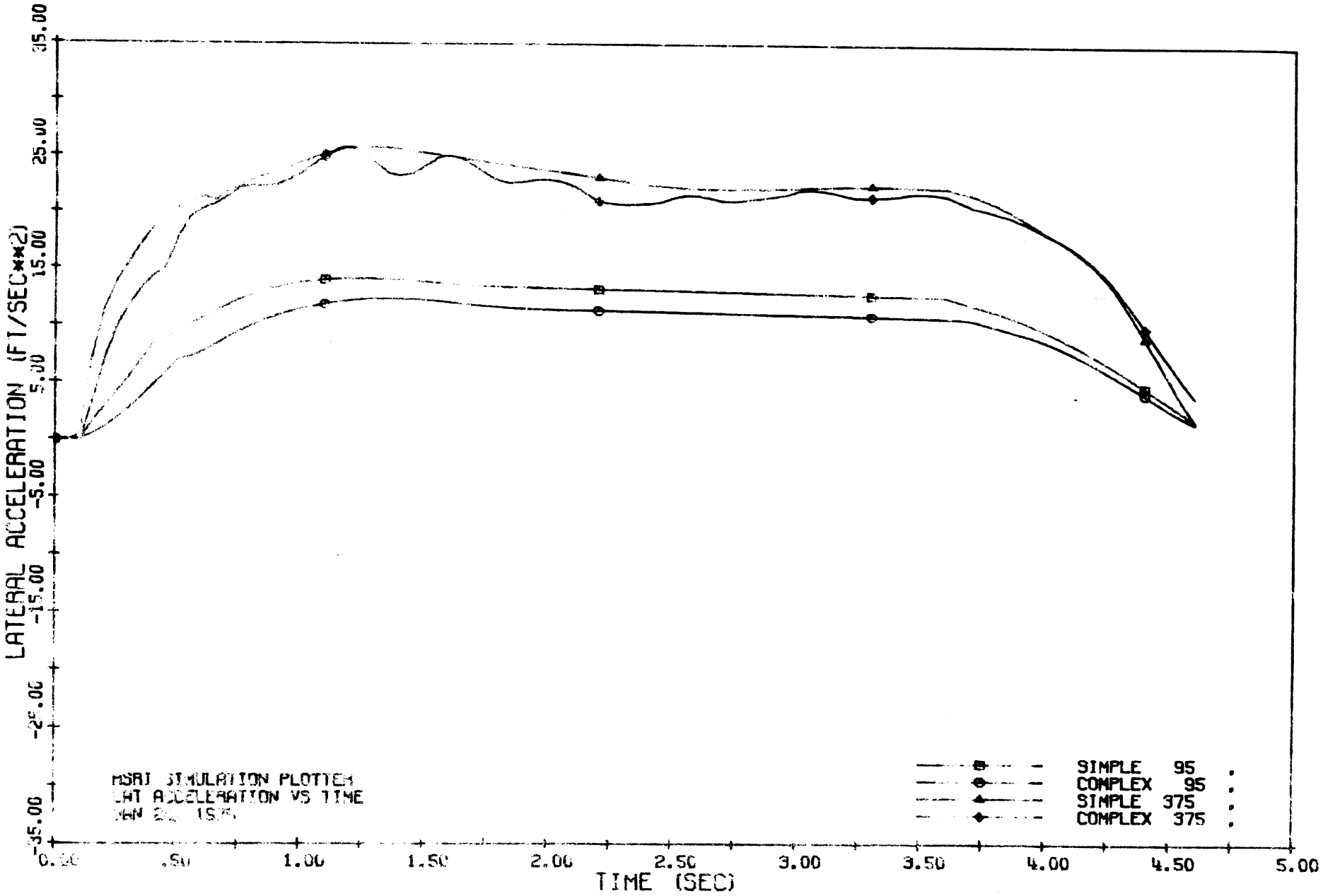

Figure B5-5a BUICK-REGAL: TRAPEZOIDAL STEER MANEUVER COMPARISION

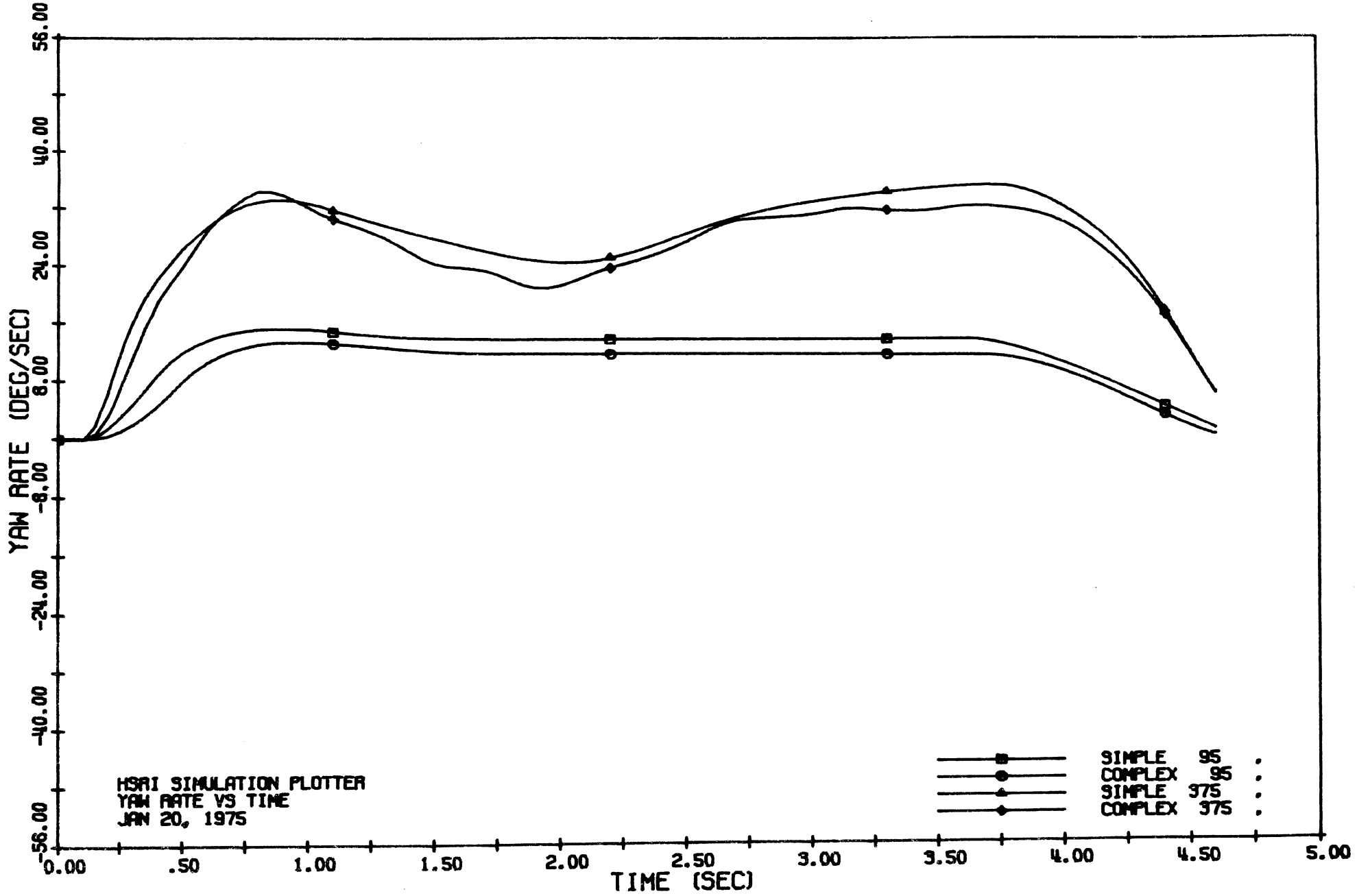

Figure B5-5b. BUICKWAGON: TRAPEZOIDAL STEER MANEUVER COMPARISION

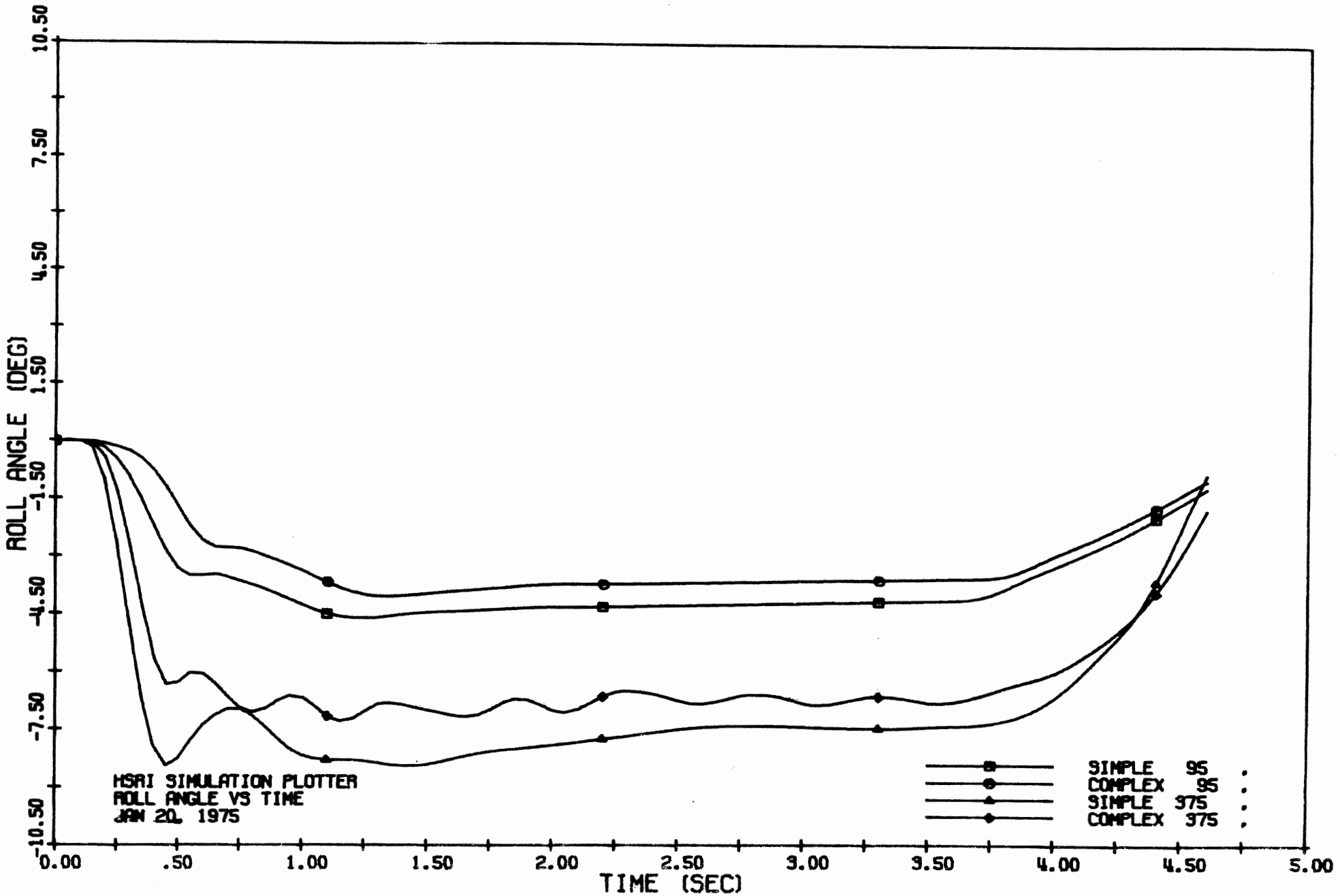

Figure B5-5c. BUICKWAGON: TRAPEZOIDAL STEER MANEUVER COMPARISION

B6. FLOW CHARTS

MAIN PROGRAM

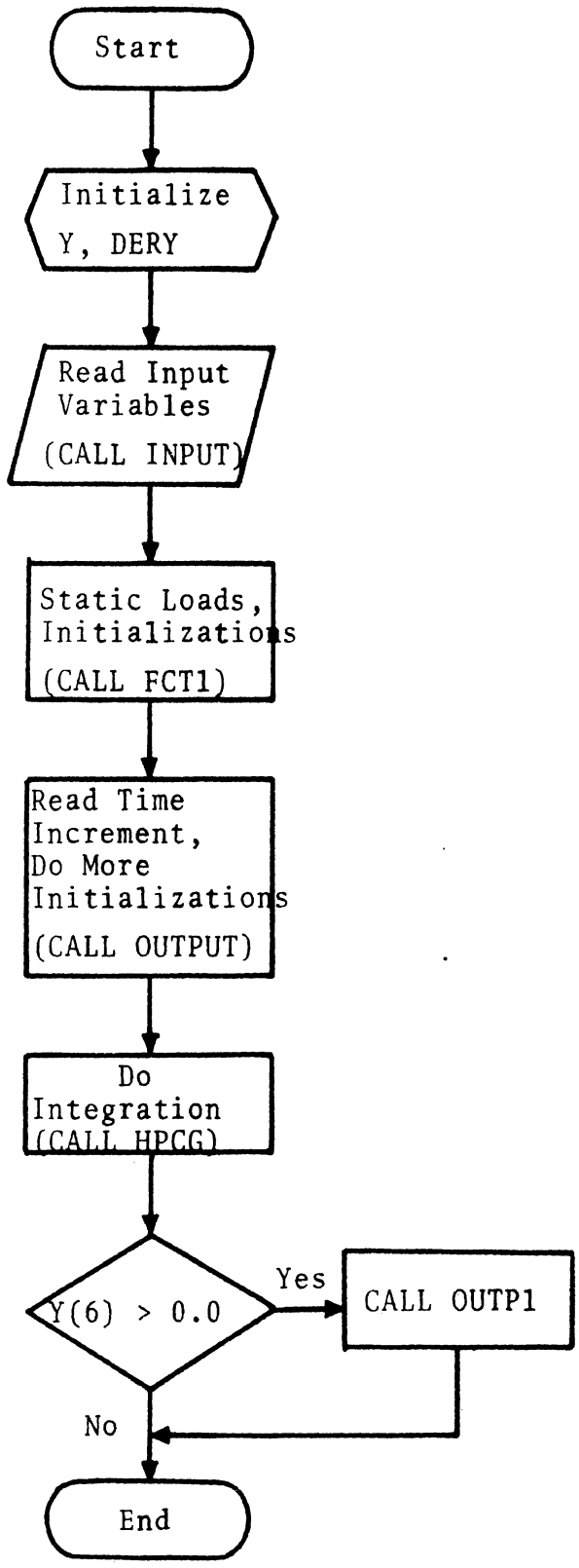

SUBROUTINE INPUT

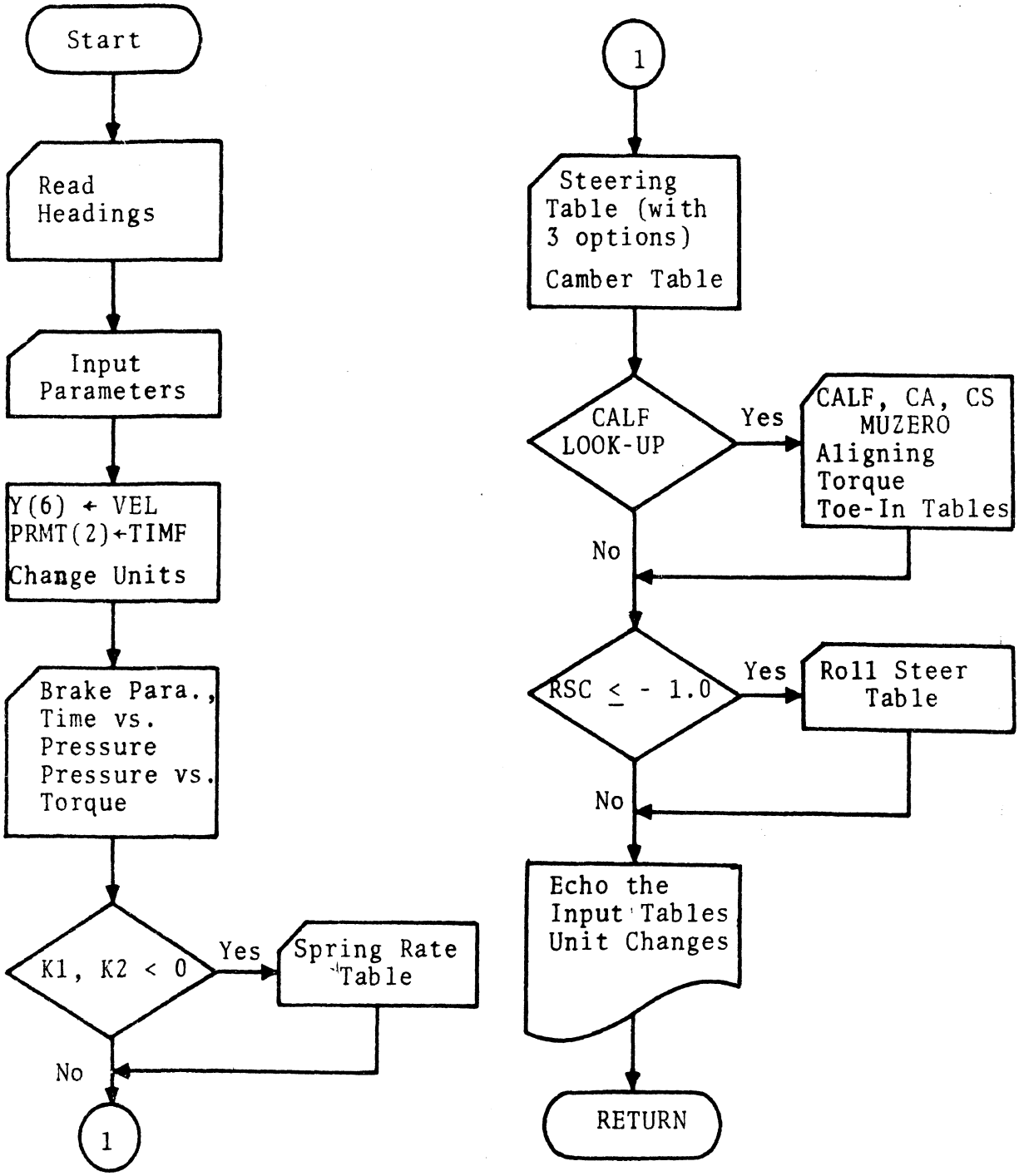

USBROUTINE FCT1

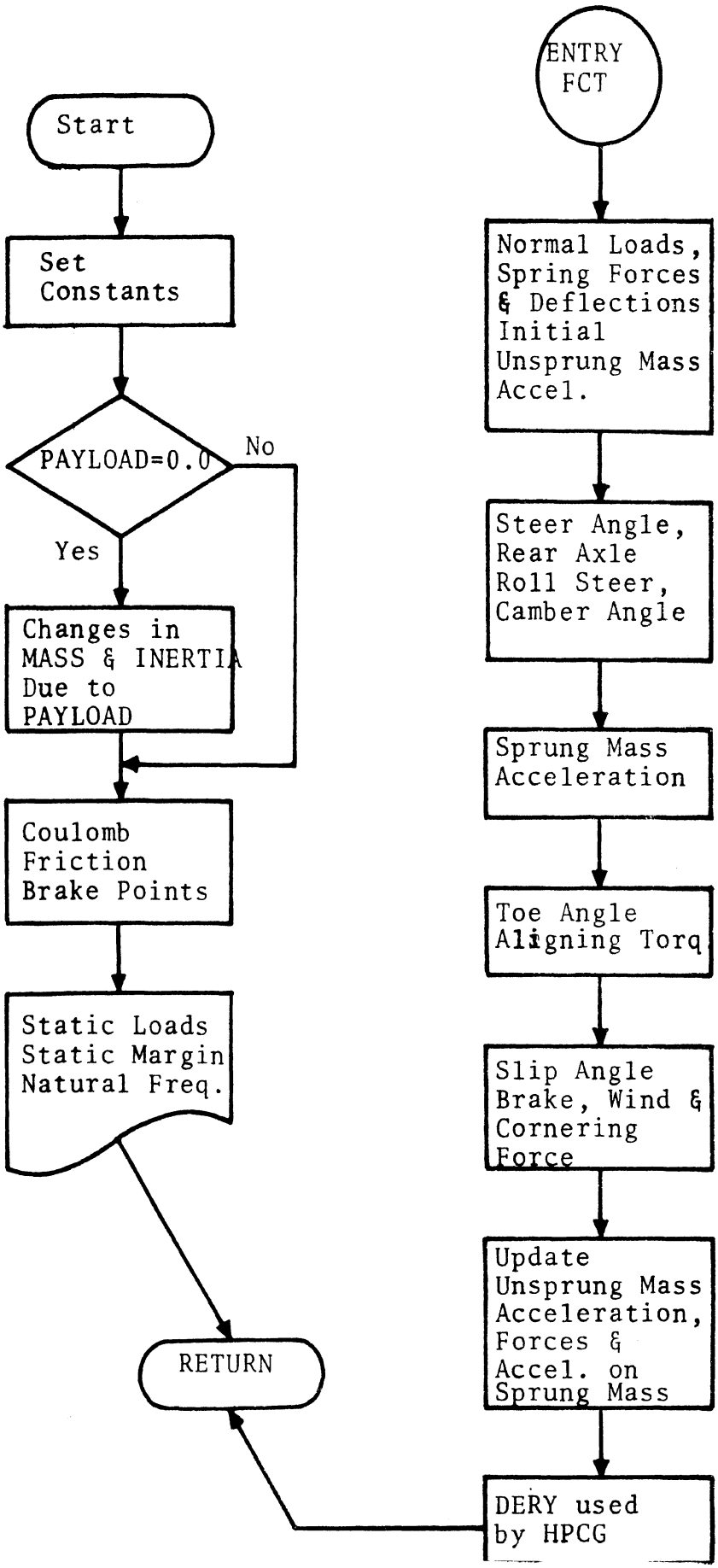

SUBROUTINE OUTPUT

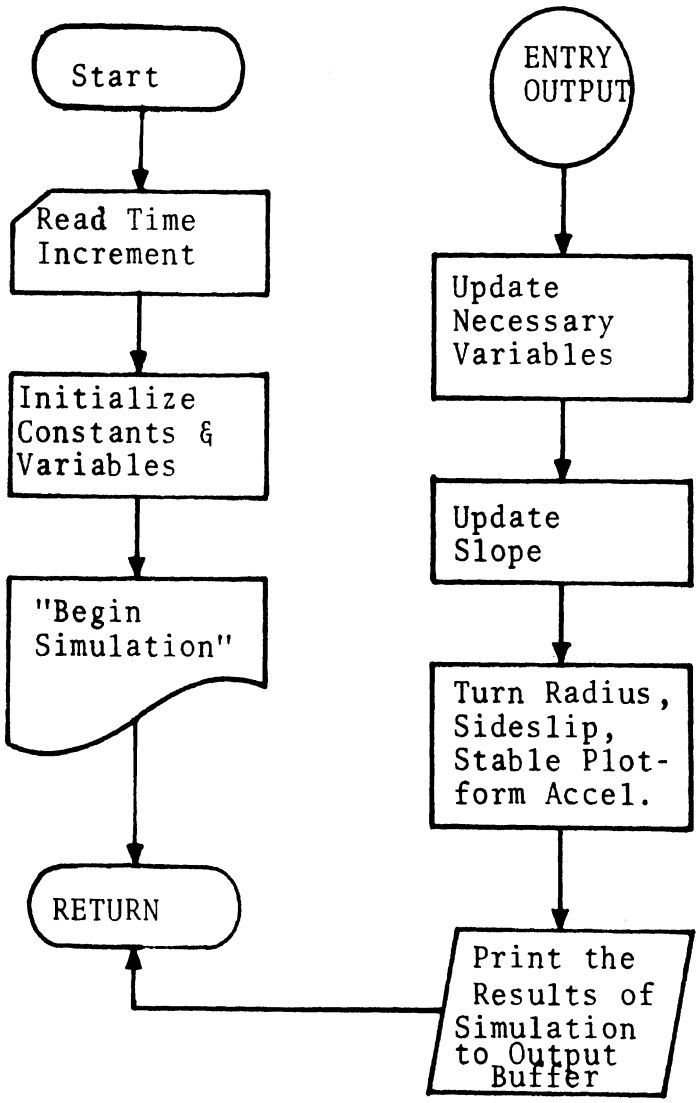

B7. REFERENCES

1. Olley, M., "Independent Wheel Suspension--Its Whys and Wherefores," SAE Transactions, Vol. 34, No. 2, 1934.

2. Ellis, J.R., Vehicle Dynamics, Business Books Ltd., London, 1969.

3. Goldstein, H., Classical Mechanics, Addison Wesley Publishing Co., Inc., Reading, Mass., June 1969.

4. Bernard, J.E., "A Digital Computer Method for the Prediction of Braking Performance of Trucks and Tractor-Trailers," SAE Paper No. 730181.

5. Bernard, J.E., "Some Time-Saving Methods for the Digital Simulation of Highway Vehicles," Simulation, December 1973.

6. Bernard, J.E., "Articulated Vehicle Simulation: A Fresh Approach to Some Recurring Problems," Winter Simulation Conference, 1974.

7. Eshleman, R.L. and Desai, S.D., Articulated Vehicle Handling, Final Report, Illinois Institute of Technology, Research Institute, April 1972.

8. Krauter, A.I. and Wilson, R.K., "Simulation of Tractor-Semitrailer Handling," SAE Paper No. 720922, October 1972.

9. Nicholas, V.T. and Comstock, T.R., "Predicting Directional Behavior of Tractor-Semitrailers when Anti-Skid Brake Systems are Used," Presented at ASME Winter Annual Meeting, New York, N.Y., November 1972.

10. McHenry, R.R. and Deleys, N.J., Vehicle Dynamics in Single Vehicle Accidents, CAL No. VJ-2251-V-3, December 1968.

11. Dugoff, H., Fancher, P., and Segel, L., "An Analysis of Tire Traction Properties and Their Influence on Vehicle Dynamic Performance," SAE Paper No. 70377.

12. Fiala, E., "Seitenkräfte am Rollenden Leiftreifen," VDI, Vol. 96, No. 29, October 1954.

13. Tielking, J.T. and Mital, N.K., A Comparative Evaluation of Five Tire Traction Models, Highway Safety Research Institute, Univ. of Mich., Ann Arbor, Report No. UM-HSRI-PF-74-2, January 1974.

14. Lipmann, S.A. and Oblizajek, K.L., "The Distributions of Stress Between the Tread and the Road for Freely-Rolling Tires," SAE Paper No. 740072.

15. Livingston, D.I. and Brown, J.E., "Physics of the Slipping Wheel. I. Force and Torque Calculations for Various Pressure Distributions," Rubber Chemistry and Technology, Vol. 42, No. 4, September 1969.

16. Livingston, D.I. and Brown, J.E., "Physics of the Slipping Wheel. II. Slip Under Both Tractive and Lateral Forces," Rubber Chemistry and Technology, Vol. 43, No. 2, March 1970.

17. Ervin R.D., et al., Vehicle Handling Performance, Final Report, Highway Safety Research Institute, Univ. of Mich., Ann Arbor, 3 Vols., NHTSA Contract No. DOT-HS-031-1-159, November 1972.

APPENDIX C

VEHICLE LINEAR ANALYSIS PROGRAM

Howard Moncarz

C1. INTRODUCTION

The linear analysis presented in this report was based on results obtained from the mathematical model and computer simulation presented in this appendix. Section C2 shows the formulation of the mathematical model, and Section C3 shows a flow chart of the computer program and a sample input-output obtained from running the computer program. The symbols used in the mathematical model and computer program are defined in the nomenclature in Section C4. Finally, Section C5 contains references designated in Section C2.

C2. MATHEMATICAL MODEL

C2.1 FORMULATION

A schematic of the model used in formulating the linear differential equations of motion for the automobile is shown in Figure C-1. Three sets of axes are shown in the figure. The x-y-z axes are fixed in the sprung mass of the vehicle, and the x'-y'-z' axes are fixed relative to the unsprung masses. With a roll angle, ϕ, of 0, the z-axis is a vertical axis which intersects the c.g. of the total vehicle. The x'-axis is along the roll axis of the sprung mass and intersects the z-axis. This point of intersection fixes the origin for both sets of axes. The x_s-y_s-z_s axes are parallel to the x-y-z axes with origin at the c.g. of the sprung mass.

C2.1.1 EQUATIONS OF MOTION. The linear differential equations of motion for the automobile in the three degrees of freedom of yaw rate (r), sideslip angle (β), and roll angle (ϕ) were derived by Segel [1]. In terms of the nomenclature at the end of this appendix, those equations are:

$$\frac{\mu}{f}\dot{\beta} + \frac{m}{f^2}\dot{p} = y_\beta\beta + (y_r - \mu)\frac{1}{f}r + y_\phi\phi + y_\delta\delta \qquad \text{(C-1)}$$

$$\frac{i_{zz}}{f^2}\dot{r} + \frac{i_{xz}}{f^2}\dot{p} = n_\beta\beta + n_r\frac{1}{f} + n_\phi\phi + n_\delta\delta \qquad \text{(C-2)}$$

$$m\frac{\mu}{f}\dot{\beta} + \frac{i_{xz}}{f^2}\dot{r} + \frac{i_{xx}}{f^2}\dot{p} = -\frac{m\mu}{f}r + \ell_p\frac{1}{f}p + \ell_\phi\phi \qquad \text{(C-3)}$$

$$\dot{\phi} = p \qquad \text{(C-4)}$$

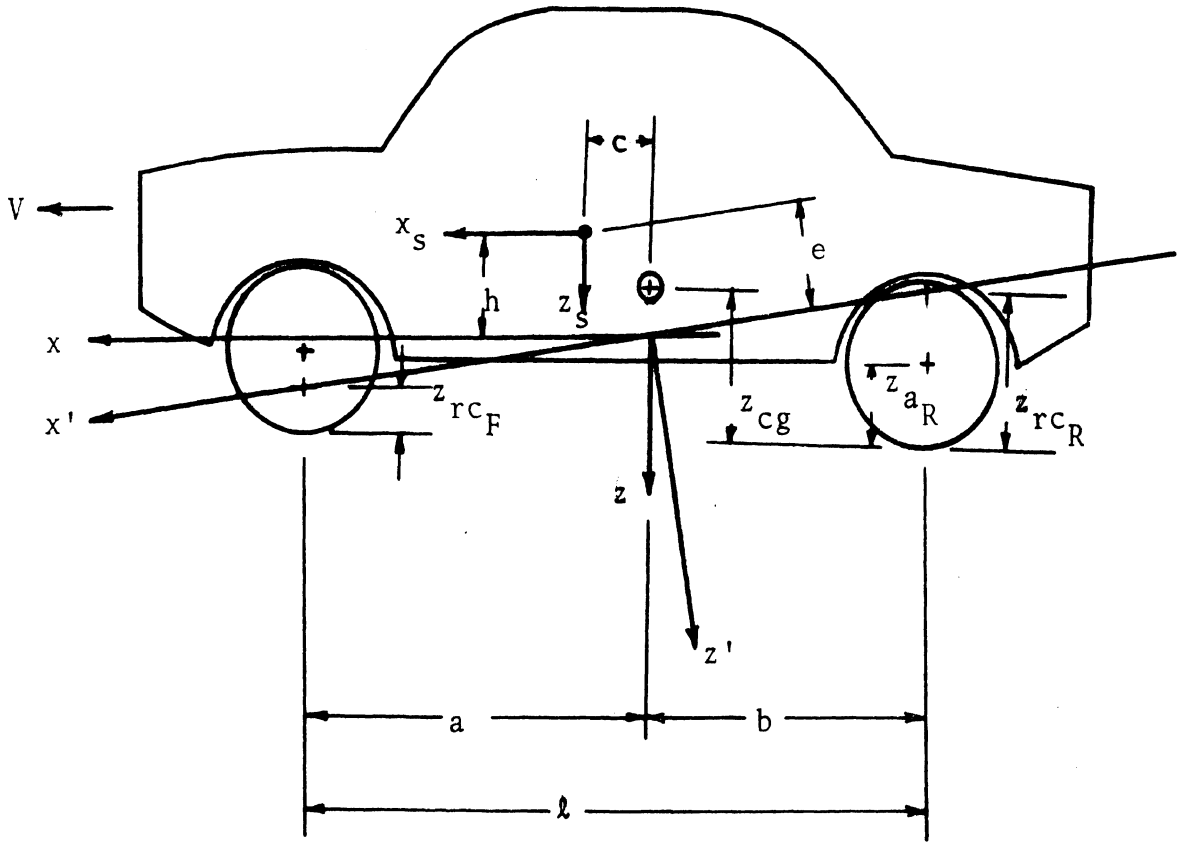

• c.g. of sprung mass

⊕ c.g. of total vehicle

y, y' and y_s-axes are directed into paper

Figure C-1. Schematic of automobile.

Equations (C-1) - (C-4) are nondimensional except for the independent variable, time, which is in seconds. The variables yaw rate (r) and roll rate (p) have dimensions of degrees per second, and the dot over a variable represents differentiation with respect to time. These equations are of first order to allow certain matrix manipulations shown later.

The terms $y_\delta \delta$ and $n_\delta \delta$ introduce the effects of steering into the equations, μ is a nondimensional velocity equal to $\frac{V}{\sqrt{\ell g}}$, m is a reduced mass defined as $M_s h/M\ell$, and f is a frequency-type term equal to $\sqrt{g/\ell}$, which provides the conversion of the equation to dimensional time.

C2.1.2 MOMENTS OF INERTIA. The nondimensional moments of inertia, i_{xx} and i_{zz}, are referenced to the x'-axis and the z-axis, respectively. The nondimensionalized product of inertia, i_{xz}, is referenced to the x'-z' axes, where $\phi = 0$. However, the moments of inertia of the sprung mass of an automobile are commonly measured about the x_s-y_s-z_s axes. Similarly, the moments of inertia of the unsprung masses are measured about axes parallel to the x-y-z axes with origin at the c.g.'s of the unsprung masses.

The moments of inertia of the sprung mass referenced to the x-y-z axes are:

$$I_{zz} = I_{zz_s} + M_s c^2$$

$$I_{xz} = I_{xz_s} - M_s h\, c$$

$$I_{xx} = I_{xx_s} + M_s h^2$$

where the subscript s indicates the moment of inertia of the sprung mass referenced to the x_s-y_s-z_s axes.

Then, nondimensionalized and referenced to the x'-y-z axes, the moments of inertia are:

$$i_{xx} = \frac{I_{xx}\cos^2\lambda - 2I_{xz}\sin\lambda\cos\lambda + I_{zz}\sin^2\lambda}{M\ell^2}$$

$$i_{xz} = \frac{I_{zz}\sin\lambda - I_{xz}\cos\lambda}{M\ell^2}$$

$$i_{zz} = \frac{I_{zz} + I_{zz_F} + \frac{W_{uF}}{g}a^2 + I_{zz_R} + \frac{W_{uR}}{g}b^2}{M\ell^2} \qquad [2]$$

where I_{zz_F} and I_{zz_R} are the moments of inertia of the front and rear unsprung masses about vertical axes through the axle centers, and λ is the inclination angle of the roll axis.

C2.1.3 STABILITY DERIVATIVES. The remaining terms in Equations (C-1) - (C-4) are stability derivatives and have been derived in the literature [1]. The stability derivatives are:

$$y_\beta = -\frac{C_{\alpha_F} + C_{\alpha_R}}{W}$$

$$y_r = \frac{-aC_{\alpha_F} + bC_{\alpha_R}}{MV\sqrt{\ell g}}$$

$$y_\phi = \frac{C_{\alpha_F}\varepsilon_F + C_{\alpha_R}\varepsilon_R + CT_F\frac{\partial\gamma_F}{\partial\phi} + CT_R\frac{\partial\gamma_R}{\partial\phi}}{W}$$

$$y_\delta = \frac{C_{\alpha_F}}{W}$$

$$n_\beta = \frac{-a^2 C_{\alpha_F} + b^2 C_{\alpha_R} + AT_F + AT_R}{W\ell}$$

$$n_r = \frac{-a^2 C_{\alpha_F} - b^2 C_{\alpha_R} + aAT_F - bAT_R}{M\ell V\sqrt{\ell g}}$$

$$n_\phi = \frac{C_{\alpha_F}\varepsilon_F a - C_{\alpha_R}\varepsilon_R b + CT_F \frac{\partial \gamma_F}{\partial \phi} a - CT_R \frac{\partial \gamma_R}{\partial \phi} b}{W\ell} - \frac{(\varepsilon_F AT_F + \varepsilon_R AT_R)}{W\ell}$$

$$n_\delta = \frac{aC_{\alpha_F} - AT_F}{W\ell}$$

$$\ell_\phi = \frac{W_s e - K}{W\ell} \cos\lambda$$

$$\ell_p = \frac{C_p}{M\ell\sqrt{\ell g}} \cos\lambda$$

The terms in the above equations are defined in the nomenclature.

In these equations the tire characteristics AT, C_α, and CT represent the sum of those respective characteristics for both tires at an axle. It should be noted, however, that when entering data, the tire characteristics are entered per tire.

The constants K and C_p are derived, representing the suspension system as the model shown in Figure C-2. The subscript R refers to a parameter associated with the rear suspension. The front suspension is similar except for the addition of a roll bar that adds a torque, K_{RB}, per unit of roll angle to the total rolling moment.

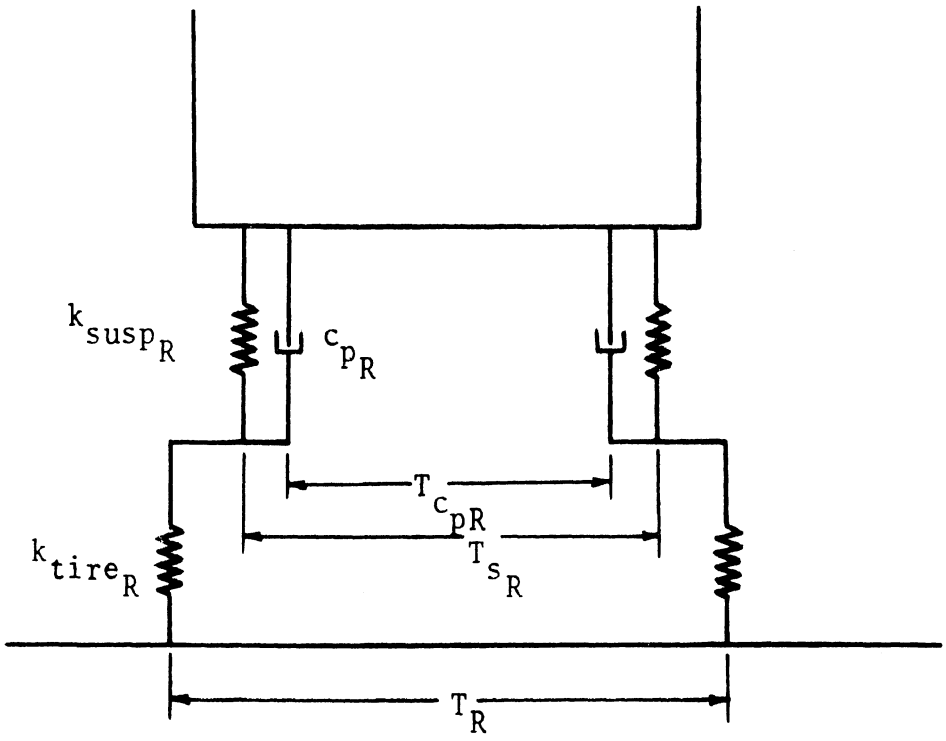

Figure C-2. Schematic of rear suspension.

The shock absorber is modeled as a dashpot with damping constant c_{p_R}. The vertical stiffness of the suspension is modeled as a spring with spring rate k_{susp_R}, and the vertical stiffness of a tire is modeled as a spring with spring rate k_{tire_R}. The distance between shock absorbers, T_{cp_R}, is assumed to be equal to the distance T_{s_R} between the suspension springs.

The moment on the sprung mass of the vehicle about the x-axis transmitted by one of the rear shock absorbers is:

$$L_{SA_R} = F_{SA_R} \chi_R$$

where F_{SA} is the force on the sprung mass in the z-direction at the location of the shock absorber and is proportional to the z-velocity of the sprung mass at this point. χ_R is the moment arm from the z-axis to the force F_{SA}. Thus

$$F_{SA_R} = C_{p_R} \frac{T_{s_R}}{2} p$$

$$\chi = \frac{T_{s_R}}{2}$$

The front shock absorbers are treated similarly. The total moment on the sprung mass about the x-axis due to the shock absorber is

$$L_{SA} = 2 \left[\left(c_{p_F} \frac{T_{s_F}}{2} p \right) \frac{T_{s_F}}{2} + \left(c_{p_R} \frac{T_{s_R}}{2} p \right) \frac{T_{s_R}}{2} \right]$$

$$= \frac{1}{2} \left(c_{p_F} T_{s_F}^2 + c_{p_R} T_{s_R}^2 \right) p$$

The moment on the sprung mass of the vehicle about the x-axis generated by the suspension stiffness to roll displacement is calculated in the same manner. In calculating the spring rate of the suspension, both the spring rate of the spring and the deflection spring rate of the tire are taken into account. As shown in Figure C-2, these two "springs" are added in series, viz.:

$$K_R = \frac{k_{susp_R} k_{tire_R}}{k_{susp_R} + k_{tire_R}}$$

where K_R is the equivalent spring rate for one side of the rear suspension, k_{susp_R} is the spring rate of a rear spring, and k_{tire_R} is the deflection spring rate of a rear tire.

The front roll bar (if the vehicle has one) adds a torque, K_{RB}, per unit of roll angle. Thus, the total moment on the sprung mass about the x-axis due to the suspension stiffness to roll displacement is

$$L_K = \left[\frac{1}{2}\left(K_F T_{s_F}^2 + K_R T_{s_R}^2\right) + K_{RB}\right] \phi$$

Note that the equations of rolling motion are written about the x'-axis. Thus L_K and L_{SA} must be multiplied by $\cos\lambda$ for use in Equation (C-3). Hence,

$$K = \left[\frac{1}{2}\left(K_F T_{s_F}^2 + K_R T_{s_R}^2\right) + K_{RB}\right] \cos\lambda$$

and

$$C_p = \left[\frac{1}{2}\left(C_{p_F} T_{s_F}^2 + C_{p_R} T_{s_R}^2\right)\right] \cos\lambda$$

C2.1.4 COMPLIANCE STEER EFFECTS. The slip angles of each tire are commonly expressed as functions of the vehicle sideslip angle (β), yaw rate (r), roll angle (ϕ), and steer angle (δ). However, there are, additionally, significant contributions to the slip angles due to compliances in the steering system and suspension system. In particular, lateral forces and moments acting on the vehicle may cause a steer change and/or a camber angle change due to these compliances.

Including these effects, the slip angles are:

$$\alpha_F = \beta + \frac{ar}{V} - \delta - \varepsilon_F\phi + \frac{F_{y_F}(x_{p_F} + x_m)}{K_{ss}} \qquad \text{(C-5)}^*$$

and

$$\alpha_R = \beta - \frac{br}{V} - \varepsilon_R\phi - K_{R\ell s}F_{y_R} - K_{Rats}M_{z_R} \qquad \text{(C-6)}$$

where the last term in Equation (C-5) and the last two terms in Equation (C-6) account for the compliances mentioned. In particular, the term

$$\frac{F_{y_F}(x_{p_F} + x_m)}{K_{ss}}$$

in Equation (C-5) is the contribution due to the compliance, K_{ss}, in the steering system. Note that

---

*The coefficients for compliance steer effects have been defined according to the convention that positive values indicate understeer and negative values indicate oversteer.

$$K_{ss} = \frac{K_{sc}(G_R)^2(2K_{s\ell})}{K_{sc}(G_R)^2 + 2K_{s\ell}}$$

where $K_{s\ell}$ is the compliance in one of the two steering linkages, K_{sc} is the compliance in the steering column, and G_R is the gear ratio of the steering system. As demonstrated in the expression for K_{ss}, the steering column stiffness is added in series with the stiffness of the two steering linkages.

The compliance of the steering system must be taken into account because the lateral force, F_{y_F}, at the tire is offset from the axle center by a distance along the x-axis equal to the pneumatic trail (x_{p_F}) plus the mechanical trail (x_m). The mechanical trail is the horizontal distance from the ground intersection of the kingpin axis to the axle center. The pneumatic trail is defined as the aligning torque stiffness divided by the cornering stiffness.

The term

$$\frac{F_{y_F}(x_{p_F} + x_m)}{K_{ss}}$$

may be replaced by $K_{Fats}F_{y_F}x_{p_F} + K_{F\ell s}F_{y_F}$ where K_{Fats} is the coefficient for front aligning torque steer. The term $K_{F\ell s}F_{y_F}$ is the front lateral force steer, which is due to a lateral force at the front axle causing a steer of the front tires because of compliances in the steering and suspension system. The terms $K_{F\ell s}F_{y_R}$ and $K_{Rats}M_{z_R}$ in Equation (C-6) are the rear lateral force steer and rear aligning torque steer, respectively.

The lateral force at the front axle (assuming no lateral force camber compliance) is:

$$F_{y_F} = - C_{\alpha_F} \alpha_F + CT_F \frac{\partial \gamma_F}{\partial \phi} \phi$$

where CT_F is the camber thrust, defined as the side force developed per unit tire camber angle, and $(\partial \gamma_F / \partial \phi)\phi$ is the camber angle due to a vehicle roll angle of ϕ.

However, because of compliances in the wheel bushings, a side force applied to the axle can alter the camber angle. This additional contribution to the camber angle is $C_{am_F} F_{y_F}$ where C_{am_F} is the camber compliance coefficient. Hence, the camber angle is:

$$\gamma = \frac{\partial \gamma_F}{\partial \phi} \phi - C_{am_F} F_{y_F}$$

Thus,

$$F_{y_F} = - C_{\alpha_F} \alpha_F + \left(CT_F \frac{\partial \gamma_F}{\partial \phi} \phi - C_{am_F} F_{y_F} \right) \qquad (C\text{-}7)$$

It is possible to retain the familiar slip angle expressions:

$$\alpha_F = \beta + \frac{ar}{V} - \delta - \varepsilon_F \phi$$

$$\alpha_R = \beta - \frac{br}{V} - \varepsilon_R \phi$$

by modifying certain coefficients to account for the compliances. This is done in the following. Both sides of Equation (C-5) are multiplied by $(-C_\alpha)$:

$$-C_{\alpha_F}\alpha_F = -(\beta + \frac{ar}{V} - \delta - \varepsilon_F\phi)C_{\alpha_F} - \frac{C_{\alpha_F}F_{y_F}(x_{p_F} + x_m)}{K_{ss}}$$

$$- K_{F\ell s}C_{\alpha_F}F_{y_F} \qquad \text{(C-8)}$$

Adding $CT_F(\frac{\partial\gamma_F}{\partial\phi}\phi - C_{am_F}F_{y_F})$ to both sides of Equation (C-8) and rearranging:

$$F_{y_F}\left[K_{F\ell s}C_{\alpha_F} + \frac{C_{\alpha_F}(x_{p_F} + x_m)}{K_{ss}}\right] - C_{\alpha_F}\alpha_F + CT_F\left(\frac{\partial\gamma_F}{\partial\phi}\phi - C_{am_F}F_{y_F}\right) =$$

$$-(\beta + \frac{ar}{V} - \delta - \varepsilon_F\phi)C_{\alpha_F} + CT_F\frac{\partial\gamma_F}{\partial\phi}\phi - CT_FC_{am_F}F_{y_F}$$

Using Equation (C-7) and rearranging again:

$$F_{y_F}\left[1 + K_{F\ell s}C_{\alpha_F} + \frac{C_{\alpha_F}(x_{p_F} + x_m)}{K_{ss}} + CT_FC_{am_F}\right]$$

$$= -(\beta + \frac{ar}{V} - \delta - \varepsilon_F\phi)C_{\alpha_F} + CT_F\frac{\partial\gamma_F}{\partial\phi}\phi \qquad \text{(C-9)}$$

Thus, the right side of Equation (C-9) is equal to F_{y_F} if C_{α_F} and CT_F are altered to C'_{α_F} and CT'_F where

$$C'_{\alpha_F} = \frac{C_{\alpha_F}}{Factor_F} \qquad \text{(C-10)}$$

$$CT'_F = \frac{CT_F}{Factor_F} \qquad \text{(C-11)}$$

and

$$Factor_F = 1 + K_{F\ell s}C_{\alpha_F} + \frac{C_{\alpha_F}(x_{p_F} + x_m)}{K_{ss}} + CT_FC_{am_F} \qquad \text{(C-12)}$$

The equation for the yawing moment of the vehicle about its total c.g. is:

$$N = AT_F\alpha_F + aCT_F \frac{\partial \gamma_F}{\partial \phi} \phi - aC_{\alpha_F}\alpha_F + AT_R\alpha_R - bCT_R \frac{\partial \gamma_F}{\partial \phi} \phi + bC_{\alpha_R}\alpha_R \quad \text{(C-13)}$$

Equation (C-13) can be broken into two equations—one for the moment due to forces at the front axle and the second for the moment due to forces at the rear axle:

$$N = N_F + N_R$$

$$N_F = AT_F\alpha_F + a(-C_{\alpha_F}\alpha_F + CT_F \frac{\partial \gamma_F}{\partial \phi} \phi) \quad \text{(C-14)}$$

$$N_R = AT_R\alpha_R - b(-C_{\alpha_R}\alpha_R + CT_R \frac{\partial \gamma_R}{\partial \phi} \phi) \quad \text{(C-15)}$$

The term enclosed in parentheses in Equation (C-14) is equal to F_{y_F}, if C_{α_F} and CT_F are modified as shown in the preceding (Equations (C-10) - (C-12)).

However, for the first term on the right side of Equation (C-14),

Let $$M_{z_F} = x_{p_F} F_{y_F}$$

$$= x_{p_F} \left[-C_{\alpha_F}\alpha_F + CT_F \left(\frac{\partial \gamma}{\partial \phi} \phi - C_{am_F} F_{y_F}\right)\right]$$

It should be mentioned here that the component of side force due to a tire camber angle is assumed to be directed along the same path as the side force due to slip angle.

$$x_{p_F} F_{y_F} = x_{p_F} \left[-C_{\alpha_F} (\beta + \frac{ar}{V} - \delta - \varepsilon_F \phi) + CT_F \frac{\partial \gamma}{\partial \phi} \phi \right]$$

$$- x_{p_F} C_{\alpha_F} F_{y_F} \left(\frac{x_{p_F} + x_m}{K_{ss}} + K_{F\ell s} \right) - x_{p_F} CT_F F_{y_F} C_{am_F}$$

Rearranging:

$$x_{p_F} F_{y_F} \left[1 + C_{\alpha_F} \left(\frac{x_{p_F} + x_m}{K_{ss}} + K_{F\ell s} \right) + CT_F C_{am_F} \right]$$

$$= x_{p_F} (-C_{\alpha_F}) (\beta + \frac{ar}{V} - \delta - \varepsilon_F \phi) + x_{p_F} CT_F \frac{\partial \gamma}{\partial \phi} \phi$$

The aligning torque stiffness (AT_F) has been defined as $x_{p_F} C_{\alpha_F}$. Hence, AT_F must be modified by the same factor as developed for C_α and CT in order to keep α in its customary form:

$$\alpha = \beta + \frac{ar}{V} - \delta - \varepsilon_F \phi \ .$$

Additionally, the term $x_{p_F} CT'_F (\partial \gamma / \partial \phi) \phi$ must be added to the moment equation. This is done very simply by increasing the distance, a, which multiplies $CT_F \ \partial \gamma_F / \partial \phi$ in the expression for n_ϕ, to $(a + x_{p_F})$.

The compliances at the rear axle are handled in the same manner as were the compliances at the front axle. The result is that C_{α_R}, CT_R, and AT_R must be modified:

$$C'_{\alpha_R} = \frac{C_{\alpha_R}}{Factor_R}$$

$$CT'_R = \frac{CT_R}{Factor_R}$$

$$AT'_R = \frac{AT_R}{Factor_R}$$

where $Factor_R = 1 - C_{\alpha_R} K_{R\ell s} - K_{Rats} C_{\alpha_R} x_{p_R} - CT_R Cam_R$. Additionally, the distance, b, which multiplies $CT_R \, \partial\gamma_R/\partial\phi$ in the expression for n_ϕ must be reduced to $(b - x_{p_R})$.

C2.2 SOLUTION OF THE EQUATIONS

C2.2.1 STATE EQUATIONS. Equations (C-1) - (C-4) can be put into the matrix form:

$$A \dot{\underset{\sim}{z}} = B \underset{\sim}{z} + f_s \underset{\sim}{\delta} \qquad \text{(C-16)}$$

where z is the state vector in Equation (C-16).

$$\underset{\sim}{z} = \begin{bmatrix} \beta \\ r \\ p \\ \phi \end{bmatrix}$$

$$A = \begin{bmatrix} \frac{\mu}{f} & 0 & \frac{m}{f^2} & 0 \\ 0 & \frac{i_{zz}}{f^2} & \frac{i_{xz}}{f^2} & 0 \\ \frac{m\mu}{f} & \frac{i_{xz}}{f^2} & \frac{i_{xx}}{f^2} & 0 \\ 0 & 0 & 0 & 1 \end{bmatrix}$$

$$B = \begin{bmatrix} y_\beta & \frac{(y_r - \mu)}{f} & 0 & y_\phi \\ n_\beta & \frac{n_r}{f} & 0 & n_\phi \\ 0 & \frac{-m\mu}{f} & \frac{\ell_p}{f} & \ell_\phi \\ 0 & 0 & 1 & 0 \end{bmatrix}$$

and

$$f_{s} = \begin{bmatrix} y_\delta \\ n_\delta \\ 0 \\ 0 \end{bmatrix}$$

C2.2.2 EIGENVALUES AND EIGENVECTORS. The solution to Equation (C-16) is obtained by summing the homogeneous and the particular solutions of Equation (C-16). The homogeneous solution is the solution to the equation

$$A \dot{z} = B z$$

If $\det A \neq 0$, then

$$\dot{z} = A^{-1} B z$$

and

$$\dot{z} - A^{-1} B z = 0 \qquad \text{(C-17)}$$

Assuming a solution in the form

$$z = \psi e^{st}$$

and substituting this into Equation (C-17)

$$(sI - A^{-1}B)\underset{\sim}{z} = 0 \qquad \text{(C-18)}$$

To find a non-trivial solution for Equation (C-18), $\det(sI - A^{-1}B)$ must equal zero. Thus, s, referred to as an eigenvalue, must be found to satisfy the characteristic equation

$$\det(sI - A^{-1}B) = 0 \qquad \text{(C-19)}$$

Equation (C-19) is fourth order, and thus there exist four eigenvalues.

The coefficients of the characteristic equation are determined using a technique developed by M. Bôcher [3]. Putting Equation (C-19) in the form

$$\det(sI - A^{-1}B) = s^4 + a_1 s^3 + a_2 s^2 + a_3 s + a_4$$

If T_q is the trace of the matrix $(A^{-1}B)^q$, where q is an integer which takes on the values 1, 2, 3, or 4, then

$$a_1 = -T_1$$

$$a_2 = -\frac{1}{2}(a_1 T_1 + T_2)$$

$$a_3 = -\frac{1}{3}(a_2 T_1 + a_1 T_2 + T_3)$$

$$a_4 = -\frac{1}{4}(a_3 T_1 + a_2 T_2 + a_1 T_3 + T_4)$$

Once the eigenvalues are found, the eigenvectors can be determined from Equation (C-18) by substituting each eigenvalue, s_i, in turn to find its respective eigenvector, $\underset{\sim}{z}_i$.

C2.2.3 RESPONSE TO STEP STEER INPUT. If U is the matrix whose columns are the eigenvectors of $A^{-1}B$, then

$$U^{-1}A^{-1}B\ U = \Lambda$$

where Λ is a diagonal matrix whose elements are the eigenvalues of $A^{-1}B$. Multiplying Equation (C-16) by $U^{-1}A^{-1}$ we get

$$U^{-1}\dot{\underset{\sim}{z}} = U^{-1}A^{-1}B(UU^{-1})\underset{\sim}{z} + U^{-1}A^{-1}\ \underset{\sim}{f_s}\delta$$

or

$$(U^{-1}\underset{\sim}{z})' = \Lambda\ U^{-1}\underset{\sim}{z} + U^{-1}A^{-1}\ \underset{\sim}{f_s}\delta$$

Defining $\underset{\sim}{y} = U^{-1}\underset{\sim}{z}$

and $\underset{\sim}{g} = U^{-1}A^{-1}\ \underset{\sim}{f_s}\delta$

then $\dot{\underset{\sim}{y}} = \Lambda\ \underset{\sim}{y} + \underset{\sim}{g}$ (C-20)

Now this set of equations is completely uncoupled since Λ is a diagonal matrix.

The solution to Equation (C-20) is

$$\underset{\sim}{y} = \Phi\ \underset{\sim}{\xi} - \hat{\underset{\sim}{g}}$$

where $\underset{\sim}{\xi}$ is an arbitrary constant vector

$$\hat{\underset{\sim}{g}} = \begin{bmatrix} g_1/s_1 \\ g_2/s_2 \\ g_3/s_3 \\ g_4/s_4 \end{bmatrix} = \Lambda^{-1} \underset{\sim}{g}$$

and $$\Phi = \begin{bmatrix} e^{s_1 t} & 0 & 0 & 0 \\ 0 & e^{s_2 t} & 0 & 0 \\ 0 & 0 & e^{s_3 t} & 0 \\ 0 & 0 & 0 & e^{s_4 t} \end{bmatrix}$$

But $$\underset{\sim}{z} = U\underset{\sim}{y}$$

so, $$\underset{\sim}{z} = U \Phi \xi - U\hat{\underset{\sim}{g}}$$

Assuming the initial conditions

$$\underset{\sim}{z}(t=0) = \underset{\sim}{z}_o$$

$$\Phi(t=0) = I \qquad \text{(the identity matrix)}$$

Then

$$\underset{\sim}{z}_o = U \underset{\sim}{\xi} - U\hat{\underset{\sim}{g}}$$

and $$\xi = U^{-1}\underset{\sim}{z}_o + \hat{\underset{\sim}{g}}$$

Hence $\underset{\sim}{z} = U \Phi U^{-1} \underset{\sim}{z}_o + U(\Phi - I)\hat{\underset{\sim}{g}}$

and $\hat{\underset{\sim}{g}} = \Lambda^{-1} \underset{\sim}{g} = \Lambda^{-1} U^{-1} A^{-1} \underset{\sim}{f_s} \delta$

$= U^{-1} B^{-1} \underset{\sim}{f_s} \delta$

so,

$$\underset{\sim}{z} = U \Phi U^{-1} \underset{\sim}{z}_o + U(\Phi - I) U^{-1} B^{-1} \underset{\sim}{f_s} \delta$$

or $$\underset{\sim}{z} = U \Phi U^{-1} (\underset{\sim}{z}_o + B^{-1} \underset{\sim}{f_s} \delta) - B^{-1} \underset{\sim}{f_s} \delta$$

for $\underset{\sim}{z}_o = \underset{\sim}{0}$

$$\underset{\sim}{z} = (U \Phi U^{-1} - I) B^{-1} \underset{\sim}{f_s} \delta$$

C2.2.4 STEADY-STATE SOLUTIONS. In the steady-state all time derivatives are 0, i.e., $\dot{\beta}$, $\dot{r}$, $\dot{p}$, and $\dot{\phi}$ are 0. Thus, Equation (C-16) reduces to

$$\begin{bmatrix} y_\beta & \frac{y_r - \mu}{f} & 0 & y_\phi \\ n_\beta & \frac{n_r}{f} & 0 & n_\phi \\ 0 & \frac{-m\mu}{f} & \frac{\ell_p}{f} & \ell_\phi \\ 0 & 0 & 1 & 0 \end{bmatrix} \begin{bmatrix} \beta \\ r \\ 0 \\ \phi \end{bmatrix} = - \begin{bmatrix} y_\delta \\ n_\delta \\ 0 \\ 0 \end{bmatrix} \delta$$

or,

$$y_\beta \beta_{ss} + \frac{y_r - \mu}{f} r_{ss} + y_\phi \phi_{ss} = - y_\delta \delta \qquad \text{(C-21)}$$

$$n_\beta \beta_{ss} + \frac{n_r}{f} r_{ss} + n_\phi \phi_{ss} = - n_\delta \delta \qquad \text{(C-22)}$$

$$- \frac{m\mu}{f} r_{ss} + \ell_\phi \phi_{ss} = 0 \qquad \text{(C-23)}$$

where the subscript ss denotes steady-state. Equations (C-21) through (C-23) can be solved for the gains β_{ss}/δ, r_{ss}/δ, and ϕ_{ss}/δ:

$$\frac{r_{ss}}{\delta} = \frac{f(n_\beta y_\delta - y_\delta n_\delta)\ell_\phi}{y_\beta(n_r \ell_\phi + m\mu n_\phi) - n_\beta[(y_r - \mu)\ell_\phi + m\mu y_\phi]}$$

$$\frac{\beta_{ss}}{\delta} = \frac{- y_\delta - \frac{m\mu y_\phi}{\ell_\phi} \frac{r_{ss}}{f\,\delta} - (y_r - \mu) \frac{r_{ss}}{f\,\delta}}{y_\beta}$$

$$\frac{\phi_{ss}}{\delta} = \frac{m\mu}{\ell_\phi} \frac{r_{ss}}{f\,\delta}$$

C2.2.5 PATH CURVATURE AND LATERAL ACCELERATION. The path curvature, defined as the inverse of the radius of the vehicle's path measured to the origin of the x-y-z axis system, is equal to:

$$\text{CURV} = \frac{\dot{\beta} + r}{V}$$

$$\text{CURV}_{ss} = (r_{ss}/V)$$

The lateral acceleration of the vehicle as measured at the origin of the x-y-z axes in the y-direction is:

$$A_y = (\dot{\beta} + r)V$$

In the steady-state,

$$A_{y_{ss}} = r_{ss}V$$

C2.2.6 STATIC MARGIN. The resultant side force caused by sideslipping of the automobile acts at a point which is located a certain distance in the x-direction from the total c.g. of the vehicle. This distance, nondimensionalized by the wheelbase, is called the static margin. The sign convention is such that if this component of side force is aft of the c.g., the static margin is positive, and if it is forward of the c.g., the static margin is negative. A positive static margin indicates understeer and a negative static margin indicates oversteer.

The static margin for the three degrees of freedom automobile is:

$$SM3D = \frac{n_\beta}{y_\beta}\left(1 + \frac{y_\phi}{-\ell_\phi}\, m\right) + \frac{n_\phi}{-\ell_\phi}\, m$$

With the roll degree of freedom neglected from the equations of motion, the static margin simplifies to:

$$SM2D = -\frac{n_\beta}{y_\beta}$$

C3. COMPUTER PROGRAM

C3.1 INTRODUCTION

The computer program developed to analyze the linear performance of the three degrees of freedom automobile consists of a main routine (MAIN) and nine subroutines. The flow chart for this computer program is presented in Section C3.2. The flow chart for the main routine includes statements from several of the subroutines to elucidate more clearly the transfer of control inside the computer program. These statements are set aside from MAIN (in the flow chart for MAIN) by dashed lines enclosing them and indicating which subroutines they are from. These statements are not meant to represent those subroutines, but only the transfer of control as it relates to MAIN. For the complete logic of a subroutine, the flow chart for the respective subroutine should be consulted. Finally, for each flow chart, it is indicated where control is transferred when a return statement is reached.

Various options, allowing for several different transfers of control, can be utilized. This is incorporated into the computer program using the vector "OPT" which is dimensioned with 10 spaces. Six of these are currently utilized. The remaining four are available for programming if desired. If ØPT(i) = 1, the option is set on. If ØPT(i) = 0, the option is set off.

The options may be set in either of two ways: (1) they are read in as data, and may be changed in the subroutine CHANGE and (2) they are set when the operator responds with "y" or "n" (for yes or no) in answer to a question printed at the terminal, i.e., the question "Degrees/g?" answered by "y" sets OPT(7) = 1, and the understeer/oversteer factor

in degrees/g is then computed and printed, using the vehicle parameters as they have been set at the time.

It should be noted that all options may be set as specified in (1) above, though not all options are available through (2).

The options available are:

ØPT(1)	Echoes matrices and intermediate computations for debugging purposes
ØPT(2)	Computes and echoes the eigenvectors
ØPT(3)	Echoes computed values from subroutine BEGIN—including geometric parameters, suspension and tire properties, moments of inertia, and static margin
ØPT(4)	Echoes data. This option is primed by question, "Print Data?"
ØPT(6)	Computes time history of response of vehicle to step steer input. This option is primed by question, "Response to Step Steer?"
ØPT(7)	Computes understeer/oversteer factor. This option is primed by question, "Degrees/g?"

Following the flow chart, a sample computer run is shown (Section C3.3).

C3.2 FLOW CHARTS

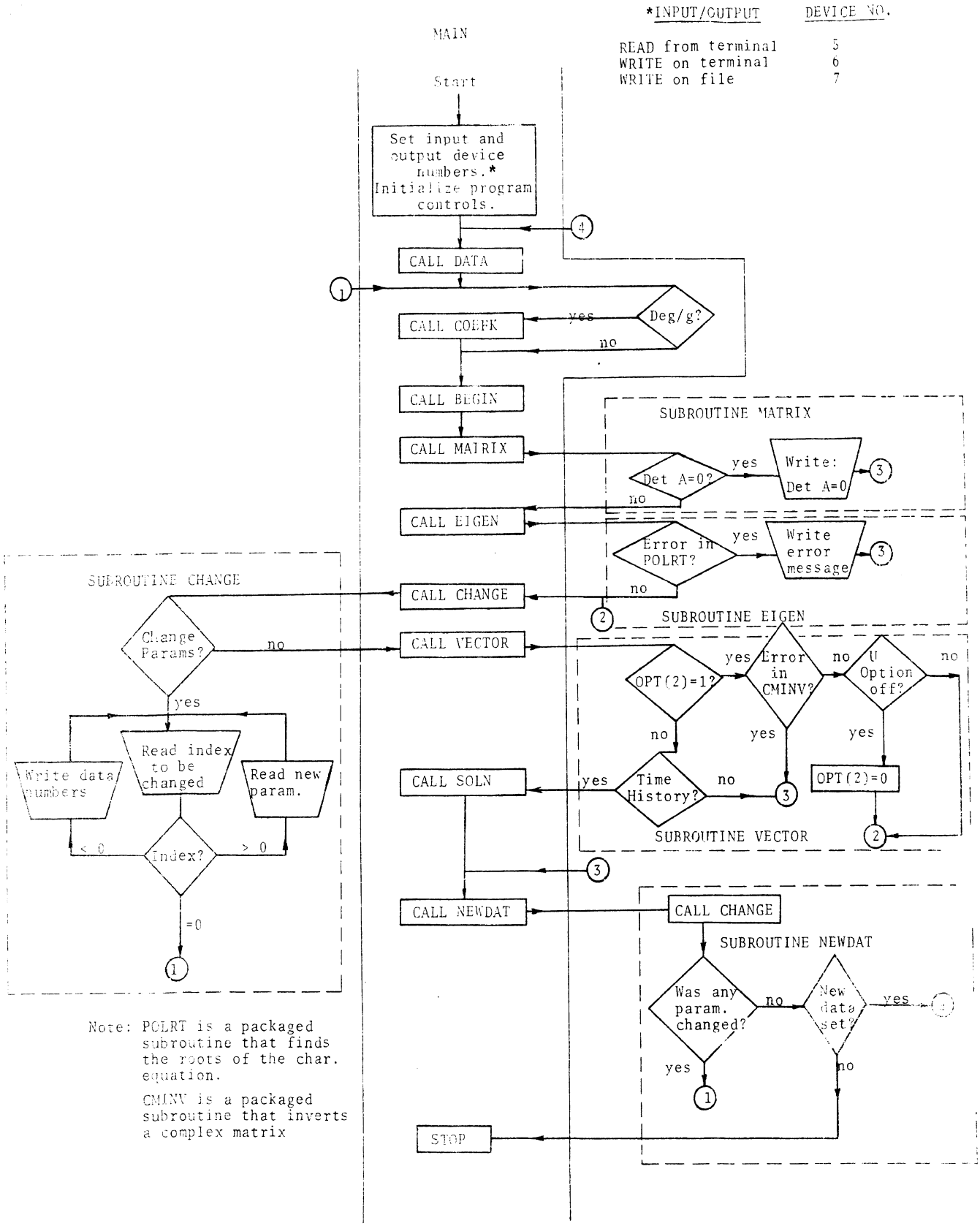

Note: POLRT is a packaged subroutine that finds the roots of the char. equation.

CMINV is a packaged subroutine that inverts a complex matrix

SUBROUTINE DATA

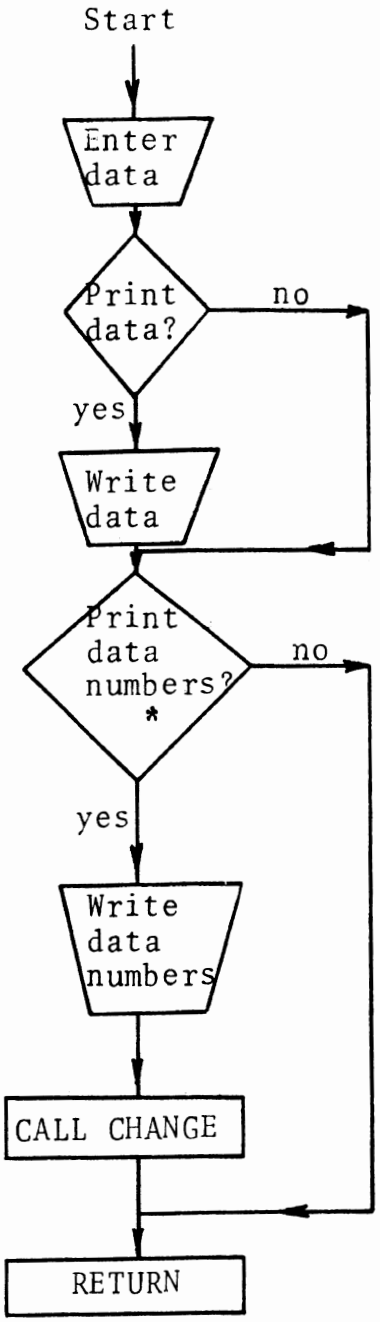

*Each parameter, including the options, have a number from 01 to 57 associated with them. These numbers are used when changing a parameter in subroutine CHANGE to key the particular parameter in question.

RETURN: Control transfers to MAIN at CALL BEGIN

SUBROUTINE BEGIN

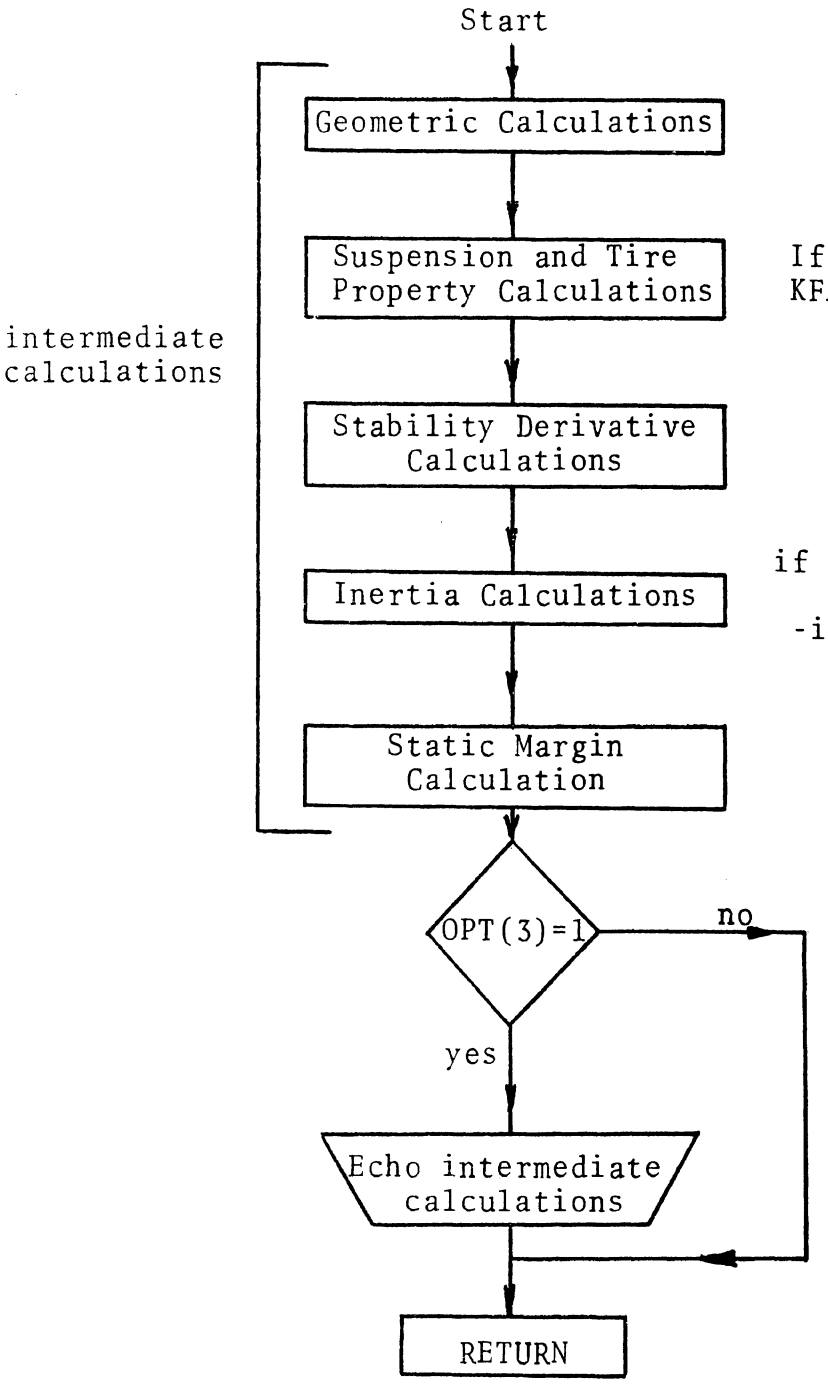

RETURN: Control transfers to MAIN at CALL MATRIX

SUBROUTINE MATRIX

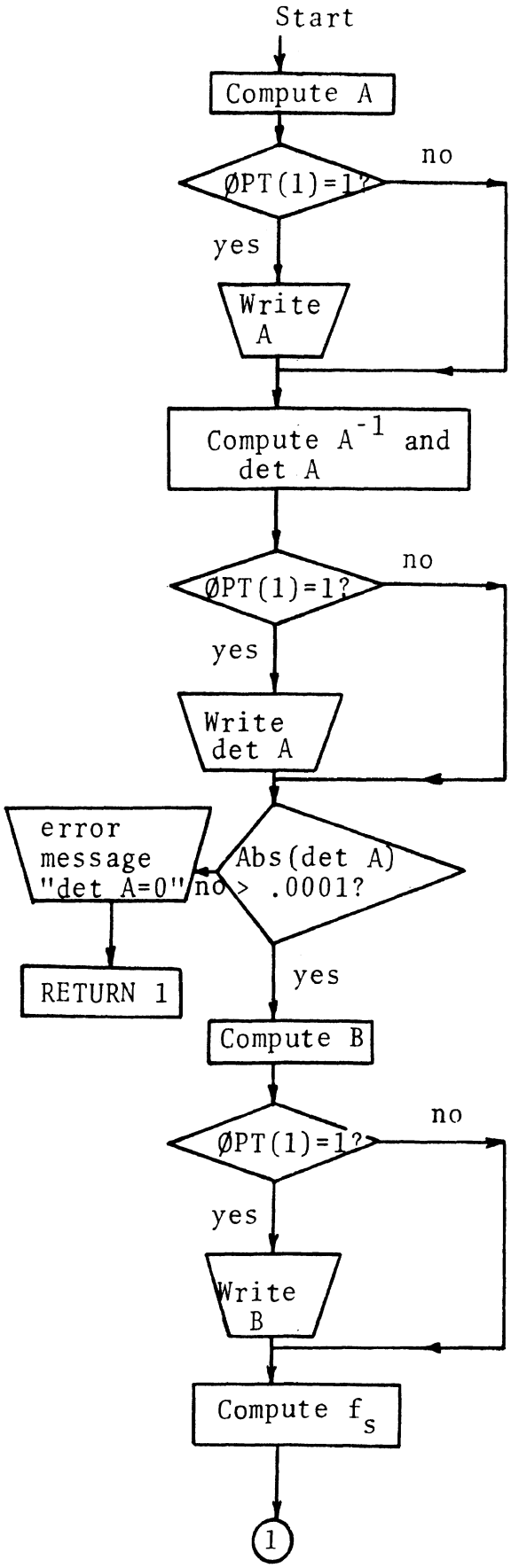

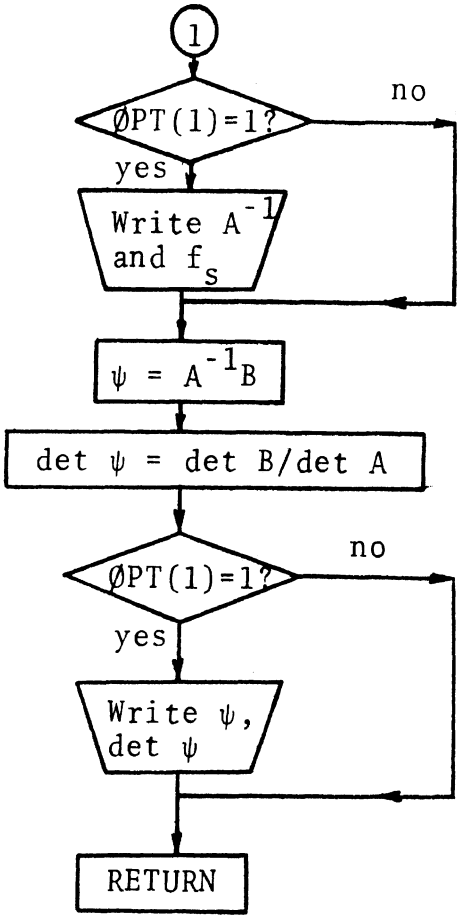

RETURN: Control transfers to MAIN at CALL EIGEN

RETURN 1: Control transfers to (3) in MAIN

SUBROUTINE EIGEN

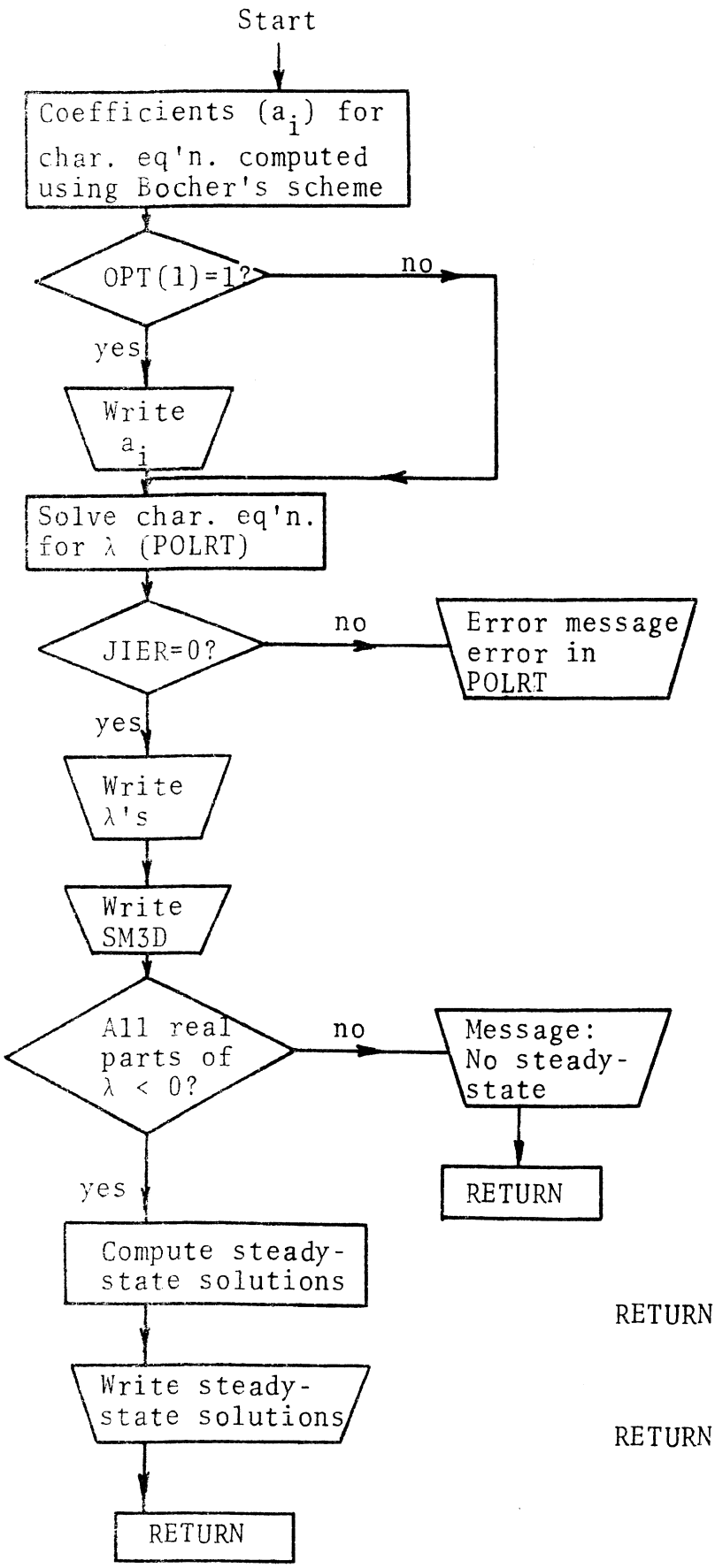

RETURN: Control transfers to (2) in MAIN

RETURN 1: Control transfers to (3) in MAIN

SUBROUTINE CHANGE

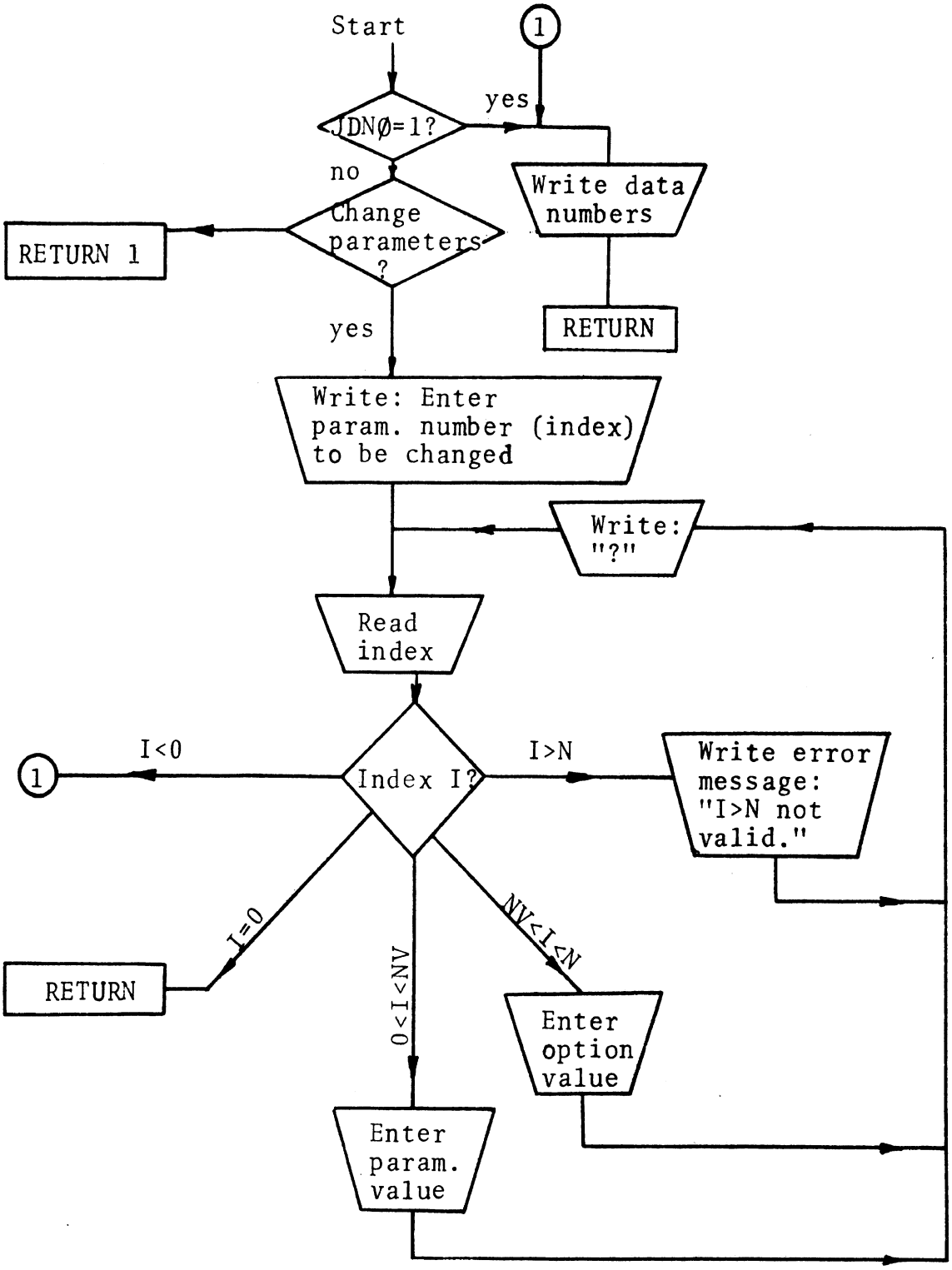

Note: NV is number of vehicle parameters

N is number of vehicle parameters plus number of options

JDNØ is an argument in CALL CHANGE statement

RETURN: Control transfers to (1) of MAIN

RETURN 1: Control transfers to MAIN at CALL VECTOR

SUBROUTINE VECTOR

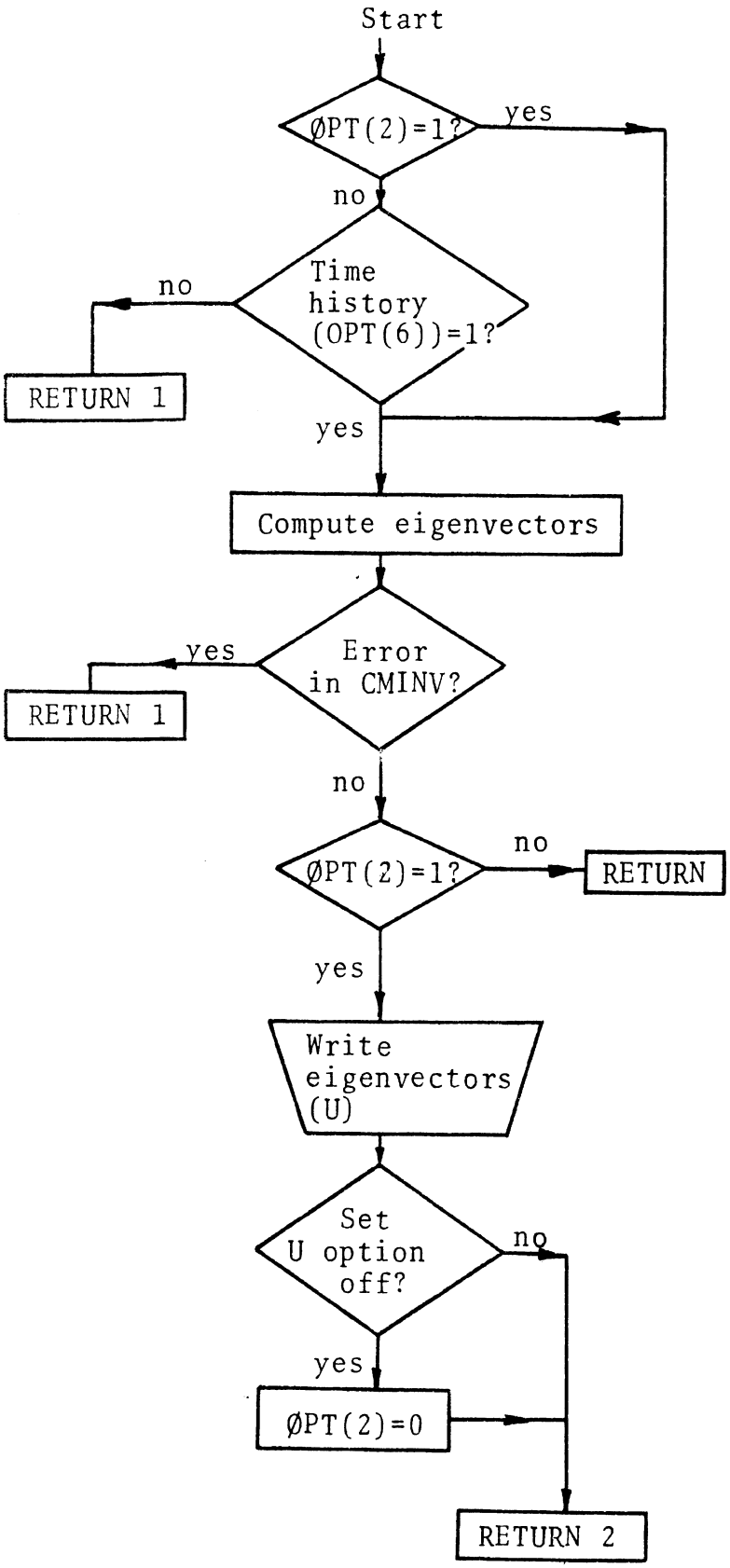

RETURN: Control transfers to MAIN at CALL SØLN

RETURN 1: Control transfers to (3) in MAIN

RETURN 2: Control transfers to (2) in MAIN

SUBROUTINE SØLN

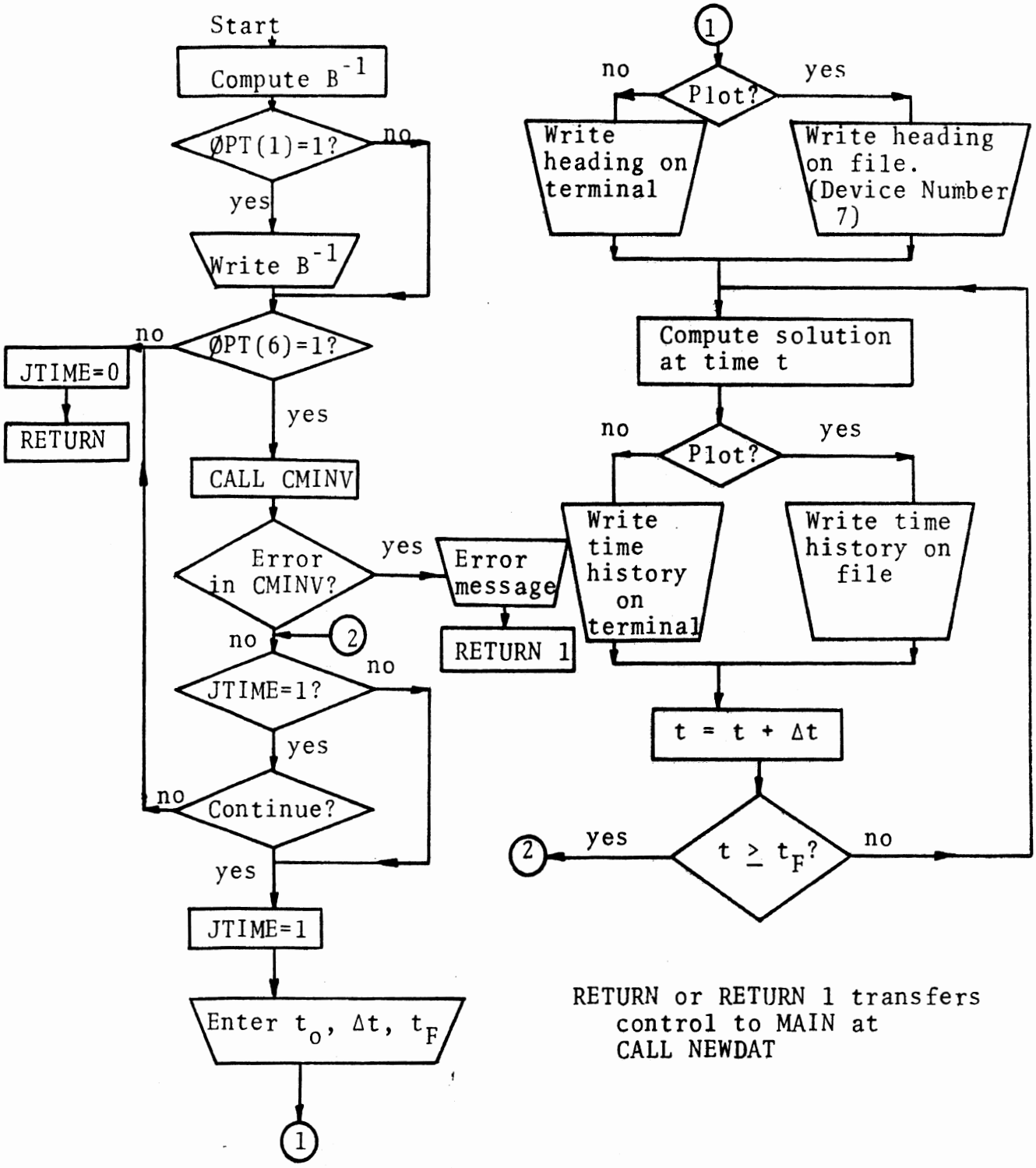

RETURN or RETURN 1 transfers control to MAIN at CALL NEWDAT

SUBROUTINE NEWDAT

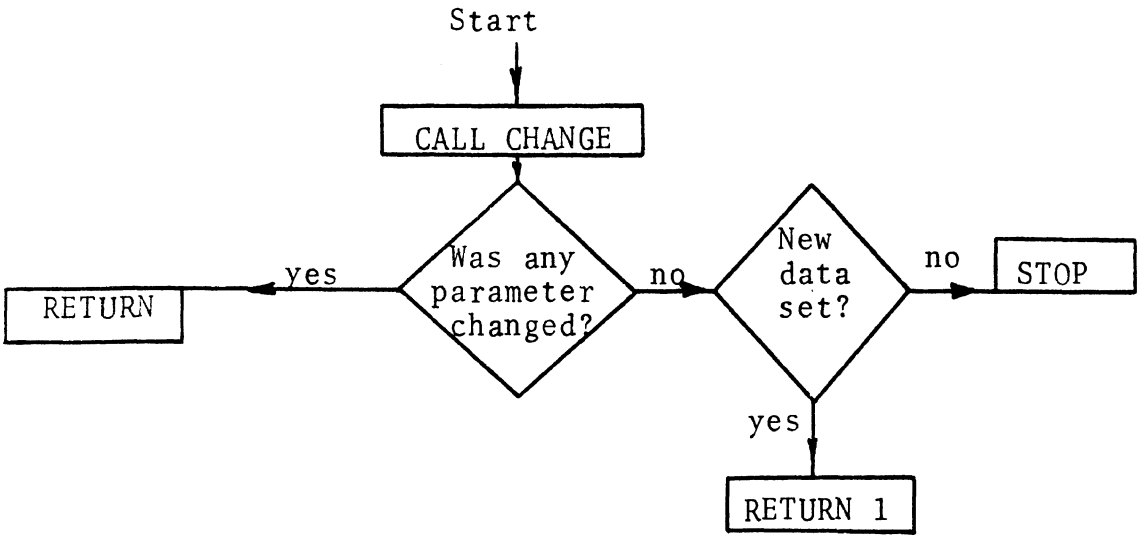

RETURN: Control transfers to (1) in MAIN

RETURN 1: Control transfers to (4) in MAIN

SUBROUTINE COEFK

The subroutine COEFK computes K, the understeer/oversteer factor in degrees/G. The schematic shown below is a very simplified version of the subroutine:

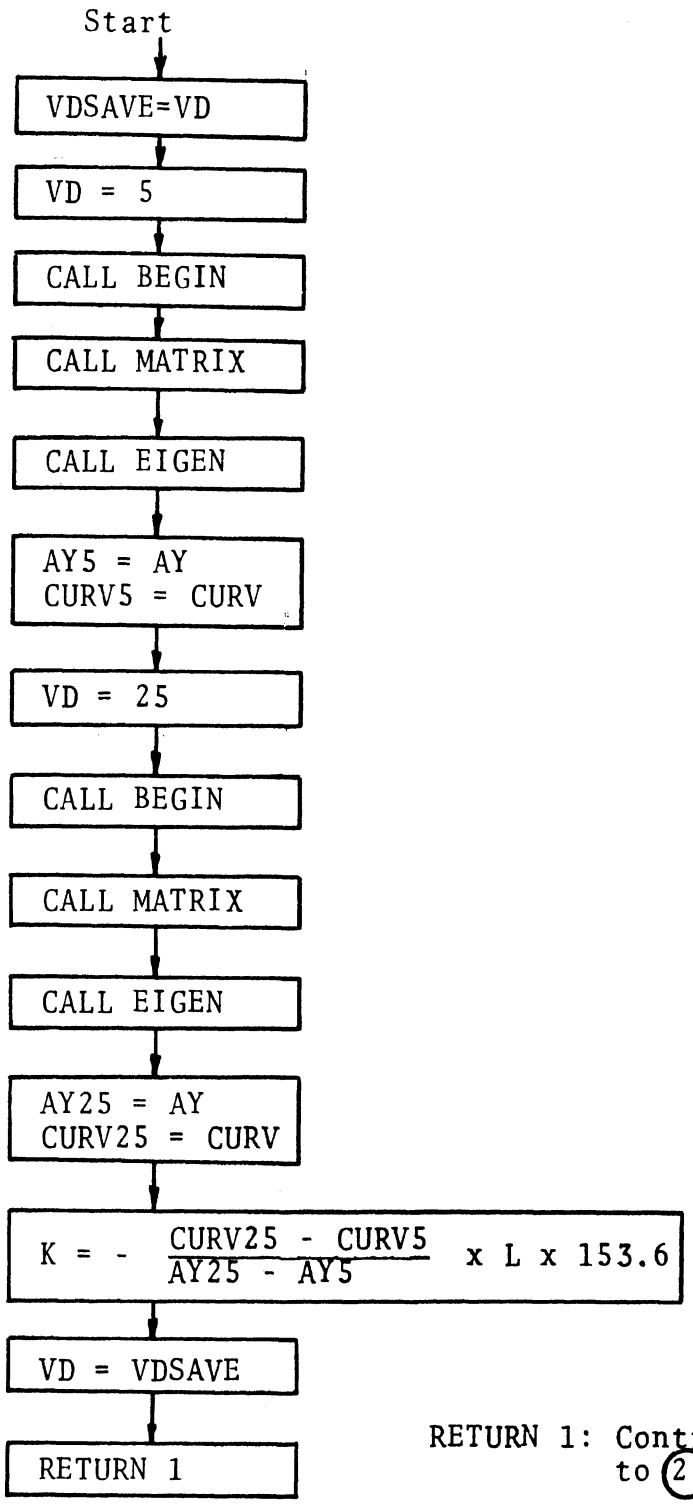

RETURN 1: Control transfers to (2) in MAIN

C3.3 SAMPLE INPUT AND OUTPUT FOR THE 1971 MUSTANG

```
run car3d(0) 5=h3data 7=lincardata
#EXECUTION BEGINS
PRINT DATA? y

A(IN)                      48.2500  ATF(IN-LB/DEG)           299.5000  ATR(IN-LB/DEG)           208.1000
B(IN)                      60.7500  CALFAF(LB/DEG)           142.5000  CALFAR(LB/DEG)           141.8000
CPF(LB/IN/SEC)              4.4800  CPR(IN/LB/SEC)             5.3350  CTF(LB/DEG)               22.0000
CTR(LB/DEG)                20.0000  DGDPHF(DEG/DEG)            0.6250  DGDPHR(DEG/DEG)            0.0
EPSF(DEG/DEG)              -0.0660  EPSR(DEG/DEG)             -0.0300  IXXS(IN-LB-SEC**2)       2970.0000
IXZS(IN-LB-SEC**2)          0.0     IZZF(IN-LB-SEC**2)       370.0000  IZZR(IN-LB-SEC**2)       600.0000
IZZS(IN-LB-SEC**2)      22600.0000  KRB(IN-LB/DEG)        151000.0000  KSUSPF(LB/IN)             87.0000
KSUSPR(LB/IN)             110.0000  KTIREF(LB/IN)            1420.0000  KTIRER(LB/IN)            1420.0000
L(IN)                     109.0000  TSF(IN)                    61.5000  TSR(IN)                   43.0000
W(LB)                    3660.0000  V(MPH)                     60.0000  WUF(LB)                  187.0000
WUR(LB)                   305.0000  ZAF(IN)                    12.7000  ZAR(IN)                   12.7000
ZCG(IN)                    20.4000  ZRCF(IN)                    0.0     ZRCR(IN)                  12.7000
GR                         22.0500  XM(IN)                      0.0     KRLS(DEG/1000 LB)          0.0
KSC(IN-LB/DEG)              9.5800  KSL(IN-LB/DEG)           4700.0000  DELSW(DEG)                22.0500
LASH(DEG)                   0.0     CAMF(DEG/1000 LB)           0.0     CAMR(DEG/1000 LB)          0.0
KFLS(DEG/1000 LB)           0.0     KRATS(DEG/100 FT-LB)        0.0
PRINT DATA NUMBERS? y
A       = 1 ;  ATF     = 2 ;  ATR     = 3 ;  B       = 4 ;  CALFAF  = 5 ;
CALFAR  = 6 ;  CPF     = 7 ;  CPR     = 8 ;  CTF     = 9 ;  CTR     =10 ;
DGDPHF  =11 ;  DGDPHR  =12 ;  EPSF    =13 ;  EPSR    =14 ;  IXXS    =15 ;
IXZS    =16 ;  IZZF    =17 ;  IZZR    =18 ;  IZZS    =19 ;  KRB     =20 ;
KSUSPF  =21 ;  KSUSPR  =22 ;  KTIREF  =23 ;  KTIRER  =24 ;  L       =25 ;
TSF     =26 ;  TSR     =27 ;  W       =28 ;  V       =29 ;  WUF     =30 ;
WUR     =31 ;  ZAF     =32 ;  ZAR     =33 ;  ZCG     =34 ;  ZRCF    =35 ;
ZRCR    =36 ;  GR      =37 ;  XM      =38 ;  KRLS    =39 ;  KSC     =40 ;
KSL     =41 ;  DELSW   =42 ;  LASH    =43 ;  CAMF    =44 ;  CAMR    =45 ;
KFLS    =46 ;  KRATS   =47 ;  OPTION1 =48 ;  OPTION2 =49 ;  OPTION3 =50 ;
OPTION4 =51 ;  OPTION5 =52 ;  OPTION6 =53 ;  OPTION7 =54 ;  OPTION8 =55 ;
OPTION9 =56 ;  OPTION10=57 ;
?
DEGREES/G?  y
    K =    3.0 DEG/G


 CHANGE  PARAMETERS? y
ENTER TWO-DIGIT DATUM NUMBER TO BE CHANGED: 06
ENTER CALFAR    : 180.
? 03
ENTER ATR       : 250.
?
DEGREES/G?  y
    K =    5.0 DEG/G
```

```
 CHANGE  PARAMETERS? y
ENTER TWO-DIGIT DATUM NUMBER TO BE CHANGED: 06
ENTER CALEAR    : 141.8
? 03
ENTER ATR       : 208.1
? 49
ENTER OPTION2   : 1
?
DEGREES/G?  n

EIGENVALUES: REAL;          -3.622          -3.622          -2.405          -2.405
          IMAGINARY;          -4.359           4.359          -8.879           8.879

STATIC MARGIN = 0.1363E 00

THE STEADY STATE SOLUTIONS ARE:
R(DEG/SEC)     BETA(DEG)     PHI(DEG)     CURV(1/FT)   AY(FT/SEC**2)
0.3474E 01    -.6650E 00    -.1408E 01    0.6890E-03    0.5335E 01


 CHANGE  PARAMETERS? n

MATRIX U:
.                                .                                .                                .                                .
.    -0.12418100   -1.58285141 .    -0.12418103    1.58285141 .    -0.31685519   -0.74880391 .    -0.31685510    0.74880391 .
.    -0.74810237   -0.07265860 .    -0.74810237    0.07265860 .    -0.21964675   -0.02896345 .    -0.21964675    0.02896345 .
.     1.02452335    2.31599903 .     1.02452335   -2.31599903 .     1.27772523    4.71780777 .     1.27772522   -4.71780777 .
.    -1.00000000    0.0        .    -1.00000000    0.0        .    -1.00000000    0.0        .    -1.00000000    0.0        .

U OPTION OFF? y


 CHANGE  PARAMETERS? n
RESPONSE TO STEP STEER? y

ENTER INITIAL TIME : 0.
ENTER TIME INCREMENT : .1
ENTER FINAL TIME : 1.0
PLOT? n

 TIME      R(DEG/SEC)    BETA(DEG)     P(DEG/SEC)     PHI(DEG)     CURV(1/FT)    AY(FT/SEC**2)
*************************************************************************************************
  0.0       0.5384E-05    -.1192E-05    -.2849E-05    -.9537E-06    0.4866E-03    0.3768E 01
  0.1000    0.2445E 01    0.5477E-01    -.4870E 01    -.2968E 00    0.3024E-03    0.2342E 01
  0.2000    0.3586E 01    -.1077E 00    -.4581E 01    -.8000E 00    0.3096E-03    0.2398E 01
  0.3000    0.3036E 01    -.3072E 00    -.2251E 01    -.1146E 01    0.4167E-03    0.3227E 01
  0.4000    0.3004E 01    -.4624E 00    -.4281E 00    -.1269E 01    0.5418E-03    0.4195E 01
  0.5000    0.4008E 01    -.5638E 00    0.1920E-01    -.1279E 01    0.6358E-03    0.4923E 01
  0.6000    0.4002E 01    -.6207E 00    -.4152E 00    -.1295E 01    0.6900E-03    0.5312E 01
  0.7000    0.3925E 01    -.6755E 00    -.8460E 00    -.1361E 01    0.7035E-03    0.5448E 01
  0.8000    0.3763E 01    -.7049E 00    -.7789E 00    -.1447E 01    0.7058E-03    0.5465E 01
  0.9000    0.3571E 01    -.7150E 00    -.2906E 00    -.1503E 01    0.7047E-03    0.5457E 01
  1.0000    0.3422E 01    -.7098E 00    0.2356E 00    -.1504E 01    0.7042E-03    0.5454E 01
CONTINUE? y
```

```
ENTER INITIAL TIME : 1.5
ENTER TIME INCREMENT : .5
ENTER FINAL TIME : 4.0
PLOT? n

 TIME      R(DEG/SEC)    BETA(DEG)     P(DEG/SEC)     PHI(DEG)     CURV(1/FT)    AY(FT/SEC**2)
*****************************************************************************************
  1.5000    0.3484E 01    -.6595E 00    -.1401E 00    -.1396E 01    0.6860E-03    0.5312E 01
  2.0000    0.3475E 01    -.6641E 00    0.1370E-01    -.1404E 01    0.6894E-03    0.5338E 01
  2.5000    0.3472E 01    -.6654E 00    0.1079E-01    -.1409E 01    0.6891E-03    0.5336E 01
  3.0000    0.3474E 01    -.6650E 00    -.3394E-02    -.1408E 01    0.6889E-03    0.5335E 01
  3.5000    0.3474E 01    -.6650E 00    -.3596E-03    -.1408E 01    0.6890E-03    0.5335E 01
  4.0000    0.3474E 01    -.6650E 00    0.3633E-03    -.1408E 01    0.6890E-03    0.5335E 01
CONTINUE? n


 CHANGE  PARAMETERS? n
IS THERE A NEW DATA SET? n
#EXECUTION TERMINATED
#
```

C4. NOMENCLATURE

a (A)*	x distance from c.g. to center of front axle (in.)
AT** (AT)	Sum of the aligning torque stiffnesses for the two tires at an axle (in-lb/deg)
A_y (AY)	Acceleration of the unsprung mass along the y-axis (ft/sec^2)
b (B)	x distance from center of rear axle to c.g. (in.)
c	x distance from the c.g. of the total vehicle to the sprung mass c.g. (in.)
c.g.	If not otherwise specified, represents the center of mass of the total vehicle
C_{am} (CAM)	Lateral force camber coefficient (deg/1000 lb)
C_p	Total roll damping moment of sprung mass (in-lb-sec)
c_p (CP)	Damping of a shock absorber (lb/in/sec)
C_α** (CALFA)	Sum of cornering stiffnesses for the two tires at an axle (lb/deg)
CT** (CT)	Sum of the camber stiffnesses for the two tires at an axle (lb/deg)
CURV (CURV)	Inverse of the radius of path in the x-y plane that the origin of the x-y-z axes is traveling (1/ft)
e	Perpendicular distance from the sprung mass c.g. to the x' axis (in.)

*Symbols in parentheses indicate the respective quantities as they appear on the computer program input-output. (The subscript F or R is omitted here.)

**The values for AT, C_α, and CT entered as data are for a single tire, though in the derivation in this document these tire characteristics are summed over the axle to provide simpler notation in the formulation.

f	Conversion factor equal to the $\sqrt{g/\ell}$ used to convert the equations of motion to dimensional time (1/sec)
g	Gravity constant equal to 386.04 in/sec^2
G_R (GR)	Gear ratio for the steering column
h	Perpendicular distance from the sprung mass c.g. to the x axis (in.)
i_{xx} (IX)	Sprung mass moment of inertia about x' axis nondimensionalized by $M\ell^2$
i_{xz} (IXZ)	Sprung mass product of inertia in x'-z' plane (with ϕ=0), nondimensionalized by $M\ell^2$
i_{zz} (IZ)	Yaw moment of inertia of total vehicle about z axis, nondimensionalized by $M\ell^2$
I_{xx_s} (IXXS)	Sprung mass moment of inertia about x_s axis (in-lb-sec^2)
I_{xx}	Sprung mass moment of inertia about x axis (in-lb-sec^2)
I_{xz_s} (IXZS)	Sprung mass product of inertia in x_s-z_s plane (in-lb-sec^2)
I_{xz}	Sprung mass product of inertia in x-z plane (in-lb-sec^2)
I_{zz_s} (IZZS)	Sprung mass moment of inertia about z_s axis (in-lb-sec^2)
I_{zz}	Sprung mass moment of inertia about z axis (in-lb-sec^2)
I_{zz_F} (IZZF)	Moment of inertia of front unsprung mass about a vertical axis through its axle center (in-lb-sec^2)
I_{zz_R} (IZZR)	Moment of inertia of rear unsprung mass about a vertical axis through its axle center (in-lb-sec^2)

k (K)	Understeer/oversteer factor (deg/G)
K	Total roll stiffness moment of sprung mass (in-lb)
K_{Fats} (KFATS)	Front aligning torque steer coefficient (deg/100 ft-lb)
$K_{F\ell s}$ (KFLS)	Front lateral force steer coefficient (deg/1000 lb)
K_{Rats} (KRATS)	Rear aligning torque steer coefficient (deg/100 ft-lb)
K_{RB} (KRB)	Roll moment of sprung mass per unit of roll due to front roll bar (in-lb/rad)
$K_{R\ell s}$ (KRLS)	Rear lateral force steer coefficient (deg/1000 lb)
K_{sc} (KSC)	Compliance in steering column (in-lb/deg)
$K_{s\ell}$ (KSL)	Compliance in steering linkage (in-lb/deg)
K_{ss}	Equivalent compliance of steering system (in-lb/deg)
k_{susp} (KSUSP)	Spring rate of a single suspension spring (lb/in)
k_{tire} (KTIRE)	Vertical spring rate of a tire (lb/in)
ℓ (L)	Wheelbase (in.)
lash (LASH)	Play in steering wheel (deg)
m	Reduced mass equal to $M_s h/M\ell$
M	Total mass of vehicle (slug)
M_s	Sprung mass (slug)
p (P)	Roll rate of sprung mass about x' axis (deg/sec)
r (R)	Yaw rate of vehicle about z axis (deg/sec)
SM2D	Static margin of 2 degrees of freedom (β and r) automobile
SM3D (STATIC MARGIN)	Static margin of 3 degrees of freedom automobile

T_{c_p}	y distance between shock absorbers (in.)
T_R	y distance between tires (in.)
T_s (TS)	y distance between suspension springs (in.)
U (U)	Matrix of eigenvectors
V (V)	Velocity of vehicle along x axis (mph)
W (W)	Gross vehicle weight (lb)
W_s	Weight of sprung mass (lb)
W_u (WU)	Weight of unsprung mass (lb)
x_m (XM)	Mechanical trail (in.)
x_p	Pneumatic trail (in.)
z_a (ZA)	Axle height (in.)
Z_{cg} (ZCG)	Height of total vehicle c.g. (in.)
z_{rc} (ZRC)	Roll center height (in.)
β (BETA)	Vehicle sideslip angle measured from x axis to velocity vector at total vehicle c.g.; positive clockwise looking down (deg)
γ	Tire camber angle (deg)
δ	Steering angle at road wheel, equal to $(\delta_{sw}$ - lash$)/G_R$ (deg)
δ_{sw} (DELSW)	Steering wheel angle (deg)
ϵ (EPS)	Roll steer coefficient (deg/deg)
λ	Angular displacement of x' axis from x axis, positive for nose down direction (deg)
μ	Nondimensional velocity equal to $V/\sqrt{\ell g}$
ϕ (PHI)	Roll angle about x' axis, positive clockwise looking front (deg)

$\frac{\partial \gamma}{\partial \phi}$ (DGDPH)	Variation of γ with ϕ

Subscripts

F (F)	Front axle
R (R)	Rear axle
ss	Steady-state

Axes

The origin of the x-y-z axes, which is coincident to the origin of the x'-y'-z' axes, is fixed by the intersection of the x' and z axes.

x' axis	Roll axis of sprung mass, positive forward
z axis	With ϕ equal to 0, this axis is vertical through the c.g. of the total vehicle
x-y-z axes	Fixed in sprung mass of vehicle, x axis is parallel to the ground and positive forward; y axis is positive to the right
x'-y'-z' axes	Fixed in unsprung mass, y' axis is positive to the right; z' axis is perpendicular to the x' axis and is positive downward
x_s-y_s-z_s axes	Parallel to x-y-z axes with origin fixed in the c.g. of the sprung mass

C5. REFERENCES

1. Segel, L., "Theoretical Prediction and Experimental Substantiation of the Response of the Automobile to Steering Control," Inst. Mech. Engrs., Proc. Automobile Div., No. 7, 310 (1956-57).

2. Weir, D.H., Shortwell, C.P., and Johnson, W.A., "Dynamics of the Automobile Related to Driver Control," SAE Paper No. 680194, 1968.

3. Pipes, L.A., Matrix Methods for Engineering, Prentice-Hall, Inc., Englewood Cliffs, N.J., 1963, pp. 59-61.